

Florian Risch

*Planning and Production Concepts for Contactless Power Transfer
Systems for Electric Vehicles*

Florian Risch

*Planning and Production Concepts for Contactless Power
Transfer Systems for Electric Vehicles*

Bericht aus dem Lehrstuhl für
Fertigungsautomatisierung und Produktionssystematik
Prof. Dr.-Ing. Jörg Franke

FAPS



Meisenbach

G m b H V e r l a g

Als Dissertation genehmigt von der Technischen Fakultät
der Friedrich-Alexander-Universität Erlangen-Nürnberg

Tag der Einreichung:	07. April 2014
Tag der Promotion:	30. Juli 2014
Dekan:	Prof. Dr.-Ing. habil. Marion Merklein
Berichterstatter:	Prof. Dr.-Ing. Jörg Franke
	Prof. Dr.-Ing. Achim Kampker, RWTH Aachen

Bibliografische Information Der Deutschen Bibliothek

Die Deutsche Bibliothek verzeichnet diese Publikation in der
Deutschen Nationalbibliografie; detaillierte bibliografische Daten
sind im Internet über <http://dnb.ddb.de> abrufbar.

ISSN 1431-6226

ISBN 978-3-87525-369-6

Dieses Werk ist urheberrechtlich geschützt.

Alle Rechte, auch die der Übersetzung, des Nachdrucks
und der Vervielfältigung des Buches oder Teilen daraus,
vorbehalten.

Kein Teil des Werkes darf ohne schriftliche Genehmigung des
Verlages in irgendeiner Form (Fotokopie, Mikrofilm oder ein
anderes Verfahren), auch nicht für Zwecke der Unterrichts-
gestaltung - mit Ausnahme der in den §§ 53, 54 URG ausdrücklich
genannten Sonderfällen -, reproduziert oder unter Verwendung
elektronischer Systeme verarbeitet, vervielfältigt oder
verbreitet werden.

© Meisenbach Verlag Bamberg 2014

Herstellung: inprint GmbH, Erlangen

Printed in Germany

Planning and Production Concepts for Contactless Power Transfer Systems for Electric Vehicles

*Planungs- und Produktionskonzepte für
kontaktlose Energieübertragungssysteme für Elektrofahrzeuge*

Der Technischen Fakultät der
Friedrich-Alexander-Universität Erlangen-Nürnberg
zur
Erlangung des Doktorgrades Dr.-Ing.

vorgelegt von

Florian Risch
aus Nürnberg

Als Dissertation genehmigt von
der Technischen Fakultät der
Friedrich-Alexander-Universität Erlangen-Nürnberg

Tag der mündlichen Prüfung:	30.07.2014
Vorsitzende des Promotionsorgans:	Prof. Dr.-Ing. habil. M. Merklein
Gutachter:	Prof. Dr.-Ing. J. Franke Prof. Dr.-Ing. A. Kampker

Vorwort

Die vorliegende Dissertation entstand während meiner Tätigkeit als wissenschaftlicher Mitarbeiter am Lehrstuhl für Fertigungsautomatisierung und Produktionssystematik (FAPS) der Friedrich-Alexander-Universität Erlangen-Nürnberg (FAU).

Herrn Prof. Dr.-Ing. Jörg Franke, dem Leiter dieses Lehrstuhls und Erstgutachter der vorliegenden Dissertation, danke ich für die wohlwollende Förderung bei der Durchführung dieser Arbeit, die vielfältigen wissenschaftlichen Freiräume und das mir stets entgegengebrachte Vertrauen. Gleiches gilt auch für Herrn Prof. Dr.-Ing. Klaus Feldmann, der mich vor allem in meiner Anfangszeit als wissenschaftlicher Mitarbeiter am Lehrstuhl begleitete. Auch für die Übernahme des Vorsitzes bei meiner Promotionsprüfung möchte ich ihm herzlich danken. Herrn Prof. Dr.-Ing. Achim Kampker, Leiter des Lehrstuhls für Produktionsmanagement der RWTH Aachen, danke ich für die wohlwollende Übernahme des Koreferates. Mein Dank gilt ferner Herrn Prof. Dr. rer. nat. Lothar Frey, Leiter des Lehrstuhls für Elektronische Bauelemente der Friedrich-Alexander-Universität Erlangen-Nürnberg als weiterem Mitglied des Prüfungsausschusses.

Allen meinen Kollegen, insbesondere des Forschungsbereichs Elektromaschinenbau (E|Drive-Center) sei herzlich für die stets sehr gute und produktive Zusammenarbeit, die konstruktiven fachlichen Diskussionen, die große Hilfsbereitschaft und gegenseitige Unterstützung in den zahlreichen gemeinsamen Projekten und die schöne gemeinsame Zeit gedankt. Besonders hervorheben möchte ich in diesem Zusammenhang Herrn Dipl.-Ing. Alexander Kühl, meinem langjährigen Bürokollegen, sowie Dipl.-Ing. Jan Tremel, Dipl.-Ing. Tobias Klier und Dipl.-Ing. Stefan Günther.

Ferner gilt mein Dank allen Studenten und wissenschaftlichen Hilfskräften für ihr großes Engagement, mit dem sie mir bei der täglichen Arbeit und bei der Realisierung von zahlreichen Ideen geholfen haben. Ohne den Beitrag anderer schmälern zu wollen, seien an dieser Stelle Dipl.-Wirtsch.-Ing. Benedikt Weiss, Dipl.-Wirtsch.-Ing. Christian Böhm, Dipl.-Ing. Martin Brunner und Dipl.-Ing. Sebastian Kraner genannt.

Mein herzlichster Dank gilt meiner Familie, insbesondere meiner Schwester Kerstin und meiner Frau Verena. Sie haben durch ihre fortwährende Rücksichtnahme und Unterstützung den erfolgreichen Abschluss dieser Arbeit möglich gemacht.

Nürnberg, im April 2014

Florian Risch

Planning and Production Concepts for Contactless Power Transfer Systems for Electric Vehicles

Table of Contents

1	Introduction.....	1
1.1	Current situation.....	1
1.2	Problem statement and need for action.....	2
1.3	Objectives of the thesis and scientific approach.....	4
2	Derivation of Fields of Application for CPT Systems	7
2.1	Medical applications and consumer electronics	8
2.2	Industrial material handling applications.....	9
2.3	CPT systems for electric vehicles.....	10
2.3.1	Comparison of EV CPT and material handling CPT systems ..	10
2.3.2	General advantages of CPT systems for EVs	14
2.4	Types of contactlessly powered transportation	19
2.4.1	Stationary contactlessly powered transportation	19
2.4.2	Semi-dynamic contactlessly powered transportation.....	22
2.4.3	Dynamic contactlessly powered transportation.....	23
3	Simulation-Based Modeling and Optimizing of CPT Infrastructure (ETEV SIM).....	30
3.1	Planning tools for CPT infrastructure allocation problems.....	30
3.2	Simulation approach to determine an optimized CPT infrastructure design.....	34
3.3	Simulation of harbor logistics	41
4	Detailed Analysis of CPT Pad Designs for Electric Vehicles	47
4.1	Physical basics of CPT systems	47
4.1.1	Energy chain of CPT systems	53
4.1.2	Main factors impacting the efficiency of CPT systems.....	55
4.2	Basic charging pad types	63
4.2.1	Comparison of single-sided circular and double-sided solenoid systems	63

4.2.1.1	Positioning tolerance and size of the pads	64
4.2.1.2	Field emissions.....	66
4.2.1.3	Future viability – inter-operability	67
4.2.2	New coil designs.....	69
4.2.2.1	Improved solenoid systems	70
4.2.2.2	Polarized single sided flux pads	70
4.2.2.3	Additional design approaches.....	74
4.3	CPT systems for RPEVs	76
4.3.1	Distributed coil structures for RPEVs.....	77
4.3.2	Lumped coil structures for RPEVs.....	80
5	Development and Implementation of Production Concepts for CPT Systems	82
5.1	Production steps for CPT systems	83
5.1.1	Plastic base parts and housing.....	83
5.1.2	Assembly of ferrites and electronics	84
5.1.3	Contacting of HF-Litz wires.....	86
5.1.4	Encapsulation	95
5.1.5	Final assembly.....	97
5.2	HF-Litz wire winding technologies.....	102
5.2.1	Analysis of coil types from a process perspective	102
5.2.2	Feeding of HF-Litz wires.....	107
5.2.3	Inherent coil stability	110
5.2.4	HF-Litz wire winding	115
6	Optimizing CPT Systems from a Process and Material Perspective.....	136
6.1	Mechanical stress profiles	139
6.2	Thermal stress profiles	153
7	Summary and Outlook.....	160
8	Zusammenfassung	164
9	List of Abbreviations	166
10	Literature	169

1 Introduction

1.1 Current situation

Over the past decade, electrification of vehicles has become an increasingly important topic for sustainable societies. It will continue to play a substantial role in emission-free transportation of the future. In the face of ever-rising fuel prices, general public demand for electrified mobility will continue to soar, and thus increasingly encourage the automotive industry to develop alternative vehicle concepts with electrified powertrains. Electrified Vehicles (EV) present several advantages. They can help reduce dependence on fossil fuel imports, as they run on electricity which can be generated using almost any fuel [1]. In combination with renewable energy production (e.g. wind, solar, hydro), it is possible to keep transportation carbon-free or at least carbon-neutral. While these benefits have triggered interest in electric vehicles since the 1990s, market penetration has remained low because of a lack of widespread consumer acceptance, mainly due to range anxiety and monetary concerns. The technology has always been expensive compared to conventional vehicles [1] due to the fact that electric vehicles require large and expensive batteries. Major improvements are required in order to achieve widespread adoption and raise user acceptance, predominantly in terms of range as well as battery life and cost.

Growing comfort and safety needs will be additional decisive aspects in achieving wide market acceptance of electric vehicles in the future. This will especially be the case for the charging procedure, as even with fast-charging solutions, electric vehicles have to be charged more frequently than vehicles with Internal Combustion Engine (ICE) need to be filled up. Charging solutions have to be found that are suitable for future vehicle and driver requirements. Early adopters, whose motivation has been to support green energy, may accept some discomfort. To win over the future main target group of average car drivers, however, the operating comfort of EVs will be crucial and the need for a simple and robust charging scheme is becoming more important. The currently preferred conductive solutions for charging EVs present problems such as potential vandalism of accessible cables, increased maintenance costs due to wear-out, and inconvenience because of the frequent plugging processes. Contactless Power Transfer (CPT) technology is the focus of research and industry to solve such basic problems of current EV concepts and to increase customer acceptance. Automatic CPT eliminates the constant and inconvenient plugging processes. All the driver of an EV has to do is park his/her car correctly over a primary CPT-infrastructure in order to charge. Problems of mechanical wear-out like damaged insulation of charging cables or breaks on the connectors can be avoided, improving the reliability of the charging process. There is no more handling and storage of dirty, wet, and heavy cables, enabling all-weather and vandalism-free charging [2], perfectly in line with the general trend towards automated parking and driving. Furthermore, the ease of charging encourages high-frequent grid

connection [3], with high-frequent charging cycles, potentially extending range and lifetime of modern batteries [4] [5]. More frequent grid-connection can also accelerate the implementation of a smart-grid approach, as EVs may be used to increase the availability of vehicles for Vehicle-to-Grid (V2G) operation and thus can be used as dispersed storage devices to stabilize the power grid [6]. Several technology demonstrators have even shown the feasibility of dynamic power transfer in vehicles while they are in motion. Roadway Powered Electric Vehicles (RPEVs) make it possible to extend the EV range with significantly smaller on-board battery capacities [3] [7] [8].

All these considerable advantages and technological progress make CPT technology one of the key market drivers for a widespread market introduction of partial or even fully electrified vehicles in the coming years, especially in terms of higher customer acceptance and the practicality of electro-mobility [7] [9]. Starting with stationary applications placed at home or at work [10], several car manufacturers and suppliers have already announced partnerships for developing CPT systems [7] [11]. Thus, based on current market conditions, the focus of this thesis lies primarily on stationary CPT systems in the range of several kilowatts. In the longer term, however, it is possible that charging systems will be built into public roadways at taxi stands, traffic lights, or even highways [12]. Therefore, this thesis also discusses electrified roadways with power transfer rates of up to several hundred kilowatts, in the appropriate fields of application and their current development context.

1.2 Problem statement and need for action

Modern CPT systems for EVs have already shown their potential of high power transfer efficiency in many prototypes and trials [7] [13]. However, CPT for EVs is a particularly demanding application and still in its early commercialization phase. There are still some barriers to overcome for a successful and large-scale implementation of CPT systems to become a preferred method for recharging EVs.

As the technology becomes increasingly sophisticated, important challenges for large-scale deployment remain, such as regulatory (standards, inter-operability, safety requirements) and business-related concerns (insecure business models, excessive cost), as shown in Fig. 1. The focus of this thesis is on business-related issues, as regulatory concerns must be solved in multi-company approaches. Several boards of standardization have already been implemented for this purpose.

Business stakeholders often bring up the concern of insecurity that comes with the very complex combination of parameters that need to be taken into account in order to thoroughly evaluate the attractiveness of different fields of application. Therefore, potential users in different fields of application, which will at first be predominantly commercial (logistics, public transport, etc.) need substantiated options for a detailed evaluation of the benefits of CPT systems.

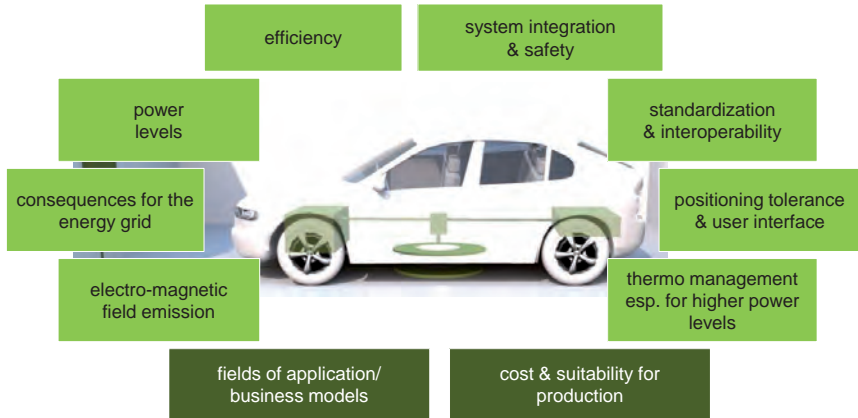


Fig. 1. Challenges for large-scale deployment of CPT systems.

Aside from this lack of planning security, another challenge to sustainably finance contactless charging is the fact that production volumes are initially low, which makes equipment costs of the first applications relatively high. For the short term, contactless charging will remain a promising add-on premium option for some years with costs ~10%-25% higher than conductive charging equipment [11] [14]. With appropriate standards in place and significant cost reduction, market research institutes like Pike Research believe that contactless EV charging equipment might make up to 30%-40% of the charging equipment market by 2020 [11]. As shown in Fig. 2, Pike Research forecasts an initially slow but steady growth of contactless EV charging systems until 2015, with sales and revenues accelerating in the second half of the decade [15] [16].

Therefore, the early stages of market development will require adaptive supply chains and a gradually adjusted degree of automation, with flexible assembly and handling technologies, to respond efficiently and quickly to increasing demand for CPT system solutions, and to thus secure a high market share [17]. Finally, increasing market acceptance with high sales numbers will require semi- and high-automated production concepts with higher process speeds. Prospective mass production with highly automated production concepts at higher process speed poses particular challenges with its requirements of reliable delivery, handling, and processing of sensitive materials [17] [18]. A manufacturer cannot afford losses caused directly by inadequate production processes or subsequently by the operation of poorly manufactured CPT systems over the entire product-life. This is crucial, as even small increases in efficiency can lead to significant annual savings and a competitive edge over other charging options.

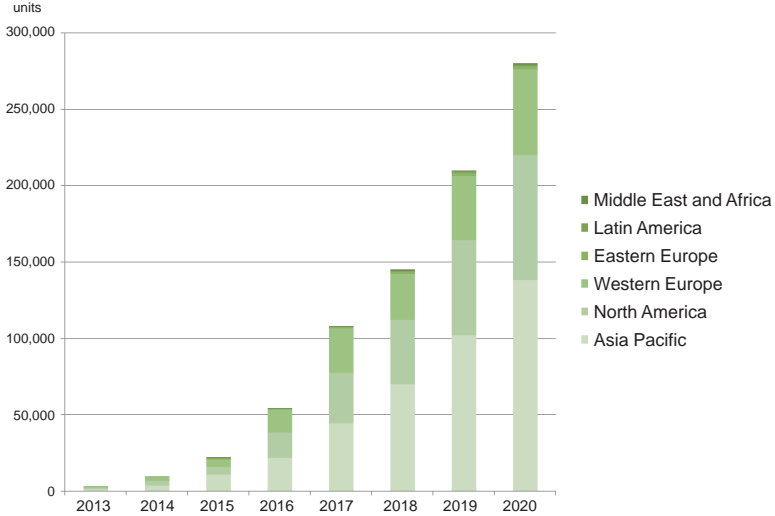


Fig. 2. Market for EV charging CPT systems by global regions 2013-2020 [16].

In consequence, the perspective of value creation must inform our understanding of the entire system. It will be vital to fully understand how to master the multi-dimensional interactions of a variety of active working materials in a variety of production processes.

1.3 Objectives of the thesis and scientific approach

The overall objective of this thesis is to help accelerate the market introduction of CPT systems for EVs. In particular, the thesis is divided in two parts, as shown in Fig. 3: firstly, emphasizing the implications of application evaluation and secondly, focusing on the production process and materials point of view. The first objective is to develop an application-specific evaluation method to assess the attractiveness of CPT-based vehicle concepts with the help of production-based planning methods (event-discrete simulation tools). The second objective is to develop automated production and testing processes to implement innovative CPT-charging pad topologies at low cost and with a reliable handling of sensitive materials.

According to the main objectives, the thesis is structured as followed:

Chapter 2 discusses the general advantages, different fields of application, and vehicle forms for CPT systems as a basis to derive a scientific approach. It further presents the differences between stationary and dynamic approaches. Subsequently, chapter 3 explains the developed approach to increase planning security, by using production simulation methods to thoroughly evaluate the benefits of diverse application fields for CPT-

based vehicle concepts. As the first objective of this thesis, the evaluation of attractive fields of application for CPT systems can be improved with this approach, supporting planning departments and authorities, and finally decision makers.

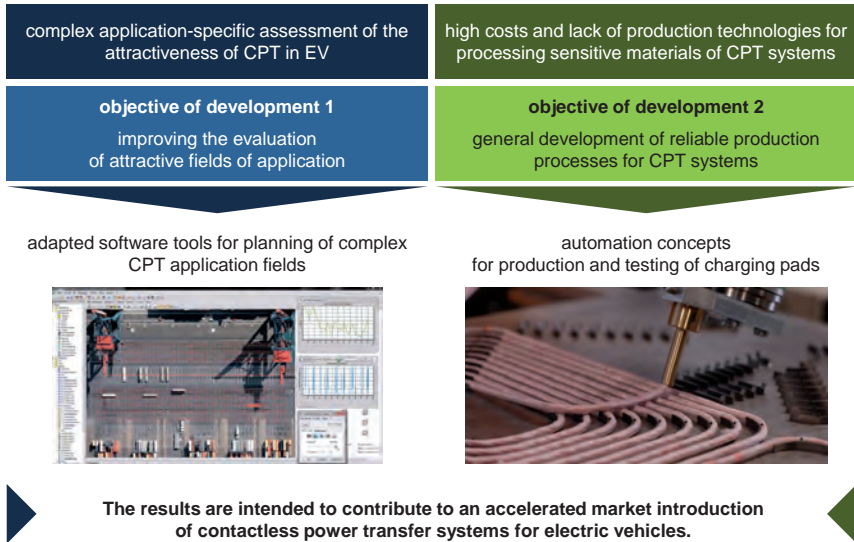


Fig. 3. Main research objectives of the thesis.

As the cost for CPT systems is still high and, in consequence, impeding the introduction of CPT systems in diverse fields of application, the second objective of this thesis is to support the development of cost-efficient, producible, and reliable CPT systems. Therefore, chapter 4 provides a detailed analysis of contactless power transfer pad designs for EVs. Starting with the physical basics of contactless power transfer and technological alternatives with their specific characteristics, this thesis elaborates innovative EV pad topologies for stationary and dynamic charging. To improve the attractiveness of the technology and to establish reliable, efficient, and flexible production structures, chapter 5 presents solutions for the production of innovative charging pads, with a focus on HF-Litz wire winding in innovative charging pad topologies. Several test set-ups are described to understand the potential impact of automated large-scale production processes (e.g. varying tolerances) and real-life material behavior. In the context of the complex correlation of diverse influencing parameters, chapter 6 proposes an automated test-bench-based verification approach for optimizing CPT systems from a process and material perspective. This allows verification of the influences of new production techniques, alternative materials (e.g. conductors, field shaping materials), failure modes during operation (e.g. mechanical and thermal stress profiles), etc. to comply

with the high demands of quality and power transfer efficiency in automotive applications, and to find further optimization potentials to reduce production costs, weight, and volume of CPT-charging pads.

Chapter 7 sums up the results and gives an outlook on future developments.

2 Derivation of Fields of Application for CPT Systems

Contactless power transfer is the transmission of electrical energy from a power source transmitter to a receiver without using any physical conductive connection. This idea of transmitting power through the air without a direct electrical connection has been around since the late 1800s and early 1900s [19], with successful proof-of-concept demonstrations around 1900 [20] [21] [22]. In the past decade, researchers have made several breakthroughs that allow the commercialization of CPT systems [23], and with its key advantages over contact-based approaches (plug-in, bar, and brush), CPT is continually finding new applications. Contactless power transfer systems are reliable and maintenance-free due to their inherent galvanic and physical isolation. Moreover, conductors and electronics are enclosed and protected in sealed watertight and explosion-proof casing, which ensures safe operation in wet or dirty environments [24]. In addition, CPT systems appeal to buyers even more because there is no need for battery replacement or a cord, the most failure-prone component [20]. CPT devices are also the more eco-friendly option, with either reduced battery size or even battery-free operation. Using grid power is much less expensive and more environmentally sound than manufacturing, transporting, and using batteries, especially when they are based on traditional electro-chemistries [20].

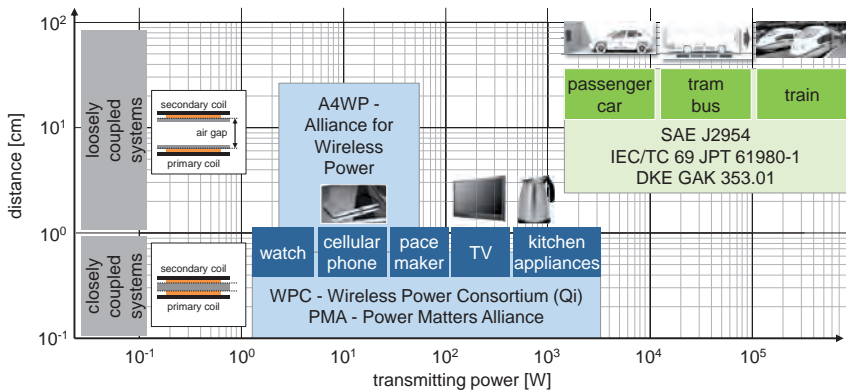


Fig. 4. Levels of transmitted power and distances for different fields of application for CPT systems.

These qualities yield a wide range of applications for CPT systems (Fig. 4, double logarithmic scale) where the use of wires is inconvenient, unreliable, hazardous, or impossible, such as powering medical and consumer electronics [25] [26] (see chapter 2.1),

factory automation [21] [27] [28] (see chapter 2.2) and - as is the focus of this thesis - electrified vehicle concepts (see chapter 2.3) [24] [29] [30].

The range of different power levels and distances for CPT applications is large. For consumer electronics, power is usually transmitted in the range of a few watts, and the focus is on closely coupled systems with a distance between transmitter and receiver of only a few millimeters. The distance of the coils and power levels for automotive vehicle applications are usually far greater. In loosely coupled systems, the air gaps that have to be covered are in the 100-300 mm range. Depending on the field of application, CPT systems today can generate an output power P_{out} of up to several hundred kW. For passenger cars, the primary focus is on lumped systems at modest power levels (3.7 kW) for home-based charging, as this is the presumed maximum power rating of a typical household main outlet (230 V, 16 A). However, as fast charging is getting more attention to facilitate the daily operation of EVs, organizations also work on larger power levels. The SAE (Society of Automotive Engineers) J2954 Wireless Charging Task Force, for example, discusses power classes from light duty home (3.7 kW), light duty private/public parking (7.7 kW) up to light duty fast charge (22 kW) [31]. The German National Electric Mobility Platform (Nationale Plattform Elektromobilität - NPE) mentions charging levels for CPT systems for the power levels 3.7 kW, 11 kW, 22 kW, and 60 kW [32]. Beyond that, other projects have already demonstrated power levels of up to 200 kW for buses, trucks, and trains [33] [34].

2.1 Medical applications and consumer electronics

Nowadays, CPT systems represent the state of the art for a wide range of medical and consumer products. Since CPT eliminates the need for cables that penetrate the human body and surgical replacement of primary batteries, commercial exploitation of transcutaneous contactless medical implants began as early as the 1960s with pace-makers [20] [35]. Since then, contactless charging systems are being further developed for other implanted medical devices including Left Ventricular Assist Devices (LVADs), heart assist pumps, and infusion pumps [20] [25] [26].

Towards the end of the 1970s, manufacturers of consumer products also began to offer contactless charging systems, starting with CPT electric toothbrushes, which are considerably safer than the contact-based chargers that had been in use before, especially in a high-humidity environment like a bathroom [36]. Due to the positive experience in the field of hygiene and personal care appliances, there has been a clear trend towards contactless power transfer in consumer electronics in recent years. Thus, there are more and more CPT-based devices, particularly in the field of portable consumer electronic equipment with its continuously rising customer demands (larger displays, faster processors, HD graphics, “always online in social media networks”), such as cellular phones and laptop computers [37] [38]. Contactless charging of mobile devices will be

even more attractive in the years ahead with manufacturer-independent interfaces of closely coupled systems, like the Qi standard (5 W at 100-205 kHz) of the Wireless Power Consortium (WPC). Higher power levels like 15 W, 200 W, 800 W, and 2.4 kW specifications are currently under development (see Fig. 4). With CPT, consumers will no longer need to carry the correct charging cable for each device. The devices can be charged by simply placing them on top of the charging pad. In the future, these pads might even be embedded in furniture and become standard in public places such as restaurants¹, hotels, or train stations. However, aside from the Qi standard, there is also the Power Matters Alliance (PMA, 5 W at 277-357 kHz) and the Alliance for Wireless Power (A4WP), potentially confusing the customers (see also problems of standardization in chapter 4.2.1.3). The A4WP is expanding to loosely coupled lumped systems, operated by non-radiative, “near-field mid-range” magnetic resonance (see chapter 4.1), with power levels of up to 22 W at 6.78 MHz. The A4WP system thus makes it possible to wirelessly power several devices simultaneously without immediate vicinity (several centimeters) to a charging base station [40].

2.2 Industrial material handling applications

CPT systems have also demonstrated their viability in another crucial and continuously growing market: The field of contactlessly powered material handling applications [30], such as Automated Guided Vehicles (AGVs), skilnet systems, monorail overhead conveyors, sorting systems for flexible manufacturing lines, or logistical systems that can operate inside or outside, in cooling facilities, and wet areas [21] [23] [30]. In the mid-1990s, the automotive industry started requesting contactless power solutions for AGVs in car factories at engine assembly lines, welding bays or paint shops, as CPT systems prove to be more robust (unaffected by chemicals or dirt) and safe with reduced maintenance than power transfer systems that rely on bus bars/brushed contacts [41]. As CPT systems do not generate fine particles that would contaminate sensitive processes, as brushed electrical contacts tend to do, CPT material handling systems are also used for processes that require a strict control of environmental pollutants, like cleanrooms in chip manufacture, achieving higher yields than any competing technology [30].

Usually, loosely coupled systems with elongated primary tracks are used here, either in the form of an overhead monorail conveyor or a floor-mounted system. A monorail conveyor system uses secondary systems with E- or H-shaped ferrite pick-up cores that encircle $\sim 270^\circ$ of the primary track (two wires at a spacing of 100 mm), operated with relatively small air-gaps, and good coupling factors at high efficiency. Floor-mounted AGVs with flat pick-ups (Fig. 5.) however, do not have such ideal operating conditions for coupling, as they do not even encircle 180° of the two primary track wires (spaced 100 mm apart and buried 10 mm in the shop floor). This results in coupling factors of a

¹ Starbucks started to adopt the concept in the U.S. in 2013 [39].

mere 50% of what is attainable with a monorail system with E- or H-shaped pick-ups [41].

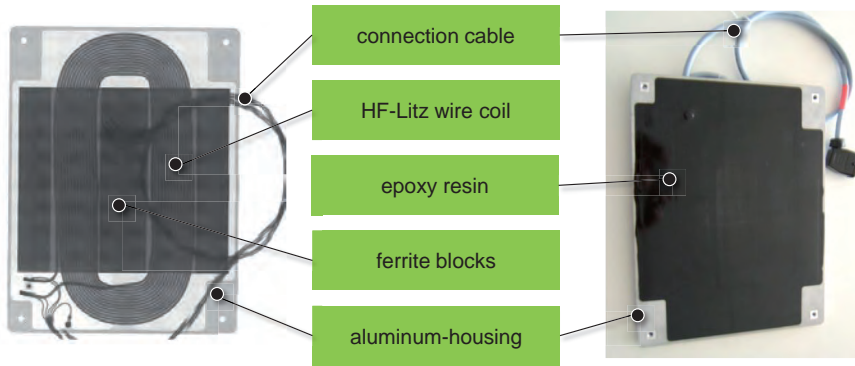


Fig. 5. Flat pick-up for floor-mounted AGVs.

However, floor-mounted AGVs with flat pick-ups can be flexibly used to leave their power supply and move around factories for some meters on battery power, e.g. to turn to the next assembly line, sensing the wire position under the concrete floor for navigation purposes.

2.3 CPT systems for electric vehicles

As emission-free electrified personal and logistics transportation systems flourish and more and more devices become cable- and wireless, the idea of having to plug your car into the wall seems at odds with the high-tech nature of electrified vehicles [4]. CPT systems for EVs actually existed for some time in early research projects in the 70s, 80s and 90s [2] [42] [43] [44], and together with recent improvements in power electronic components and the technology used in material handling industrial applications as described in chapter 2.2, technological progress for automotive CPT systems is rapidly evolving.

2.3.1 Comparison of EV CPT and material handling CPT systems

The existing components used in CPT-based material handling are inadequate for EV charging. The systems have to be adapted significantly, as larger air gaps in the kW range in EV CPT applications make it much more technically challenging to achieve sufficient performance. Tab. 1 shows the differences between material handling systems and automotive EV charging.

Tab. 1. *Design specifications for material handling and EV CPT systems (based on [45]).*

	industrial material handling systems	automotive EV CPT systems
system efficiency [%] ²	~25%-90% (depending on infrastructure layout: lumped vs. distributed primary systems)	above 90% [20] [46] (lumped systems)
air gaps	small, closely coupled, mm-range [30]	large, loosely coupled, several cm
tolerance to misalignment ³	intolerant	tolerant
power level [kW]	100's W up to several kW's	well above several kW's
specific power density [kW/kg] ⁴	~0.02-0.34	target values of the automotive industry: 3.7 kW with 5 kg ~0.74
volumetric power density [kW/m ³]	~30-300	above 1,000
electronics/packaging	big	small
field guiding material/ferrites	only secondary side	primary and secondary side
frequency [kHz]	~20-25	~85-140
emissions and safety	EMF limited to international safety regulations [47]	EMF limited to international safety regulations [47], and additional FOD ⁵ , LOP ⁶

The direct comparison shows the weak points of material handling systems and thus the need for action from a product point of view. Industrial systems are built simple and their actual degree of efficiency, air gaps, tolerances to misalignment, and power rating are far (10-100 times) from sufficient to meet the stringent requirements for modern automotive EV applications [41]. Additional difficulties arise from the needed stricter safety requirements in EV charging equipment compared to industrial systems operated by skilled workers.

To prevent adverse health effects, many national governments have established safety limits for human exposure to various frequencies of electromagnetic energy, mainly based on ICNIRP (International Commission in Non-Ionizing Radiation Protection) guidelines [20]. In consequence, companies take these ICNIRP regulations into account as they develop and configure CPT systems for EVs [41]. In the frequency range that is

² End-to-end efficiency (AC input to DC output) [20].

³ Always depending on coil diameter and air gap.

⁴ Always depending on whether power electronics are included/integrated or not.

⁵ Foreign Object Detection (FOD): for the presence of metal objects in the magnetic field that may be heated (induction heating).

⁶ Living Object Protection (LOP): for the presence of persons or animals in the magnetic field, e.g. using GHz radar sensors to pick up any movement between the charging pads.

being discussed for CPT EV charging (~85 kHz), humans should not be exposed to magnetic field strengths above 6.25 μT (ICNIRP 1998) [47]. In this context, the German Association for Electrical, Electronic & Information Technologies VDE (Verband der Elektrotechnik Elektronik Informationstechnik) developed an initial application guide VDE-AR-E 2122-4-2 [48]. Among other aspects, the application guide defines safety zones, as shown in Fig. 6.

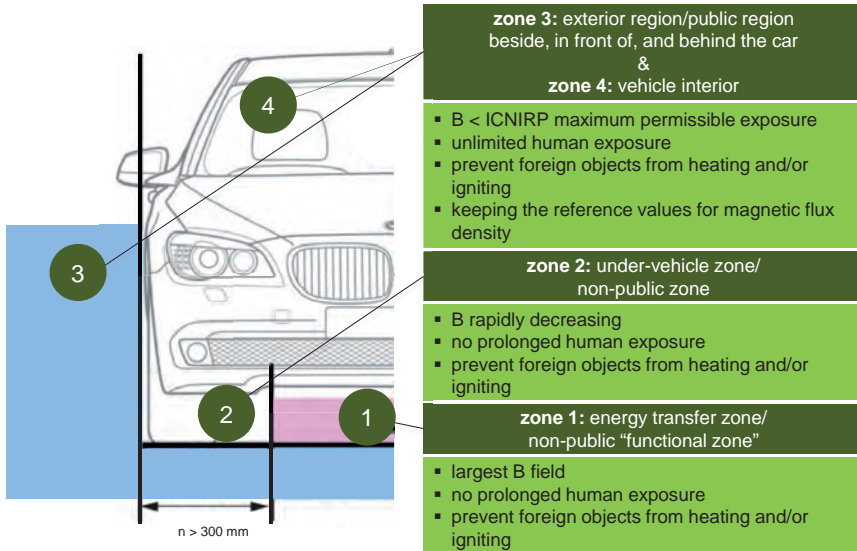


Fig. 6. Safety zones according to the application guideline VDE-AR-E 2122-4-2 [48].

The magnetic field has to comply with the international recommended limits in zones that are easily accessible to humans in and around vehicles that are charged contactlessly. This pertains to the interior or the rocker panels at the lower edges of the car, located at least 300 mm from the CPT system. Especially in a garage with little space between vehicle and garage wall, it is important that the magnetic field outside the footprint of the car does not exceed field leakage limits [47] [49]. It is therefore clear that operating CPT systems should have appropriate safety features that detect or generally prevent the presence of humans or animals in the high-field zone (Fig. 6, zone 1 and 2) between the coils underneath a vehicle like sensors [50], Animal Deterrent Devices (ADDs) [51], and/or other special protection/cover devices [52] [53].

Moreover, industrial applications are too heavy and too big with large aluminum housing blocks (see Fig. 5). In contrast, automotive pads should be as thin and light-weight as possible to minimize overall vehicle energy consumption [54]. The specific power densi-

ties of diverse CPT systems are shown in Fig. 7 with the target values for automotive EV CPT systems.

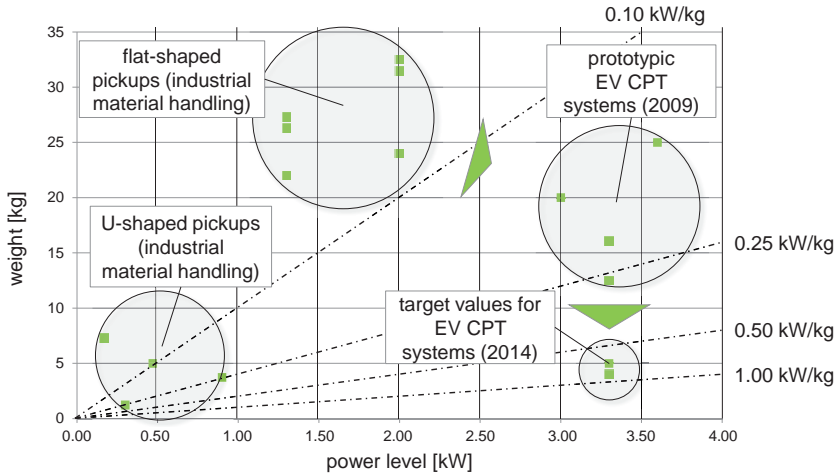


Fig. 7. Specific power densities of different CPT systems.

For low-power applications of 3.3-3.7 kW, circular CPT receiver pads featured in research projects around 2009 had dimensions of $\sim 1 \text{ m}^2$ and a weight of more than 20 kg (0.185 kW/kg) [55] [56]. The receiver pads of the next generation already had physical dimensions below 0.25 m^2 and a weight of $\sim 15 \text{ kg}$ (incl. on-vehicle rectifier) (0.25 kW/kg) [57]. Recent systems have dimensions of 0.126 m^2 to 0.0625 m^2 and a weight of $\sim 5 \text{ kg}$ (0.74 kW/kg) [58]. Bombardier recently published a 7.2 kW CPT system (max $P_{\text{out}}=6.6 \text{ kW}$) with a total on-board weight of $<6 \text{ kg}$ (1.1 kW/kg) [34]. Such smaller pad sizes, however, cause other concerns due to the flux-density. Further safety (temperature sensors, detection of objects, shielding, etc.) and heat dissipation measures have to be considered. In addition, such small systems may have limited interoperability with higher power levels and RPEV applications (see future viability of pad systems in chapter 4.2.1.3), and need large primary pad structures for an acceptable tolerance to misalignment.

This illustrates that research projects in the past few years have successfully demonstrated the feasibility of contactless charging for EVs with CPT systems that are by far more powerful, safer, more efficient, with an improved tolerance to misalignment, and are able to handle even larger variations in coupling [30]. Companies from different fields have been involved in these research projects. Based on the solid know-how that industrial material handling CPT applications have provided, companies like Conductix-

Wampfler [27] [56], SEW [59], and Vahle [55] [60] have adapted their contactless battery charging concepts to EVs in recent years. Aside from this, quite a few companies from other technological fields have also begun to develop EV CPT systems [34] [57] [58] [61]. Car manufacturers started supporting this technology in the past years. German and Japanese Original Equipment Manufacturers (OEMs), in particular, started to study wireless charging approaches and developed test vehicles with integrated CPT systems. Toyota, however, stands out as the pioneer of Plug-in Hybrid Electric Vehicles (PHEVs) with a consistent pursuit of (partial) electrification of the powertrain. Toyota took up CPT activities as early as the 90s in the field of industry automation [62], and already participated in developing and using a CPT solution with the closely coupled MagneCharge SAE J1773 inductive charging paddle standard in the late 1990s [63].

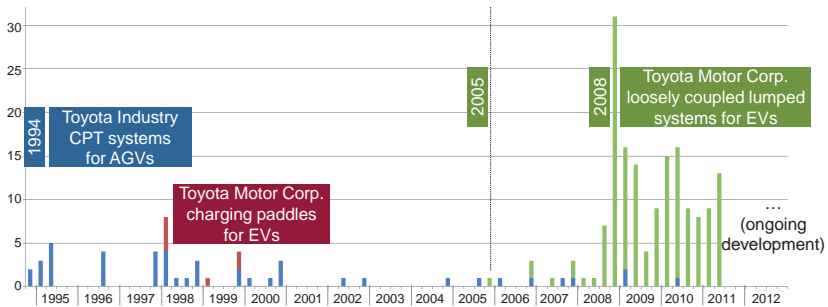


Fig. 8. Toyota's patent activities for CPT systems over the last 20 years.

Since 2005, after several years of a passively waiting, Toyota has once again shown significant patent activities for static and dynamic EV CPT charging concepts (see Fig. 8), especially in diverse positioning, battery management, and system integration concepts for CPT systems [14] [64], among others. Moreover, Toyota publicly announced various CPT activities and launched collaboration with Witricity [65]. In addition, it developed futuristic-looking vehicle concepts like the Fun Vii, which features CPT along with other analogies to mobile devices, like massive LED-screens around the entire exterior surface of the vehicle [66]. In summary, significant progress and continuous development of CPT systems is evident in the research projects of suppliers and OEMs in the past few years [55] [56] [61].

2.3.2 General advantages of CPT systems for EVs

It could be shown that in contrast to conductive charging solutions, CPT systems are safe, durable, and vandal-resistant with lower maintenance [67], as charging outlets of conductive solutions may become a safety hazard, especially when installed outdoors. Fig. 9 summarizes several problems with cables and plugs.

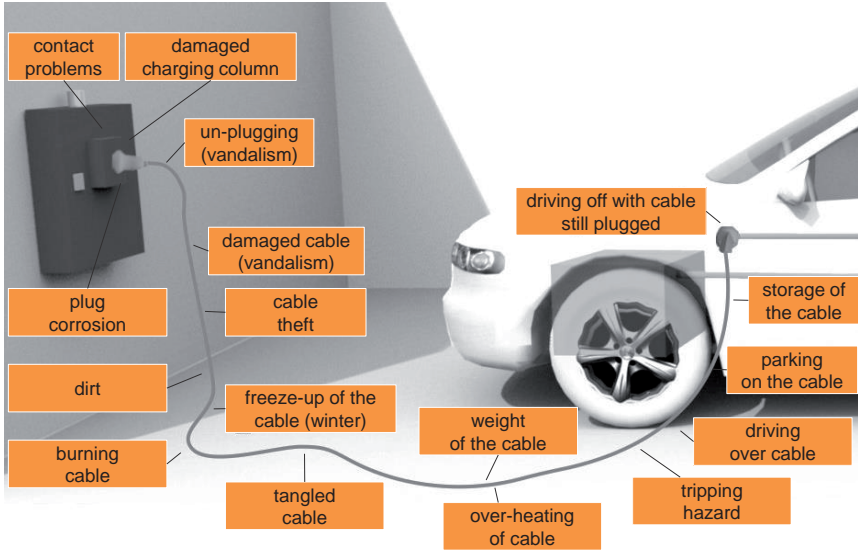


Fig. 9. Problems with conductive cable-based charging equipment for EVs (based on [68]).

CPT avoids problems like permanent degradation of contact surfaces, insulation, and cables, as well as general abrasion of the plastic plug casing due to mechanical and chemical stress (e.g. corrosion) [69]. One of the main benefits of contactless power transfer is that automatic contactless charging requires no handling and storage of dirty, wet, and heavy cables [67]. The constant and inconvenient plugging process is completely eliminated by simply positioning the vehicle secondary pad correctly over the primary infrastructure pad. Thus, user-friendliness and safety are especially strong and decisive advantages of automatic contactless charging systems. Beyond this, CPT solutions are also particularly attractive in public places. In recent years, roadways, sidewalks, and curbs have been cleared out in many downtown areas to facilitate maintenance, cleaning, and snow removal. Parking meters, for example, have been replaced by central parking machines, which can be placed at the peripheral area of the sidewalk. In this context, it will hardly raise acceptance amongst customers and authorities if there was a massive and ubiquitous intrusion in the form of EV charging columns and cables dangling along the sidewalks [70]. Therefore, contactless charging stations that are integrated into the environment almost invisibly can help build an adequate infrastructure network while still preserving aesthetic cityscapes [69] [71]. Another major benefit is that automated CPT charging technology improves battery charging management, especially considering that electro-chemical vehicle traction battery systems

largely determine overall vehicle characteristics. Even modern lithium-ion-batteries remain the main bottleneck of electric mobility today in terms of cost (up to 2,000 US\$/kWh with a long term goal of 100 US\$/kWh) [72], range, and weight (specific energy density of 130-200 Wh/kg versus 10,000 Wh/kg for petroleum) [72], charge rate limitations due to the electro-chemical processes in the battery (power density of 350-400 W/kg versus 2,000 W/kg for ultra-capacitors) [72], durability, and environmental costs associated with their production and final disposal. Consequently, most OEMs are also investing in PHEV and Range Extended Electric Vehicles (REEVs). With today's conventional plug-in hybrid vehicles, however, it is obvious that EV owners will not always use the cable to charge their batteries, as it is a major inconvenience. Instead of physically plugging-in at the end of every short journey, customers prefer to go to the next gas station to get fossil-fuel-based vehicle range, as they have the combustion engine on board, anyway. In contrast to contact-based charging, hands-free automatic CPT significantly facilitates charging. Such a process is truly opportunistic and can be repeated many times per day, after each trip, whenever the opportunity arises ("opportunity charging"), rather than irregular and longer charging operations [3] [41]. In consequence, charging is more likely and frequent, as customers can no longer forget to plug in [3] [45]. Especially vehicles that are set mainly to electrical driving-mode and therefore have larger battery systems, like REEVs (electrically driven vehicles with combustion engines for an extended range) and BEVs (purely battery-powered vehicles) benefit from automated, more convenient, and thus more frequent wireless charging. It reduces battery wear-out by minimizing the depth of battery discharge, which can extend battery life. Additionally, CPT increases the electrical driving range and driving-mode portion of hybrid vehicles, as batteries are more likely charged up [45] [73]. CPT can thus help reduce the range problem and lower cost with extended battery life or smaller, more frequently charged batteries [1] [69], all crucial aspects that enable OEMs to sell EVs at a larger scale and reduce Total Cost of Ownership (TCO) [4]. However, the monetary benefits of potential extended battery life and increased electrical driving-mode portion are restricted for PHEVs with only very small batteries. For them, the benefits of CPT are 'limited' to comfort and safety [45].

Moreover, easy access to regular and more frequent grid connection is also of specific importance to the power grid as such, as there is a clear trend towards "green" power and more renewable energy sources with little or no carbon footprint. It is impossible to accurately forecast the amount of power yielded by a supply mix of solar, wind, wave and tidal power, all of which are fluctuating in nature. Thus, grid frequency cannot be held as precise and stable as is the case with traditional central energy sources like nuclear power [3]. In this context, reducing peak load effects and stabilizing the grid frequency through controlled EV charging is very promising and can become a highly attractive business model in the future. In this concept, the car of the future becomes far more than just a transportation medium. With large-scale deployment, battery EVs could

form one gigantic electricity storage fleet and act as a controlled, widely dispersed load that automatically improves the stability of any supply network. At times of surging wind, a lot of wind power is added to the power system, increasing mains frequency [3]. However, wind turbines do not need to be shut off, as electric cars can charge up very cheaply with the surplus power in the system. Conversely, in situations with calm wind conditions and acute energy shortages, EV charging can be reduced [3] [6]. In theory, EVs could even feed power back into the grid to meet a temporary demand. In August 2009, Germany's pumped storage power plant capacity totaled approximately 6.7 GW. Assuming that the accessible power of a vehicle battery can peak at $P=20$ kW, 340,000 EV batteries together could essentially substitute Germany's entire pumped storage power plant capacity [69]. However, when considering a power flow back to the mains, the potential additional battery stress and extra electronics costs need to be justified. Moreover, [74] [75] claim that unidirectional power flow and demand control strategies can provide much of the same benefits with little more than a smart control algorithm. These approaches may reduce the amount of spinning reserve that governments need and could increase the wind power penetration without a significant increase in grid demand-supply balancing cost [3]. Such "energy services" would improve the quality of power supply from renewable sources if they could be reliably established. To achieve this, it would have to be guaranteed that numerous controllable EV batteries are connected to the power grid simultaneously to stabilize daily load curves and thus avoid peak loads in the grid. This endeavor would be greatly compromised if motorists do not keep their batteries well charged at all times. It can be assumed that drivers would not make a constant effort to manually plug and unplug at home, and certainly not in public unless it was absolutely necessary [69]. Automated CPT can mitigate this problem, as CPT leads to better, more regular grid connection and allows the battery to be more frequently available for grid services.

For validation, a load profile scenario has been developed in the scope of this thesis comparing stationary contactless versus contact-based charging with traffic data from the study "Mobility in Germany 2008" [76]⁷, as shown in Fig. 10. Two charging scenarios were considered, "charging after every trip" (blue curves) and "charging only after last trip" (green curves). One assumption is that the operator of a conductively charged vehicle only charges his/her vehicle with a State of Charge (SOC) of below 50% (assuming that the operator will handle the charging cable only if necessary). In the "charging after every trip" scenario (blue curves), charging and usage of grid power is widely distributed throughout the day, in contrast to the "green curves" that show a sharp peak in the evening hours. It can also be seen that without central power management, contactless charging may in theory even have a negative impact on the grid with slightly higher load peaks compared to conductive charging. This is due the fact that as CPT vehicles

⁷ $N=22,043$ vehicles, only passenger cars, $P=3.7$ kW, $\eta_{\text{conductive(AC-mains_to_DC-battery)}}=95\%$, $\eta_{\text{contactless(AC-mains_to_DC-battery)}}=90\%$, battery-capacity=25 kWh, weighted average energy consumption=0.174 kWh/km.

return home in this scenario, charging starts automatically regardless of the SOC⁸, while owners of conductively charged vehicles wait to plug in and charge until their car battery's SOC falls under 50%⁹. However, this last point has to be put into perspective: Contactless charging automatically leads to "charging after every trip" (blue curves - e.g. charging at home and attractive, convenient opportunities to charge during the day in front of shopping centers, at work, etc.) and thus helps distribute the power load in the grid, even without any central grid power management. With central grid power management, CPT can help further distribute the load profile and in consequence can become a key technology to reduce peak loads and thus promote the expansion of decentralized, fluctuating renewable energy sources such as wind or solar.

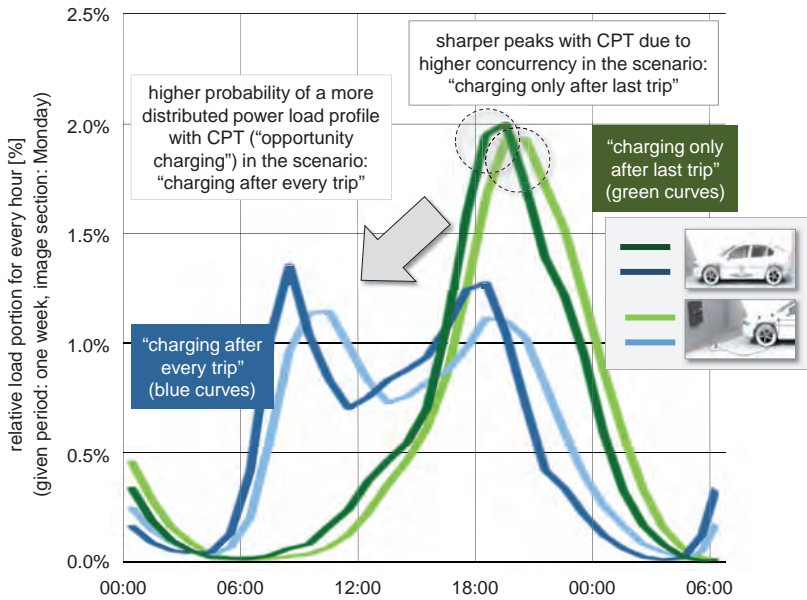


Fig. 10. Comparison of contactless and contact-based stationary charging strategies without central power grid management.

Beyond that, CPT opens up yet another possibility to further reduce on-board battery capacities. Since no cable connection is required, vehicles can even be powered while in motion [1] [3], and applications can be classified by speed in stationary, semi-dynamic, and dynamic CPT, as shown in Fig. 11. The energy transferred and collected by the EV thereby depends on the length of the powered road and vehicle speed.

⁸ Slightly higher concurrency, slightly narrower distribution of the load profile.

⁹ Slightly lower concurrency, slightly wider distribution of the load profile.





	stationary CPT	semi-dynamic CPT	dynamic CPT	
				
power rates	3.7-22 kW	3.7-22 kW	>20 kW	>20 kW
examples	home-based charging, work, shopping center	taxi ranks, traffic lights	along gas stations on motorways	separated charging lanes on motorways

Fig. 11. Classification of different fields of application for CPT-based EV systems.

Initial technology demonstrators have shown the feasibility of such Roadway Powered Electric Vehicles (RPEV). In theory, their vehicle range is unlimited, with significantly smaller or no batteries, and thus reduced vehicle cost and weight, lower maintenance, fewer safety concerns, and less vehicle down-time [3] [30] [68]. Delivering power directly to the motor of a driving vehicle rather than to the battery translates into further efficiency gains, as energy loss during transfer into and out of even modern battery packs can amount to 10%-20% [77]. In combination with business models that charge variable toll rates depending on the time of day and thus encourage electrified traffic during off-peak hours, RPEV could also significantly support the development of a smart energy grid [3]. Such electrified RPEV traffic is a substantial and flexible method to 'drain' energy from the grid when needed, and to thus compensate off-peak "energy valleys", which is of special interest in an economy that uses fluctuating renewable energy sources. Again, this goes to show the outstanding attractiveness of electrification of transport together with potentials and synergies of the energy grid.

2.4 Types of contactlessly powered transportation

With all the advantages and potentials described in chapter 2.3.2, CPT technology can help popularize EVs by making them quicker and easier to charge. CPT can thus turn out to be one of the key market drivers for a wide diversity of different electrified vehicle concepts and applications, as presented in the following.

2.4.1 Stationary contactlessly powered transportation

Motorized transportation consists mainly of private passenger cars. Their trips are usually not very long and the average car is parked most of the time, either at home or at work. The typical daily travel time for private cars in Germany is 32 minutes, with an average driving time of 21 minutes, an average driving distance of 15 km, and a majority

of private trips shorter than 40 km [76]¹⁰. For small cars with energy storage capacities of about 20 kWh that give it a range of about 150 km, power rates of 3.7 kW and charging times of about 5-6 hours overnight¹¹ are sufficient for normal commuter services. It is relatively easy to install stationary CPT infrastructures at parking spaces at home or at work. Therefore, the most promising initial target group for a market introduction would be vehicle owners who own a parking space or garage. This group represents 43% of vehicle owners in urban areas and 71% outside of urban areas [79]. However, as battery systems are still limited today, drivers with a long commute rely on range extender concepts or additional (semi-)public infrastructure. In order to increase the rate of electrical driving, commuters and users that park on the street and do not have a home garage at which to charge (57% inside urban areas, 29% outside urban areas [79]) need publicly accessible charging options. They are thus the main target clientele for public and semi-public charging options. The currently relatively low battery capacities of EVs resulting in limited range mean that charging is more frequent and more time-consuming than conventional refueling of vehicles with Internal Combustion Engine (ICE). Consequently, higher power levels of up to several dozen kW are on the table to shorten charging times (aside from DC conductive fast charging solutions, 22 kW CPT-systems of, for instance, a fast-chargeable 20 kWh battery within less than an hour)¹². The assumption is that these power levels are necessary for consumer acceptance of EVs, and to make them as attractive as vehicles with ICEs, even for longer distances. In addition, to guarantee high utilization of public charging spots and to make such a public infrastructure profitable within a short break-even period, it is vital that charging systems are inter-operable (see chapter 4.2.1.3).

Retro-fitting public spaces is more or less complicated depending on the kind of pavement surface (asphalt-paved, concrete, cobblestones), location (parking spaces, bus stations, roadway, etc.), and accessibility of connection lines to the grid peripherals. The main costs arise from the depth of the pit that is necessary in a sub-terrain environment with telephone cables and fibers, and also prescribed by guidelines like the German DIN 1998 that specify how power cables have to be installed in public areas [81]¹³. This becomes far more complex in dense inner-city areas. All systems also have to meet basic requirements, especially in terms of load profiles of all street-legal vehicles, including the impact of braking forces on road surfaces, or in terms of thermal profiles, as for example under severe weather conditions. As a solution, primary systems for stationary charging are usually integrated in public parking spaces in standardize-able underground systems [34] [59] [82] [83] [84], which makes parking spots easy to equip. The components are integrated in a modular way, safely protected, and installed invis-

¹⁰ In the U.S., the average driving distances are twice as long as they are in Europe [78].

¹¹ With CPT systems, as has already been successfully demonstrated, an efficiency of more than 90% from grid to battery is possible within certain operational constraints (see also chapter 4.1.1) [20].

¹² Tesla Motors, Inc., uses conductive 135 kW-fast-charging stations [80].

¹³ According to German DIN 1998, power cables in public areas have to be installed between 0.6-1.6 m below street level.

bly in the ground. The coil module (pad) usually lies in a metal frame as a cover on top of the cable pit. It is therefore easy to access components in the cable pit at any time by simply lifting the base pad. However, the coils have to be sufficiently protected from mechanical impacts. To make public charging points more durable, the primary-side charging module must be encased, for example with resin-bonded concrete types (polymer concrete) [83]. If needed, concrete or asphalt may also be laid over the pad, making it even more durable and vandal-resistant. If components are buried and not easily accessible for maintenance and inspection purposes, operational stability is key, especially since mechanical and thermal stresses due to frequent on/off cycles negatively affect the service life and reliability of the components. Moreover, drains need to be put in the shafts to avoid problems with incoming water, e.g. during rain storms, as already reported in [2]. Higher power levels require integrated cooling systems, which further complicates shaft systems [84].

Since such a public charging infrastructure is expensive and difficult to pre-determine, especially due to the variability of private traffic routes [45], it may increase profitability to focus on highly-frequented locations, which, on the other hand, may result in insufficient coverage of CPT charging stations throughout the city. The short range of the EV requires a dense network of charging points, far exceeding the density of today's conventional gas stations, at a variety of suitable (semi-)public areas like car parks, in front of shopping centers, at workplaces, and traffic lights [6]. In order to achieve overall user acceptance, any user who wants to charge his/her car must be able to quickly find a free charging point nearby. This need for widespread availability makes it even harder to establish a profitable business with a public stationary CPT system, as a large number of available charging stations spreads both demand and profit over a larger number of competitors.

The idea of electrifying car sharing makes the problem of a large number of widespread public charging stations even more obvious. Car sharing concepts in general, and particularly with EVs, have come back as an attractive business field in the past few years, as more and more EVs are available on the market [32] [84]. There are two fundamentally different concepts for 24-hour car sharing services. The first concept has customers return the shared vehicles to pre-defined locations. The second concept, which is called free-floating, allows customers to park the shared vehicle in any parking space in the city [7]. The current free-floating concept discourages the use of BEVs in car sharing, as it would require not only charging capabilities at the car sharing stations, but also a widespread public charging infrastructure. Nevertheless, CPT technology offers major advantages to car sharing companies that still are willing to embark on BEV/PHEV concepts: It reduces maintenance costs and simplifies charging for customers and employees who are in charge of keeping the fleet fully charged (see also advantages in chapter 2.3.2) [70]. In 1997, the Praxitele project in Saint-Quentin-en-Yvelines near Paris used

EVs with contactless charging for car sharing. The project showed promising results, but was finally terminated due to a lack of public funding and the persisting high cost of EVs [43] [85].

Aside from passenger cars, CPT is also an attractive technology for other vehicle concepts, e.g. for catenary-free electric buses. Vehicles make short stops, charge enough power to continue along their route, and can thus stay in circulation all day long [4]. Moreover, CPT is a key lever to make electric buses a commercial alternative to today's Diesel-fueled buses in public transport, or at least to increase the electric driving portions of contactlessly charged hybrid buses. In addition, catenary-free solutions help preserve aesthetic historic cityscapes. The increasing number of CPT bus projects confirms the attractiveness of this field of CPT application in local public transit [2] [27] [34] [86].

2.4.2 Semi-dynamic contactlessly powered transportation

As a further step to future scenarios with RPEVs, semi-dynamic charging is particularly suited at traffic lights or slow-driving road sections in urban environments [3] [5] [87] [88]. This is of special interest in fields of application where conductive plug-in systems are impracticable because vehicles have to be charged very frequently, due to their daily driving ranges. Such automatic semi-dynamic CPT is particularly attractive for taxis with their long and predictable idle times at taxi stands, moving slowly from one position to the next while waiting for customers [12]. Charging can be activated at each single primary pad underneath the road surface of the taxi stand as soon as the receiving pads of the taxis are roughly aligned with each pad below. In addition, the CPT infrastructure at the taxi stands can also directly supply auxiliaries such as air conditioning. This keeps drivers comfortable as they wait for customers in extreme warm/cold weather conditions, at no cost to range or battery life, because grid power is used rather than discharging the batteries. Moreover, the high turnover of waiting taxis and permanent movement of vehicles at the taxi stand prevents the problem of blocking charging spots with vehicles that are already fully charged. An average taxi driver with a 12-hour shift is driving for 3.5 hours (29.2%), and waiting at the taxi stand for customers 70.8% of the time. The majority of taxi trips are under ten kilometers. However, the travel profile of taxis is very heterogeneous. Special events like international trade shows or weather cancellations in air and/or rail transport cause a peak in demand and thus a need for longer range. Days with more frequent and/or longer taxi rides are economically beneficial for taxi drivers, and vital for the one-man taxi businesses that are typical in Germany [7]. Taxi drivers are therefore particularly dependent on long range, available at any time. This still is a problem with BEV, which makes taxis with range extenders more attractive, but also more expensive. In summary, CPT systems make sense for taxi companies with a larger fleet. They make good pilot projects to test CPT in public, as it is relatively cheap, in absolute terms, to install CPT at the rather few clearly defined taxi

stands in a given city. CPT taxis may be particularly promising in larger metropolitan areas that are burdened with heavy traffic and high pollution, as a single taxi covers the transport needs of numerous people per day and runs a much higher mileage than a private car over the course of its product life, making it the optimal and most eco-friendly way to use a car.

Another example for operating a semi-dynamic CPT infrastructure is the vision of charging EVs statically or slow-dynamically at highly frequented traffic sections in urban areas where great numbers of vehicles are stopping or slowly passing an infrastructure, like during idle times at traffic lights [5] [12], main and arterial roads, etc. (city-wide CPT network). Vehicles can be charged on an actively used public roadway and do not need to be driven to specific charging spots. However, such an infrastructure would essentially have to be installed instantaneously in order to convince potential user groups like commuters and street parkers to buy BEVs, as they would require a high number of CPT-equipped traffic lights to cover their energy needs in all possible traffic situations. In addition, one must recognize the challenge presented to CPT systems at a semi-dynamic charging infrastructure: as vehicles pass an intersection, the time period they are exposed to the CPT system is short, and the amount of transferred energy small. Even assuming optimistic electricity prices and margins and a large number of CPT-vehicles on the roads, investments do not repay within a reasonable time period by electricity sales alone. This shows the importance of innovative future mobility services that provide sufficient range [km], and do not rely only exclusively on selling energy [kWh]. The necessary higher power levels also have to be seen in the context of battery life. Depending on the battery type, high-charging currents may have a strong detrimental effect on the number of charging cycles and battery life [5].

Aside from technical and economic problems, CPT presents additional difficulties as it encourages traffic behaviors that are in conflict with transport authorities' idea of optimal traffic flow. For example, drivers might obstruct traffic by slowing down over charging segments, or even cause accidents by sharply braking for a yellow light to catch some power from the CPT system. It will be necessary to adapt traffic rules to prevent such problems. In summary, city-wide networks with contactless traffic lights do not appear to be economical in an urban environment without massive government subsidies. As high installation and maintenance costs make public CPT energy more expensive than energy from a home- or office-based infrastructure, it may not even be used much by BEV drivers, who most likely already have access to charging at work or at home.

2.4.3 Dynamic contactlessly powered transportation

Purely-battery electric vehicles that are currently available have to sell themselves to users despite the major inconvenience that they carry all of their energy in the form of expensive, low-range, slowly charged and short-lived batteries. Consequently, the next

market step up from semi-dynamic could be powering vehicles 'on the move', even at higher speeds. While stationary contactless charging eliminates the need for the charging cable, on-demand dynamic charging reduces or even eliminates dependence on the battery. Keeping the energy in the grid, reducing battery size, which leads to cheaper and lighter vehicles with unlimited range is a promising approach.

Academic interest in RPEV picked up as early as the late 1970s when BOLGER, ROSS, and others began publishing papers on electric highway systems [89] [90]. The first major project was then coordinated by the 'Partner for Advanced Transit and Highways' (PATH) project, led by researchers of the University of California, Berkeley [2] [42]. This project to develop roadway-powered CPT vehicles like buses and passenger cars (see Fig. 12) was active through the 1980s and 1990s [30] [91].



Fig. 12. Roadway-powered electric bus and roadway track system of the PATH project, California [2].

The main vision of the project was nothing less than reduce pollution in the Los Angeles Bay area with a substantial transition of traffic to RPEVs. Business studies accompanying the PATH project showed that life-cycle costs of RPEV travel was similar to gasoline vehicles [2]. Although the business studies were promising and the major technical project goals were met, the roadway electrification part of the PATH project was terminated in the mid-90s. Even after several years of development, intensive tests, and many improvements in infrastructure, costs were still higher than anticipated. Moreover, achieved efficiency rates (~65%) and air gaps (7.5 cm) were limited due to conductor materials and power electronics available at that time [2] [30] [41] [42]. However, the promise of freeing EVs from expensive and heavy batteries through contactlessly powered roadway systems with transmitting coils embedded in roadways remains so inspiring that dynamic charging has recently begun to receive renewed attention. Even "na-

tion-wide electrified roadway networks" as an intense modification of the conventional highway infrastructure are once again subject of extensive discussion. Similar to the PATH business studies [1] [2], BROOKER et al. [92] show that hypothetically, the only type of EV that can hope to compete with a conventional vehicle for cost of ownership from a customer perspective is the (hybrid)-RPEV with smaller batteries, picking up electrical energy from the roadway in-motion. In this context, it is important to note that the final infrastructure for such a dynamic charging system could be relatively small, as highways make up only a small percentage of installed roadway miles, yet carry a significant percentage of overall vehicle miles. In the U.S., for instance, 1% of roadway miles carry 22% of all vehicle mileage [1] [87] [93]. However, as the PATH project showed, it is quite a complex undertaking to put a public dynamic roadway infrastructure into the ground [2]. High voltage levels, especially, may cause issues. Installation and maintenance costs for such systems have to be reduced by newly developed roadway construction methods like new track laying technologies and machines [94]. Highly automated roadway construction is especially important, as recent research results of the Belgium Flanders' DRIVE project "inductive charging" show performance deviations due to roadwork tolerances of cables that are laid in the ground manually [95].

However, it is hardly possible today to come up with a business model and win stakeholders for a nation-wide electrified roadway network with public dynamic charging for private passenger cars, because everything, infrastructure and vehicles, would have to be built up from scratch. Any consideration of such an infrastructure depends on the utilization rate of CPT EVs, which is simply not high enough in early stages of market development. A massive and costly intervention in and replacement of the existing infrastructure, with widespread use of contactless charging for passenger cars, requires long-term government initiatives and the cooperation of all stakeholders to ensure industry will be able to implement viable business models. The approach of RPEV could be compared to business models in the mobile phone industry. In the case of RPEVs drivers will pay for the mobility service [range in km] in form of road tolls based on distance or time. These billing methods will also be vital to finance construction and maintenance of a RPEV infrastructure network, as revenues from sales and taxes on fossil fuels decline. However, as such an installation is expensive, smaller step-by-step installation scenarios are also being discussed. For a market introduction, the systems could be implemented on dedicated lanes of major arterial roads e.g. on busy long-haul routes between major cities like Hamburg-Berlin, Shenzhen-Hong Kong, or Los Angeles-San Francisco. Another example for successive installation is the option of "high-power electrified roadway segments" along highways to charge up vehicles for routes ahead that have no charging infrastructure. Users thus do not have to stop for charging. However, the vehicle must drive as slowly as possible to maximize the amount of transferred energy. To avoid impeding traffic flow, the infrastructure should not be installed directly on the highway lanes, but on a short section parallel to the highway, for example

next to a gas station (see Fig. 11) or along a steep uphill section. This way, like the branches of a tree, the technology could spread out to more roads and grow into a tightly-knit RPEV infrastructure.

Compared to RPEVs, stationary high-power CPT systems along highways (as Tesla Motors, Inc. is already implementing with conductive 135 kW-fast-charging stations [80]) are also expensive and still require a wait time until the vehicle is charged up. Yet, for the next few decades, they seem more promising than the idealistic vision of a dynamic, nation-wide CPT infrastructure for passenger cars.

Different scenarios and strategies have been elaborated to promote the topic of RPEVs for passenger cars nonetheless. One very promising approach is motor sports, especially since power transfer will play a major role in the strategy and tactics of electrified motor sports in the future, similar to today's tire changes during pit stops. Moreover, CPT could bring a boost to electrified motor sports, as CPT tracks could even be embedded in the race tracks, enabling race cars to power up as they pass over designated portions of the course. In September 2013, the company Qualcomm HalolPT announced a multi-year agreement with Formula E Holdings (FEH) to become an official founding technology partner of the FIA Formula E Championship. CPT charging in the pits was subsequently included in the preliminary status of the FIA Formula E Championship Technical Regulations at the end of 2013 [96]. In 2014/2015, CPT systems will be fitted into the safety cars to familiarize people with it, and from 2015/2016, CPT will be installed in the race cars. CPT systems will then be installed in the pits to simplify charging and to improve safety by removing loose cables and exposed connectors. In a next step, the race cars will also be able to charge while slowly moving along the lane to a pit stop or back onto the race track. Finally, in the battle for ever better times, the long-term goal is to equip the race track itself with CPT segments for dynamic charging. When battery power decreases, drivers could head their vehicles for specially equipped dynamic CPT segments on the route to get additional power. This offers exciting new possibilities for future racing strategies with a reduced or even eliminated need to stop the cars for recharging during a motor race. The main benefit of pioneering CPT in the domain of motor racing will most likely be the experience gained and thereby possible technology transfer from racing cars to series-production vehicles, as was the case for many automotive technologies that are taken for granted today. Motorsport applications will rapidly drive development, pushing mechanical and materials development, resulting in safer, lighter, more efficient, and more reliable systems. Events like the Formula E are also educating the public about the attractiveness of EVs, planting the notion that EVs can charge continuously and hassle-free around a track in the public mind [4] [97]. As described in a market research study with *puls* Marktforschung GmbH [7], such

RPEV demonstration projects with high public visibility may help significantly increase buying interest in electric vehicles¹⁴.

In the past few years, other challenging vehicle concepts like electrified roadway networks for long-haul trucks were also considered alternatively to passenger cars [33] [92] [98] [99]. So far, the necessity of heavy and expensive batteries forbade the electrification of long-distance heavy-truck freight transport. The large power demand cannot be met, especially as most of heavy-truck traffic takes place on highways at higher speed. The batteries would have been so heavy that they would have left almost no carrying capacity. Therefore, trucks on long-distance trips need to be powered in-motion directly while driving on the highway. Continuous power transfer to trucks in-motion would mean significantly smaller and lighter batteries, enabling total or at least partial electrification of long-distance heavy-truck traffic. The right lanes of highways would need to be electrified to power trucks in-motion, especially on steep uphill slopes that require large amounts of power. In contrast to EV passenger cars, where a power input of 10-30 kW on electrified roadways is sufficient [89] [93], a fully loaded truck (40 tons) needs much more power to pass an uphill highway section. If highways were equipped with CPT segments, CPT hybrid heavy-duty trucks (for highway sections without CPT systems) would be able to drive up steep highway sections on electric power only. Additionally, stationary power transfer points at parking lots along the highways could be used to charge batteries during mandatory rest periods. To address this topic, several test tracks with different technology approaches have recently been set up at different research locations [33] [98] [100] (see Fig. 13).




contactless power transfer	contact-based power transfer	
contactlessly powered coil systems	power rail	catenary system
ground-based system		overhead-wire-based system
source: Bombardier	source: Volvo/Alstom	source: Siemens AG
		
test track: Mannheim, Germany	test track: Volvo testing facility Hålleröd/Gothenburg, Sweden	test track: Uckermark, Germany

Fig. 13. Comparison of alternative power transfer solutions for electrified trucks.

¹⁴ In the *puls* Marktforschung research study [7] with N=1,001 participants, buying interest increased from 44% up to 59% with the option of charging vehicles in-motion.

Aside from CPT systems, another RPEV technology is Scania's cooperation with Siemens that proposes electric truck traffic on roads with overhead contact lines [33] [100]. However, depending on external conditions at the locations in question, ground-based systems like contactless electrified roads [33] or power-rail systems [98] are more flexible and have multi-use capabilities for various types of other, including smaller vehicles. A greater number of potential users to help pay back the large investment in the road network as well as the preservation of aesthetic landscapes speak for ground-based systems like CPT and power rails. A project example for the electrification of heavy traffic with ground-based systems is the research program "Swedish Electric Roads" of the Swedish Energy Agency (SEA) in collaboration with Scania, Volvo, Bombardier, Alstom, and other companies within the transport industry [33] [101]. These technologies show quite some potential, even for the very challenging and visionary application of nationwide electrified roadway networks with long-distance haulage. The ongoing research projects in Sweden and Germany will help to derive installation and maintenance costs for such solutions. Thereby, even with significant roadway construction, electrified heavy traffic could be quite economically profitable in the future in the face of rising fuel prices and in the context of promoting a smart-energy grid that relies on renewable resources, as discussed in chapter 2.3.2 [3].

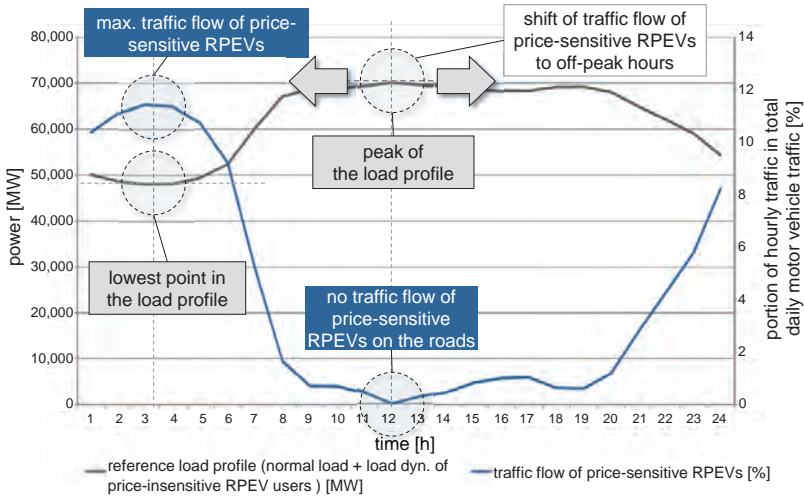


Fig. 14. Sample load profile with normal RPEVs (gray curve) and proportion of shifted price-sensitive RPEVs in the course of one day (blue curve).¹⁵

¹⁵ Based on traffic data from the study "Mobility in Germany 2008" [76], the proportions of price-sensitive RPEVs that adapt their mobility behavior in this scenario are: 10% of passenger cars, 40% of light commercial vehicles (as they have big cost pressure, but are largely tied to a daily business rhythm), 70% of heavy commercial vehicles (as they are most price-sensitive, having the biggest cost pressure).

Shifting electric truck traffic to off-peak hours with the help of time-based toll-rates might become a very attractive business model in a context of fluctuating renewable energy sources, especially wind power. The very significant power demand of electric heavy-truck traffic could serve as a substantial and flexible energy sink, filling off-peak “energy valleys”, as shown in Fig. 14. This is of special interest as the majority of Germany’s freight transport, 72% in the year 2006, consists of heavy trucks with a permissible maximum weight of 40 tons [102]. Making electrified heavy trucks economically viable has enormous potential both for the national economy in terms of job creation and for environmental protection, as it would lead to a massive reduction of concentrated carbon dioxide emissions [100].

With promising results and higher power rates in the research projects for CPT-powered trucks [33] [98], CPT technology is also being considered for vehicle types like high-speed trains [86] [103]. Today’s catenary systems limit train speed to less than 300 km/h because pantographs are subject significant wear-out (in particular at low temperatures with ice on the overhead wires), cause noise pollution and present substantial aerodynamic resistance at increasing speeds [103]. Contactless transmission can free the train of this encumbrance, allowing it to reach faster speeds and reducing life-cycle costs of the overall system. Another major advantage is that the primary coil segments can be integrated into pre-fabricated ballasted track and slab track systems between the rails in a very compact way. Since this eliminates the need for overhead lines, tunnel diameters can be smaller, which significantly lowers construction costs [103].

The examples for RPEV fields of application and the promising results of the research projects show the potentials for CPT-based transportation in the future. However, it also becomes obvious how difficult it is to derive reliable final statements on the practicability of RPEVs, since scenarios are highly complex with a variety of possible influential parameters, hardly predictable infrastructure costs¹⁶, and difficult-to-determine system boundaries. This is especially the case with complex, non-predictable driving behaviors of individual passenger cars, and extreme scenarios that have to be addressed in such traffic-models [2]. Ongoing research projects help gain more and more knowledge and verified parameters from a technical and economic point of view. It is thus reasonable to start with smaller, fleet-operated CPT system applications with clearly defined system boundaries in the first phases of market development. Even these, however, may become very complex in verification as many parameters have yet to be factored in. Therefore, the following chapter will present a developed planning approach (called ETEV|SIM – Energy Transfer for Electric Vehicles Simulation) to evaluate CPT-based fields of application, based on event-discrete simulation software to solve complex CPT infrastructure allocation problems.

¹⁶ The predicted costs for the infrastructure vary from ~€0.3 M/lane/km [45] to ~€1.25 M/lane/km [92].

3 Simulation-Based Modeling and Optimizing of CPT Infrastructure (ETEV|SIM)

There is a variety of possible attractive fields of application for a step-by-step market introduction of CPT systems. In spite of all the advantages and several successful initial projects [34] [86], the use of CPT systems for EVs still presents a number of uncertainties for a variety of potential applications, especially in terms of system stability and achievable vehicle range - factors that are still significantly impeding acceptance and spread of CPT systems [7]. This is even more critical in fast evolving environments (e.g. expansion of logistics and warehouse space in the context of company growth) as the initial system set-up of the expensive charging equipment, number of vehicles, power levels, etc. may have to be upgraded. To avoid planning errors and costly subsequent changes, infrastructure will have to be planned very carefully with continuous adaptation to demand [104]. At this time, there are no clear and user-friendly planning and decision-support tools for evaluating the technical and economic attractiveness of contactless power transfer to electric vehicles in different fields of application. In this context, this chapter presents a new model-theoretical planning approach (ETEV|SIM) that can solve even complex CPT infrastructure allocation problems by adapting discrete event simulation tools, which are usually known for planning extensive production processes and logistics operations.

3.1 Planning tools for CPT infrastructure allocation problems

CPT tools for infrastructure allocation problems need to map out all interconnections and interactions between different activities in their temporal context so that the complexity of the decision-making problems can be handled adequately in the model [104]. In this context, the initial state of the system and input variables have to be transferred into output variables to evaluate the system stability, depending on the events within the simulation (e.g. number of charging operations).

To implement CPT systems and to solve the planning conflict between infrastructure investment and battery costs, a tool as simple as a spreadsheet calculation can deliver a rough estimate of their feasibility. On the one hand, these tools are characterized by a fast learning curve, and can be expanded with visual basic for applications (VBA) for more extensive calculations and data analysis. On the other hand, they are by no means a detailed planning approach for more complex traffic scenarios. They do not offer sufficient simulative capabilities, which are necessary for a detailed evaluation of CPT infrastructure scenarios. In addition, they cannot illustrate complex systems behavior and interactions with vehicles. For the present task, these tools are only useful for calculating applications with low complexity and/or a high level of abstraction.

Traffic simulation software tools like VISSIM (Verkehr In Städten - SimulationsModell)¹⁷ and SUMO (Simulation of Urban Mobility)¹⁸ provide another alternative for simulating CPT infrastructure designs. The traffic simulation software VISSIM is basically used to model and analyze complex situations like traffic congestion, and to optimize traffic routing in inner cities. It supports integration of public transport, cyclists, and pedestrians [105]. The open-source simulation package SUMO is particularly suitable to represent large-scale traffic scenarios. With SUMO, entire cities can be displayed in a time-lapse view with up to 100,000-200,000 individual vehicle movements [106] [107]. Therefore, VISSIM and SUMO make it possible to model and simulate traffic in urban road networks as well as on highways, and to thus develop, apply, and/or optimize new traffic-control strategies, e.g. to prevent traffic congestion [106]. This is specifically important as ever-increasing urbanization and motorization comes with major traffic disruptions. Both programs have been successfully used in numerous infrastructure projects and generate realistic results and it is generally possible to simulate CPT-based traffic with these software tools [108]. However, VISSIM and SUMO are only partly useful to simulate and subsequently determine an optimally designed CPT infrastructure. Extensive data about traffic volumes and an enormous amount of work are required in order to generate the driving profiles of the virtual vehicles in a CPT simulation. Moreover, the output parameters are primarily designed to collect data on average speed between stops and traffic volumes. Thus, if the goal is to model detailed and precise traffic scenarios that take into account the existing infrastructure, like expected wait times (e.g. boarding and exiting passengers, or delays caused by backed-up traffic), known wait times (such as the rhythm of light-signal systems or public transportation schedules), and traffic rules (e.g. driving behavior, restrictions, joint use of charging stations by private and public drivers) the tools are capable and useful for public traffic scenarios [108]. On the other hand, it makes the tools complex and unsuitable to easily determine the optimal design of different CPT infrastructures with desired output parameters system stability and achievable vehicle range (especially as not only public transportation but also logistics scenarios are possible applications for CPT systems).

To address these barriers, a new approach has been developed in the scope of this thesis to economically allocate CPT infrastructures with the appropriate power transfer rates and vehicle battery capacities, in theory suitable for all possible CPT fields of application. Therefore, the discrete-event simulation software *Plant Simulation* by Tecnomatix, which is already successfully used in the planning of complex production lines and logistics operations, was adapted to the field of electrical logistics transportation and expanded with the necessary parameters and traffic flow information (Fig. 15) [109]. This makes it possible to visualize, simulate, analyze, and finally optimize individual scenarios with potential users, providing a solid decision-making basis for substantiated

¹⁷ <http://vision-traffic.ptvgroup.com/de/produkte/ptv-vissim/>

¹⁸ <http://sumo-sim.org/>

technical and economic feasibility studies. The powerful simulator with open-system architecture enables the creation of individual, customized attributes with good graphic display options. In addition, *Plant Simulation* has capable analysis tools and a simple easy-to-use interface. As shown in Fig. 15, this approach allows to select pre-defined modules individually and to modify them as needed for CPT operations. This facilitates the study of CPT traffic scenarios in many different possible combinations and experimental set-ups. The basic components of a simulation model are traffic networks, methods (vehicle control strategies), routes (modeling of transport routes), static elements (e.g. charging stations), and mobile elements (passive elements such as goods/payloads that are to be handled and active elements such as vehicles).

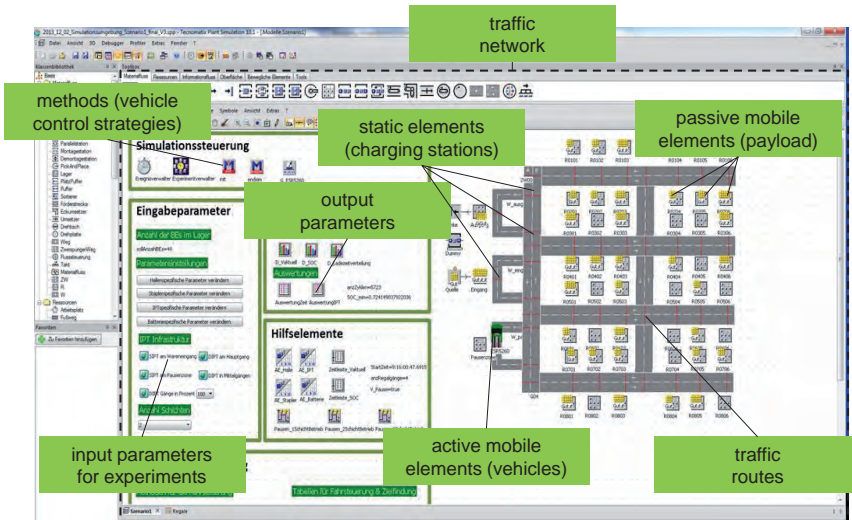


Fig. 15. *Plant Simulation* software to calculate CPT traffic scenarios, here showing warehouse logistics with reach trucks.

However, *Plant Simulation* has not yet been used to simulate charging infrastructures of electrical mobility concepts. As with any simulation tool, the initial simulation of new infrastructure requires some time for programming and implementing the necessary networks, methods, etc. Each application thus usually requires its own modules and networks, since, for example, the driving/travelling routes of public transport differ from that of harbor logistics. Nevertheless, the model of one field of application, e.g. intra-logistics vehicles, can inform a model for similar fields of application with similar system behavior and traveling routes, e.g. harbor logistics. The more fields of application are simulated, the higher the probability that existing modules and networks can be re-worked to suit new applications. Thus, the modules of a new simulation model will require only slight

adaptions and less time to program. *Plant Simulation* also presents limitations that have to be considered, for example the fact that the software can neither simulate very large traffic networks with a huge number of mobile elements (see SUMO) nor detailed interactions of a large number of participants in an open transport system. Tab. 2 summarizes the obstacles and potentials that arise from using *Plant Simulation* for a CPT simulation.

Tab. 2. *Suitability of Plant Simulation for the simulation of a CPT infrastructure.*

potentials for the simulation of a CPT infrastructure	obstacles to the simulation of a CPT infrastructure
<ul style="list-style-type: none"> ▪ customer-defined attributes ▪ powerful simulator ▪ requires only simplified traffic flow network ▪ comes with comprehensive analysis tools ▪ allows modeling of complex drive controls ▪ object-oriented, hierarchical models ▪ open-system architecture ▪ designed to run simulations with alternative experimental setups ▪ simple interface ▪ comes with standard vehicle objects available (from logistics operations) 	<ul style="list-style-type: none"> ▪ no professional traffic simulator ▪ no applications yet in the simulation of traffic infrastructure ▪ average training time ▪ performance boundaries with very large number of mobile objects/vehicles ▪ interactivity of the mobile objects/vehicles is limited

In summary, depending on the specific traffic scenario and field of application, different possible simulation approaches have to be considered in order to keep the planning effort appropriate to the task at hand. This will depend on the main parameters of traffic routing and operating range. The different fields of application for CPT systems can thus be classified and summarized, as shown in Fig. 16.

For a simple traffic scenario with small operating ranges and deterministic, pre-defined travelling routes, simple spreadsheet tools appear sufficient for a rough evaluation of a CPT infrastructure. With less defined system boundaries, complex interactions of vehicles in intense traffic situations (traffic jams, traffic control strategies, less-predictable driving behavior, etc.) and varying options of complex traffic routing in large transit networks complex traffic simulation approaches like SUMO may be appropriate, as described by [108]. For traffic scenarios whose system boundaries are at least locally clearly defined (e.g. around planned charging stations), the idea of adapting *Plant Simulation* production and logistics planning software to efficiently evaluate CPT infrastructure allocation is promising. This becomes even more obvious when considering that

allocation problems with many input variables and complex correlations can be seen as a subtask of production and logistics planning, anyway [104].

		operating range of the vehicles			increasing planning complexity ↓
		small operating range trips with stops in-between (<5 km radius)	medium operating range - trips with fewer stops in-between (5-50 km radius)	large operating range trips with almost no stops in-between (>50 km radius)	
traffic routing	pre-defined fixed routes	leisure park routes/trolley trams/ AGV intra-logistics with fixed routes	local public transit	fixed long-distance heavy truck routes, trains	
	occasionally varying routes	AGV intra-logistics with from time-to-time varying routes	commuter, city logistics	special delivery long-distance freight operations	
	always on different routes	intra logistics (forklift, reach truck), AGV harbor logistics/ airport logistics	city traffic, car-sharing, taxis	business representatives, vacation trip	
increasing planning complexity →					

Fig. 16. Classification of fields of application for fleet-operated vehicles using CPT systems.

3.2 Simulation approach to determine an optimized CPT infrastructure design

The Plant Simulation-based planning approach is shown in Fig. 17. First, to fulfill the functional requirements of a CPT simulation, diverse technical input and output factors have to be determined depending on the individual traffic scenario. The input values, for example, vary with the consumption models of different vehicles and depend on parameters like rolling resistance etc. ($input_{vehicle}$). In the case of REEV, for instance, an internal combustion engine powering an electric generator must be added into the simulation model. The power sink of the simulation model is furthermore defined by vehicle motion profiles (drive cycle parameters with speed and acceleration profiles etc.) ($input_{routes}$) and energy prices. Using *Plant Simulation*, a simplified traffic flow network can be modeled in order to simulate vehicle behavior. To ensure that vehicle behavior is realistically represented, the deviation of vehicle parameters compared to real-life vehicle behavior (e.g. parameters collected by data loggers) must be verified. Therefore, small test networks have been implemented.

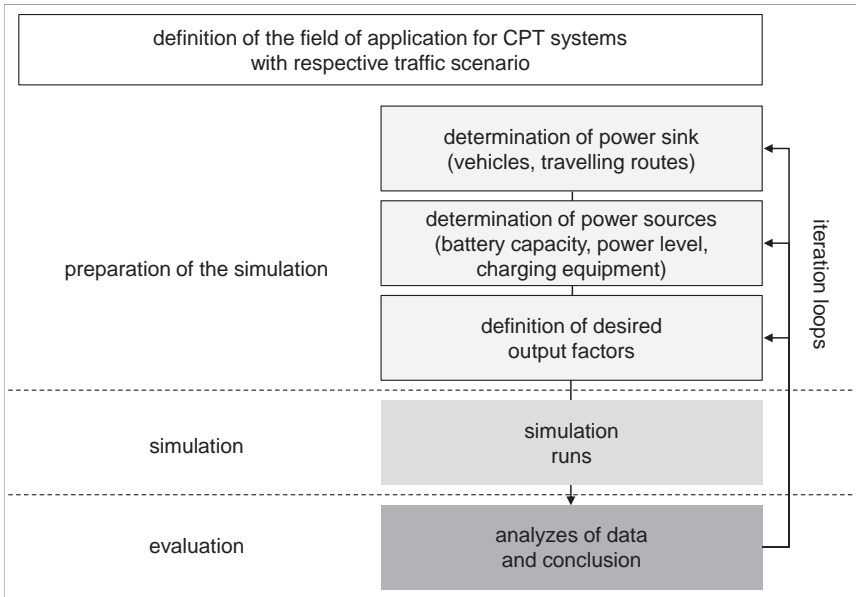


Fig. 17. Plant Simulation-based planning approach for a CPT-based infrastructure.

Fig. 18 shows a sample testing environment created with *Plant Simulation* for the scenario of a reach truck carrying out the VDI 2198 consumption test for material handling equipment (reproducible driving and lifting cycle with a payload of 2,000 kg)¹⁹ [110]. In this example, energy consumption in the simulation model deviates from real consumption values of the respective reach truck only slightly (~1%). Similar tests can be conducted with *Plant Simulation* for other scenarios with given consumption data for the vehicles that are to be analyzed (see chapter 3.3).

In addition to this basic input data for the power sink in a traffic scenario (ideally verified with such testing environments as described above), the input data of the power source has to be determined, as well. The input factors for the power source are mainly the allocation and total length of the installed power transfer segments along the vehicles' travelling routes [m], its power transfer rate [kW] [111], and the required vehicle battery size [kWh]. Thus, the goal of the optimization is to determine the trade-off between infrastructure investment ([m] and [kW]) and storage capacities ([kWh]) in a way that meets range requirements for stable system behavior at the lowest possible cost.

¹⁹ The load height while driving is 0.5 meters above ground level. The forward travel speed is 3.3 m/s. For driving in reverse, speed is 2.1 m/s. The time of the consumption test is exactly 60 minutes. By the end of the consumption test, exactly 60 load cycles will have been performed.

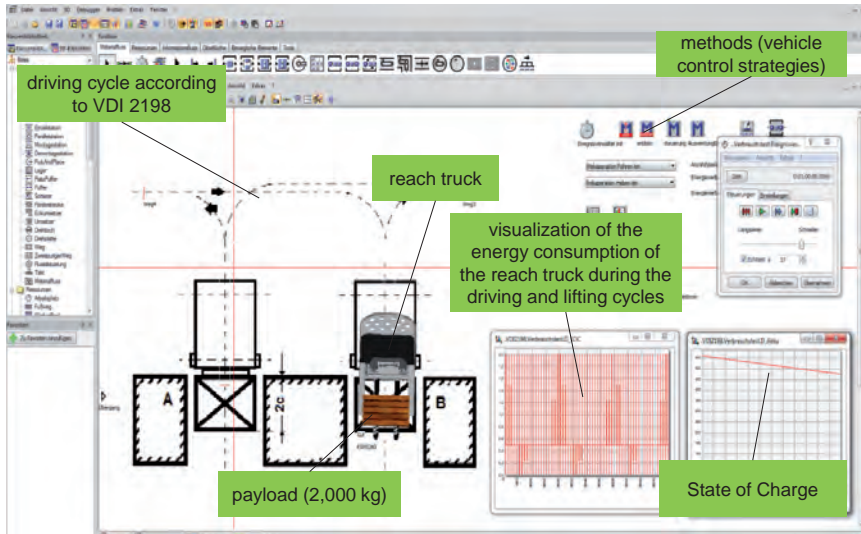


Fig. 18. Test track for consumption test for reach trucks with travelling routes according to VDI 2198 [110].

The basic correlations of these three parameters are described in detail in the following:

Battery size [kWh]: A higher number of infrastructure installations along the road with high power transfer rates translates into more frequent charging of vehicles and thus smaller necessary battery sizes. Smaller battery capacities in electric vehicles means less weight and thus less power necessary to move the vehicle. This further improves vehicle cost. However, lower battery capacity also leads to range reduction and higher dependence on infrastructure allocation [m], infrastructure power rate [kW], and battery type specific charge rate (C-rate)²⁰.

Power transfer rate [kW]: Higher power transfer rates with a high degree of power transfer efficiency η_{CPT} mean that fewer meters of infrastructure segments are required, since more power can be provided on a shorter length. A high transfer rate also makes it possible to reduce battery capacity as the batteries can be charged faster, e.g. in case of a fast-chargeable battery system, or with integrated super capacitors. However, high-power components, which are required for the generation (inverter), transfer (pads), and storage (batteries, super caps) of high power transfer rates also cause higher costs.

²⁰ The term C-rate signifies a charge or discharge rate in correlation to the capacity of a battery.

Infrastructure allocation [m]: Overall cost greatly depends on the right allocation of power transfer segments with stationary and/or in-motion CPT facilities along the roads, and varies depending on the application and charging strategy of the infrastructure and vehicle operators. A generous distribution of power transfer infrastructure leads to more frequent power transfer to the vehicles, which means battery capacity and/or the power transfer rate can be reduced. An excessive allocation of charging infrastructure, however, comes with high installation costs.

General rules for infrastructure allocation have been developed to further reduce the complexity of the optimization problem. These rules help determine an appropriate trade-off between infrastructure investment and necessary battery size with a set of parameters that has already been limited prior to the experiments. This yields clearly defined and structured allocation rules for installing a charging infrastructure for various fleet-operated vehicle scenarios from an energy ("help with energy") and a power ("help with power") perspective as shown Fig. 19.

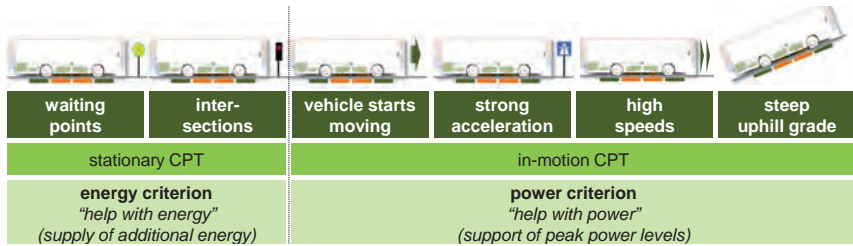
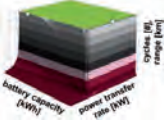
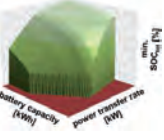
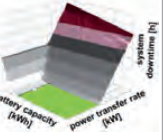
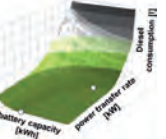


Fig. 19. Allocation rules for the installation of a CPT infrastructure.

The energy collected by the EV depends on the length of powered road and vehicle speed. Powered sections are particularly suitable where average vehicle speeds are low. Therefore, the power transfer infrastructure should primarily be placed at stops, intersections or even at specific points along the route, raising or maintaining the State of Charge (SOC) of the battery in order to meet total energy needs ("help with energy") [112]. Especially stops with longer-than-average wait times are attractive, as an adequate charging infrastructure can be gradually introduced there at comparatively low cost [8] [69]. Additionally, it is desirable to place powered track sections where peak power needs are high, during strong acceleration or on steep uphill sections of roadway, as heavy charging and discharging may cause even modern lithium-ion-batteries to deteriorate much more rapidly [5]. Therefore, CPT systems at these sections can directly power the battery, vehicle drivetrain, and/or vehicle auxiliary loads (e.g. air conditioning unit) ("help with power"). This helps limit the discharge rates of the vehicle battery and thus extends battery life [3] [87]. Moreover, it allows for smaller batteries, and/or in hybrid vehicles, a larger portion of purely electric drive mode.

Subsequently, in order to evaluate a CPT implementation, adequate output factors ($output_{simulation}$) have to be derived, depending on different traffic scenarios and vehicle types, representing the degree of system stability. In purely electric vehicles with CPT systems, system downtimes due to depleted batteries are unacceptable. Vehicles would have to be towed to the next charging station and be unavailable for their main transportation task while they are being recharged. Thus, to simulate CPT systems with purely electric vehicles, the most meaningful output factors representing system stability are “minimal actual SOC” [% of SOC_{min}], “number of conducted transportation cycles” [#], or “achieved range” [km]. Alternative vehicle concepts should be assessed by other output factors as they have different requirements regarding system stability. In battery swapping or hybrid-concepts, for example, system downtime can be limited with built-in “back-up systems” (extra battery capacities in battery swapping stations, ICE in hybrid-vehicles). Battery swapping systems have inherent downtimes as they move to the battery swapping stations (incl. wait times), which have to be kept to a minimum. Hence, for vehicles with battery swapping concepts, system downtime [h] is the most meaningful output factor. The most meaningful output factor for hybrid CPT vehicles is Diesel consumption [l] which has to be kept as low as possible to drive in purely electric mode under almost any circumstances. Tab. 3 provides an overview of possible charts for the evaluation of different traffic scenarios.

Tab. 3. Overview of possible charts for the evaluation of different traffic scenarios.

output factors	cycles [#], range [km]	min. SOC _{tot} [%]	system downtime [h]	Diesel consumption [l]
charts for the evaluation of different traffic scenarios				
traffic scenarios	BEV CPT systems	BEV CPT systems	battery swapping concept	hybrid CPT vehicles

The x- and y-axis is thus reserved for combination values like charging power [kW] and battery capacity [kWh]. The z-axis represents the respective output factor. Thereby, one can derive different possible charts with clearly demarcated areas of stable and unstable system behavior. The “iceberg” model (Tab. 3, BEV CPT systems), for instance, lends itself to backup-less BEV CPT systems, which have to be recharged over longer time periods if they run out of battery. In consequence, the charts show easily discernable demarcations between stable and unstable system behavior. Traffic scenarios like battery swapping concepts or hybrid CPT vehicles do not fail completely due to their back-up systems. However, battery swapping concepts need more frequent battery changes, resulting in a staggered increase of system downtimes, which represents the transfer times to the battery swapping terminal. With hybrid CPT vehicles, insufficient

battery capacities or power levels result in a gradual increase of Diesel consumption to compensate the limited range. This favors the use of inverse “valley” models with transitions between stable (purely electric) and unstable (back-up systems are needed) system behavior (Tab. 3, battery swapping concepts and hybrid CPT vehicles). In addition, it keeps values at the z-axis ascending from min to max from the bottom to the top (base values of the z-axis in the diagrams: range = 0 km; number of cycles = 0; min. SOC_{tot} = 0%; Diesel consumption = 0 l; system downtime = 0 h).

Fig. 20 summarizes all input and output factors of the optimization problem and their inter-relations that have to be considered for the evaluation of a CPT traffic simulation in an energy model.

The simulation runs in *Plant Simulation* can furthermore be structured by the following equation:

$$n_{\text{simulation}} = n_{\text{combinations}} \times n_{\text{experiments}} \times n_{\text{observations}} \quad (3.1)$$

Thereby, the number of total simulation runs $n_{\text{simulation}}$ to derive the desired output factor (depending on the traffic scenario min. SOC_{tot} [%], cycles [#], range [km], Diesel consumption [l], system downtime [h], etc.) is made up of the multiplication of possible combinations of battery [kWh] and charging equipment performance [kW] ($n_{\text{combinations}}$), with the number of studied experiments ($n_{\text{experiments}}$), which represent possible CPT traffic layouts (transportation network, payloads, number and type of CPT segments, work shifts, etc.), and the number of observations ($n_{\text{observations}}$). It is vital to perform several observations per experiment to ensure adequate validity and comparability of the conducted simulation runs. By performing several observations, certain input values like the detailed traffic routes in a traffic network are set randomly and vary continuously for all vehicles. This ensures that the vehicles generally do not drive in the same order or cycles etc. in every simulation run, which helps reduce the influence of possible extreme values of the individually defined experiments and helps reflect real-life system behavior. With this repeated random sampling, the planning approach shows the characteristics of a Monte Carlo method²¹.

²¹ Monte Carlo based methods rely on repeated random sampling for simulating systems with many coupled degrees of freedom [113].

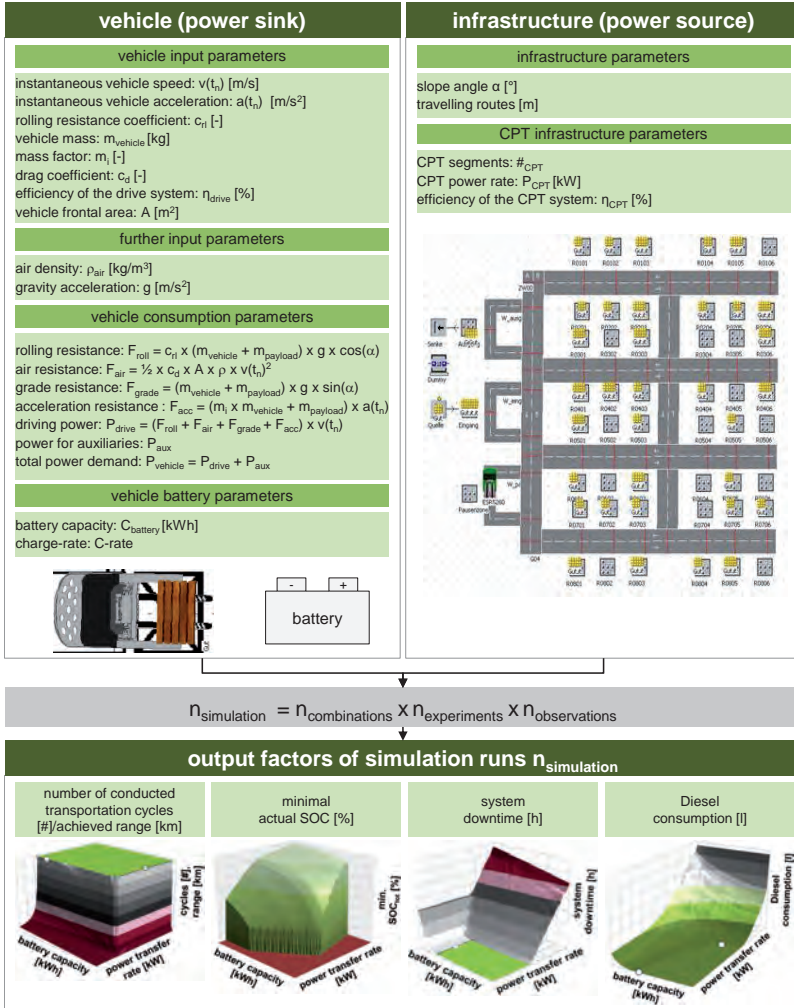


Fig. 20. Basic calculation model with main input and output parameters.

The next chapter verifies the aptitude of this approach for harbor logistics with AGVs. For the AGV simulation model, 625 combinations of battery size [kWh] (25 different values) and charging performance [kW] (25 different values) are studied in seven experiments with different infrastructure layouts, and finally observed five times. In this case, this results in a total number of 30,625 simulation runs. These numbers emphasize the

advantage of *Plant Simulation*, as it permits a solid verification of a large quantity of different experiments.

3.3 Simulation of harbor logistics

The following will verify the developed simulation approach with the example scenario of CPT systems for AGVs in harbor logistics, which are used for handling containers between quay and storage areas [7]. This scenario is of specific interest to verify the simulation approach, as planning complexity increases dramatically when vehicles have no strict routing, as is the case for AGVs in harbor logistics. The operating radius is in fact limited, but the AGVs are in 24-hour operation and their routes between the quay and the storage area vary. In addition, in the almost continuous movement of vehicles in a 24-hour operation, driving times significantly exceed wait times. This makes a clearly defined allocation of CPT infrastructure almost impossible. However, although selected paths are variable, at least the basic travelling profiles show recurring behaviors. All basic routes have the same type of cornerstones on the quay and storage areas (waiting positions, loading positions, main travelling lanes). Therefore, the driving route of an AGV includes: waiting for a new job in a waiting position, driving towards the container bridge, once again standing on a waiting position in order to maintain the correct sequence, loading containers from the container bridge, driving to a storage area, unloading containers at the storage area, and driving to a new waiting position until the next assignment. The AGVs' average travel time at a given container terminal is four minutes and the average path length of one assignment is 460 m.

Research projects for AGVs in harbor logistics focus on substituting currently used Diesel-based AGVs with battery replacement systems [114]. Battery exchange systems force the B-AGVs²² to drive to a battery swapping station as soon as their SOC reaches a certain level, causing downtimes and thus reducing productivity [114]. CPT systems can avoid this drawback and enable continuous 24-hour operation of zero-emission AGVs without any non-productive auxiliary process times. Therefore, the following compares CPT systems to battery swapping AGVs. This will demonstrate the feasibility of the simulation approach not only for CPT systems, but also for other electric vehicle concepts (in this case battery swapping). Moreover, detailed final data from the B-AGV research project in Hamburg (2010-2011) [114] can be used to verify the input data for the simulated vehicles.

To compare B-AGV and CPT-AGV approaches, several experiments have been defined with different parameters of power source and/or power sink. Fig. 21 shows the results for B-AGVs. The displayed diagrams are set up as described in chapter 3.2. The main output factor at the z-axis for B-AGV systems is downtime [h], which is unavoidable because of the transfer to the swapping stations, and which should be minimized. This al-

²² Battery Swapping-Automated Guided Vehicle

allows for an easy comparison of different numbers of batteries, rack-feeding systems, and battery charging equipment in the battery swapping stations in different experimental set-ups.

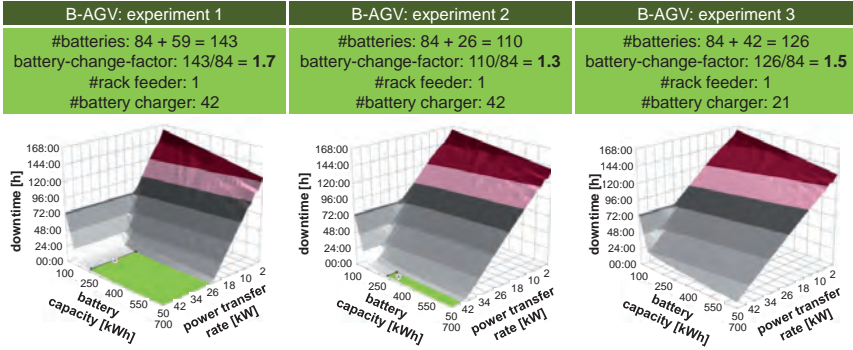


Fig. 21. Comparison of simulation run results with different B-AGV experimental set-ups.

Currently, the research project features the combination of 84 vehicles with 59 extra batteries in the battery swapping station, one rack feeder, ~36 kW charging equipment, and two different lead acid battery types (288.0 and 331.2 kWh) [114]. The chosen parameters can be verified by simulation to be sufficient. Moreover, the simulation shows one of the negative effects of battery swapping concepts. With a reduced number of extra batteries (in Fig. 21, the battery-change-factor is reduced from 1.7 in experiment 1 to 1.3 in experiment 2), the range of possible combinations of battery sizes, and charging levels drastically decreases in the battery swapping concept. A significant number of extra batteries must thus be provided together with a sufficient number of battery chargers in the swapping stations at substantial extra cost. Experiment 3 in Fig. 21 shows the even more negative effect of reducing the number of battery chargers. This goes to show that reducing batteries is the preferable strategy for optimizing the system, as more batteries always require more battery swapping facilities (chargers and fully automated rack feeders), further increasing cost and required space. Moreover, batteries have to be replaced altogether after several years of service. By comparison, CPT systems require little extra space as the charging equipment is installed in the ground. This is another decisive parameter, in particular for container terminals in harbor cities, with limited expansion options and space constraints. From a technical point of view, there are several possibilities for infrastructure allocation as verified in the simulation. Waiting, container bridge and storage area positions are specifically attractive for stationary CPT points. Thus, the battery of the AGV can be charged while it is waiting, picking up, and unloading containers. In principle, it is also possible to envision in-

motion CPT along the main travelling lanes, directly supporting the AGVs' powertrains as they move between the different target positions ("help with power"). The results of the simulation runs for CPT systems is shown in Fig. 22 with 100% (experiment 1) and 50% (experiment 2) coverage of stationary CPT systems at waiting positions, and 50% coverage of the main travelling lanes (experiment 3).

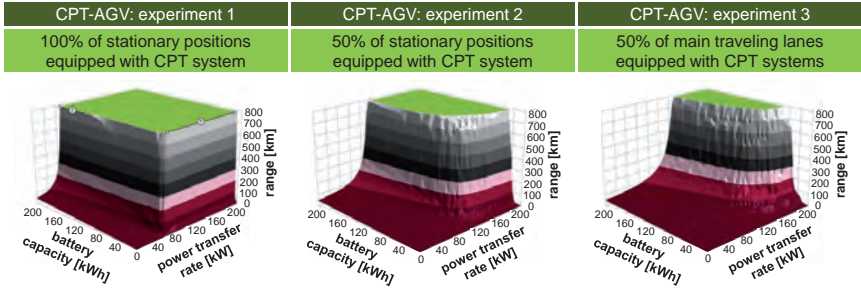


Fig. 22. Range in km achieved by CPT equipment with different infrastructure allocations (100% and 50% coverage of stationary positions, 50% coverage of travelling routes).

Thus, simulations of a sample container terminal with AGVs show that in theory, even if waiting positions or travelling lanes are only partially equipped with CPT, it is possible to maintain the SOC and achieve stable system behavior (green surface in the chart). However, this requires large batteries and higher power transfer rates. Thus, from an economic point of view, and as it is the goal to reduce battery capacities with CPT systems, all waiting positions at the storage blocks should be equipped with stationary power segments (experiment 1). In theory, battery capacities can thus be drastically reduced compared to battery swapping concepts. However, the feasibility of this approach is limited by the charging rates, especially as higher charging current results in heat dissipation in the batteries due to internal resistance of the battery cells, which can reduce battery life [5] [115]. Fig. 23 includes C-rates²³ to show what this means for possible combinations of different power levels and battery capacities.

Limiting the charging power to 1, which is the typical rate of charging for lithium-ion batteries, reduces the number of valid combinations by half (Fig. 23, experiment 1b). If charging rates are below 0.2 (technical limit with lead-acid batteries), no stable system behavior can be achieved when 100% of all waiting positions are equipped with stationary CPT segments (Fig. 23, experiment 1c).

²³ C-rates refer to the current carrying capacity that a battery can sustain. It generally signifies charge or discharge rate equal to the capacity of a battery in one hour. In this case, it is assumed that voltage changes only slightly between 30-80% SOC, thus correlating to [W] and [kWh].

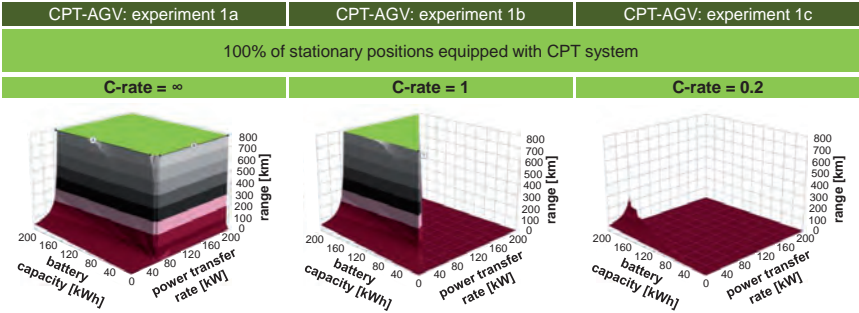


Fig. 23. Consequences of including C-rates in the possible CPT power level and battery capacity combinations (100% coverage of all waiting positions with stationary CPT segments).

Tab. 4 summarizes the technical comparison between B-AGVs and CPT-AGVs for harbor logistics systems. The direct comparison shows that CPT systems allow for a significant reduction of batteries. B-AGV systems require more and much larger batteries (battery-change-factor: 1.5, battery capacity: min. 250 kWh) with lower charging power rates (min. 30 kW). In contrast, CPT systems need batteries that can be charged with C-rates that are close to one. In this case, lead-acid batteries with typical C-rates of C/5 cannot be used and more expensive lithium-ion batteries have to be installed. For CPT-AGVs with installed lithium-ion batteries (charging rate = 1C), experiment 1b in Fig. 23 shows a possible combination of a power transfer rate of 52 kW and a fast-chargeable battery capacity of 52 kWh.

Form a technical point of view, CPT systems present various advantages over battery replacement systems. However, expensive CPT infrastructures and lithium-ion batteries are currently still a limitation. In the coming years, this limitation should be minimized as costs go down, C-rates for lithium-ion batteries go up, and the costs of CPT infrastructures decrease. However, further real-world high-power CPT demonstrations must be set up to verify the technical input parameters and attainable infrastructure and maintenance costs of CPT systems. This is of significant importance because ground settlement behavior at newly deposited harbor quays may cause severe problems as there are strict rules to renew road surfaces quickly and regularly. In addition, integrating high-voltage cables in the ground in busy harbor environments entails safety aspects that have to be studied.

Tab. 4. Example results of the simulation-based comparison of B-AGV and CPT-AGV approaches for harbor logistics.

	B-AGV	CPT-AGV
power transfer rate [kW]	30	52
battery capacity [kWh]	250	52
charging rates	up to C/5	up to 1C
battery concepts	lead-acid batteries	lithium-ion batteries
energy density [Wh/kg] [72]	35	130
battery weight [kg]	7,143	400
battery-change-factor	1.5	1
uninterrupted daily operation at maximum capacity of the terminal [h]	12.5	24
idle times due to charging system per week per AGV	about 4 h	0 h
space required for charging infrastructure	high	low
system reliability	low	high
flexibility of the vehicles	high	medium
charging infrastructure elements	battery swapping station, chargers, rack feeder, exchange batteries, grid connection	CPT charging segments, grid connection/distribution network

In conclusion, it can be said that adapting the event-discrete simulation software *Plant Simulation* is a promising solution to evaluate CPT traffic allocation problems, even for complex logistics operations. The simulation models show sufficient precision, verified by checking the simulated data against real vehicle behavior. The essential parameters and correlations of individual traffic scenarios can easily be derived by setting up appropriate simulation run experiments. In addition, the approach with *Plant Simulation* shows a large number of further evaluation options. The approach can help derive the best suitable vehicle and powertrain concept (PHEV, REEV, BEV) and correlated operating strategy (using power to charge the battery versus directly powering the drive system). Especially as infrastructure costs are significant and should be reduced, *Plant Simulation* can ultimately help derive the appropriate infrastructure set-ups in detail, by match-

ing detailed vehicle power consumption profiles with needed CPT charging infrastructure.

To further help accelerate the market introduction of CPT systems for electrified vehicles, system cost has to be steadily reduced. Therefore, the following analyzes and presents basic CPT system set-ups (chapter 4) to develop appropriate production technologies (chapter 5).

4 Detailed Analysis of CPT Pad Designs for Electric Vehicles

Chapter 4 analyzes various possible basic physical principles of contactless power transfer technologies and alternative system designs with their specific characteristics. It shows the main factors needed to achieve high power transfer efficiencies in order to derive the research needs and scientific approach of this work from a production and material perspective.

4.1 Physical basics of CPT systems

The use of contactless charging technologies in EVs has various implications for the power transmission system and its components. Power must be transferred at the level of several kW and virtually loss-free power transmission needs to be attained with the relatively large air gap (~100-300 mm) that is necessary for underbody ground clearance (in the case of underbody system integration) [3]. There are several basic coupling mechanisms to attain contactless transfer of power for EVs, as presented in Tab. 5.

Because of the advantages mentioned in Tab. 5, experiences from the latest research projects, and the necessary distances, inductive coupling is at the main focus of development in both industry and science. The basic principle of inductive power transfer is thereby based on electro-magnetic interactions between two mutually arranged conductor structures and basically works on the same principle as conventional transformers. Michael Faraday studied the basic principles of electromagnetic induction, which is the basis of electric motor, generator, and transformer technologies, as early as 1831. Faraday discovered that a copper wire in motion within a magnetic field produces an electrical current. In the same way an alternating current in a copper wire creates a time-varying magnetic field. This is used in conventional transformers with a primary and a secondary coil wrapped around a highly magnetic permeable iron core. An AC current generates a magnetic field in the primary coil, which induces an electrical voltage in the secondary coil. The permeable iron core links the wound coils and increases the strength of the time-varying magnetic field, so that the iron channels most of the magnetic flux through both coils with a tight coupling, thus minimizing power losses with low stray fields. The main difference between contactless power transfer systems and such a conventional transformer is that the magnetic circuit is not closed by a highly magnetic permeable iron core, but by an air gap. In these circumstances, power is transferred by induction from one coil to another without physical contact [41].

Tab. 5. Classification of different contactless power transfer technologies.

	capacitive coupling	inductive coupling (near-field, near-range)	inductive coupling (near-field, mid-range)	radiative coupling (far-field)
principle	<ul style="list-style-type: none"> power transfer by electro-static field [5] 	<ul style="list-style-type: none"> magnetically coupled coils comparable to operation of a conventional transformer resonance used to enhance the efficiency [20] 	<ul style="list-style-type: none"> same principle as with magnetic induction resonance used to enhance the efficiency [20] 	<ul style="list-style-type: none"> use of electro-magnetic far field
range	<ul style="list-style-type: none"> short-range (mm) (field is concentrated between two conductive sheets) [5] 	<ul style="list-style-type: none"> closely-coupled coils with relatively high coupling coefficient $k > 0.1$ loosely-coupled coils with coupling coefficient $k > 0.01$ [5] distance between coils: $-0.33 \cdot 1 \times$ coil radius 	<ul style="list-style-type: none"> very loosely-coupled systems with relatively low coupling coefficient $k < 0.01$ [5] distance between coils: larger than coil radius 	<ul style="list-style-type: none"> long-range (up to even kms) distance between transmitter and receiver: typically much larger than the wavelength of the transferred signal [5]
frequency	<ul style="list-style-type: none"> MHz-range [117] 	<ul style="list-style-type: none"> kHz-range (10-200 kHz) [5] 	<ul style="list-style-type: none"> MHz-range [5] 	<ul style="list-style-type: none"> GHz-range [99]
advantages	<ul style="list-style-type: none"> easy matching of impedance and resonance frequency [117] 	<ul style="list-style-type: none"> well-known system approach lower efforts for safety-measurements due to small air gap (especially for closely-couple coils) 	<ul style="list-style-type: none"> larger air gaps with more freedom in positioning of the coils 	<ul style="list-style-type: none"> power transfer over larger distances [5]
bottle-necks	<ul style="list-style-type: none"> large capacitor plates or small distance needed between them to achieve high degrees of efficiency [118] high influence on the surroundings high voltages [69] dependence on weather conditions [117] 	<ul style="list-style-type: none"> primary and secondary coil must be located in relatively close proximity (depending on the tuning: non-resonant within mm, resonant within cm) [20] 	<ul style="list-style-type: none"> complex system configuration: due to high quality factors, power transfer dwindles rapidly with even small detuning [5] high frequencies: safety and health issues [5] 	<ul style="list-style-type: none"> high directivity of the transmitting antenna is needed [5] radiation based power transfer methods interact strongly with living organisms and certain metallic objects [116] limitations for an efficient operation with high frequencies due to the currently available semiconductor devices [3]
EV applications	<ul style="list-style-type: none"> only laboratory test set-ups 	<ul style="list-style-type: none"> non-resonant: used for closely coupled EV systems resonant: considered to be best suitable for practical use in loosely-coupled electric vehicle battery charging [5] [69] 	<ul style="list-style-type: none"> only laboratory test set-ups 	<ul style="list-style-type: none"> only laboratory test set-ups

As air has a high magnetic reluctance, the power transfer is less efficient, especially as the air gap increases. To still operate efficiently, the coupled coils need to operate in what is called a strongly coupled regime with a high magnetic link potential [5] [119]. The magnetic link potential X is thereby represented by the product of the coil's quality factors Q_{c1} and Q_{c2} and coupling coefficient k of the coil system [120] [121] [122]:

$$X = k^2 Q_{c1} Q_{c2} \quad (4.1)$$

The maximal link efficiency is described by

$$\eta_{link,max} = \frac{X}{(1 + \sqrt{1 + X})^2} = \frac{k^2 Q_{c1} Q_{c2}}{(1 + \sqrt{1 + k^2 Q_{c1} Q_{c2}})^2} \quad (4.2)$$

The quality factors

$$Q_{c1} = \frac{\omega L_1}{R_{c1}} \quad (4.3)$$

and

$$Q_{c2} = \frac{\omega L_2}{R_{c2}} \quad (4.4)$$

can be described by the ratio of its impedance to its AC resistance at the operational frequency [67]. They include the coil's inductances L_1 , L_2 , and their equivalent resistances R_{c1} , R_{c2} , representing the losses that may be inherent to the induction coils at a specified signal frequency ω [121]. The higher the operating frequency ω , the more intense the induction effect and the greater the transmittable power, which makes for a smaller and lighter system set-up [27]. However, the selection of the operating frequency ω is typically a compromise between efficiency, cost, coil size, and safety concerns due to regulations on flux leakage [5] [41] [123] [124].

Thus, approaches to maximize the magnetic link potential X also inherently depend on the coupling coefficient k . The coupling coefficient k is a dimension-less parameter representing the fraction of the main magnetic flux Φ_m received in the secondary coil to the total flux produced by the transmitting coil Φ_{total} , consisting of the main magnetic flux Φ_m and the leakage flux Φ_σ [125].

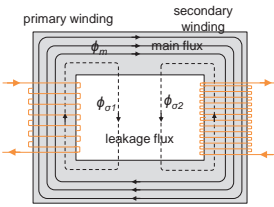
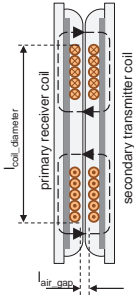
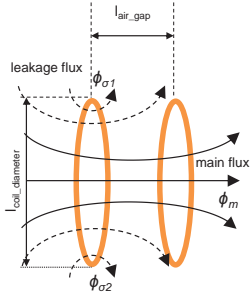
$$k = \frac{\Phi_m}{\Phi_{total}} = \frac{\Phi_m}{\Phi_m + \Phi_\sigma} \quad (4.5)$$

k has a magnitude between zero (no coupling) and 1 (all flux is coupled) and thus depends on the design of and the distance between the coils. In conventional transformers with closed iron cores, k is typically in the order of $k > 0.95$ with a strong magnetic coupling compared to CPT systems with $k \sim 0.01-0.5$ [24].

In analogy to current literature [5] [67], CPT systems can be distinguished into closely coupled-systems and loosely-coupled systems, depending on coil diameters $l_{coil_diameter}$ and air gaps l_{air_gap} , as shown in Tab. 6.

Tab. 6. Inductive coupling approaches depending on air gap.

coupled by closed iron core	closely- coupled	loosely- coupled
high coupling factor, no air gap	high coupling factor, small air gap	low coupling factor, large air gap
$k \sim 0.95$	$k \sim 0.5$	$k < 0.1$
$l_{air_gap} = 0$	$l_{air_gap} \ll l_{coil_diameter}$	$l_{air_gap} \leq l_{coil_diameter}$
conventional transformers	charging paddles, license plate solutions	underbody systems with air gap

The lower the ratio of the air gap to the coil diameter ($l_{air_gap} \ll l_{coil_diameter}$), the higher the magnetic coupling. Therefore, early approaches of air-gap couplers in the 1990s used closely-coupled systems with the primary and secondary coils located within close proximity (high coupling factors $k > 0.1$) [126]. To transfer power efficiently, coils were designed with very large cross-sectional areas [2] or carefully positioned, usually within millimeters [20] [70]. This “near-field near-range” non-resonant inductive coupling can be used for systems that require only small air gaps and low positioning tolerances. This results in very low leakage inductance compared to magnetizing inductance, adding a level of safety. The objects to be charged have to be placed directly on top of, or very close to the base pads, or may even require a cradle to hold the receiving device. Closely-coupled systems with fixed or guided positioning mechanisms represent an interesting alternative as they are comparatively simple and inexpensive, as well as efficient and safe, especially for high-power applications (as no foreign or living object detection is necessary between the coils). One example of such an inductive coupler is the hand-held insert-type Magne Charge charging paddle proposed for electric vehicles in the early 1990s [127] [128]. Other examples are license plate solutions [12] [60] [129] [130] [131]. However, license plate solutions with small air gaps and high coupling fac-

tors may not be accepted due to their crash sensitive position. Adaptive underbody systems that can be lowered are also possible to reduce the air gap and thus increase coupling factors (called z-lifters) (see Fig. 24).

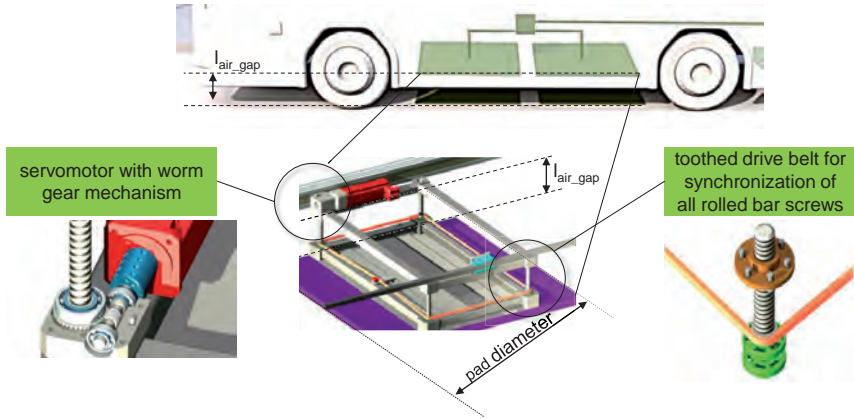


Fig. 24. Adaptive pick-up systems to reduce the air gap between the primary and secondary charging pads.

These systems have already been installed, e.g. in high-power applications (60–200 kW) like bus systems to position the pick-up directly on the ground at bus stops [2]. Wampfler uses a scissors-based lifting system [27], whereas Bombardier and Viseon [95] [132] use a special swiveling device to lower the pick-up, which is also equipped with rolls to ensure adequate spacing between the pick-up and the ground and protect it from damage. With adaptive systems in buses, the Flanders' DRIVE project reports better EMF control and a weight reduction of the pick-up of 100 kg [95]. Adaptive pick-up systems for passenger cars have also been the subject of intense discussion for several years now [133]. However, it is not prudent to integrate adaptive systems into the underbody of passenger cars, which are quite small compared to bus systems, as they also cause potential problems with space and weight requirements (smaller pick-ups, but additional weight due to the z-lifter). This is even more important with vehicles that may operate at higher speeds with induction coils preferably integrated flush with no protruding parts [134]. In addition to these adaptive vehicle-sided systems, adaptive positioning support systems for the primary infrastructure are also under discussion, featuring functionalities like lifting, lowering, or rotating to accurately orient the coils [6] [70] [135]. Z-lifters to avoid air gaps have, for example, already been integrated on the primary side of the Praxitele car sharing system in 1997. Although the CPT system worked in a “satisfactory” manner, the special z-lifter posed problems with the mechanical sys-

tem [43]. In consequence, adaptive systems should be avoided in passenger cars as they can malfunction as well as create significant costs and maintenance problems.

In contrast, loosely-coupled systems operate with a significant air gap. One way to make loosely-coupled systems work gained enormous popularity after it was presented and promoted by MIT researchers in 2007²⁴ [119] is called the “near-field mid-range” inductive resonant coupling approach. The distance between the coils is usually larger than the coil diameter ($l_{\text{air_gap}} \gg l_{\text{coil_diameter}}$). Unlike a tightly-coupled transformer, significant flux exists in the primary and secondary windings as well as in the space in-between. The bottlenecks of this approach are its relatively low efficiency with very large air gaps ($l_{\text{air_gap}}/l_{\text{coil_diameter}} > 1$) [121]. This approach with very loosely-coupled coils ($k < 0.01$) only achieves a strongly-coupled regime with sufficient quality factors Q_{c1} and Q_{c2} (1,000 and above). The MIT researchers used for their resonant coupling approach core-less coils with no shielding and an operating frequency in the MHz range [119]. Resonance induction works on the same principles as non-resonance induction, but uses resonance to enhance the efficiency of the power transfer between two coils [20]. The needed high Q-values, however, make it harder to control the tuning of compensation-circuits to maintain resonance. Therefore, this approach is sometimes referred to as “highly resonant” contactless power transfer [20]. Safety and health issues have to be considered, as well [5]. In terms of efficiency and range, this method is a compromise between the “far-field radiative” approach and the “near-field near-range” approach (see Tab. 5), currently showing promise only for low-power applications that can tolerate lower efficiencies, such as cell phones, medical equipment, and other small IT devices [41].

The alternative that is used far more often for EV-charging is called “near-field near-range” inductive resonant coupling. This approach uses a relatively high coupling coefficient ($k > 0.01$) and a moderate frequency from 10-200 kHz, which requires moderate values for the coil quality factors Q_{c1} and Q_{c2} . However, practical needs in EV charging dictate a certain economy of space and weight for the pads, which means that a certain Q value (above 100) is still needed to achieve higher overall efficiency at limited pad sizes (see Fig. 25). This approach can transfer a large amount of power while maintaining controlled resonance in the compensation-circuits [5]. The described advantages, along with the ability to efficiently transfer power across air gaps that are appropriate for EV charging, make “near-field near-range” inductive resonant coupling using resonant tuned coils the best suitable and practical method for electric vehicle battery charging [5] [20] [41] [69] (see also Tab. 5).

²⁴ Laboratory test set-up: two identical helical copper-coils, $r_{\text{coil}}=30$ cm, distance=2 m, P=60 W, resonant frequency $f=10.56 \pm 0.3$ MHz, $\eta \sim 40\%$, $Q_{\text{measured}} \sim 950 \pm 50$.

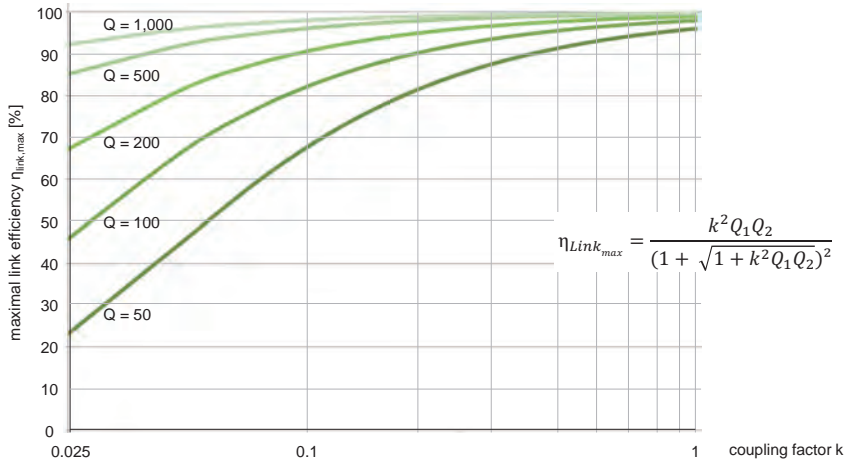


Fig. 25. Relevant system parameters to determine the system efficiency.

The following describes the core components of contactless power transfer systems based on “near-field near-range” inductive resonant coupling to clarify the key factors of highly efficient, reliable, and safe systems that are necessary for automotive applications.

4.1.1 Energy chain of CPT systems

The basic structure of CPT systems for electric vehicles consists of a Base Charging Unit (BCU) and a Vehicle Charging Unit (VCU) (Fig. 26). The BCU consists of primary electronics for the power supply, compensation (C_1), and a road-side transmitting coil (L_1). The VCU consists of an on-board receiving coil (L_2) to capture magnetic flux, secondary electronics including compensation (C_2) and rectification [30] [54] [87]. Moreover, both sides need appropriate communication and surveillance systems.

In the power supply, an AC/DC rectifier block converts the AC mains voltages of typically 50/60 Hz (AC_{in}) to DC power at a suitable voltage level. Then, a DC/AC switching amplifier converts the DC voltage into a high-frequent AC voltage to drive the source resonator (primary transmitting coil) [71]. Together with a corresponding on-board receiving coil, the coils form an inductive transmission path. Thus, loosely-coupled systems, which have smaller coupling coefficients and larger air gaps with large leakage inductances, need appropriate reactive power compensation in a compensation network so that they can still attain an inductive transmission path with strong coupling and highly efficient power transfer rates [121].

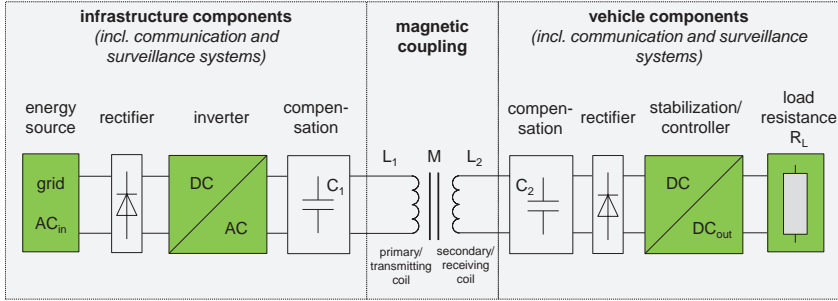


Fig. 26. Exemplary schematic arrangement of a contactless power transfer system (based on [54]).

Therefore, capacitors are used to extend the system on the primary and secondary side to attune the resonance frequencies of the primary and secondary circuit to each other, making the resonant circuit oscillate harmonically between the coil and the compensation capacitor with larger amplitude [69]. When operating an inductively coupled coil pair that resonates at the same frequency, the efficiency of the power exchange improves dramatically as it reduces damping losses. The operating frequency for inductive power transfer systems is commonly set between 20-140 kHz [30]. There are several possible ways to arrange capacitors (i.e. reactive tuning components) to form a resonant circuit. The capacitors may be placed in a serial or parallel configuration or a combination of both with a base induction coil to emit an electromagnetic field at a desired frequency. Systems with different set-ups have already been presented [6] [121] [136] (Fig. 27).

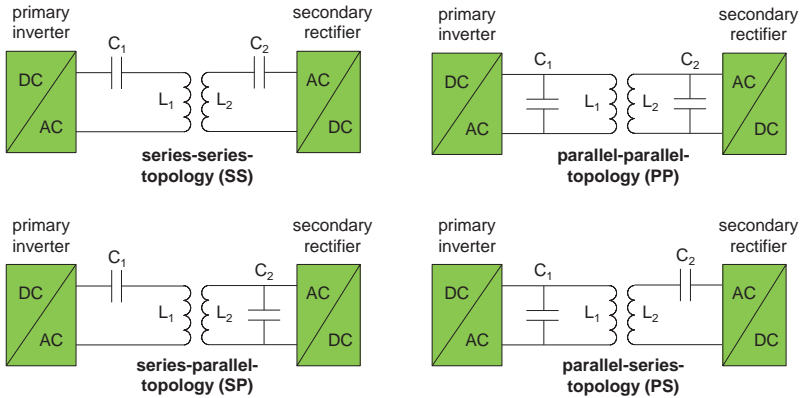


Fig. 27. Different resonant topology combinations (based on [137]).

This way, the reactive components in the transmission system are compensated and the classic transformer is functionally replaced by two inductively coupled resonant circuits at a coupling-dependent resonant frequency. It is thus possible to transfer energy efficiently at lower coupling rates, at greater distances, and/or with more positional freedom than is otherwise possible, eliminating the need for precise positioning between source and device [20].

Aside from the receiver pad inductance L_2 (receiving coil) with compensation capacitors (C_2), the secondary side of the CPT system in the vehicle also includes circuits for rectification from the operating frequency AC voltage back to DC, as well as a switch mode controller for voltage stabilization, at a voltage level matched to that of the vehicle DC link. The stabilized DC voltage is fed to the vehicle DC link and managed by the Battery Management System (BMS) to either charge vehicle storage systems (e.g. high-voltage battery and/or a super capacitor) or to power a load directly.

4.1.2 Main factors impacting the efficiency of CPT systems

One of the decisive factors of contactless charging systems is the degree of efficiency they can attain. High system efficiencies save the scarce resource of energy in the spirit of sustainable green mobility and avoid slow charging, overheating components, and eventually higher energy costs for the customer [10]. Therefore, a high power transfer efficiency rate is key to achieve a competitive advantage over conductive charging solutions. It is even possible that industry and policymakers will prescribe a minimum efficiency for power transfer to avoid wasting energy [46]. The end-to-end efficiency of CPT systems²⁵ can be defined as the amount of usable electrical energy that is available to the powered device, divided by the amount of energy that is drawn from the power source:

$$\eta = \frac{\text{amount of usable electrical energy}}{\text{amount of energy drawn from the power source}} \quad (4.6)$$

For EV charging in the kW-range, stationary prototypic CPT systems have demonstrated end-to-end efficiencies of $\eta > 90\%$, even across larger air gaps of about 20 cm [1] [20]. Such efficiencies require careful design in each stage of the system with an efficiency of $\eta \sim 96\%-98\%$ or greater [20] [41], as shown in Fig. 28.

It is promising that such high efficiencies (above 90%) are attainable, especially considering that in comparison, conductive charging solutions usually only marginally exceed these efficiency rates ($\sim 93\%-97\%$), as there are also losses in insulation and control circuitry, components, connectors, and cabling [73] [95].

²⁵ End-to-end efficiencies commonly refer to AC_{in} (energy grid connection) to DC output at the battery connection.

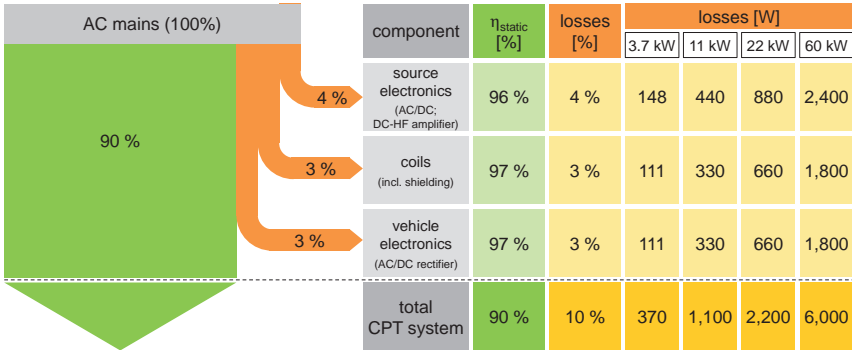


Fig. 28. Power-flow diagram with end-to-end efficiency of EV CPT systems (based on [138]).

It is important to know the influence factors and correlations that affect CPT efficiency in order to find out which production technologies and process parameters yield high performance automotive CPT systems. Along with the above-mentioned aspects of improved k - and Q -values, higher efficiency rates for CPT systems with larger air gaps highly depend on the availability, performance, and cost of suitable materials (shielding, magnetic field guidance, conductor) and suitable power electronics [3]. Therefore, the following explores possibilities to improve the system power level and efficiency along the energy chain.

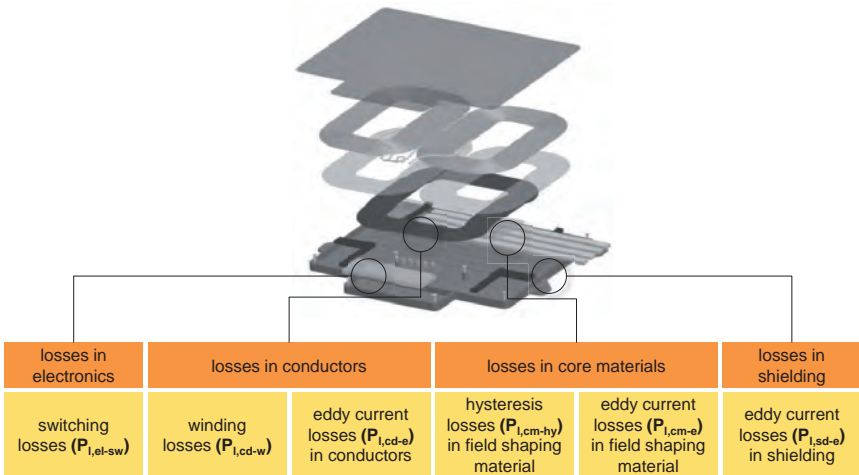


Fig. 29. Losses in CPT systems (based on [69] [87] [139] [140] [141] [142]).

Along the energy chain, several forms of loss occur correlating with the frequency (f), magnetic flux density (B), and current rating (I) that have to be considered, as shown in Fig. 29. Switching losses in the used power electronics, particularly in the input rectifier, increase with increasing switching frequency ($P_{l,el-sw} \sim f$) [69]. As the frequency mounts, inverter switching devices become less efficient at turning DC power into AC. In the past, the needed higher frequency rates were unachievable with the available electronic circuitry. The PATH project, for instance, used only ~ 400 Hz-8,500 Hz [2]. However, modern power electronics, e.g. based on silicon carbide semiconductors, reach very high efficiencies for power supplies and secondary electronics, even at higher frequencies, without deterioration. Power supply efficiencies are typically $\sim 95\%$, while the secondary electronics and controls can have efficiency rates as high as $\sim 96-97\%$ when operating under ideal conditions [41]. Moreover, continuing research into control and circuits for high-power CPT systems will further increase the efficiency of CPT systems and provide opportunities for reducing electronics size. Reductions in the size of metal housings, printed circuit boards, connectors, etc. will help further reduce per-unit costs with an increase in scale.

Aside from the semiconductor devices, losses in the field guiding and conductor materials may cause significant losses in the pads. Two effects have to be considered in the conductor materials for CPT systems: winding losses and eddy current losses. Winding losses mainly arise from the ohmic resistance of the conductor material. They are proportional to the square of the current coil load (due to Ohm's law) according to the equation $P_{l,cd-w} = I^2 \times R$ (I : coil current, R : winding resistance) [69]. Thus, winding losses are highly dependent on the load, as higher current rating results in greater winding loss due to resistance in the wires that reduce efficiency [87]. These undesirable winding losses have to be minimized, e.g. by employing conductors made from low-resistivity metals with higher electrical conductivities, such as copper. Especially for higher power transfer applications of several dozen kW, additional cooling measurements may have to be implemented (see chapter 6.2).

In addition to winding losses, another negative side effect is that at higher frequencies, AC currents create a magnetic field that results in eddy currents in the wire. Such eddy currents induced within conductors create losses (skin effect, internal and external proximity effect).

$$P_{l,cd-e} = P_{l,skin} + P_{l,prox,int} + P_{l,prox,ext} \quad (4.7)$$

Aside from the current ratings, the resistance of a conductor carrying AC current (and hence the effectively used cross-sectional area) also depends on the frequency ($P_{l,cd-e} \sim B^4 \times f^4$) [141]. Eddy currents counteract the current flow, and as AC resistance is strongest at the center of a conductor, the current is distributed irregularly over the conductor diameter - the material at the center is not being used effectively. Since the area

that carries current is reduced, the effective ohmic resistance of the conductor increases. Current density increases at the outer edges of AC conductors in what is called the skin effect, basically causing the major part of the current to flow in a thin ring near and on the conductor's surface (current displacement effect) [143]. The penetration depth of the current of each individual conductor is inversely proportional to the square root of the frequency and can be approximated with the following equation [141] [144]:

$$\delta = \sqrt{\frac{2\rho}{\omega\mu}} = \sqrt{\frac{2}{2\pi f\mu_r\mu_0\sigma}} = \sqrt{\pi f\sigma\mu_0}^{-1} \quad (4.8)$$

δ is the penetration depth of the skin effect [mm], ω the angular frequency ($2\pi f$) [Hz], μ the magnetic permeability of the material [H/m], μ_r the relative magnetic permeability, μ_0 the vacuum permeability ($\mu_0 = 4\pi \times 10^{-7}$ [Vs/(Am)]), ρ the resistivity [Ωm], and σ the electrical conductivity [S/m] of the material. As a consequence, massive single conductors with a large cross-sectional area are impractical for inductive charging pads with frequencies in the kHz-range. The impact of the skin effect and AC resistance factor at higher frequencies can effectively be reduced by using multiple thin individually insulated wire strands (up to several thousand with diameters of 0.018 mm up to 0.500 mm [145]) through which the AC current can travel with reduced conductor diameter d , called HF-Litz wires²⁶, as shown in Fig. 30.

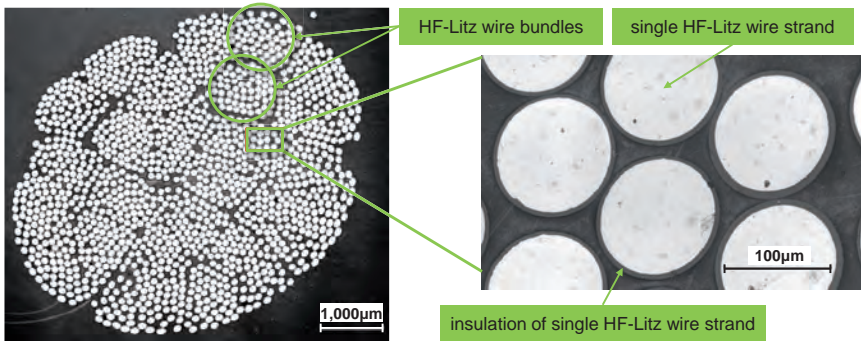


Fig. 30. Cross-section of a HF-Litz wire.

Thus, fine HF-Litz wires with $d < 2\delta$ are used for the entire diameter of the conductor in which AC current can travel at high frequency [6]. In order to protect the Litz wires electrically, thermally, and mechanically, each individual wire strand is surrounded by a non-conductive insulating layer. This layer consists of either a ceramic enamel coating or a polymer film [15]. For external insulation, the bundle of strands can be wrapped with

²⁶ The term "Litz wire" comes from the German term "Litzendraht" and is used for conductors carefully constructed according to a precisely prescribed pattern [143].

polyester film "Mylar", nylon, or natural silk sheaths to protect the thin insulation of the individual wire strands against mechanical damage, moisture, or the like. External insulation materials are needed especially to create HF-Litz wires in special shapes, e.g. rectangular to use available winding space more efficiently. Since HF-Litz wires require high electrical conductivity, they are traditionally based on copper. Another alternative conductor material is aluminum with base material costs of only a quarter of copper and lower price fluctuations compared to Cu ($Al_{03-26-2014}=1.27 \text{ €/kg}$ vs. $Cu_{03-26-2014}=4.75 \text{ €/kg}$). Innovative bi-metallic HF-Litz wire compounds with copper being clad-ded onto an aluminum core (copper clad aluminum: CCA) allow the combination of the preferred properties of both metals. With CCA, conductivity increases slightly, problems with the oxide layer of aluminum can be mitigated, and the same contacting techniques as for copper conductors can be used [145]. However, there remains a tendency to form aluminum oxides which, without appropriate insulation, will degenerate the entire conductor, especially at the terminals [146]. In addition, HF-Litz wires already make up a large proportion of pad costs [24], and CCA makes them even more expensive. Tab. 7 compares the main characteristics of the three relevant conductor materials copper, aluminum, and CCA.

Tab. 7. Comparison of different conductor materials for CPT systems [145].

	copper	aluminum	CCA10%	CCA15%
volume fraction of copper [%]	100	0	10	15
density [g/cm^3]	8.9	2.7	3.3	3.6
conductivity [$\text{m}/\Omega \times \text{mm}^2$]	58.5	36	37.7	39.2
breaking strength [N/mm^2]	220-270	120-140	130-180	230-280

In addition to the skin effect, the proximity effect is causing losses that have to be considered. The proximity effect is similar to the skin effect, with the difference that the eddy current losses are caused by alternating magnetic fields of adjacent wire strands within the Litz wire bundle (internal proximity effect) and by alternating magnetic fields of adjacent Litz wire bundles (external proximity effect). Currents travelling near each other tend to increase the AC resistance as they redistribute current flow in undesirable patterns. The smaller the distance between two conductors, the greater the proximity effect. Thus, to mitigate the internal proximity effect, the individual Litz wire strands have to be twisted together in such a way that, viewed over the length of the Litz wire, each conductor weaves evenly towards and away from the core of the Litz wire. On its way along the length of the entire Litz wire, each individual wire strand crosses each possible position in the overall cross-section of the Litz wire, thereby reducing the internal proximity effect. The length of lay thereby describes the length of the path traveled by a

single wire strand for one complete revolution (360°) around the center of the Litz wire [141] [143]. According to [144] and [147], a reduced copper filling factor in AC applications in the kHz-range may be preferable to reduce R_{AC} . Therefore, alternative set-ups for loss-minimized HF-Litz wires have been proposed, with Litz wire strands arranged in areas of reduced magnetic field strength (e.g. along the lateral surface) or thicker layers of wire/bundle insulation.

With increasing frequencies, HF-Litz wires clearly show reduced skin effect losses compared to solid wires. However, as the frequency rises above the megahertz range (MHz-GHz), current flows in an ever-thinner surface layer. Above a certain frequency (800 kHz in a model consideration of [148] with a 20×0.08 Litz wire), the internal proximity effect leads to increasing losses in the Litz wires. In this situation, solid round wires are once again the better alternative, as they cannot induce internal proximity effects in adjacent internal wire strands. Therefore, to generate the alternating magnetic field, Litz wires are especially effective below 500 kHz and rarely used above 2 MHz [143] [148]. This is absolutely sufficient for the proposed CPT systems frequency of 20-140 kHz. As magnetic design has a significant impact on competitiveness and capability of the system transmission path, it becomes clear that Litz wires play a crucial role. This, in turn, means that power transfer systems are also limited by the availability and cost of suitable Litz wires.

Highly permeable ferromagnetic core material (like ferrites) positioned below the coils are commonly used, as they provide a path of low magnetic reluctance for the flux with minimized field leakages and hence improved coupling [67] [149]. However, increasing frequency also increases losses due to magnetization reversal (hysteresis losses) as well as eddy currents in the applied core materials [69], which together are described as core losses. By changing magnetic fields (AC), induced loops of eddy currents generate resistive losses that can occur in any material with a conductivity of $\sigma > 0$ (non-zero resistivity). Eddy current losses are proportional to the square of the frequency and to the magnetic flux density predominant in the material ($P_{l,cm-e} \sim B^A \times f^2$) [69] [139] [142]. Moreover, they are proportional to the area of the loops and inversely proportional to the resistivity of the core material. Thus, eddy currents can be minimized by selecting magnetic core materials of low electrical conductivity, like ferrites with high-resistance grain boundaries between the ferrite phases, or by using thin sheets of magnetic material with insulating coating in a plane normal to the flux, known as laminations. [150] [151]

In addition to eddy current losses, the core also experiences hysteresis losses (magnetization losses) arising from the work that needs to be applied in alternating magnetic fields to re-magnetize the core in the rhythm of the frequency. They only occur in materials with a relative permeability $\mu_r > 1$, for example in all ferromagnetic materials. Microscopic friction losses that result from the constantly changing orientation of the inner elementary core structure in an external magnetic field cause heating. Each time a

magnetic field in the core is reversed, a small amount of energy is lost due to hysteresis within the core. The amount of energy lost in the material in one cycle of the applied field is proportional to the area inside the hysteresis loop, and is dissipated as heat. The coercivity H_c is the degree of magnetic hysteresis and caused losses in the core materials. Since the energy lost in each cycle is constant, hysteresis power losses increase exponentially with frequency ($P_{l,cm-hy} \sim B^A \times f$) [140] [142]. Therefore, highly permeable core materials are used for field guidance in CPT systems, e.g. with a relatively high magnetic permeability μ_r , high saturation B_s (more than 200 T), and also very small coercivity H_c . To minimize core losses in high frequency applications like CPT systems, non-conductive magnetic materials, like ferrite (low conductivity σ , high permeability of $\mu_r \gg 1$) are perfect for field guidance and mainly used as a suitable core material in CPT systems. With small coercivity H_c and a high saturation induction of the ferrite B_s , they have low hysteresis losses. Ferrites are available in a wide variety of material compositions with different magnetic and mechanical parameters. For the frequency range of CPT systems (20-145 kHz), manganese-zinc (MnZn) ferrites are commonly used [150] as they have high permeability (typically in the range of 300-18,000, usually 2,400 [123]), small coercivity H_c (5-100 A/m), high saturation flux density (0.2-0.5 T), and good performance at frequencies from a few kHz up to as high as 1 MHz with low losses [142].

Aside from commonly used MnZn materials, there is a significant number of alternative soft magnetic core materials, featuring high saturation induction, high initial permeability, and low core loss in relation to frequency. Various soft ferrites and a number of non-ferrite materials including Fe-group amorphous alloys, Fe-Al-Si and nano-crystalline alloys can also in theory be used as core materials in CPT systems [152] [153]. However, alternative materials like powder-/particle-based ferrite cores, iron flakes, and nano-crystalline iron foils all do not attain the characteristics of conventional ferrite at higher frequencies. Even though research results are sobering regarding their magnetic characteristics, the opportunities that arise from magnetic conductive compounds made of plastics are still enticing from a production perspective. The use of nano-crystalline iron foils still seems to be promising, as well, as there are more and more system designs that try to adapt their magnetic design to the use of "amorphous" nano-crystalline iron foils. Hybrid core structures have been developed that consist of MnZn ferrites and nano-crystalline iron foils at different areas of the pads in order to combine the optimal characteristics of both materials [154] [155]. However, it is quite challenging to apply such a material with its directional dependence particularly in loosely-coupled CPT systems because of its stray leakage, which will result in higher losses and heating.

Coils without any core material as shown in [119] are generally unsuitable for high power applications. Coreless coils need to be operated at higher frequencies in the MF to VHF band (range of hundreds of kHz to MHz) to compensate for lower coupling and to

maintain good efficiency [3]. In addition, especially in EV underbodies with conductive or ferrous materials in close proximity to the system, eddy currents caused by high leakage-flux and hysteresis losses will heat up vehicle chassis and floor pans that are typically steel-based (medium conductivity σ , high permeability μ_r) and severely reduce Q [126]. It is therefore crucial to block such leakage flux in EV charging. This topic becomes even more important for future lightweight structural vehicle components like GFRP with a permeability of $\mu_r=1$ and negligibly low electrical conductivity. They are essentially “transparent” to magnetic fields, which means the magnetic field from the primary coil would penetrate the vehicle underbody practically unhindered [69]. Shielding magnetic alternating fields is generally achieved at the expense of power transfer efficiency, as eddy currents are induced in electrically conductive shielding materials [121]. Therefore, thin (~ 0.1 -3.0 mm) aluminum shielding back plates (high conductivity σ , low permeability μ_r) are typically used to block flux leakage above the pad and thus shield the EV chassis and surrounding area from stray magnetic fields in compliance with magnetic field exposure guidelines [87] [156]. Aside from conduction shielding, the magnetic flux should be channeled in a way that it cannot radiate unimpededly toward the chassis during operation, anyway. In this context, ferrites can act as additional passive shielding, resulting in lower overall leakage paths with increased magnetic coupling coefficient k , and preventing excessive energy loss in surrounding materials [3] [41] [67] and/or to protect electronics (communication, rectifier, etc.) in the charging devices [83] (see also tests with several different degrees of ferrite damage in chapter 6.1). Tab. 8 summarizes the properties of different materials with their effects caused by AC magnetic fields.

Tab. 8. Comparison of different materials and the effects caused in the materials by AC magnetic fields.

	permeability μ_r	electrical conductivity σ [S/m]	effects caused by AC magnetic fields
steel, iron	ferromagnetic (~ 300 -10,000)	conductor (10.02×10^6)	heating
copper, aluminum	dia-/para- magnetic (~ 1)	conductor (58.00×10^6)	field-shielding
ferrites	ferromagnetic (~ 10 -15,000)	semiconductor (MnZn), isolator (NiZn)	field-shielding and guiding
GFRP	diamagnetic (~ 1)	isolator ($\sim 10^{-13}$)	no effect

It has thus become clear that CPT depends on recent developments in power electronics and magnetic materials (especially Litz wires and core materials) [41]. Thus, the focus of this work is to derive the production challenges for these sensitive materials. The following presents a detailed set-up of materials in current charging pad designs.

4.2 Basic charging pad types

With continuous improvements in power electronic components, the performance and efficiency of a contactless power transfer system is largely determined by the magnetic design and the arrangements of receiver and transmitter coils and field guiding materials [54] [87]. Thus, magnetic design is one of the main distinguishing features between the various pad types [67], which has led to continuous development of new coil design approaches. A presentation of different coil designs will subsequently reveal the resulting challenges for the in the scope of this thesis developed production processes in chapter 5.

4.2.1 Comparison of single-sided circular and double-sided solenoid systems

The following generally compares the two common practical base charging pad types, single-sided circular and double-sided solenoid, and compares their main characteristics concerning positioning tolerance, field emission, and their future viability, e.g. regarding to inter-operability.

Derived from pot cores, single-sided circular magnetic structures with a single circular wound Litz wire in the form of a flat spiral are the most intuitive coil designs [67] and therefore the most commonly proposed to couple flux between a primary transmitter and secondary receiver over the past decade [67].

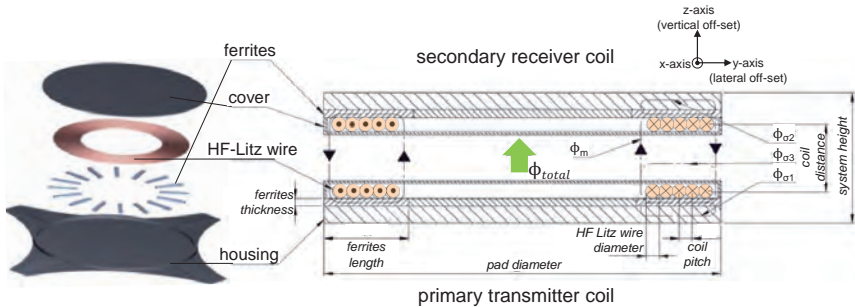


Fig. 31. Cross-sectional view illustrating magnetic field lines in a circular pad.

As shown in Fig. 31, it is a simple structural design like a circular pancake coil positioned on a material with small magnetic reluctance. Usually, I-shaped cores are used

for traditional circular coupler designs, as ferrite magnetic pot-, U-, or E-cores are too thick and hence unsuitable for EV charging [54]. Circular transmitters essentially produce a symmetric vertical magnetic field ($\phi_{total} = \phi_m + \phi_{ox}$) around their center points [3] [64] [123]. Thus, the magnetic field distributions of circular pads are toroid-shaped like a fountain [29]. This coil design has been used in several research projects [55] [56] [61] [157] and is at the focus of a wide range of companies [58] [83].

In addition to the above-mentioned single-side flat circular pads, alternative topologies are developed based on solenoid couplers. They are typically a rectangular flat ferrite core with a solenoidal coil wrapped along its length. This makes solenoid pads thicker than single-sided pads, as shown in Fig. 32.

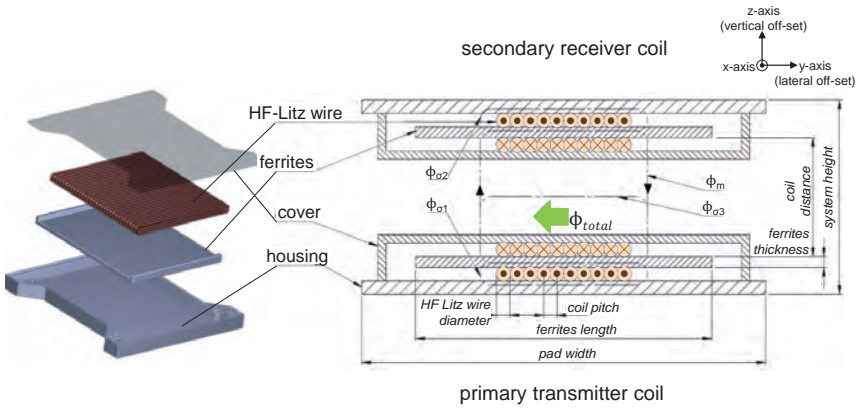


Fig. 32. Cross-sectional view illustrating magnetic field lines in a simple solenoid pad.

The coil arrangement channels the flux along the length of the ferrites from one pole to the other. In consequence, the direction in which magnetic flux passes through the coils is different from that of circular pads. Polarized solenoid transmitters essentially create a horizontal flux profile (Fig. 32) compared to the vertical field lines of circular pads (Fig. 31). Thus, the magnetic field of these transformers is arched, emerging on both sides of the pad [29] [44]. This coil design is also studied in several research projects by several universities and companies [51] [64] [124] [158].

4.2.1.1 Positioning tolerance and size of the pads

It cannot be expected that a driver will always park the vehicle perfectly over the primary charging pad. If the need to park very accurately becomes a hassle, it will negatively affect customer acceptance. Accordingly, positioning tolerance is a main convenience factor for CPT-based electric vehicles. This is even more important as large positioning

inaccuracies may also bring large losses. Suppliers and OEMs are developing automated parking solutions which support the idea of CPT even with smaller CPT systems and smaller charging zones. These systems automatically position vehicles until an adequate alignment has been reached and the charging operation can be activated [6]. To do this, the vehicle has to be equipped with power steering, sensors (optical, quasi-optical, and/or ultrasonic), and the ability to detect when the electric vehicle is properly placed for contactless power transfer [6] [134]. However, as not every car may be equipped with an automated parking system, simple pad designs with sufficient tolerance to lateral (y-axis) and longitudinal (x-axis) misalignment are still necessary to allow for easier parking.

Therefore, circular and solenoid systems need to be compared regarding their tolerance to horizontal misalignment (Δx and Δy). Circular systems have the advantage that a vehicle can approach them from any direction [41]. However, their flux pattern also limits circular pads regarding operational air gap and horizontal tolerance [24]. For conventional circular pads with identical primary and secondary pads, the fundamental flux path height²⁷ is a quarter of the pad diameter [67]. In addition, flux cancellation effects create a power null in the power profile at a horizontal off-set of approximately 40% of the primary pad diameter. In this position, the flux directions from opposite sides of the transmitter pad coil cancel each other, effectively reducing mutual coupling to zero and resulting in almost no induced voltage in the receiver pad coil [3] [120] [159]. Thus, in order to obtain a coupling coefficient that is sufficient to deal with large air gaps and misalignments, the pad diameter needs to be scaled up substantially [120]. These aspects have to be considered when developing circular pad systems with large air gaps or higher power levels [24]. Nevertheless, circular designs with smaller secondary sided pads (secondary side ~250x250 mm, primary side ~700x800 mm [58], secondary side ~300x300 mm, primary side ~500x500 mm [160]) have recently been presented that are sufficient for low-power 3.7 kW transfer systems.

In contrast, polarized pads like solenoids produce a horizontal field, which presents significant improvements in coupling [10] [159] [161]. The fundamental flux height is approximately half the length of the pad [24], while the maximum flux heights of circular pads are less than one fourth of the overall pad diameter [3]. Consequently, polarized pads essentially produce twice the flux height of a circular coil with the same linear dimension, which translates into a 20-25% higher coupling factor k [41]. If minimized pad size is the most critical factor, double-sided pads can achieve the same coupling factor k as a circular single-sided pad at half the size. However, solenoid pads have different flux patterns depending on the direction in which the vehicle approaches the pads, limiting tolerance to misalignment in one direction [41]. This has to be considered as first

²⁷ The flux path height corresponds to the ability to throw flux to a receiver pad placed above.

research results on parking behaviors show that drivers have more difficulty handling longitudinal misalignment (x-direction) than lateral misalignment (y-direction) [55]. However, misalignment in longitudinal x-direction can much more easily be corrected by the driver or even avoided than lateral misalignment in y-direction, for example by simple mechanical aids like wheel chocks or other simple guides. It is therefore preferable to orient polarized (solenoid) pads inside the vehicle longitudinally (x-direction along the central vehicle axis) (Fig. 33) [24] [161].

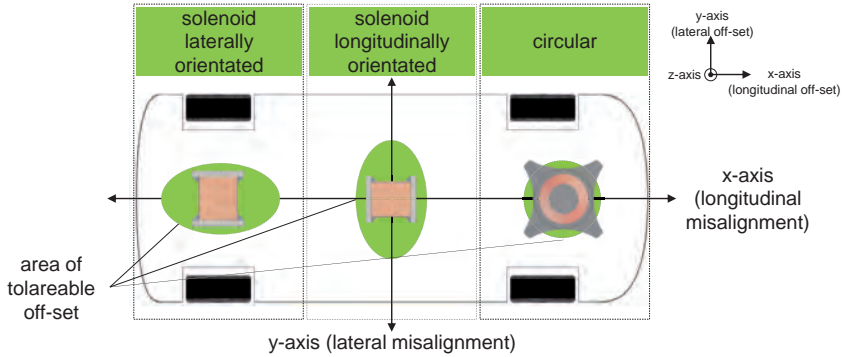


Fig. 33. Direction-dependent integration of different pad designs in the vehicle underbody in the context of tolerable off-sets.

Thus, on the one hand, double-sided solenoid systems allow for smaller pad dimensions than single-sided circular pads in compact light-weight designs [161]. On the other hand, solenoids present different performances in lateral and longitudinal misalignment that have to be considered.

4.2.1.2 Field emissions

Aside from positioning tolerance, field emission is of major importance for OEMs, as the systems have to comply with emissions regulations and guidelines such as ICNIRP [47] [67]. CPT systems may cause issues due to their flux pattern when integrated in the vehicle underbody (see safety zones in chapter 2.3). CPT must not harm living organisms (humans, animals) and may also not interfere with other devices such as keyless entry systems, electronic control systems, pacemakers, or radio-frequency identification (RFID) systems [124] [162]. The PATH project, for instance, reported problems with magnetic fields that interfered with the electronic engine controls of non-RPEVs passing the CPT segments [2].

The structure of circular pads naturally results in a desirable single-sided flux pattern, ensuring low loss and leakage levels [24]. Moreover, the coils sit above ferrite strips

guiding the majority of the flux out of the front of the pads upwards towards a receiver, thus avoiding unwanted rear flux paths [10]. Especially larger circular pads and ferrite layers that extend beyond the coil area essentially re-capture returning main flux ϕ_m and help containing leakage flux ϕ_σ . Circular pads therefore have comparatively low field emissions [41] [157]. Aluminum shielding added to the back of the pad blocks and thus minimizes stray fields in surrounding metallic materials, like steel chassis under an EV [67]. Shielding has only little effect on pad efficiency, as it only acts to stop leakage flux ϕ_σ rather than main flux ϕ_m . This is particularly beneficial for electromagnetic compatibility (EMC) on the vehicle-side pick-ups and hence one of the main reasons why circular power pads have been well researched and optimized for EV charging systems.

In contrast, solenoid systems produce strong horizontal flux out of the ends of the pad with equal flux paths on both sides (front and back, see Fig. 32) [161] with field leakage which is particularly difficult to suppress [54] [163]. Additional shielding is therefore needed to avoid low coupling factors and EMC issues [120] [161]. Shielding, however, leads to additional losses, which may significantly reduce the native Q of the coil and hence drop system efficiency below practical levels for an EV charging system. [41] documents expected magnetic losses as high as 10%, compared to target values of no more than 2-4%. Researchers are working on several solutions for this problem and further adaptations to the magnetic design, as presented in chapter 4.2.2.

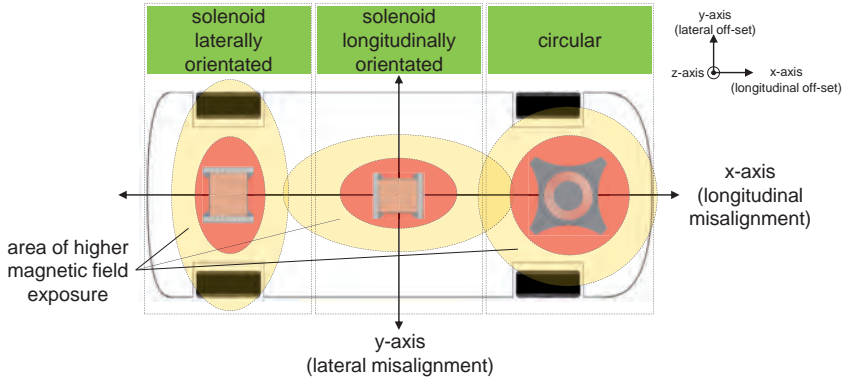


Fig. 34. Direction-dependent integration of different pad designs in the vehicle underbody in the context of potential EMC issues.

4.2.1.3 Future viability – inter-operability

Another very decisive aspect of different coil designs is their future technological viability, which must be considered carefully with regard to global market introduction and a

potential future public charging infrastructure. Different coil designs will not be inter-operable, which means that not every car will be able to use every charging spot. Standardization of CPT systems is thus one of the main challenges, but vital to open up new fields of application [41]. As other fields have shown (diverse conductive plugs²⁸/low-power CPT applications²⁹), different standards that evolve simultaneously can cause problems and potentially slow down market introduction and widespread commercialization, as the future of the products is difficult to predict [165]. Without standards and inter-operability, infrastructure providers will not be willing to invest in a public infrastructure. Most importantly, there is a danger of alienating customers when the existence of several standards impedes sales and thus economies of scale. On the one hand, standardization processes slow down technical development to some extent. On the other hand, however, standards that are set prematurely can also impede development, especially in a very fast evolving technology field like CPT (see new coil designs in chapter 4.2.2).

The issue of circular versus solenoid base pad designs make the problem with inter-operability obvious. The magnetic field patterns of the two pad designs differ greatly (mainly vertical versus horizontal flux pattern). A circular transformer produces magnetic flux from the center pole to the outer pole in all directions, whereas a solenoid core transformer produces magnetix flux in only one direction [166]. As a result, the two types are incompatible without further adaptations. If a vehicle fitted with a circular receiver parks over a polarized transmitter, there will likely be some loss of power and significant leakage flux, which might breach field exposure limits [10] [47]. Moreover, operation between different coil types might not meet tolerable levels of minimum efficiency (~90% [46]). Fig. 35 illustrates different possible misalignment situations between circular and solenoid pad designs.

As can be seen, in the case of a longitudinally orientated solenoid secondary and a circular primary, and lateral misalignment (y-axis), there is almost no magnetic coupling between the circular and the solenoid system. This is also the case if a circular and solenoid pad is perfectly aligned one over the other. Magnetic fluxes from the base circular pad attempt to pass upward through its coil center. However, the shape of the center portion of the secondary solenoid pad does not allow the magnetic fluxes to pass. As a result, no magnetic circuit can be formed. With longitudinal misalignment (x-axis), magnetic coupling remains possible between the two pads [64]. This correlation becomes quite more complex with additional pad designs and shows the necessity to study the inter-operability of a receiver pick-up with several types of transmitters. As a result, intense research efforts are dedicated to comparing different coil structures in all possible misalignment situations of the x-, y-, and z-axes [46] [167].

²⁸ Several standards for different types of plugs including IEC62196, SAE's J1772 and CHAdeMO [164].

²⁹ Competing approaches like the Qi-Standard (Wireless Power Consortium), Power Matters Alliance, A4WP (Alliance for Wireless Power) or even company-specific approaches.

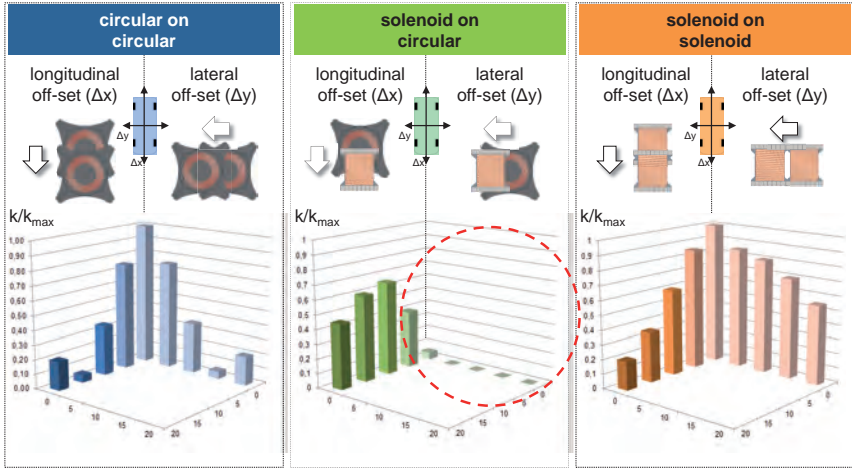


Fig. 35. Circular-solenoid pad design correlations for inter-operability (based on [64]).

Aside from the principal flux design (e.g. circular versus solenoid), inter-operability involves a number of other decisive factors, such as power levels, operating frequency range³⁰, communication standards, system performance (minimal efficiency), system safety, pad location in the underbody, misalignment tolerances, and alignment techniques [41]. Inter-operability improves as these parameters are more precisely defined, which, however, limits technology providers' possibilities for differentiation. Therefore, the past few years have seen a number of standardization boards and industrial consortia push for specifications and standards on the application and commercialization of contactless power. The Society of Automotive Engineers (SAE) recently announced that it will complete the Technical Information Report (SAE J2954 Wireless Charging Task Force) for wireless power transfer for light duty, electric, and plug-in electric vehicles, which involves field data confirmation in 2014 [31]. Outside of North America, other international (IEC/TC 69 JPT 61980 Electric vehicle wireless power transfer systems) and national organizations (e.g. the Japanese Automobile Research Institute or the German Commission for Electrical, Electronic & Information Technologies - DKE GAK 353.01³¹ [48]) are doing the same in collaboration with industry [20].

4.2.2 New coil designs

As traditional single-sided circular coils and simple double-sided solenoid coil structures still have some drawbacks, this thesis presents the new magnetic designs, providing greater flux height and versatility.

³⁰ In 2013, the SAE J2954 announced that it would issue a frequency of 85 kHz [31] [167].

³¹ The DKE GAK 353.01 developed the application guide VDE-AR-E 2122-4-2 as a first step towards establishing a standard [48].

4.2.2.1 Improved solenoid systems

To further improve the efficiency of solenoid systems and to adequately control field leakage, [163] [168] introduce H-core designs for solenoids that have additional ferrite “wings” on both sides of the main ferrite plate to guide the flux towards the receiver pad. This is to ensure good coupling and to further improve tolerance to horizontal misalignment [3] (Fig. 36).

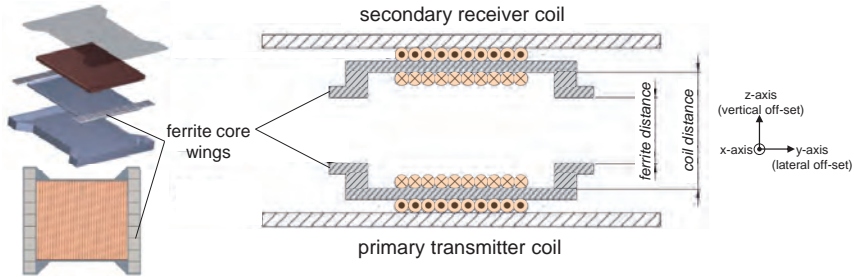


Fig. 36. Double-sided H-core pad design (based on [163] [168]).

The University of Auckland found similar ways to improve the efficiency of the solenoid systems. In 2010, [54] published a specially formed solenoid type transformer with a flux pipe. Analogous to the H-core approach of [163] [168], both pole ends of the flux pipe are designed as wings with a minimal amount of extra ferrite [3] [54]. The flux pipe is created by positioning two coils at the ends of the mid-section of a solenoid pad, resulting in a comparable set-up as proposed in [163] [168]. This polarized dual-loop design channels flux from one pole end along a maximum length of ferrite to the other pole end. Due to the separated coils and longer ferrite strips, the field naturally achieves a higher flux path height with minimized inductance, thus improving the coupled power rate [3]. Unfortunately, as these solenoid topologies are essentially double-sided, they produce equal flux paths on both sides of the pad (front and back) which entails the problems described above in the presence of metallic materials [67]. In addition, as the coils are wrapped around the ferrite core in a double-sided winding pattern, pads are thicker than single-sided pad designs.

4.2.2.2 Polarized single sided flux pads

In order to reduce the rear flux and still maintain the advantages of polarized pad designs, [24] derived a single-sided flux-pipe pad from the double-sided solenoidal flux pipe pad. Placing two flat circular coils in close proximity to each other on top (rather than wrapped around) creates a magnetically permeable core with a single-sided pad design that still shows a polarized field pattern [67] [169]. This topology, called Double-D (DD, butterfly) pad (Fig. 37), reduces pad height as the coils do not need to be wrapped around a ferrite [54].

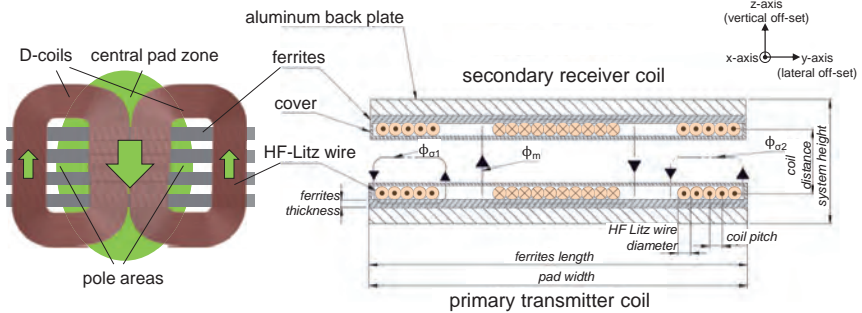


Fig. 37. Single-sided DD pad design.

As with a single-sided circular pad, aluminum shielding can be placed underneath with little impact on Q , as it only needs to shield stray fields, resulting in little leakage flux below the coils and negligible loss [170]. The two D coils are arranged in a way that they meet along a common line in the pad center, at right angles to the ferrites [41]. AC current passing through the lengths of the HF-Litz wires flows in the adjacent portions of the two D coils in the same direction in the center part of the pad [170]. The lines of magnetic flux arch between the coils in the form of a zone of high flux concentration [10] [170]. As a result, a polarized field pattern is created and the two D coils act as pole areas.

[24] further discovered that DD-pads do not need solid pieces of ferrite, as ferrite strips interspersed spaced along the length of the pad - forming a flux-pipe in the center of the pad - can obtain similar performance. This use of relatively little ferrite makes the structure lighter and changes reluctance since the plate is more permeable along the ferrite and less permeable across [41]. As with the solenoid flux pipe, the section of this central flux pipe between the coils should be made as long as possible to achieve high intra-pad flux. Therefore, windings outside of the center of the pad are laid closer together than those windings in the center of the pad between the pole areas [169]. This is advantageous, as it minimizes the remaining length of the coil and thus saves copper and reduces R_{AC} . This eventually results in coils shaped like Ds. As in the case with solenoids, the fundamental path height (h_z) is proportional to half of the pad length, which makes them superior to conventional circular pads. DD-systems are ideal for stationary charging, as DD-systems in general have a much wider horizontal coverage in both x- and y-directions and throw flux so high in the z-direction that smaller-sized couplers can potentially be used for the same power transfer if required.

Due to the mainly horizontal flux pattern created by DD primary pads, single-sided DD primary pads and double-sided solenoids are inter-operable. This allows also for small secondary solenoids with larger primary DD ground pads as described in [158] (Fig. 38).

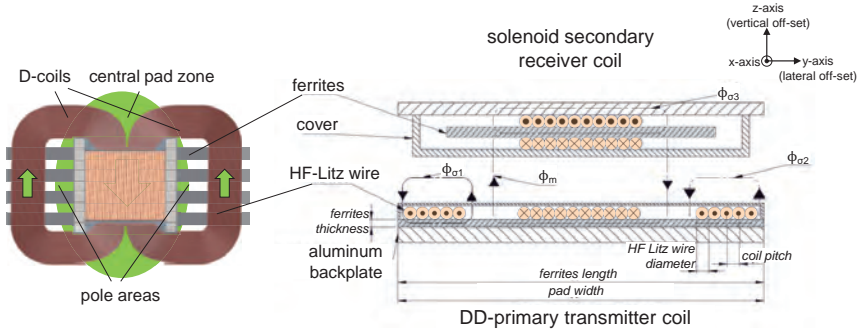


Fig. 38. DD-solenoid approach (based on [158]).

However, data from initial DD-pad system simulations indicates that, comparable to solenoid systems, coupling and power transfers are better suited for large air-gaps, but with the set-up in Fig. 38 the performance in x-axis (longitudinal) is better than in y-axis (lateral). This is due to the fact that DD-receivers mainly couple horizontal flux components in x-direction, horizontally along the central axis of the pad. A coupling null occurs when horizontal misalignment is $\sim 34\%$ of the pad length in the y-axis. At this position, flux enters and exits the same coil, inducing almost no voltage at all. This imposes a fundamental y-axis tolerance limit for DD coils similar to circular pads [24]. Therefore, to significantly improve the performance in the y-axis, [24] [67] propose adding a third circular coil, called “quadrature” to the DD-system in the center of the secondary pick-up side, as shown in Fig. 39. This Q-coil is essentially a flat circular or rounded square Archimedean spiral coil and is placed symmetrically across the line where the two original coils meet in the DD pick-up pad.

Although the quadrature coil sits under the DD-coils, its position ensures that it is magnetically decoupled from the DD-receiver coils [24]. The quadrature coil can be treated independently, as it is independently tuned and rectified before being added to the DD output [23] [24]. Thus, combined with the DD coils, a DDQ pick-up can capture both the vertical (Q-coil) and horizontal (DD-coils) components of the magnetic field [171] [172], which enables inter-operability. In addition, in a pick-up situation that includes vertical and horizontal components of the magnetic field, the pick-up coil is sensitive to both of them and can take power from both of them. This creates sufficient horizontal misalignment tolerance relative to the transmitter pad. As the coupling of one coil reduces, the coupling of the other coil increases [10]. Based on this, [41] shows that DDQ pick-ups

can achieve a power zone about three times larger than matched circular-circular or matched polarized-polarized combinations. Ground-based transmitter pads can also be modified into a DDQ-coupler. However, this should only be considered if interoperability with a range of different receivers is needed. A DD-primary eliminates the need for a second synchronized power supply to separately drive the independent coils (D and Q) [41]. Moreover, for a DDQ-receiver, a DD-primary already produces the desired flux pattern [24].

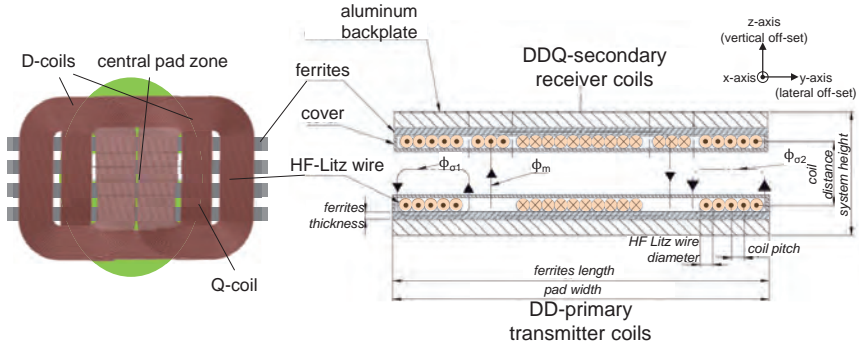


Fig. 39. Single-sided DDQ pad design (based on [24]).

However, while DDQ-systems provide superior performance and position tolerance, their windings require larger amounts of copper. Therefore [10] [123] propose a polarized multi-coil coupler, called bipolar pad structure (BP), to create a receiver which uses 25-30% less copper, whose performance is almost identical to that of a quadrature pick-up, and which is also able to capture both the vertical and horizontal fields [123]. Moreover, it is simpler to construct and to produce as only two coils are used [41] [123]. [173] also proposes the use of a bipolar pad structure (BP) for the primary side. BP pad design consists of two coils that are identical, coplanar (except in one spot where one of them passes over the other) [10], partially overlapped, and ideally totally mutually decoupled from one another, with one side sitting immediately next to a ferrite structure [10]. The overlap between the two coils is designed to ensure that ideally, energizing one coil will induce no voltage in the other (mutual inductance/coupling is zero). Such mutual decoupling enables the two coils to be driven (tuned and controlled) independently, with independent outputs [10]. Zero mutual inductance is difficult to achieve in practice. It is important to minimize mutual interference between the coils to avoid harm to the inverters [10]. In consequence, inter-operability with circular receivers can be achieved by operating just one of the bipolar pad coils (whichever is best aligned with the receiver) to produce a vertical field suitable for a circular coupler [10]. However, combining circular and polarized systems requires careful consideration. When using a

large circular primary and a BP polarized secondary, a perfect alignment of the pads will actually lead to inefficient power coupling. A vehicle must purposefully park off-set to properly align only one of its BP coils to a circular primary [41], which can in turn cause issues of flux leakage and heating effects, and thus a potential violation of guidelines and vehicle safety zones as described in chapter 2.3.

4.2.2.3 Additional design approaches

In addition to the circular and polarized pad designs described above, a wide range of further design approaches has been developed to enhance inter-operability between different pad designs and power levels, and to improve tolerance to misalignment in the x-, y- (horizontal) and z-direction (air gap variations). To improve inter-operability between circular and solenoid systems, [14] and [166] recently presented several approaches with double-sided multi-coil solenoid winding patterns. They added a central magnetic pole to a solenoid by dividing a coil of the H-shaped core transmitter into two, creating an H_c -core with two solenoid coils, as shown in Fig. 40.

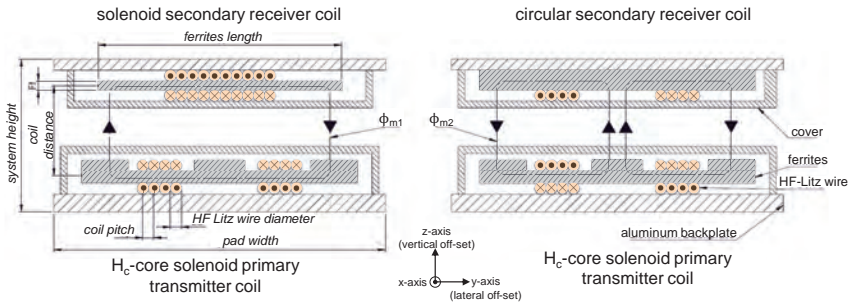


Fig. 40. H_c -core solenoid-circular approaches - H_c -core-solenoid, H_c -core-circular (based on [14] and [166]).

The magnetic field structure can thus change depending on whether the central magnetic pole is used or not. This makes it possible to power both solenoid-shaped core receivers (central magnetic pole is not used) and circular receivers (central magnetic pole is used) with one single pad design. [161] also presents a multi-coil solenoid winding pattern that is inter-operable with normal and rapid charging (in this case 1.5 kW & 10 kW). Hence, the primary winding structure is split into two or more and alternately connected in serial to avoid high primary terminal overvoltage [161]. [174] also proposes a multi-coil solenoid system to further improve lateral tolerance. A number of switchable coils are arranged in the primary side transversely to the vehicle's longitudinal x-axis. Thus the effective length of the primary side coil can be adjusted since the secondary side in the vehicle has to be kept as small as possible. This solu-

tion selectively activates only those coils that are located near the vehicle's receiver coils, making it possible to compensate lateral misalignment (y-axis) of the vehicle. This also prevents generating electromagnetic fields out of alignment with the respective other coil. In summary, such double-sided solenoid-based multi-coil approaches can improve inter-operability by using different sizes of coils for different vehicle sizes. In case of air gap variation, coil sections can be switched on or off to maintain the required voltage level of the secondary coil, which can also help adjust transmittable power levels. [161] [174]

[60] [175] describe a similar multi-coil approach based on single-sided circular pad designs with mutually spaced-apart winding turn regions of different sizes (one inside the other) that can be activated separately. This again results in a variable magnetic field with adaptively optimized coupling factors for different charging situations (air gaps, power levels, during start-up procedure, etc.). [170] proposes a single-sided polarized multi-coil approach with two or more partitioned HF-Litz wires continuously wound into two poles each, as shown in Fig. 41.

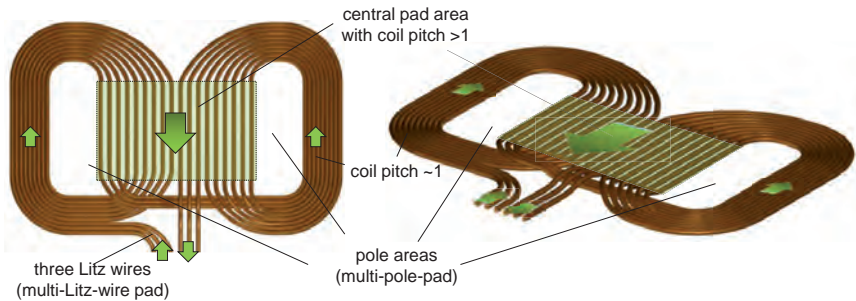


Fig. 41. Multi-pole multi-Litz wire pad topology (based on [170]).

In this approach, coils are arranged in such a way that the current always flows in the same direction as diagonally-opposed coils, and in the opposite direction to adjacent coils, creating a flux pipe when AC current passes through the coils [170]. The more separately arranged HF-Litz wires are in a pad, the greater the range of inductance values that can be connected by switching devices. The pad can thus be flexibly adapted to different charging situations, such as opposing pad designs with differing inductances, power levels, and air gaps. In addition, misalignment tolerance can be increased, as additional Litz-wire parts in the pads can be activated to cover larger areas, depending on the pad design.

Pad designs that are compatible and inter-operable with stationary and dynamic charging infrastructures make the vision of RPEV [10] even more appealing and future-proof.

Therefore, the following presents RPEV system topology and coil design options that are currently being considered.

4.3 CPT systems for RPEVs

Literature has been discussing electrified roadways that power moving RPEVs [171] for four decades. Early US patents [176] [177], amongst others, show first proposals of track and coil designs that allow vehicles to pick up power contactlessly while driving. More and more projects have been developed and hardware test tracks with several different coil design approaches have been built [2] [33] [95]. These research projects focused on testing diverse challenges of a RPEV infrastructure, e.g. how to transfer sufficient power levels to RPEVs over relatively large and varying air gaps. For an EV with an air gap of 175 mm to the road and a track system in the road covered by 75 mm of asphalt/concrete, the de facto air gap is 250 mm. Ideally, the tolerance to vertical (Δz) and horizontal (Δx and Δy) misalignment should be even greater at higher power levels for RPEVs [24]. Vertical and horizontal misalignment causes significant changes in the magnetic circuits that couple the power from the roadway to the vehicle and make it difficult to tune the system [30]. For unguided vehicles at higher speeds, the required misalignment tolerance could easily be as high as ± 300 -600 mm to enable a vehicle to receive full power across the width of the lane [87]. This makes (semi-)automated driving assistance attractive for RPEV-systems, as well (as already discussed for stationary systems), with automatic tracking that keeps the vehicle in an optimal lateral position over the infrastructure [3] [67]. In the PATH project [2] [42] and recently in the "Partnership for Roadway Electrification and Automation" [178] the advantages of connecting roadway electrification and automated driving (roadway automation) have already extensively been discussed. To comply with safety requirements, the energized roadway coils should only be activated to produce a magnetic field when a sensor detects the presence of a passing vehicle [179]. Other road users will not be exposed to the magnetic field, as only those parts of the roadway directly underneath a passing EV are energized. In the absence of a receiving device, or if the receiving device no longer needs to capture power, the power source should automatically revert to a power-saving "idle" state. This ensures that conventional vehicles can travel on the roadway unaffected by magnetic fields. Under special circumstances, for example in case of debris, animals, or humans on the roadway (traffic jam, accidents, etc.), the systems must shut off or at least drop to safe flux levels within ICNIRP limits [47]. Systems must also ensure that objects in the gap do not overheat in an unsafe manner [41].

The magnetic design of the power track is critical to minimize costs and maximize efficiency in a large-scale implementation. The sequence of coils in a continuous strip along the road tends to be different from stationary systems and can basically be divided into distributed (elongated conductor structures in the two-digit meter range) [180]

[181] and lumped pad-based system approaches (segments with a length of about 1 meter), as shown in Fig. 42 [24] [87].

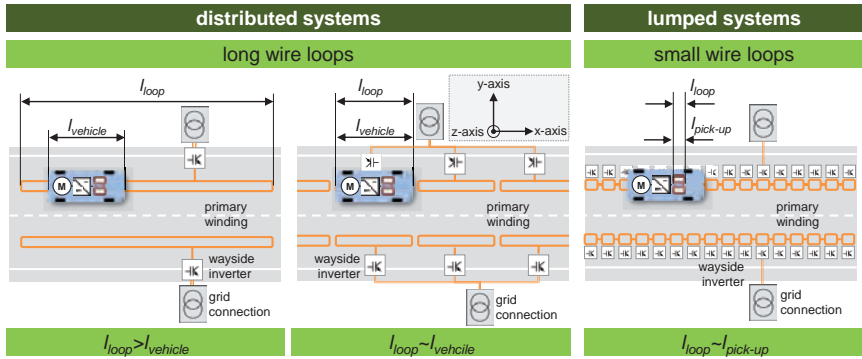


Fig. 42. Basic magnetic structures for RPEV-systems.

4.3.1 Distributed coil structures for RPEVs

Distributed systems are often used for RPEV applications. Conventional single-phase RPEV systems essentially use elongated loops [180] [182] (Fig. 43).

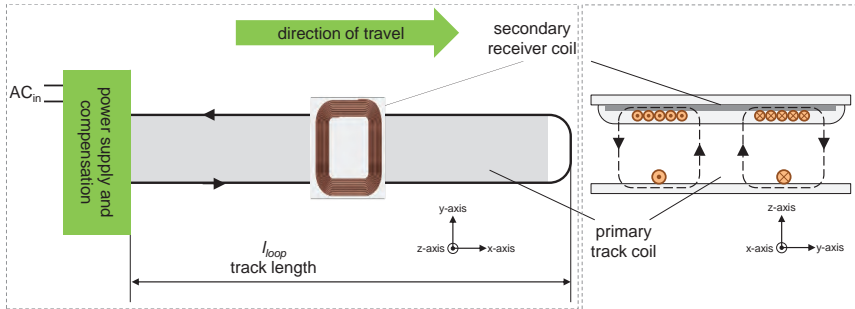


Fig. 43. Single-phase RPEV system (based on [180] [182]).

Such “single-phase track systems” can be set up at relatively low cost, but have so far been impractical for unguided EVs. This is mainly due to the fact that single-phase CPT tracks always have a lateral magnetic field cancellation (power null) resulting in low horizontal tolerance [183]. The needed horizontal tolerance (~ 700 mm) and ground clearance (150-200 mm) for EVs would require automatic guidance systems [87] [90].

In order to improve lateral tolerance (y-axis) for RPEV systems, a single phase track based on a DD-topology has been proposed with solenoid-shaped pick-ups [182] and DD-based pick-ups [184] (Fig. 44).

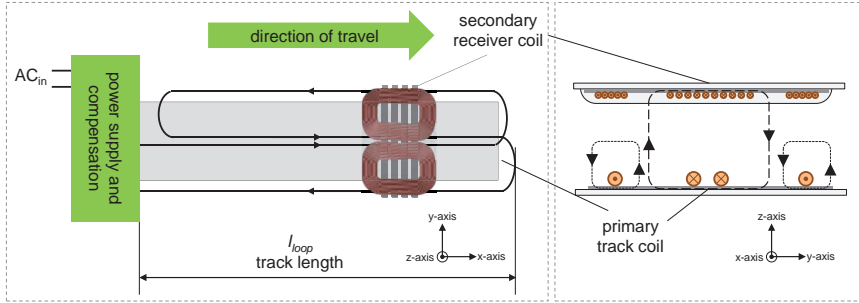


Fig. 44. Single-phase RPEV track system for RPEV based on a DD-topology (based on [182] [184]).

Another approach to improve lateral tolerance (y-axis) for RPEV systems has been proposed by [180] with a “bipolar three-phase track” topology, which has several elongated track cables along the direction of vehicle movement (x-axis) [183] (Fig. 45).

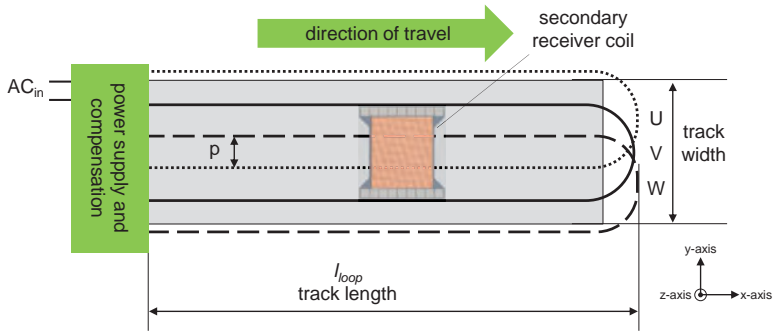


Fig. 45. Bipolar three-phase track topologies (based on [87]).

This track topology uses overlapping wires powered from a three-phase inverter and is called bipolar because a pick-up is exposed to both forward and returning currents to the supply [87]. The distance between the conductors is called the pitch p of the track. This creates a travelling field across the width (y-axis) of the track and provides a smooth power distribution along the track cables. The horizontal flux that is so created can be captured by suitable receivers like solenoids- or DDQ-pick-ups [3]. The windings

on the primary side of this three-phase CPT system operate in a fashion similar to a three-phase linear induction motor. In contrast to a linear induction motor, however, the traveling magnetic field in a CPT system moves at such high speed that positive and negative sequences are of little relevance, because the concept of slip does not apply [41]. However, overlapping tracks do cause mutual inductance between adjacent phases [3]. Another problem is the limited lateral tolerance of bipolar three-phase tracks. Lateral tolerance is improved compared to single-phase systems, but the outer conductors are still not covered and power transfer drops significantly at the edges of the track [87]. In consequence, [87] proposes an alternative “uni-polar three-phase track layout” with three meander-shaped conductors along the width of the track (Fig. 46).

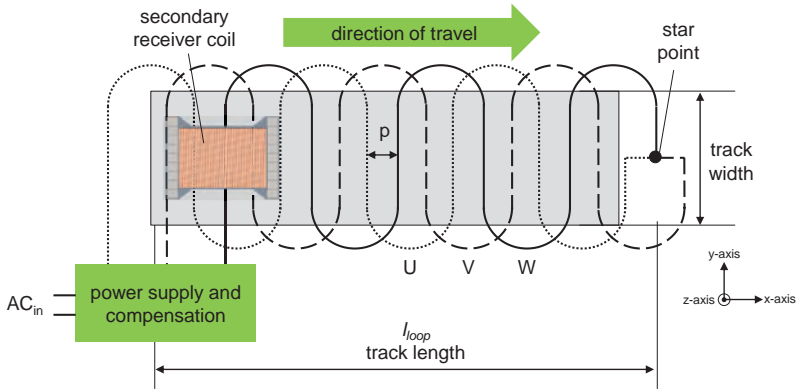


Fig. 46. Uni-polar three-phase track topologies (based on [87]).

This topology is referred to as “uni-polar three-phase track” because there are no explicit return conductors. In this case, the time-varying constructive addition of flux from each conductor results in travelling magnetic pole pairs along the length of the track, in the direction of travel (x-axis) [103], and not along the width (y-axis). This track topology has balanced mutual inductance between phases, making it easier to drive than the bipolar design. Another advantage is improved horizontal tolerance, as the lateral tolerance of a pick-up is determined by the width of the track rather than by its resonant current rating, as shown by the shaded area of full power transfer in Fig. 46. Power is maintained all the way to the edges of the track where the wires loop back [3]. Lateral tolerance can be extended by increasing cable length and widening the track. Adding cable length presents only a linear increase in copper loss and cost, which makes it a much better method than increasing track currents, which leads to an quadratic increase of losses ($P_w \sim I^2 \times R$) (see also chapter 4.1.2) [87].

Matched three-phase to three-phase CPT systems have recently found application particularly with higher power levels in larger vehicles like light rail and buses [34] [41]. The track lengths and three-phase pick-ups are large and well suited for large vehicles, but not for smaller private vehicles [41]. In this context, alternative options of smaller single- or two-phase pick-ups with solenoids, DDQ- or BP-pick-ups are also being discussed intensively [41]. Distributed track topologies present more challenges, as large elongated primary tracks pose a great risk of flux leakage if the smaller secondary cannot capture the field. [185] presented a comparative case study of different single-phase track layouts. The results show that lumped systems improve the coupling coefficient and overall system efficiency, while minimizing the magnetization current, supply voltage ratings, and stray fields [185]. In consequence, the following chapter studies alternative roadway systems whose primary magnetic structure is based on short lumped pads from stationary charging.

4.3.2 Lumped coil structures for RPEVs

[112], and recently also [3] [179] [186] propose the installation of a lumped RPEV roadway system with many smaller pre-fabricated energized ground pads, placed end-to-end along the center of a road lane. For safety and efficiency reasons, they should ideally be smaller than a vehicle's length (no bigger than one or two square meters), so that only those sections that are completely underneath a vehicle at a given moment generate a magnetic field, avoiding energizing and heating unwanted loads [3]. The pads can activate directly under a given moving vehicle at a set power level that is suitable for that particular vehicle (e.g. a higher current may be used for a vehicle with higher power and road clearance demands), creating a wave of power where secondary pick-ups can be localized. [41] therefore propose that each coil segment should be capable of delivering 30-40 kW and above for charging and propelling a vehicle. Such a system can also be used by larger vehicles. The primary track system may couple to two or more vehicle pads simultaneously to enable the transfer of even higher power rates. However, in contrast to distributed track systems, lumped track systems require embedding a larger number of smaller pads in the road. Each pad also needs to be connected to power supply cabinets, which involves significant roadway construction efforts [95] [187]. Nevertheless, lumped systems are advantageous as they are more modular and create redundancy. If one pad (or its associated power supply) fails, only a small section of the roadway stops providing power. Several pads could fail before it affects the functionality of the powered roadway to the extent that pad replacement becomes inevitable [10] [87] [186].

In general, there are several ways to design the primary pad for lumped systems in dynamic roadway applications. Circular pads placed side by side along a highway would entail unavoidable power nulls in power transfer profile between pads. The null occurs at 40% of the pad diameter, so even if transmitter pads touch along a highway, the

power output inevitably passes through zero before moving on to the next transmitter [120]. It is thus difficult to obtain a smooth power profile [67]. Moreover, circular-to-circular pads provide a useful flux height of only approximately $\frac{1}{4}$ of the pad diameter. In consequence, roadway applications require significantly larger circular pads to ensure adequate power transfer. These fundamental restrictions mean that circular pads are only of limited suitability for a dynamic roadway system [3]. To overcome the shortcomings of the circular pad structure, different alternative power transfer structures for RPEV lumped systems have been proposed. [41] and [179] propose the use of lumped DD primary (road level) with DD- or ideally DDQ- or BP-pads on the secondary vehicle side to capture both the vertical and horizontal magnetic fields above a track. This system can provide magnetic flux over a much wider surface, enabling a vehicle to travel from pad to pad coupling power dynamically, and avoiding power nulls. Hence, DD pads do not have to be placed side by side in the direction of travel. They can be placed at expedient spacing (pad pitch) and still provide a smooth power profile and high coupling over a practical working area [41] (Fig. 47).

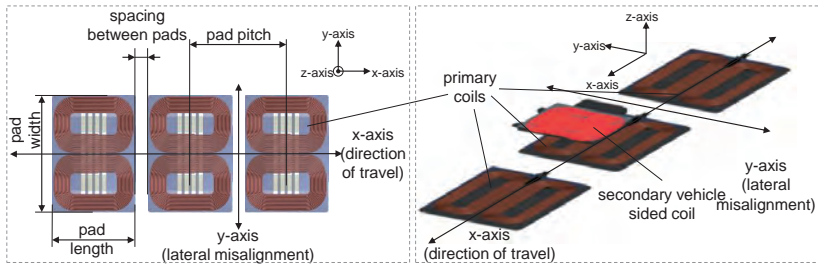


Fig. 47. Inductively powered roadway using many lumped pads (based on [3]).

Moreover, using DDQ-secondaries above DD-primaries works particularly well for RPEV systems. Due to the “quadrature-nature” of a DDQ-secondary to capture vertical and horizontal flux, the RPEV system is not only tolerant to longitudinal misalignment along the direction of travel (x-direction), but also particularly tolerant to lateral misalignment (y-direction) with a reduced need for automated track guidance systems even at higher speeds.

To fulfill commercial potentials, this large (and steadily increasing) variety of capable but complex coil designs has to be considered from a production perspective. In order to make these pad designs marketable and affordable, they have to be suitable for mass production, which calls for automated production concepts as developed in the following chapter.

5 Development and Implementation of Production Concepts for CPT Systems

In view of increasing global interest in EV CPT system launches [11] [12], considerable new potentials for value creation opened up for car manufacturers and their suppliers, in combination with a general increase in demand for EVs. The next few years will be of great opportunity to increase demand for CPT systems, as it is not only purely electrically powered vehicles, but especially plug-in hybrid EVs that will favor CPT systems. Therefore, aside from the factors efficiency, safety, etc., the prospect of mass-producing contactless power transfer components puts manufacturers before further challenges of sophisticated system integration approaches (weight, space, temperature, and EMF requirements), cost reduction, and cycle times. CPT systems will make EVs in a first step more expensive as all EVs will continue to also have a standard plug in the next years. Further down the road, CPT will make its way into mass market vehicles in cheaper price segments, and thus cost will eventually become the most decisive factor for system competitiveness [7]. So far, contactless power transfer systems, e.g. for AGVs or prototypic EV systems, have been produced manually with rigid coil structures due to small unit numbers. This often results in quality variations in the pads [18]. However, as quality is paramount in the automotive industry, it is important to ensure product quality with well-established and reliable production processes with material-specific analyses to control production tolerances and to avoid imperfections. A lack of quality can result in lower efficiency (e.g. because of winding tolerances of HF-Litz wires, cracks in ferrites, etc.) or even be dangerous for the driver and other road users (e.g. HF-Litz wires jutting out of a damaged pad, losing parts of a damaged pad during driving), and may result in expensive recalls accompanied with a loss of reputation. Additionally, the high volatility of the forecast and uncertain sales potentials call for flexible, modular and standardized assembly and handling technologies [16] [17]. Moreover, it is yet unclear to what extent charging pads will have to be adapted to individual vehicle architectures, even with standardized charging pads.

In this context, capable supply chains need to be set up step-by-step as demand evolves - from sub-suppliers all the way to integrating components into the vehicle at the manufacturing plants. It will generally help market development if CPT system designs are optimized for manufacturing and process complexity with ultimately reduced costs [7] [71]. Suitable materials and their specific shapes have to be carefully selected as they determine system function and also have a great impact on associated production processes. Thus, various production technologies and disciplines need to be considered. This chapter covers the entire value chain (5.1) with a focus on the process of winding HF-Litz wire coils (5.2). This process step is especially relevant for product properties and quality, harbors several failure risks, and shows potential for further ra-

tionalization. Therefore, plausibility checks are needed to test different magnetic coil designs for their suitability for manufacturing and assembly.

5.1 Production steps for CPT systems

Charging pads, as shown in the exploded view in Fig. 48, consist of several components and materials with different functions and material behaviors that need to be processed in successive production steps.

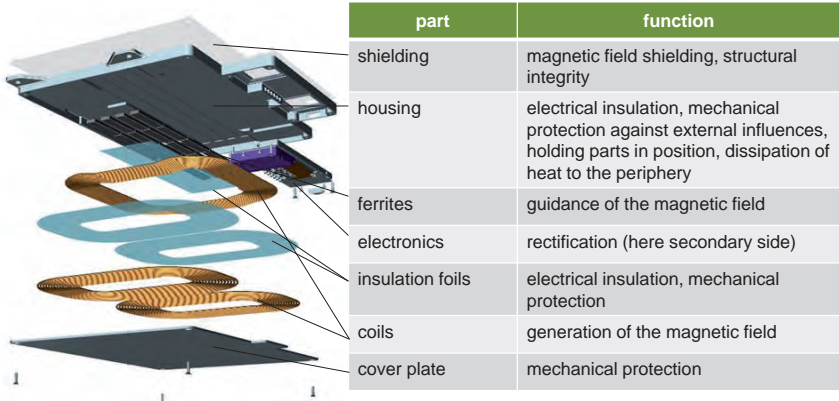


Fig. 48. Exploded assembly drawing of a contactless charging pad based on a DDQ-system topology (secondary side based on [123]).

The production processes for primary and secondary pads vary to some extent, depending on pad size (primary pads are typically much larger), level of electronics integration, sensor systems (e.g. radar sensors for LOP only on primary side), and quality efforts (strict automotive ISO/TS 16949:2009 requirements).

5.1.1 Plastic base parts and housing

First, the plastic base parts and housing of the primary and secondary charging pads need to be produced. The function of the housing is to clearly and robustly position the active materials (coils, ferrites, electronics, etc.) (Fig. 49). Moreover, the housing needs to conform to mechanical, chemical, thermal, and electrical requirements and also has to be suitable for production.

Industrial CPT systems often have heavy and expensive aluminum housings. In contrast, the base parts of automotive charging pads have to be as lightweight as possible and at the same time resistant to mechanical stress. Materials like fiber-reinforced polymers can be used with local stiffeners and ribs to reduce system weight and provide

high bending and tensile strength, and thus a generally high level of wear resistance. Moreover, lightweight housing with ribs and thin walls facilitates the production process, as potential problems like varying shrinkage and thus distortion in the plastic can be avoided.

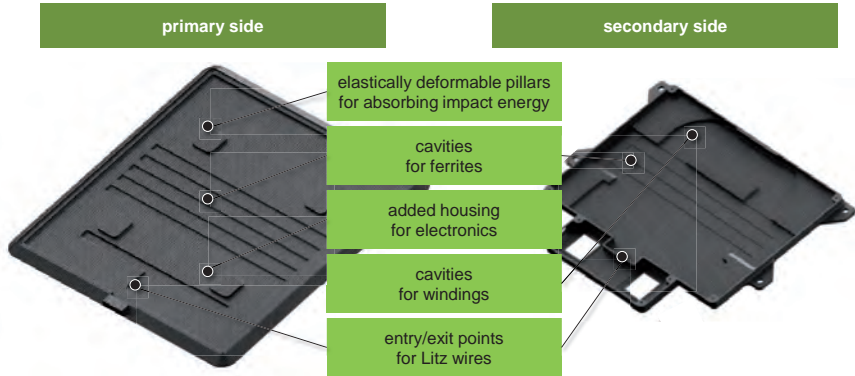


Fig. 49. Charging pad with grooves for ferrites, windings, and electronics.

5.1.2 Assembly of ferrites and electronics

Next, ferrite materials have to be handled and assembled into the provided slots to achieve the desired power transfer flux path [3]. This has to be done carefully since ferrite is brittle and prone to breakage. In addition, ferrite shrinks when sintered resulting in geometric irregularities, which means that ferrite tolerances must always be considered when designing charging pads and especially ferrite cavities. Maintaining correct dimensional tolerances as well as preventing breakage are fundamental concerns of the manufacturing process [188]. Instead of ferrite plates, smaller standardized ferrite bars (e.g. N87 I-cores 93 mm × 28 mm × 16 mm) [24] are commonly used. Although such smaller ferrite bars require more handling steps, procurement cost and risk of fracture can be reduced. For a higher automated process, parallel kinematic robots or SCARA³²-robots with simple vacuum gripping systems offer reliable and safe processing from specific trays or special delivery mechanisms (conveyor belts) to the final position of the ferrites in the pad. Even though the positioning repeatability of SCARAs is higher, the process speed of parallel kinematic robots is superior, ideal for simple pick-and-place applications. However this strongly depends on pad design. For example, cycle times for placing ferrites are less critical in smaller polarized pad designs with smaller ferrite plates or ferrite strips [123] compared to some of the larger circular pad designs that use large amounts of ferrite like [83] [157].

³² Selective Compliance Assembly Robot Arm.

Ferrites should be set into the housing with caution, as higher temperatures may be necessary when fixing/impregnating ferrites that are prone to crack under temperature variations. Optical inspection and flux leakage testing (different permeability caused by cracks in the ferrites) may be included prior to assembly or in-line. It would require further detailed process analysis to determine how to handle and insert alternative materials like nano-crystalline iron foils or thinner ferrite materials into the base parts.

In addition, depending on the packaging of the pads, diverse electronic components need to be assembled (rectifier, inverter, capacitors, positioning-, communication-, and surveillance-systems). In early product generations, coils and electronics can be physically separated in different housings in order to minimize the physical footprint in the vehicle underbody of given vehicle architectures. This facilitates installation at locations with space limitations or generally complex space requirements [6]. This means there should be no physical hard-wired cable connections between the components. Instead, there have to be removable connections e.g., as proposed in [6], plugs with protrusions and sockets with a mounted latch to catch and connect plug and socket. This may be particularly useful when components are manufactured in different facilities and also facilitates system installation, repair, storage, and transport. This is of specific importance when different vehicle installation set-ups, power level requirements, etc. dictate various combinations of different coil systems and rectifying units [6]. On the other hand, a physical separation of coils and electronics means that further down, the value chain has to deal with a partial pre-assembly and a separate delivery of individual components. In higher system integration, it makes sense to have electronics close to the effective working location, e.g. close to the coil and ferrite carrier plates, as high frequency AC voltage outside the pad should be avoided [83] [157]. This limits problems of shielded high-voltage HF-cables and connectors, weight, package volume, and costs.

Additionally, higher system integration also benefits the primary side, as customer acceptance of charging systems strongly depends on how easy and intuitive they are to handle. Bulky and extensive primary side charging systems (~20 kg, ~800x800 mm) are not only challenging for vehicle assembly and integration, but also for transport from vehicle dealership to the end user. Integrating electronics is appealing but has to be done without adding much additional weight. This goes to show once again why complex and hard-to-adapt systems with “z-lifts” should be avoided.

Ultimately (as shown on the right side of Fig. 50), it makes sense to strive for a higher degree of electronics integration on both primary and secondary side while - depending on the field of application and market introduction phase - always with a reasonable degree of component modularization from one product generation to the next.

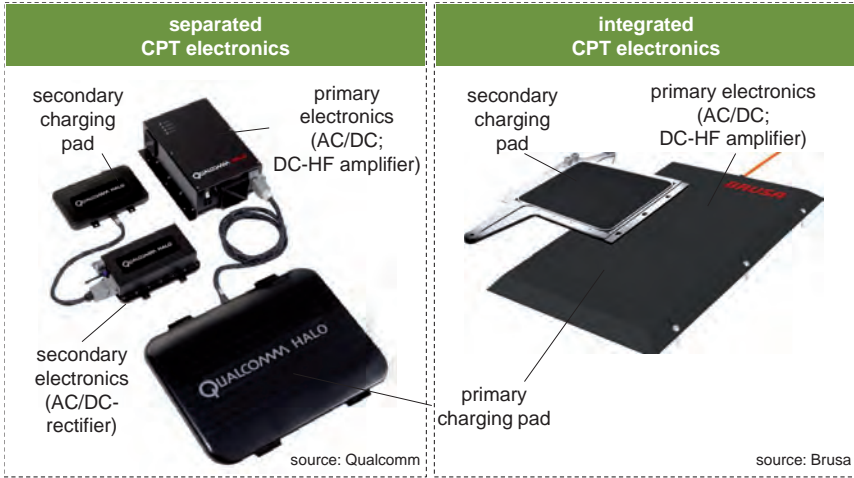


Fig. 50. Levels of electronics integration for CPT systems.

5.1.3 Contacting of HF-Litz wires

To realize high quality coil structures, the coils have to be wound in the specific shape required by their magnetic design and also assembled in the pad. This can be done with rotation-based or wire-laying techniques. As the focus of this work is on production challenges of coil structures, the needed winding concepts will be discussed in detail in chapter 5.2.

Aside from the winding operation, another important coil production step is contacting HF-Litz wire ends. In a CPT system, the ends of HF-Litz wires in a coil have to be electrically connected to a power source, rectifier, etc. Contacting is an essential process step impacting the reliability of charging systems, as the contact can be a weak point if not executed in an adequate manner. Especially HF-Litz wires for CPT systems present some connection difficulties, due to the demanding operating parameters that come with AC currents in the kHz-range and the specific set-up with several hundred individually insulated single wire strands. In order to reap the benefits of HF-Litz wires and to create a conductive pathway between the strands and the connector, insulation has to be stripped off and reliably removed from each strand at once [6], which is a big challenge for manufacturers. It is therefore necessary to consider procedures for reliable, large-scale-enabled contacting of HF-Litz wires to terminals. Process alternatives like insulation displacement connectors (IDC), (cold-)crimping, and splicing are not appropriate for HF-Litz wires as they cannot adequately remove the insulation coating. Mechanical and/or chemical methods for stripping wire insulation are also impractical as they harm the sensitive individual fine strands of HF-Litz wires. Stripping the insulation with the

help of laser-based systems is difficult as the LASER needs access to the entire surface of the single wires that have to be stripped. This is difficult as the several hundreds of individual strands are tightly packed in twisted bundles. Other techniques like removing the insulation by induction [189] or electric plasma as proposed by [190] are investigated in ongoing research activities. One major drawback of all these techniques is that a second process step is needed for stripping insulation and establishing contact to a highly conductive copper-based terminal (small plates, pins, cable sockets, etc. coated with tin, nickel, or silver).

A suitable option for contacting HF-Litz wires described in [6] is the use of pins or cable sockets where HF-Litz wires are soldered into the recessed ends of a socket. The HF-Litz wire ends can be simultaneously dipped into a pot that contains solder heated to 350-450°C (depending on the material characteristics). The solder permeates the gaps between strands, electrically interconnects them and strips the enamel coating from each strand [6]. This creates a continuous connective path between the strands and the pin. This method presents the advantage that it applies less mechanical stress on the Litz-wire strands. Soldering HF-Litz wires in pins is a proven contacting process alternative for fast, small-scale production of prototypes. Thermally stripping the insulation off the HF-Litz wires in soldering pots is commonly used for industrial material handling of CPT pads. However, soldering HF-Litz wires in soldering pots poses problems in higher automated production lines as their high temperature has to carefully be monitored and maintained [6]. Each HF-Litz wire dipped in the soldering pot cools the temperature down, which requires constant monitoring and regulation with the help of sensors. This makes the process energy-intensive. Aside from the need to regulate the temperature, the soldering pots require frequent cleaning. There is also a risk of brittle solder joints, which may turn out to be weak points in demanding operating conditions like vehicle underbodies.

Another promising technique for contacting HF-Litz wires is called hot crimping. Here, HF-Litz wires and cable socket are connected by thermal and mechanical deformation in one process step. Similar to resistance welding, hot crimping is based on heat, generated by the electrical resistance of the welded material and the force applied by a welding head to hold cable socket and HF-Litz wire together. Ideally, applying heat removes the insulation entirely from the cable socket. Within milliseconds, the welding head releases enough current to generate a temperature of about 700°C at the terminal. This temperature is high enough to vaporize the insulation and connect the wire strands to each other and the terminal. However, thermally or mechanically caused damage to the individual wire strands should be avoided and complete stripping off the insulation of the individual wire strands must be ensured in the contact area for a force-fitted, gas-tight crimp connection that is suitable for the demanding operating conditions in CPT systems. A properly hot-crimped HF-Litz wire therefore has to fit perfectly with

the cable socket in both shape and size. The following investigates the main tool and process parameters to test the option of hot-crimping HF-Litz wires for CPT systems.

Several different process parameters can be varied for hot crimping cycles. The main application-specific parameters are crimping pressure and current, crimping pulse duration, pause time, and number of pulses. Fig. 51 shows the course of the crimping current over time for the first pulses of a crimping cycle. The first pulse of a cycle begins with a ramp-up phase whose length is defined by the ramp time $t_{\text{ramp-up}}$, until the crimping current reaches the required value. This ramp-up phase is needed for a good connection between cable socket and crimping tool to avoid wear-out and potential damage to both crimping tool and cable socket. The ramp-up phase $t_{\text{ramp-up}}$ is followed by the crimping phase with several pulses, separated in pulse duration t_{pulse} and pause times t_{pause} . Each subsequent crimping pulse comes without a ramp-up phase.

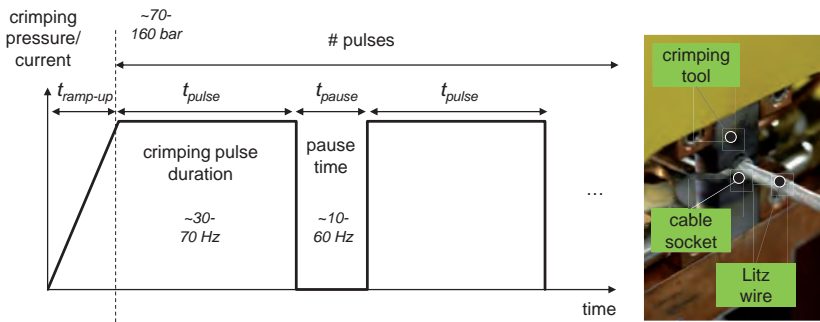


Fig. 51. Schematic process flow of hot crimping.

The basic requirements for crimp connections are defined in norms like DIN EN 60352-2 etc. which describe mechanical tests (pull-out force, insulation grip effectiveness), electrical tests (contact resistance), climatic tests, shaker, and corrosion tests, tests on current carrying capacity, and optical detections with a polished micrograph section or X-rays to achieve a high quality connection for the individual field of application.

Experiments on a CASTECH GFA301000 hot crimping machine have shown, that resistance can significantly be reduced by increasing the process parameters crimping current and number of crimping pulses. Insufficient crimping current and number of crimping pulses will not completely remove the insulation. However, excessive crimping current increases resistance, as the joint suffers damage under high crimping currents. In addition, crimping pressure is significant, as, in contrast to soldering, crimped connections present a risk of air gaps and improper connections between inner and outer Litz wire strands. Higher crimping pressure leads to better compaction and thus fewer

voids in the wire package, resulting in higher pull-out forces. However, it has to be noted that excessive crimping pressure could also keep the melted insulation from flowing out of the cable socket. Pull-out force increases with higher welding pressure because this higher pressure compacts the individual wires more intensely, resulting in a better form-fitting connection with fewer voids. Polished micrograph sections in Fig. 52 show that insulation is also more easily pressed out of the cable socket at higher crimping pressures. Crimping pressure rises from left to right. On the left, there are still many voids, as low crimping pressure is insufficient to completely compress the individual wires. As crimping pressure increases, the amount of voids decreases.

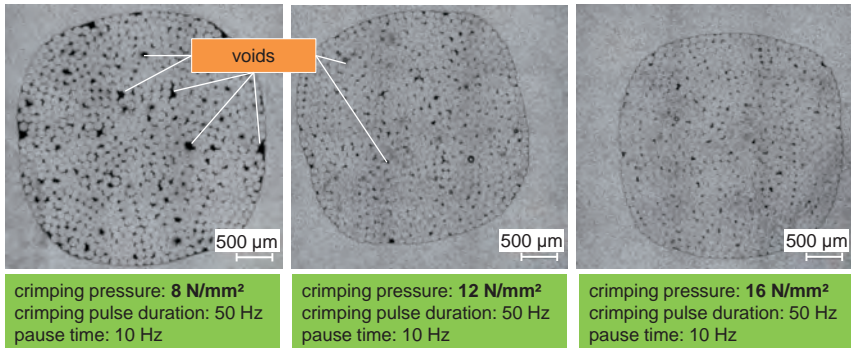


Fig. 52. Polished micrograph section of 810 x 0.12 mm HF-Litz wires at different crimping pressures.

At the smallest crimping pressure setting, some insulation rests remain, mainly at the edges of HF-Litz wire at the cable socket (see close-up picture in Fig. 53, left). The insulation rests weaken the pull-out force. Such crimping results are unacceptable for the demanding operating conditions in CPT systems (AC currents in the kHz-range) and cause safety hazards at heated terminals. At increased crimping pressure, these insulation rests disappear and reveal the potential of the hot crimping process for CPT systems. However, the correct process parameters always have to be configured for each individual HF-Litz wire selected for a given CPT system. In addition, increased crimping pulse duration heightens the probability that insulating coating is melted completely, yet also increases the possibility of welding spots (Fig. 53, right). Lastly, without pause times in the hot crimping process, the resulting heat increase also poses the risk of welding spots between single wire strands. The application of crimping current in the hot crimping process is therefore not continuous, but applied in several pulses with brief pauses. Longer pause times, however, require more pulses and it will take longer to remove the insulation.

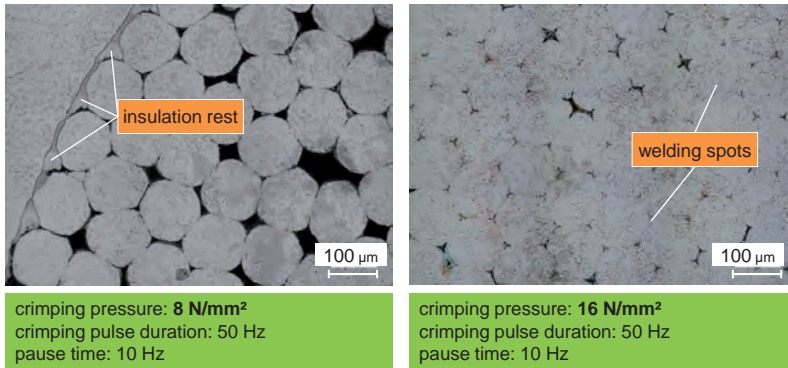


Fig. 53. Close up of 810 x 0.12 mm HF-Litz wire at low crimping pressure (left) and high crimping pressure with long pulse duration (right).

To explore how meaningful images of cross-sectional planes could be obtained at a reasonable effort, the samples have also been analyzed in an X-ray CT. The effort needed to create such X-ray CT images is quite moderate. The samples simply have to be clamped in a special rack in the machine. The machine then creates the images in ~30 minutes. Subsequently, the machine's software allows for viewing the samples from any perspective. Compared to the complex process chain for creating cross-sectional images, which involves sawing, embedding, polishing, etc., X-ray CT analysis requires relatively little effort and time. Fig. 54 shows images of the sample at different planes A-C along the cable socket. Size and quantity of voids can be detected and analyzed very well with such images. The fact that there is no limit on the location in the cable socket and quantity of images is particularly advantageous. In a polished micrograph image, the analysis is limited to a single cross-sectional plane. Moreover, the sample is always destroyed, including the risk of missing the desired target plane. Such problems do not arise in an X-ray CT image.

However, polished micrograph images show by far more details, for example wire deformations, insulation rests or welding spots. The resolution of today's X-ray CT quickly reaches its limits, especially with thin 810 x 0.12 mm HF Litz wires. In conclusion, an analysis with an X-ray CT offers many opportunities and has some clear advantages; however, certain details can still only be observed with polished micrographic images.

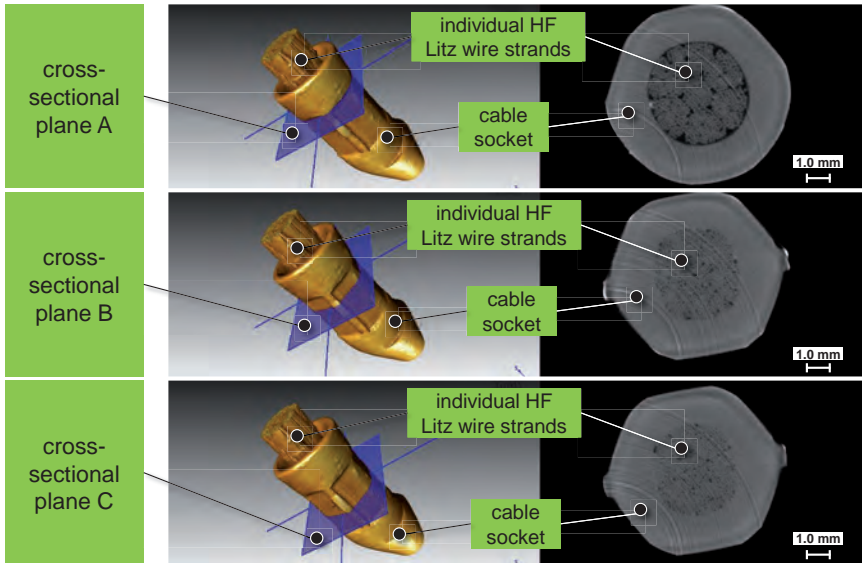


Fig. 54. X-ray CT images of different cross-sectional planes A-C of a 810 x 0.12 mm HF-Litz wire (crimping pressure = 8 N/mm², crimping pulse duration = 50 Hz, pause time = 10 Hz)

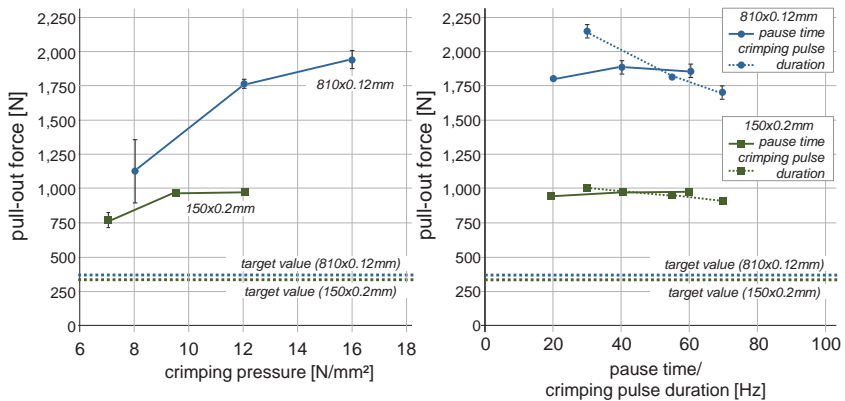


Fig. 55. Pull-out forces in correlation with crimping pressure, crimping pulse duration, and pause time ($n = 6$).

With appropriate set machine parameters (in this case for 810 x 0.12 mm HF Litz wires (number of pulses >5, crimping current >35%³³, crimping pressure >10 N/mm², pause time >20 Hz, crimping pulse duration >30 Hz), all the measured pull-out forces surpass the specifications of DIN EN 60352-2 (see Fig. 55).

In addition, neither climate nor vibration test have significantly damaged the probes. In conclusion, hot crimping can be considered a promising alternative contacting method for HF-Litz wires. It is cost-effective and can easily be integrated in higher automated production lines. However, as could be shown, different possible HF-Litz wire types, cable socket forms, crimping tool designs, and process parameters (crimping pressure, crimping pulse duration, pause time, crimping current, number of pulses) make for a multi-parameter process whose correlations have to be carefully analyzed for each field of application (e.g. for CPT systems - thermal and mechanical impacts resulting from vehicle underbody installation/base parts in the ground, AC-currents in the kHz-range, etc.), especially when also considering other adverse factors such as tool wear etc.

Another option to contact HF-Litz wires is called ultrasonic-welding. Ultrasonic-welding is done by locally applying high-frequency ultrasonic acoustic vibrations to work pieces which are held together under pressure to create a solid-state weld. In ultrasonic-welding, sound is used to vibrate the surfaces of the parts that are to be welded together. Interfacial friction and surface absorption generate the necessary heat to melt the joining pieces, achieving a tight connection. Ultrasonic-welding has relatively short welding cycles due to the high amount of locally applied energy. Moreover, ultrasonic-welding can easily be automated with repeated accuracy, as it is fast and creates clean and precise joints. Ultrasonic-welding is usually used for plastics, thin metallic foils, connections between coated wires, or for connections of coated wires on copper plates [191].

However, ultrasonic-welding is rarely used for contacting coated HF-Litz wire bundles. Welding tools (called sonotrodes) can be smeared with remaining insulation of coated HF-Litz wires after contacting. Ultrasonic-welding also presents the disadvantage that adjacent handling devices or other areas may also vibrate. Moreover, if process parameters and welding tool designs are configured incorrectly, the sharp edges of the sonotrode and the intense local energy in the vibrating metal can easily lead to single wire cuts of the fine Litz wire strands.

To find a way to use US-welding to contact HF-Litz wires despite the above-mentioned drawbacks, first tests were conducted with closed cable sockets and 150 x 0.2 mm HF-Litz wires. The prepared micrograph images (Fig. 56) show that the insulation was completely removed, but many voids remained. In addition, the sharp edges and serrat-

³³ Machine parameters for crimping currents of CASTECH GFA 301000 are given in %.

ed jaws of the sonotrode produced sharp edges in the cable socket, which might turn out to be weak points. Sonotrodes without serrated jaws should solve this issue.

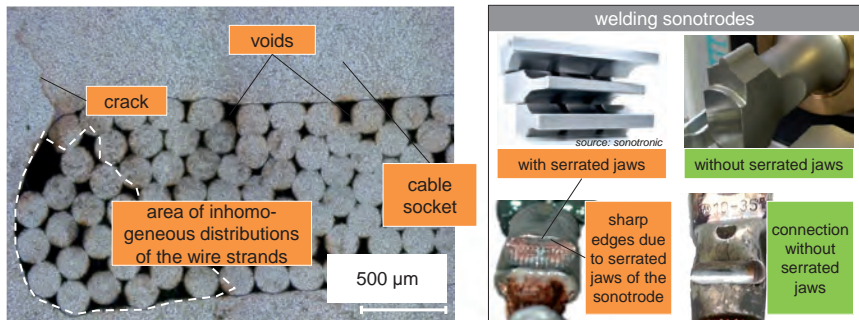


Fig. 56. Polished micrograph section of an ultrasonic-welded 150 x 0.2 mm HF-Litz wire with a cable socket.

Despite all these challenges, first test results on the samples indicate that ultrasonic welding is a suitable method for HF-Litz wire contacting if several adaptations are made. Another promising advantage is that although intense heat is applied to the cable socket, less heat is applied to the HF-Litz wires, allowing them to retain more of their original flexibility. In consequence, ultrasonic-welding can be a promising alternative to soldering or hot crimping.

Further comprehensive tests are necessary to demonstrate the impact of process parameters, especially AC current carrying capacity with frequencies in the kHz-range and resistance to environmental stresses. These tests, however, must be conducted with an adapted cable socket and welding tool design, as the geometry of the sonotrode and anvil greatly influence the welding result. In summary, ultrasonic-welding using sonotrodes without serrated jaws, and not pressing directly on the Litz wire strands but using cable sockets is a new process variation with promising initial results, which still has to be investigated in further detail.

Tab. 9 summarizes the options soldering, hot crimping, and ultrasonic-welding for HF-Litz wires.

Tab. 9. Direct comparison of process alternatives for contacting HF-Litz wires.

	soldering	hot-crimping	ultrasonic-welding
removal of insulation	thermal	thermal	ultrasonic sound/thermal
advantages	<ul style="list-style-type: none"> ▪ simple process ▪ strong connection 	<ul style="list-style-type: none"> ▪ high dimensional tolerance ▪ high level of automation ▪ no additives 	<ul style="list-style-type: none"> ▪ high dimensional tolerance ▪ high level of automation ▪ no additives ▪ low energy consumption ▪ short cycle times
bottlenecks	<ul style="list-style-type: none"> ▪ low level of automation ▪ soldering additives ▪ rigidity of the wire after the process ▪ long cycle times ▪ complex wire handling 	<ul style="list-style-type: none"> ▪ costly iterative process testing for each wire/cable socket combination ▪ high energy consumption ▪ abrasion/wear-out of tool 	<ul style="list-style-type: none"> ▪ little experience with HF-Litz wires ▪ costly iterative process testing for each wire/cable socket combination
automation	low	high	high
automotive-level	low	high	high

As next steps, alternative wire forms like rectangular HF-Litz wires and alternative materials like aluminium or copper-clad aluminum should be included in the test series. For the contacting of aluminum, further parameters have to be considered due to aluminum's creep-fatigue deformation behavior that eventually tends to lose fixed connections over time. Exposed to air, the surface of Al-Litz wires without insulation will very quickly be covered in a durable oxide layer (corundum). This layer provides excellent corrosion protection and is electrically non-conductive. However, it cannot be used as reliable insulation, as it is brittle and difficult to wind (additional failure mode especially at corners/bends). This oxide layer is also difficult to remove for contacting. Therefore, [192] propose electric plasma for the removal of Al-wires insulation layers. Copper-clad aluminum wires can be a promising alternative, as they combine the properties of copper and aluminum. As a result, electrical conductivity increases slightly and problems with the oxide layer of the aluminum are avoided, making it possible to use the same contacting techniques as for copper. However, this alternative HF-Litz wire type is more expensive as the cladding of copper adds production steps.

In addition, solutions for higher degrees of automation have to be reflected, especially for pads with a higher number of connections. The number of connections depends on the pad type (single-coil, multi-coil, number of phases). Especially internal connections inside the pad (e.g. compensation capacitors that are dispersed throughout the winding to reduce inductance, meet voltage limits, and/or achieve inter-operability [161]) inherently increase the production effort and may reduce pad reliability [120]. This shows the importance of a comprehensive, fully studied automation solution, with handling tools to

secure the limp ends of HF-Litz wires in a fixed position and to insert them into the connector devices prior to the contacting process. Fig. 57 shows two different contacting cells based on hot crimping for different levels of automation.

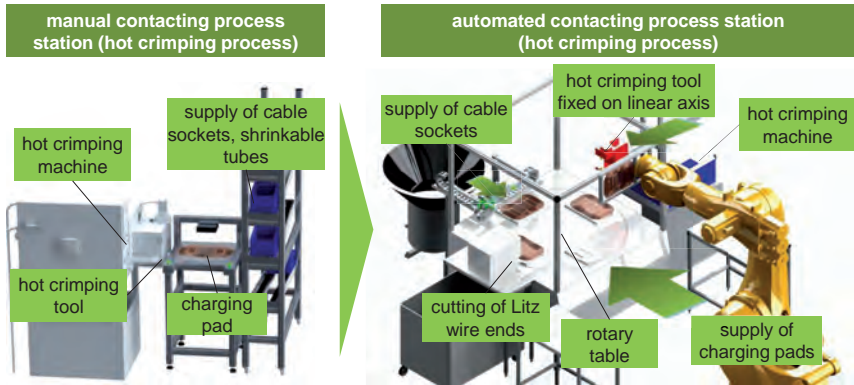


Fig. 57. Manual versus automated contacting of HF-Litz wires.

One problem with the above-described connections are the losses caused by the skin effect, when all HF Litz wire strands are connected and thus form a solid wire in the cable socket. Alternative designs for cable sockets are needed to reduce the skin effect in connectors. [193] propose a connector where all HF Litz wire strands are arranged circularly in one layer along the inner surface of the connector. With this measure, considerably smaller losses have been observed in the frequency range between 30-300 kHz.

Finally, in areas of significant voltage difference, voltage insulation is needed to avoid malfunction or even sparks which could cause a fire. The wires have to be protected with shrinkable tubes at crossing as well as entry and exit points to the power electronics. Insulation foils (e.g. Kapton® tape or Mylar® film [134]) have to be placed [170] e.g. between coils in multi coil systems and at HF-Litz wire crossings. Such insulation foils may also be useful to separate coils from the ferrite material, in a trade-off between magnetic coupling and ferrite hysteresis losses [134].

5.1.4 Encapsulation

All designs have to be analyzed in terms of individually applied stress profiles (see also chapter 6). Therefore, the last production step must add a robust (vibration and shock resistant), electrically insulating, and water-tight casing to fully protect the components (coils, ferrites, electronics, connections) from external environmental influences and to ensure reliable operation over the entire lifetime of the pad (Fig. 58).

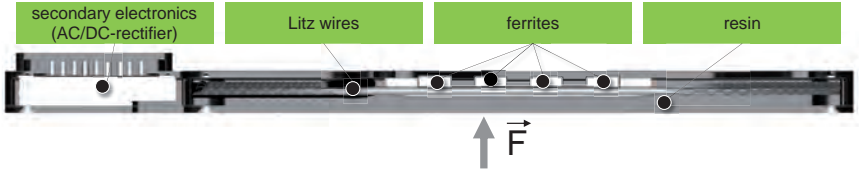


Fig. 58. Secondary pad cross section.

Fully encased transmitter and receiver pad housing may distribute external compression forces more evenly across the power pad [71]. However, complex multi-layer set-ups, especially, may cause problems with appropriate resin flow throughout the housing. Low-viscosity resin is needed to avoid unwanted air pockets. In addition, several layers of a loosely woven nylon sheath (e.g. as produced by Sofilec™) can be used as an external insulation to assist penetration into the HF-Litz wires to lock them into an epoxy matrix inside the casing. High frequency vibrations can then be applied to the pad during the encapsulation process, causing the resin to move around all of the components within the housing, avoiding any air pockets, as shown in Fig. 59 [134].

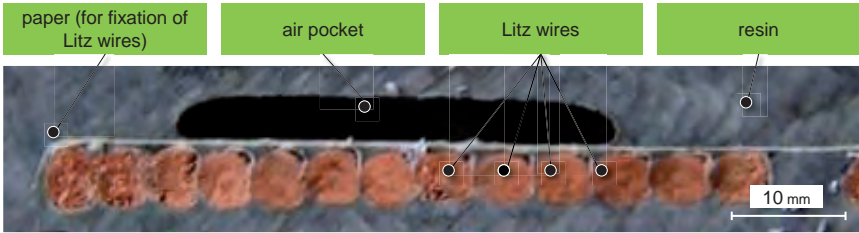


Fig. 59. Air pocket in an AGV industrial CPT system with epoxy resin.

For this process step, process temperature has to be carefully selected to avoid damaging the HF-Litz wire insulation materials (polyester for insulating HF-Litz wires with temperature stability up to 150°C) [145]. Usually, polyurethane-based resins are used for the final encapsulation. However, there is quite a range of alternative materials like silicones, epoxy resins, and foams, as shown in Tab. 10. However, while encapsulation and fixation of individual materials improves life-cycle durability, it also adds weight and cost. Moreover, encapsulation is not only an issue in terms of strict cost and weight targets, but also involves required cycle times to harden the material, a likely bottleneck in the value chain as it impedes the constant flow of materials.

Tab. 10. Alternative encapsulation materials for CPT systems.

	curing time	mix viscosity at 22°C	density	temperature range	bending strength	thermal conductivity	recommendation
polyurethane resin	- - -	o	o	+	o	o	long processing time, limited moisture resistance
polyurethane foam	++	n/a	+	n/a	++	-	limited moisture resistance, insecure
silicone resin	-	++	+/-	++	o	o	good material properties but expensive
melt adhesives	+++	n/a	o	-	-	o	fast and precise processability, problem of thermal resistance
epoxy resin	+	+	o	++	+	o	good processability, high media resistance
unsaturated polyester resin	o	+++	o	+	+	o	good processability, high media resistance but brittle

This speaks for alternative housing concepts where encapsulation is only applied locally and/or combined with lightweight solutions like PU foams where possible. A compromise that avoids full encapsulation yet still provides physical protection for the pad components might be the integration of several elastic insulation layers to minimize the air in the interior of the housing. Elastic insulation layers can compensate unevenness in the ferrite layer and distribute pressure that arises, for instance, from driving on the pad [157]. [71] therefore propose a malleable, deformable, gel-like, or gelatinous material like polyurethane-based closed-cell foam rubber sheets. To further reduce weight, another solution is a mere mechanical fixation (clips, bolts, screws), which has advantages for repair and maintenance. However, this solution shows low resistance to mechanical stress over the product lifecycle. The choice between the alternatives - full encapsulation, local encapsulation, elastic insulation layer sheets, or just mechanical fixation of the parts - depends on the mechanical stress profiles during the product-life as discussed in chapter 6.1.

5.1.5 Final assembly

Finally, a shielding element has to be attached to the pad to avoid stray flux exiting the side or rear of the pad (e.g. to the engine sub-frame or passenger compartment) depending on the magnetic pad design and vehicle integration concept. Such shielding can be assembled before or after the encapsulation in the pad housing, depending on the pad structure. Shielding plates may also be specially shaped for passive cooling by convectional heat dissipation of pads and power electronics (e.g. with cooling fins - see chapter 6.2) [51].

As a last step of the total pre-assembly line for charging pads (see Fig. 60), pad functionality has to be tested.

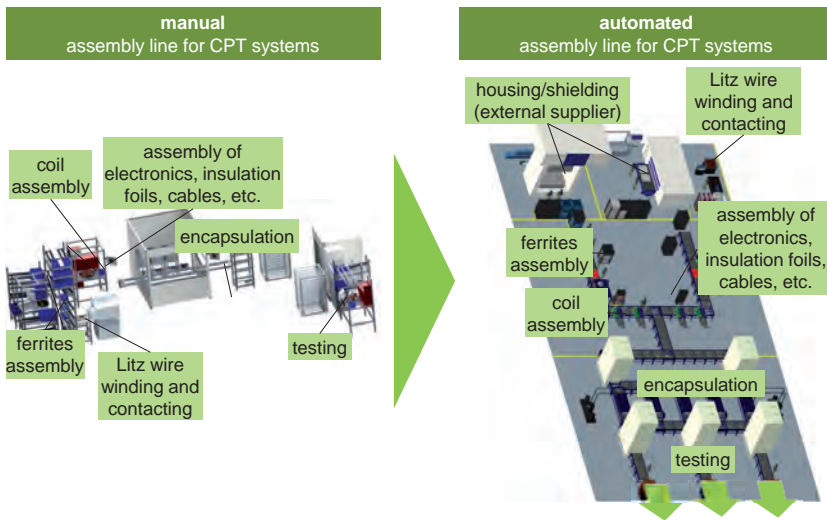


Fig. 60. Exemplary assembly lines for CPT charging pads.

From a production perspective, the main parameters of charging pad designs can be analyzed in terms of material cost, material weight, and cycle times of individual production steps, as shown in Fig. 61 for an exemplary circular pad design.

In the case of this example of a circular pad design, from a material cost perspective, ferrites and HF-Litz wires are critical, and from a weight and cycle time perspective, encapsulation is critical.³⁴ In summary, the material use, HF-Litz wires, ferrites, shielding, and encapsulation should be minimized altogether. The amount of HF-Litz wire and ferrite must always be justified in terms of added weight and cost versus performance [24]. Multi-coils enhance performance and inter-operability but significantly add to the cost and weight of the pad. It must always be clear how much conductor and core material is necessary for each individual vehicle type (needed air gaps, power levels, tolerance to misalignment, etc.) to the point where no significant additional improvement can be achieved without oversizing the systems [123]. In practice, first prototypic systems tended to overdesign the use of HF-Litz wire and ferrite thickness for robustness (due to the brittle nature of ferrite), and there is room for adjustment [23]. If possible, encapsulation should be avoided to reduce production cycle times. In chapter 6, a test bench ap-

³⁴ It has to be noted that weight, cost, and process times will, of course, vary with different alternative pad designs (number and type of coils and ferrites), used electronics (communication and surveillance systems), type of encapsulation, etc.

proach is presented to support a precise validation of different materials (type and quantity).

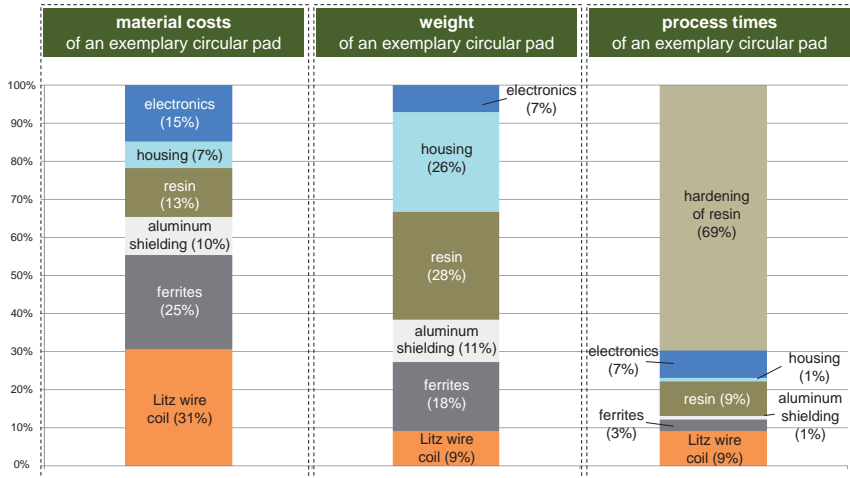


Fig. 61. Composition of a primary side circular pad design from the perspective of material cost, weight, and process time.

Those numerous correlating parameters depend on pad designs (single-coil design with less HF-Litz wire but more ferrite versus multi-coil design with more HF-Litz wire but less ferrite, or, among others, approaches with more homogenous field distribution with less current and thus less wire and thinner ferrite [60] [175]). Fig. 62 also shows weight reduction potentials compared to industrial systems by substituting heavy aluminum housing with plastic base part housings.

In addition, development has shifted from the 1st prototypical CPT-system generations with a copper to ferrite ratio of ~ 0.2 (similar to the ratio of already well-known non-resonant powered material handling CPT-systems), to ~ 4.75 with resonant inductively operated multi-coil systems and a sophisticated and thus economical usage of ferrite (Fig. 62). This helps reduce pad weight, but the cost of Litz wires has to be carefully considered in multi-coil pad systems.

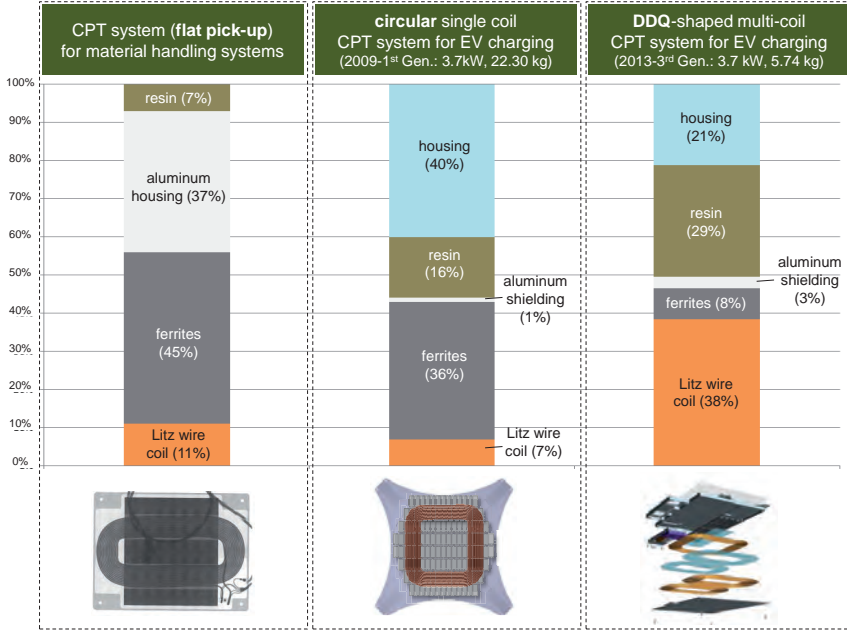


Fig. 62. Comparison of different charging secondary side pads from a material weight perspective (relative numbers in %, without electronics).

Another interesting aspect that has to be considered is complexity of production steps with potential failure modes for the individual materials. Here, handling and contacting HF-Litz wires is not a tact-time limitation. It is the sensitivity of HF-Litz wires and their high cost that make this the most complex production step, especially in the case of complex coil designs, as described in chapter 5.2. Aspects like mechanical and thermal stress also have to be taken into account when considering what affects materials during operation over the product-life of the pad, with major failure modes for HF-Litz wires and ferrites (see chapter 6). Such considerations are especially important as, with suitable automation concepts, rising production volumes will significantly reduce proportionate labor and machine costs, making material costs an even weightier factor, as shown in Fig. 63 with production costs for different unit numbers of a sample circular primary pad design (without electronics).³⁵

³⁵ The 3.3 kW-CPT systems (240V, Level 2, primary and secondary pad including electronics) from Evatran Plugless Power to retrofit Chevrolet Volt and Nissan Leaf are available for \$2,970 (not including installation) [194]. In the mid-term, the addressed average sales price for a complete CPT system (primary and secondary pad including electronics) are in the range of €1,500-2,000 [73].

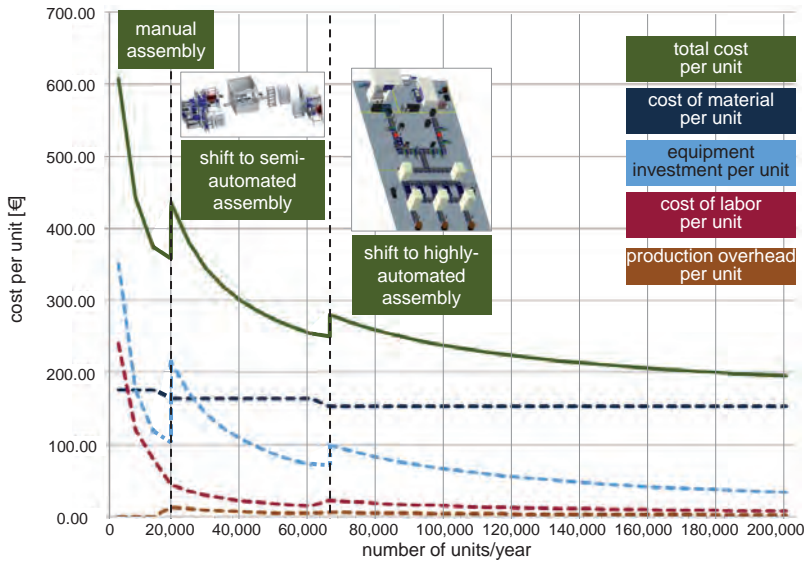


Fig. 63. Total costs for a sample circular CPT pad (without electronics).

The pad pre-assembly described above could be done at several different points in the supply chain [18]. It is possible that value creation shifts to the suppliers of underbody plastic structures or even of battery modules in the context of future comprehensive vehicle sub-floor settings [195]. For the sake of higher system integration, engine and underbody shielding could even take over the function of the cover plate, improving aerodynamics and additionally cooling the electronics with added air flow and - in the case of PHEV-powertrains - integrated heat shielding (Fig. 64).

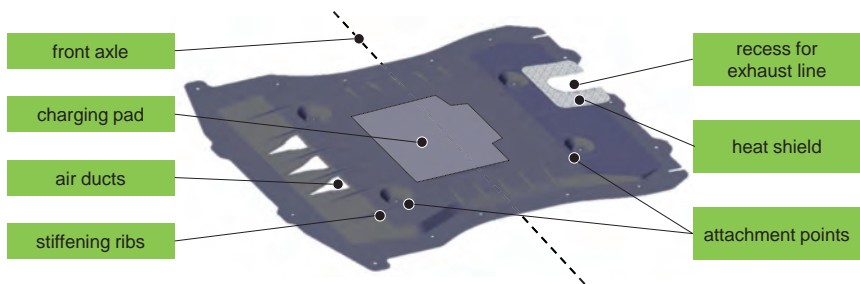


Fig. 64. Underbody shielding with CPT system integration.

Such protective underbody shielding made of materials with extreme corrosion resistance is especially useful for pads that are integrated in areas exposed to splash water, road salt, etc. Moreover, they can protect the pads from mechanical impacts (see chapter 6.1). This would additionally upgrade the value of the underbody structure and at the same time streamline the logistics chain [196]. However, it would also add weight and bulk to the systems, causing problems (automated handling systems, larger logistics packaging units, etc.) for the delivery process and final assembly in the plants [18].

In later phases of market development, vehicle manufacturers may in-source the production of CPT systems in the event that, despite current efforts to standardize contactless charging systems, they will become one of the key competitive vehicle components, and adapting modules to the individual underbody structure of the total vehicle architecture will be increasingly complex (e.g. due to complex field guidance in underbody sub frames). The intense R&D activities by Toyota, which develops its own pads integrated in the underbody, already point in this direction [14] [64].

5.2 HF-Litz wire winding technologies

HF-Litz wires, in particular, need adequate production processes as a wide range of diverse and increasingly complex magnetic designs are being developed [17] (Fig. 65).



Fig. 65. Different degrees of complexity for the production depending on the complexity of the coils structures.

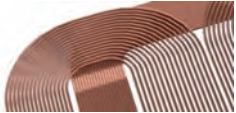

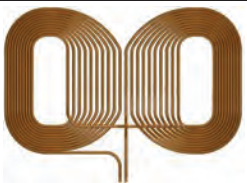
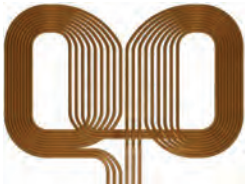

Today, coil structures for CPT systems are wound manually, which results in inferior laying precision unsuitable for mass production, as well as low productivity, which can be tolerated in small series, but is not profitable for mass production. In consequence, there is a need to reflect coil structures of CPT systems (chapter 5.2.1) for the purpose of developing automated production technologies (chapter 5.2.2-5.2.4), as presented in the following.


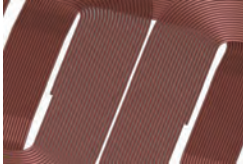

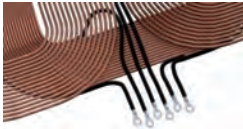
5.2.1 Analysis of coil types from a process perspective

Coil shapes are one of the main differences between pads, because coil structure impacts the main function of power transmission. In the first phase of development, mainly simple winding forms were considered. In the past few years, coil shapes for CPT sys-

tems have been increasingly adapted to the desired functionality and the resulting complex coil design parameters. The main coil parameters that pose production challenges are shown in Tab. 11.

Tab. 11. Coil design parameters resulting in production challenges.

coil design parameter	diverse functions achieved by the coil parameter	coil example
3D contours	<ul style="list-style-type: none"> ▪ helical coils for long-distance power transfer ▪ transition between the layers of multi-coil systems ▪ compressed coil edge to further reduce pad dimensions 	
multi-coil systems	<ul style="list-style-type: none"> ▪ inter-operability (receiving different flux parts) ▪ larger active field areas ▪ improved tolerance to misalignment 	
multi-pole coils	<ul style="list-style-type: none"> ▪ improved magnetic design ▪ reduced number of connections ▪ minimized material usage 	
multi-Litz-wire coils	<ul style="list-style-type: none"> ▪ attains variable inductances ▪ different power levels ▪ improved tolerance to misalignment 	
coil pitch	<ul style="list-style-type: none"> ▪ optimized ferrite coverage ▪ larger active field areas ▪ homogenization of magnetic flux density ▪ electrical and/or thermal insulation ▪ integration of electronics ▪ reduced external proximity effect 	

varying radii	<ul style="list-style-type: none"> ▪ minimized pad dimensions ▪ minimized material usage/costs ▪ minimized wire length/loses 	
winding tolerances	<ul style="list-style-type: none"> ▪ precise magnetic field design especially at active pad areas ▪ avoiding “fanning” at radii which may result in leakage flux 	
transitions/crossings	<ul style="list-style-type: none"> ▪ needed in every coil, especially demanding to attain multi-pole- and multi-Litz-wire designs 	
position of the Litz wire ends	<ul style="list-style-type: none"> ▪ for subsequent winding operation ▪ accurate feeding to contacting process step 	

For EVs, the focus is especially on thin flat CPT coils, as 3D-helical coil designs [119] or even solenoid systems might be too large in the z-direction and thus too bulky to fit the very restrictive space requirements of the OEMs. However, innovative pick-up systems like DDQ or BP may have a slight 3D-elevation, consisting of several overlapping coils with transitions [123], adding additional complexity to the production process.

Multi-coil systems may improve inter-operability (e.g. receiving vertical and horizontal components of the magnetic field), achieve larger active field areas, or improve tolerance to misalignment. Therefore, different pad designs have been proposed, from simple arrangements of several identical coils side by side or partially overlapping [130] [131], to flat circular coils with winding turn regions that are spaced at different sized gaps (one inside the other) [175], to DDQ or BP. The challenges of multi-coil designs consist in handling and fixing these more complex structures.

Another complicating aspect of new multi-pole coil designs is that manufacturers may want to build them with a single HF-Litz wire that extends across over even several poles [154] [170] [179] for improved magnetic design, fewer connections, and minimized material usage. In order to create a flux pipe as described in chapter 4.2.2 of such multi-pole coil designs, the electric current must flow through the lengths of adjacent Litz wire

coils in the center pad region in the same direction. This means coils have to be wound against one another, one pole clockwise and the other counter-clockwise [170], as shown in Fig. 66. In consequence, it does not suffice to simply wind by rotation, and wire laying is needed to fix the wires to a base material.

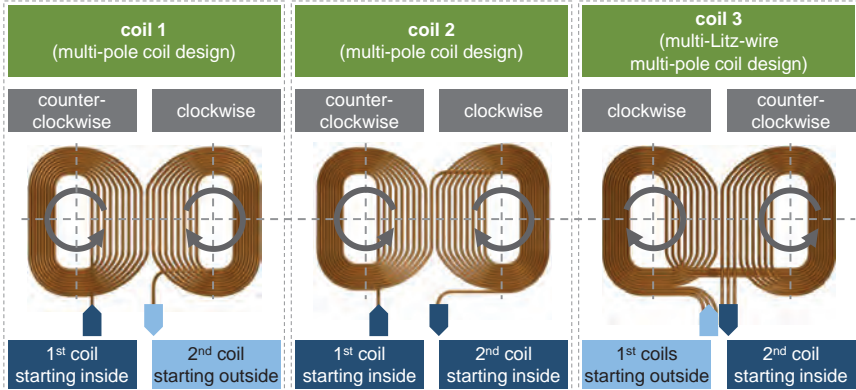


Fig. 66. Winding arrangements with multi-pole coils.

In addition, such winding arrangements should result in low voltage differences between adjacent Litz wires to avoid losses and a need for excessive insulation material [170]. For instance, minimal voltage difference between adjacent HF Litz wires is achieved by coil 1 (Fig. 66) where the outermost winding of one pole is immediately connected to the outermost winding of the other pole with no wires crossing between the coils. However, winding from the outside to the inside makes it more difficult to lay the material down in the desired coil arrangement. In consequence, coil 2 is the easiest to produce because the material can be wound from the center to the outside around a centrally positioned object inside each coil, and each new loop can be placed immediately outside the previous loop [170]. Furthermore, it may even make sense to integrate several parallel Litz wires, resulting in more complex multi-Litz-wire coil designs. Multi-Litz-wire coils create on/off possibilities to increase/decrease inductance that can make pads inter-operable for different power levels and/or show an improved tolerance to misalignment in the x-, y-, and z-direction. Coil 3 in Fig. 66 shows a multi-Litz-wire coil wound over several poles (which is actually a “multi-Litz-wire multi-pole coil”).

Another decisive parameter of coil design complexity is the coil pitch. The coil pitch describes the distance between adjacent turns of individual windings. Simple geometries are primarily circular windings with a coil pitch of one. A coil pitch of less than one (*coil pitch* < 1) results in multi-layer coils and adds undesirable thickness to the pad [24]. Different or even varying coil pitches with a greater distance between the wires may be

necessary for field shaping (e.g. homogeneous low magnetic flux density avoiding local field maxima [60] [175]), ferrite coverage, insulation, heat dissipation, reduced outer proximity effects [143], and material savings. In addition, larger coil pitches make it possible to integrate further electronic components (ICT, LOP, FOD) in the empty spaces between the windings [197]. One example of a coil design that uses coil pitches larger than one is the DD-pad. DD-pads, especially, rely on their specific design in the pad midsection to create a flux pipe. The height and hence effectiveness of the intra-pad flux pipe is created by adjusting coil width in the midsection of the pad and depends on the number of turns as well as on coil pitch [24] [67]. [24] found that the coupling coefficient could be improved by separating the wires slightly (*coil pitch* > 1). Experiments have shown that coils wound with a larger pitch (*coil pitch* >> 1) have a shorter effective flux pipe length. If the pitch is greater than a few wire diameters, flux will leak out of the gaps between the turns, causing the air gap flux to collapse effectively, resulting in a short flux pipe. This is because the resulting small flux loops around the separated conductors do not increase coupling and add significantly to pad inductance, eventually reducing the coupling factor [24]. Winding coils with an adequate coil pitch moreover can achieve an optimal percentage of covered ferrite strip, utilizing ferrites more effectively. A coil pitch of about twice the wire diameter in the central pad midsection was used for further tests. This helps improve material usage as it optimizes the correlation between used ferrite and Litz wires [24] [120]. Outside the flux pipe, the remaining coil length of a DD-pad should be minimized with gapless winding (*coil pitch* = 1) to save copper, weight, cost, and to lower its AC resistance R_{AC} [24]. This results in an even more complex pad design, as varying coil pitch and thus different curve radii have to be considered in the coil production process. In addition, the pad designs are very sensitive in terms of stray fluxes. Therefore, precision in winding is a major factor to attain the desired magnetic field design. Especially in areas like the above-described flux pipe, precise winding is important to avoid problems like leakage flux that is due to “fanning” at radii. These sophisticated coil designs, particularly multi-Litz-wire and multi-pole designs, result in an increased number of transitions/crossings that complicate winding operations. Finally, HF-Litz wire ends have to be accurately positioned for the subsequent winding operation and for the contacting process.

All these aspects show the wide range of potential challenges for HF-Litz wire winding of CPT-coil designs. Since researchers who invent coil designs are focused on coil performance and not particularly preoccupied with easy coil winding [198], winding techniques have to meet high demands, as described in the following. To create a finished coil structure that can easily be integrated in the housing of the pad, several process steps need to be carried out. The following presents possibilities that have been developed for HF-Litz wire feeding (chapter 5.2.2), to establish inherent coil stability (chapter 5.2.3), and different winding techniques to attain the coil designs described above (chapter 5.2.4).

5.2.2 Feeding of HF-Litz wires

Research projects from the past show that one of the main tasks for implementing innovative winding concepts is the proper and reliable feeding of limp products like wires, flat-bands, or cables to the subsequent production steps [199]. General requirements are feeding paths with reduced danger of wire damage, twists, etc. with as little bending as possible and wider radii. A short feeding path with horizontal de-spooling reduces the risks of twists in the HF-Litz wire, especially with rectangular HF-Litz wires, and enables higher process speed. The handling of HF-Litz wires along the supply path can be divided into Litz wire storage, external tool supply, and internal tool supply (up to the laying point).

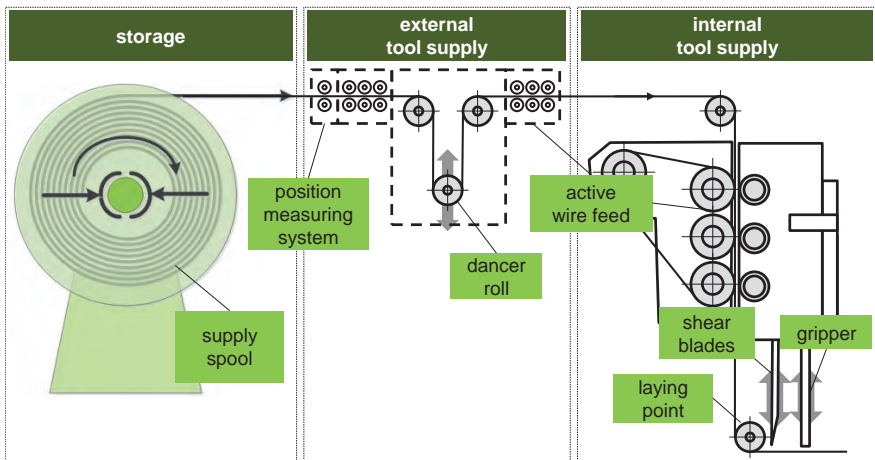


Fig. 67. Supply path for HF-Litz wires.

HF-Litz wires could basically be stored and fed to the process by unwinding from supply spools, or already pre-cut to a certain length [199]. However, large spools (usually delivered wrapped on standardized wire spools) with a continuous supply of several hundred meters of wire ensure reliable feeding and reduced handling and set-up times as it takes longer until the spool needs to be replaced.

Twists in the HF-Litz wires seriously impact the electrical parameters of the system, especially with respect to the proximity effect (chapter 4.1.2). A HF-Litz wire may be twisted depending on the way it is fed (passive or active) and the winding technique as described in chapter 5.2.4. Twists can be avoided by using actively movable supply spools that move to compensate twists, as shown in Fig. 68.

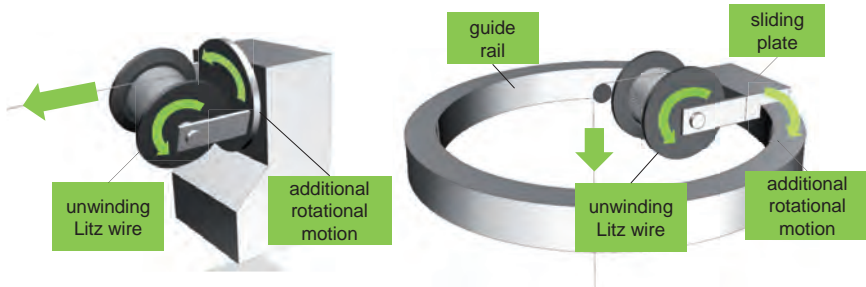


Fig. 68. Active supply spools for the feeding of HF-Litz wires.

Twists can also be avoided by rotating the wire in synch with the rotation of the supply spool and/or laying tool [17] (Fig. 69). This, however, further complicates the winding process.

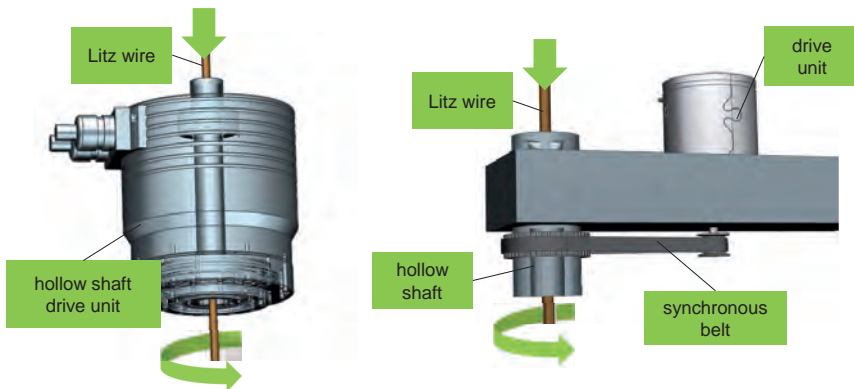


Fig. 69. Rotation axis with central HF-Litz wire guidance.

Several HF-Litz wires can be fed from spools in or close to the winding machine simultaneously for multi-Litz-wire pads (see Tab. 11). In doing so, correct wire tension becomes a major influencing parameter. The wire tension must be selected according to wire size and kept as constant as possible at the right level through the entire winding process to obtain a product of high quality [198]. Changes in wire tension occur during the acceleration and deceleration phases of the winding process and affect the process flow, as considerable fluctuations in wire take-off speed affect wire tensile force. This is of specific importance at higher winding speeds and for rectangular winding shapes [198]. For HF-Litz-wire-based charging pads, winding speeds are moderate. It is critical to compensate the movement of the laying tools relative to the supply spools, as insuffi-

cient wire tension leads to variations in wire feeding speed and loose turns. To control the unwinding of the HF-Litz wire, for example, a tensile-force- or torque-controlled brake can be attached to the supply spool, limiting possible damage to HF-Litz wire insulation. In addition, such relative movements and resulting speed variations in the laying tool and storage spools can be compensated by a dancer roller or a dancer arm that can tauten “slack” or “back” tension.

However, the spools can become too heavy for traditional feeding devices, controlled only by brakes and wire-tension elements. For large spools, accelerating the coil unevenly can thus lead to very high wire tension. Excessive wire tension causes problems of slippage and wire damage if tensile elastic limit is reached, producing permanent cross-section and length deviations. This can impact the electrical resistance of the coils or even cause wire breaks and mantle deformations as well as shift the individual fine Litz wires amongst each other. All this leads to increased scrap and machine downtime [200]. In this case, actively powered spools have to be used for tension-free feeding and subsequent turning HF-Litz wires to the laying tool and base material with a wire tensioner as mentioned above. If flexural rigidity causes too much friction and wire traction for passive guidance, additional active elements along the feeding path are also needed. Depending on the specific construction, active drive elements have to be added at one or several points of the supply path. Ideally, HF-Litz wires are actively guided by rubber-based belt systems that are clamped to the wire, e.g. using gas pressure springs between the rubber belt and two pinch rollers with specially formed guiding grooves to provide additional guidance and to avoid point loads that cause slippage and deformation (see Fig. 70).

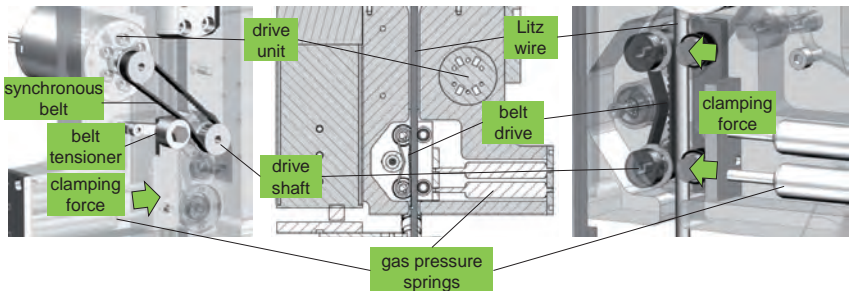


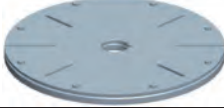

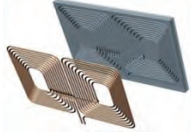

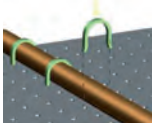



Fig. 70. Rubber-based belt-systems for an active supply of HF-Litz wires.

To achieve complex coil designs as described above in chapter 5.2.1, the coils have to be fixed to a base material to create inherent stability, as described in the following.

5.2.3 Inherent coil stability

Complex coil designs need to be inherently stable for several reasons, depending on the coil form and base material. Stability facilitates logistics (e.g. transport of the pre-wound coils from the winding machine to assembly in the housing), and helps protect sensitive materials in the pads from damage. It is easier to position components, and helps maintain even complex shapes, e.g. correctly spaced coil pitches [71], and/or reduce process time. Depending on how the coils will eventually be fixed in the pad, e.g. with full encapsulation, they may only need to be inherently stable for a short time. There are several possibilities for coil carrier materials and fixation methods, as shown in Tab. 12.

Tab. 12. *Alternative base materials and fixation methods to achieve inherently stable coils.*

mechanically-fixed coils		adhesively-fixed coils	
rigid coil-formers/templates		liquid adhesives	
base parts with grooves, pillars, hooks		strong spray adhesives	
clamping bracket/staples		adhesive foils/paper/tapes	
wire on foams/textiles		thermoplastic wire coatings/self-bonding wires	

The easiest way to attain inherently stable coils is the use of mechanically fixed rigid coil formers/templates. The use of a rigid coil former/template with a base and a top (thereby creating a clearly defined winding space for the HF-Litz wires) makes winding fast, guarantees secure handling of the wound coils, and allows for complex shapes with coil pitches if used in combination with emerging pins or locally applied glue, as described in [201]. However, templates add extra space, weight, and cost to the pad (as the parts need to be produced separately with extra tooling costs, logistics, etc.). Moreover, tem-

plates allow only for rotation-based winding concepts, and it may be difficult to fill the spaces below the rigid coil former, even with low-viscosity resins.

In the same way, the use of spool carriers with grooves adds extra bulk, weight, and cost to the pad. However, grooved base parts make it easier to create complex coil designs with accurate and inherently stable coils as grooved spool carriers allow more freedom for rotational winding and also enable wire laying approaches. To ensure a tight mechanical fit of the coil winding while preventing the wire from sliding out of the groove, the grooves have to be slightly narrower than the actual wire diameter at the top and then open to a circular shape to receive the individual HF-Litz wire [157]. This has to be designed in a way that will not damage the wire insulation as the wire is clamped into the groove. Fig. 71 shows an example of such a base part with grooves.

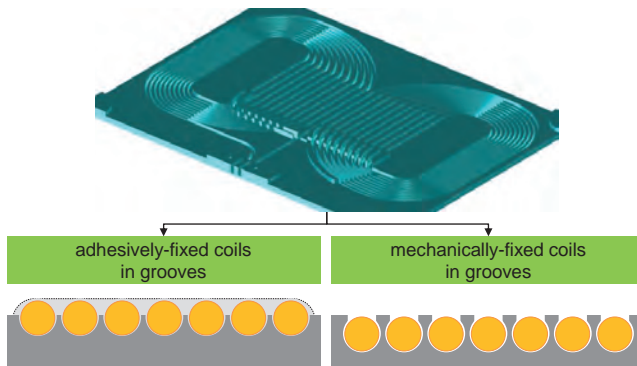


Fig. 71. Alternative types of base parts with grooves to attain inherently stable coils.

Cutting the HF-Litz wire ends to a specific length, and then positioning them exactly and reliably in the contacting machine (e.g. hot crimping, ultra-sonic welding) is critical to attain reliable higher automated process steps, especially as the HF-Litz wire ends are limp. It is helpful to use base parts that can be carried with workpiece carriers, with special grooves to fix HF-Litz wire ends. It facilitates transport of the coils to the next process step, in this case the contacting of the HF-Litz wires ends, as shown in Fig. 72.

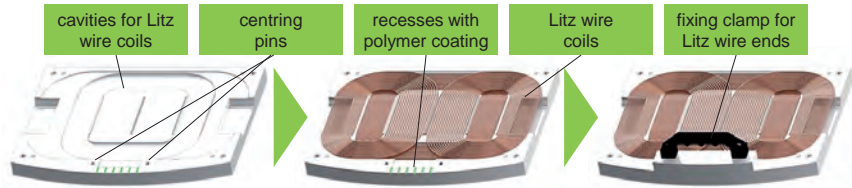


Fig. 72. Base-plate with grooves for accurate feeding of HF-Litz wire ends.

Aside from the above-described concepts, coil windings can also be fixed by sewing the wires onto a base material, e.g. with industrial sewing machines. To do this, the HF-Litz wire is placed in front of the sewing head of an industrial sewing machine and subsequently fixed to a base material with needle and thread. Many different materials can be used as a base structure like technical textiles, thermoplastic foils, foams, etc. This approach allows a flexible fixation to a base material, but also poses several potential problems, e.g. the danger of hitting the wire and low tolerance when fixed on limp textile structures, as described in detail in chapter 5.2.4.

Adhesives are yet another alternative to mechanical fixing options. Coils can be partially fixed by winding or laying the wires in grooves, accompanied by a fixing tool with special ink jet nozzles that locally applies liquid or strong spray adhesives into the grooves. The used adhesive, specific application tool, and process parameters (pressure, speed of the laying tool, base-part-adapted trajectory, quantity of applied adhesive per surface area, curing time, keeping temperatures below the melting point of the wire insulation material, etc.) have to be carefully selected to ensure reliable adhesion between the base material and wires. Especially the curing time of the adhesives is a limiting factor in terms of needed process speed. Curing must be sped up with high-energy radiation (e.g. ultraviolet light) or heat etc. These aspects complicate the process alternative of fixing coils adhesively, and all parameters have to be studied in detail before choosing this process option.

Another alternative to reduce system weight is using light-weight base materials like adhesive foils, papers, or tapes to fix the winding structure to simple plates or directly into the housing. This is a simple and cheap solution without mechanical or thermal stress on HF-Litz wire materials. This process alternative is favored for small production volumes and prototypic systems. However, it is not be very precise and significant deformations and ripples may occur if not processed accurately with automated handling tools, as shown in Fig. 73.

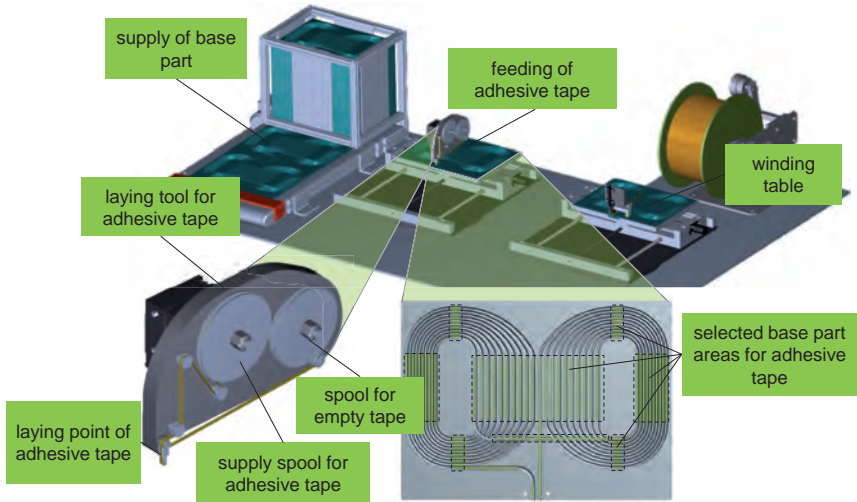


Fig. 73. Laying tool with automated feeding of adhesive tape.

In addition, to avoid deformations, pressure rollers can be used to press HF-Litz wires onto base materials such as adhesive paper and fix them to their final position. Even complex coil structures with coil pitches etc. can be attained in this way with wire laying and pressure tools, as described in detail in chapter 5.2.4.

Aside from fixing the coil to an adhesive base material, thermoplastic coatings or self-bonding wires can also create inherently stable coil structures which can be unloaded from the winding station. In addition to the primer insulating layer, bonding wires have an additional adhesive overcoat made of polyvinyl-butyral or polyamide. Once the temperature reaches 150°C, the adhesive overcoat melts while the prime insulating layer still resists due to its significantly higher softening point of over 200°C [145], which bakes the individual windings together. In this manner, appropriate forming tools can achieve sophisticated, easy-to-handle coil shapes, even with 3D-contours. To create coils with a coil pitch larger than one, wires can be added to base materials with a self-bonding layer [197]. There are several methods to connect individual self-bonding enameled wire types. One option is using solvents, with the decisive disadvantage that solvent residues might get on the wire surface, which can damage the enamel insulation. Therefore, it is more common to use heat to bond the wires. This can be done either by heating the coils in an oven (slow, but controllable), by intense current pulses/resistance heating (faster, but risk of overheating with damage to the insulation), by hot air stream (fast, controllable and can be applied directly during the winding process), or by LASER light (extremely fast, precise fixation points/areas). Furthermore, the last

two options (hot air, LASER) can be integrated in a HF-Litz wire laying tool directly after the pressure rollers, as shown in Fig. 74, to fix the (self-bonding-)Litz wire to a (thermally activated self-adhesive) base material.

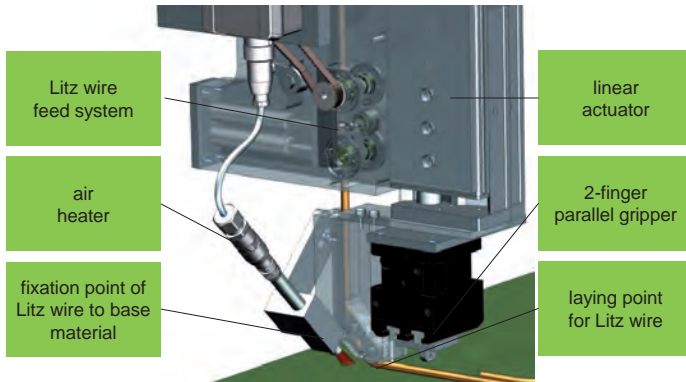


Fig. 74. HF-Litz wire laying tool with hot-air tool to fix the HF-Litz wires to a base material.

Aside from laying wires directly onto an adhesive base material, they can also be pre-wound in a winding station and subsequently transferred to adhesive foil or a base part.

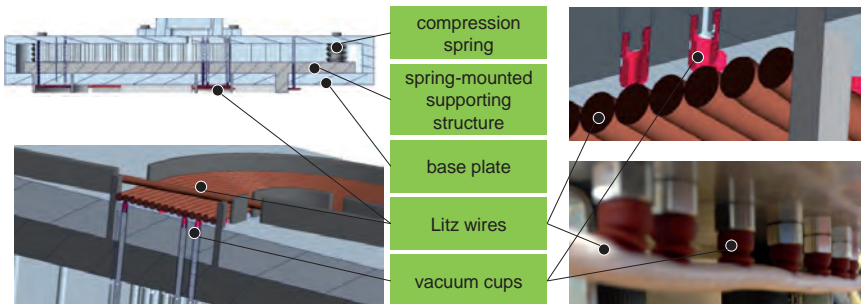


Fig. 75. Cross-section of a vacuum gripper for HF-Litz wires.

Special air grippers with vacuum cups can be used to maintain the inherent stability of the coil design, especially for coil pitches. The gripper must have a contour that is inverse to the coil geometry, with support structures e.g. in the area of coil pitches and bends. The position and shape of the vacuum cups are crucial for this handling option to guarantee a reliable transfer of the coil from the winding station to the next process step. As shown in Fig. 75, the vacuum cups should protrude from the gripper to a cer-

tain extent and should mirror the form of the individual HF-Litz wires as precisely as possible.

After pre-winding the coil, the air gripper picks it up and transfers it to another gripper that is mounted to a lifting table. The vacuum gripper is subsequently turned 180° to a reel-to-reel system with adhesive foils. Pressure and hot air can be used to connect the coil and the adhesive foil to generate inherent coil stability.

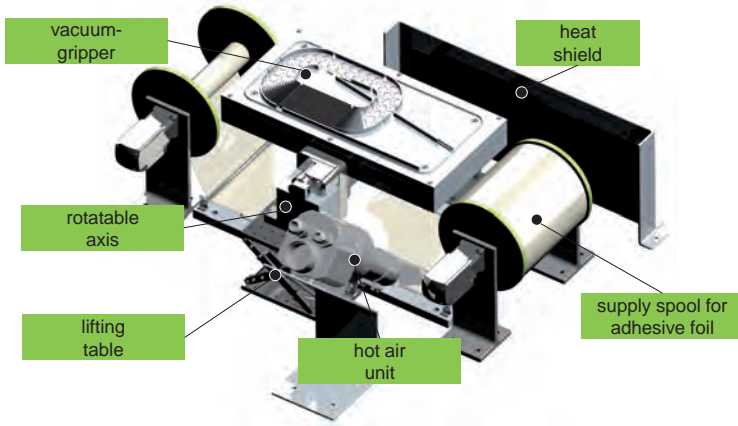


Fig. 76. Reel-to-reel system with adhesive foils and vacuum gripper.

With all the above-described process alternatives, it has to be considered that limp base materials (paper, foams, foils, textiles, tapes) are inherently problematic due to their limpness with low tolerance values, especially when removed from a support frame to the next process step (see test set-up with textile-based materials in chapter 5.2.4).

5.2.4 HF-Litz wire winding

HF-Litz wires are expensive, sensitive, and can significantly weaken pad performance when not processed appropriately. HF-Litz wires consist of several hundred twisted, individually insulated thin wire strands (see also chapter 4.1.2 for the detailed set-up of HF-Litz wires). The process of winding HF-Litz wires is specifically demanding when it comes to smaller bending radii, spreading wire strands, wire tension, wire feeding, etc. and must be examined carefully, as shown in Fig. 77.

To guarantee the performance of the pad design over the entire product-life, mass production must ensure high reproducibility and meet manufacturing tolerances. In [120] [123], winding tolerances of ± 3 mm have been reported with manually-created prototype constructions. Winding imperfections and manufacturing tolerances (Fig. 77 - 1, 2)

may result in reduced pad performance. Moreover, square coil corners help reduce pad size and material usage (shorter wire length) [87].

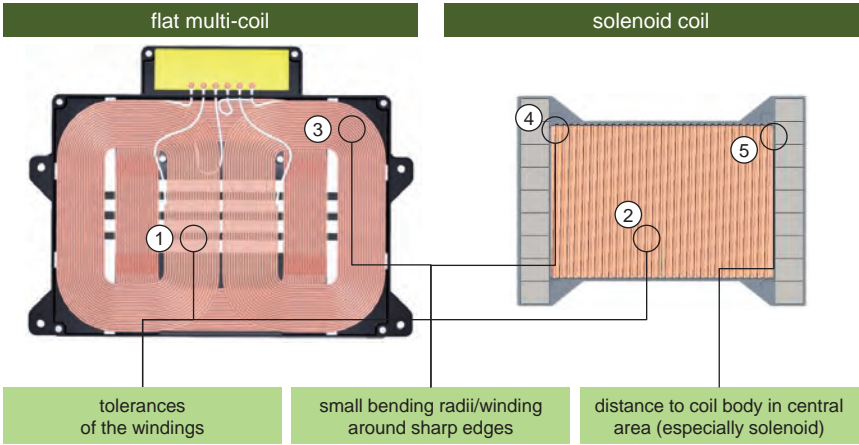


Fig. 77. Potential failures in the HF-Litz wire winding process.

In practice, however, HF-Litz wires will be damaged when bent too sharply, which favors a design with rounded corners (Fig. 77 - 3). HF-Litz wires may also be damaged as they are wrapped around sharp edges (Fig. 77 - 4) in the ferrite base plate. In addition, pad performance may suffer due to gaps between winding and ferrite base plate, e.g. in solenoid pad designs (Fig. 77 - 5), but also due to imprecisely wound and fixed circular pad designs.

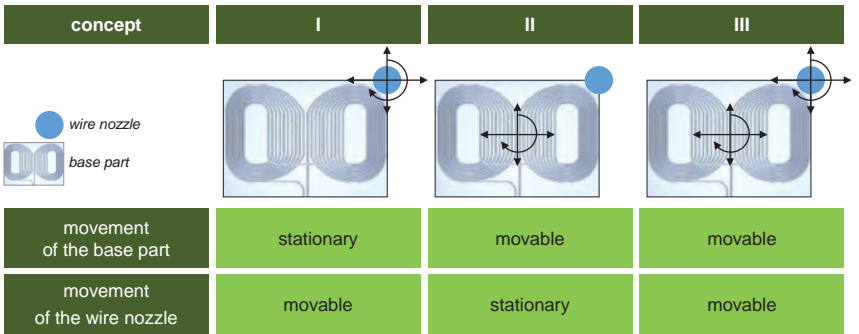


Fig. 78. Possible basic kinematic concepts for HF-Litz wire winding.

There are several possible basic kinematic concepts to perform the relative movements between the base parts and the wire nozzle in automated HF-Litz wire winding processes, as shown in Fig. 78. The focus is mainly on single-sided coil types described in chapter 4.2.

There are special tools and specifically developed kinematic concepts and winding stations to create different winding concepts. However, as shown in Fig. 79, the present thesis also uses robot-based concepts, due to several aspects and advantages, similar to the concepts studied for round wires [17] [198] [202].




concept	I	II	III
			
movement of the base part	stationary	movable	movable
movement of the wire nozzle	movable	stationary	movable

Fig. 79. Possible robot-based kinematic concepts for HF-Litz wire winding.

Test set-ups are expensive and time-consuming, as numerous variables need to be considered when designing charging pads [24]. Moreover, manually-produced prototypes have shown winding imperfections and manufacturing tolerances (± 3 mm), making it difficult to use simulation results to exactly verify different pad structures and compare results and effects in detail [123]. In this context, industrial robot-based concepts present the very decisive advantage that they are more precise than manual winding procedures, combined with a high degree of freedom and thus system-immanent procedural flexibility. Trajectories can easily be derived with CAD-CAM chains and kinematic simulations for different, even complex winding products, as shown in Fig. 80.



Fig. 80. CAD-CAM-based procedure to create test-coils.

This is also important as the behavior of HF-Litz wires during processing cannot be directly compared with the behavior of simple solid round wires. Thus, beside the kinematic simulation models to verify the principle of the production concepts, several real test set-ups have been implemented to optimize tool design and to derive potential problems with winding imperfections, as shown in Fig. 81.

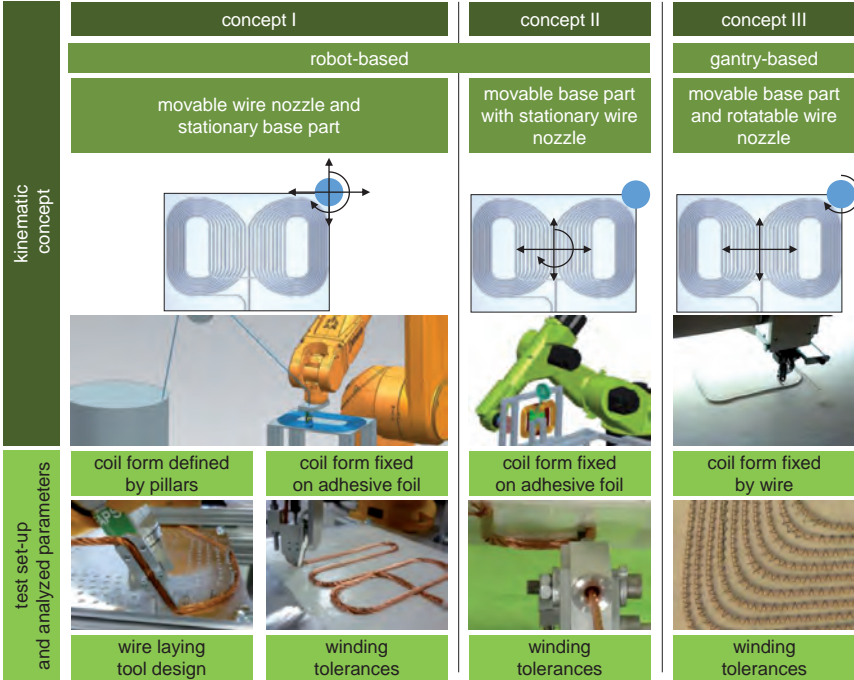


Fig. 81. Test set-ups to identify suitable trajectories and analyze material behavior.

This facilitates prototypic process development and evaluation of different coil concepts and enables a faster and more precise set-up of test designs compared to manual winding procedures. Aside from procedural flexibility to create different possible winding concepts, robot-based approaches also provide functional flexibility. Additional functions may be loading and unloading coils from the winding station or accurate positioning of HF-Litz wires for automated contacting. Such a robot-based approach is thus especially helpful during early stages of market development, as it allows product adaptations without intense investment in new basic assembly structures, increasing the range of product variants [198] [202].

The first concept (concept I, Fig. 78) of a movable wire nozzle and a stationary base part is used when the coil former/base material of the desired winding product does not rotate at all and stays in a fixed position. This is the case for the flyer winding concept, where a flyer rotates at high speed around a stationary fixed coil former. However, this process is hardly practical for HF-Litz wires, as wires may be twisted especially at larger wire diameters and/or alternative wire geometries. Moreover, since the flyer arm can only rotate, it does not allow for complex winding geometries without additional guiding elements. As the flyer winding option is limited, kinematic concepts with more flexible, movable wire nozzles on stationary base parts/coil formers are better suited, especially in order to fundamentally analyze different winding geometries. Approaches with linear gantry systems that move the winding nozzle across an x-y-plane are of limited suitability for HF-Litz wire handling without an additional degree of freedom to avoid sharp corners at the laying points, which may damage the HF-Litz wires. Robot concepts offer the most freedom and flexibility for wire laying on different base materials.

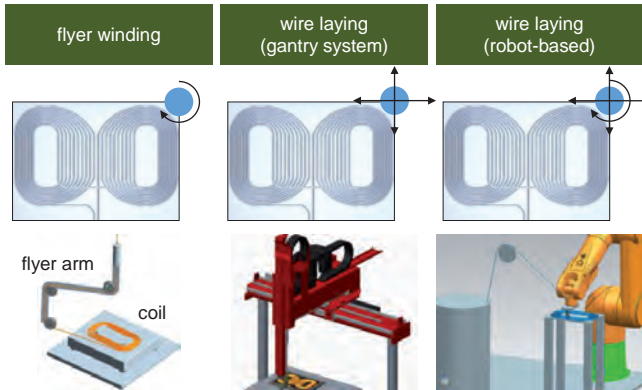


Fig. 82. Kinematic concepts with stationary base part and movable wire nozzle.

In order to verify the robot-based wire laying approach, a test has been set-up with a movable wire nozzle and a stationary base part (coil form defined by pillars), as shown in Fig. 83. The optimal parameter combination of the wire laying tools have been investigated with HF-Litz wire types (300x0.2; 1,500x0.1), with (silk) and without external insulation. The run-out radius of the wire nozzle and the tool-setting angle at the run-out point of the HF-Litz wire are the essential parameters, as they potentially cause friction or shear stress to the HF-Litz wire, which can damage it. Therefore, to identify the limits of used HF-Litz wires and derive appropriate tool design, tests were conducted starting with a large run-out radius of 5 mm (~diameter of the investigated HF-Litz wires) and different tool setting angles, from a non-critical 45° up to a challenging 90°. As shown in Fig. 83, a radius of 5 mm caused no damage to the HF-Litz wires. With a radius of

2 mm and 1 mm, the external insulation (silk) of the HF-Litz wires was damaged with tool setting angles above 75°, but the individual HF-Litz wires themselves remained intact in all test settings upon visual inspection.

run-out radius of the wire nozzle: 5 mm tool-setting angle: 90°				tool-setting angle					
Litz wire	run-out radius								
300°0.2 backlack 300°0.2 silk/one layer 300°0.2 silk/two layers 1,500°0.1 silk/two layers	5 mm	45°	60°	75°	90°				
						+	+	+	+
						+	+	+	+
						+	+	+	+
300°0.2 backlack 300°0.2 silk/one layer 300°0.2 silk/two layers 1,500°0.1 silk/two layers	2 mm	45°	60°	75°	90°				
						+	+	+	+
						+	+	+	+
						+	+	+	+
300°0.2 backlack 300°0.2 silk/one layer 300°0.2 silk/two layers 1,500°0.1 silk/two layers	1 mm	45°	60°	75°	90°				
						+	+	+	+
						+	+	+	+
						+	+	+	+

Fig. 83. HF-Litz wire laying test results.

This shows that the concept of laying HF-Litz wires is generally possible. However, to avoid damage to the HF-Litz wires, it will always be necessary to study the laying tool in detail, depending on the HF-Litz wire. This is especially crucial if the laying process changes the internal structure of the HF-Litz wire, with negative effects on pad performance.





	small pressure roll	large pressure roll	step-by-step deviation
	 <ul style="list-style-type: none"> small diameter of the pressure roll 90° deflection high deformational energy 	 <ul style="list-style-type: none"> large diameter of the pressure roll 90° deflection reduced deformational energy limitations with the laying radii 	 <ul style="list-style-type: none"> smaller diameters of the pressure rolls step-by-step deflection reduced deformational energy

Fig. 84. HF-Litz wire laying tool parameters.

The same is true for HF-Litz wires that are pressed onto base materials (adhesive foils, into grooves, etc.) with movable wire laying tools, as shown in Fig. 84. Deformation energy on HF-Litz wires can be reduced by using bigger radii on the pressure roll or by step-by-step re-routing, as shown in the Fig. 84. By using two pressure rolls and guiding the HF-Litz wire step-by-step, deformational energy can be further reduced while still maintaining high laying precision, as the lower pressure roll inside the tool is still quite small.

The attainable bending radius of HF-Litz wires is another important parameter, as smaller radii help reduce material usage but may damage internal structure. To determine minimum viable radii in HF-Litz wire winding, a test layout was developed that has different radii, parts with parallel windings, and a crossing for a fast and individual assessment of minimal HF-Litz wire radii (Fig. 85)

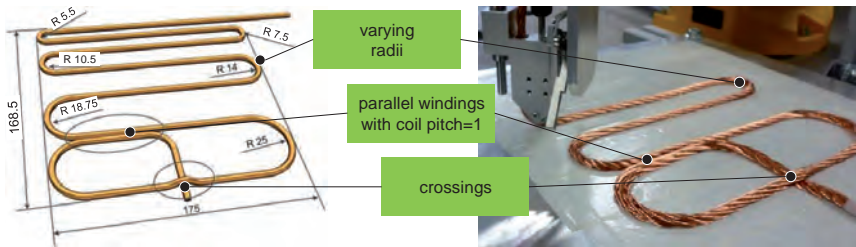


Fig. 85. HF-Litz wire laying test layout.

The experiment with this test layout was also based on the general kinematic winding concept with a movable wire nozzle and stationary base part (concept I, Fig. 78). This experiment with a 768 x 0.1 mm HF-Litz wire easily shows the limits of the laying radii, in this case at 14 mm. At this radius, the wire can no longer be reliably fixed onto the adhesive surface. It also shows the specific problem of HF-Litz wires without external insulation. The HF-Litz wires are deformed as they are pressed onto the foil, and their cross-section becomes oval-shaped. The low dimensional stability of HF-Litz wires without external insulation thus results in a reduced Litz wire quality parameter λ_p , as described in [203].

The serial-linked robots that have been used in the above-described initial test set-ups, still present some disadvantages for HF-Litz wire laying. The multitude of joints in the robot reduce stiffness of the kinematic and, in consequence, laying accuracy. This type of robot is also limited in its flexibility to lay sophisticated coils with several turns. Aside from serial-linked robot kinematics with rotary joints, parallel kinematic robots also can be used. Especially parallel robot concepts based on linear delta arrangements, as shown in Fig. 86, are well suited for laying HF-Litz wires. Linear actuators are assem-

bled sturdily in a “cage”, enabling large working volumes and providing high robot stability and rigidity. They also have a small footprint, saving shop floor space. Moreover, an infinitely rotating robot axis at the base platform can be added to enable rotation around the wire feed-axis (here z-axis). Thus, wires can be fed through the robot flange with a laying tool attached at the free end of the base platform. In summary, such a robot end-effector can move in three translational directions (x, y, z) and also has rotational degree of freedom of movement (α of more than 360°) around its z-axis for comprehensive positioning and orientation of the HF-Litz wire and a reduced risk for twists in the wire (see also wire feeding topics in chapter 5.2.2).

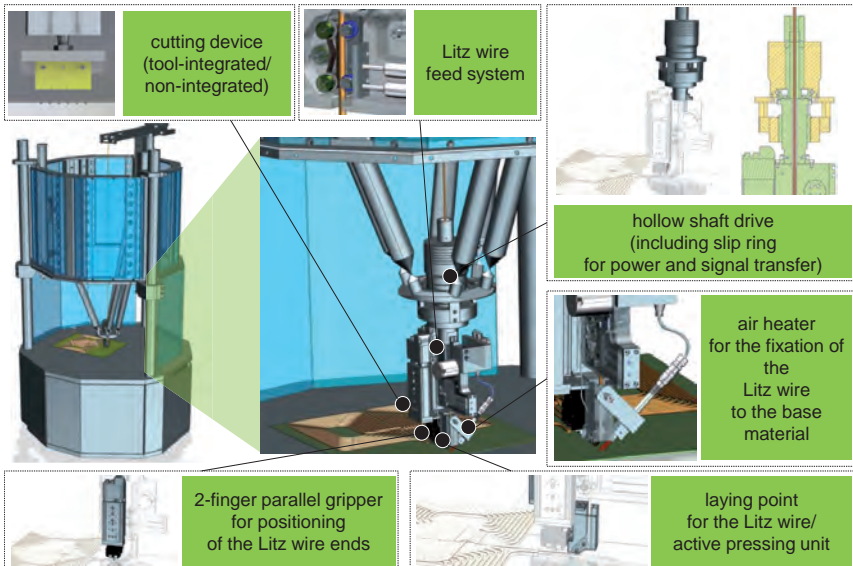


Fig. 86. Delta kinematic arrangement and laying tool with wire feed through robot flange.

Fig. 86 also shows the delta kinematic arrangement with an advanced tool that shows possible integrated functions that are needed for the wire laying operation. In order to integrate several functions in a laying tool with an infinitely rotating robot axis, slip rings for the transfer of power and control signals to the rotating tool are necessary. In consequence, the tool is capable of laying Litz wire coils in a flexible manner. However, the integration of functions in the movable laying tool should always be reflected for cost reduction compared to the option of integrating functions in the stationary base part elements.

Laying tool complexity can also be reduced with a stationary wire nozzle and movable base part (concept II, Fig. 78). Fig. 87 therefore shows alternative kinematic set-ups for this concept.

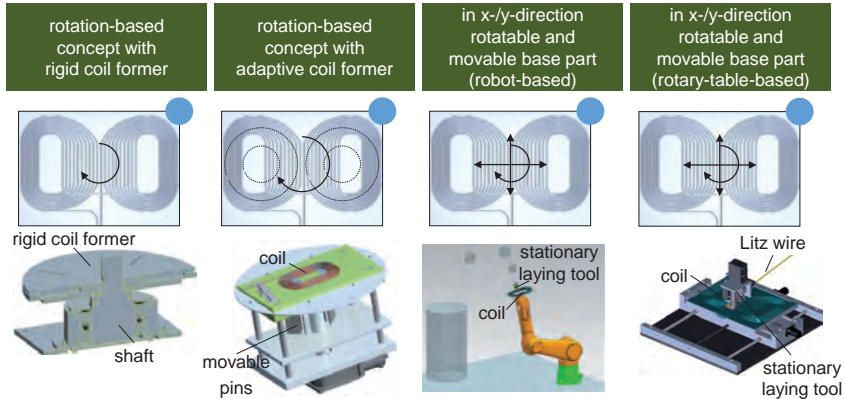


Fig. 87. Kinematic concepts with movable base part and stationary wire nozzle.

The simplest concept is thus to wind with a stationary winding nozzle onto a rotating base part. The winding device consists of an upper part to pneumatically or electrically open and close the machine and a base part with a motor for rotating the winding bobbins. The shaft of the upper part is not self-driven, and only rotates along with the base winding device. The rotation of the coil former pulls the wire, which minimizes wire stress and winds precisely without twisting wires. Thus, even coils with rectangular HF-Litz wires can be realized. It is also conceivable to wind several coils simultaneously [201].

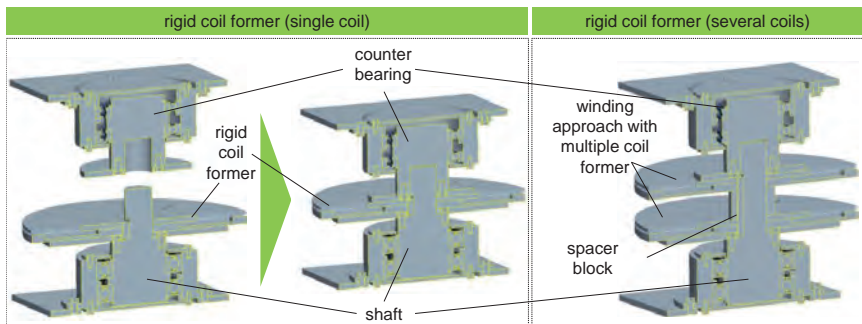


Fig. 88. Rotation-based winding concept with rigid coil former.

For this purpose, several base parts/bobbins would have to be mounted on the shaft, as shown in Fig. 88. However, the deficits of this inflexible standard winding technique and the expected increase in demand for increasingly sophisticated coil designs, e.g. with a larger or even varying coil pitch and/or 3D-contours, call for alternative winding methods.

A spindle winding process with adaptive coil formers has been developed to create pads with a larger (*coil pitch* > 1) or even varying coil pitch. After a defined number of winding turns, the coil shape is altered, e.g. by coil shaping elements (e.g. movable pins) that jut out from different spots of the base coil part [197] [201] (Fig. 89).

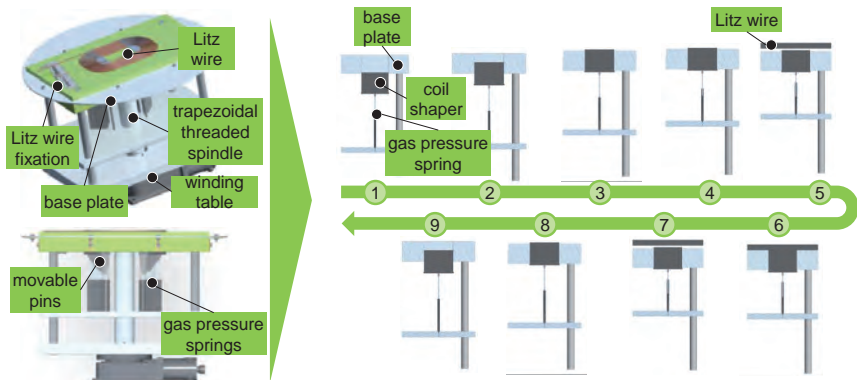


Fig. 89. Winding table with adaptive coil former.

Once the pins are pushed out through the base plate, the following winding turns have to take a different, longer path than the previous windings [197]. In this way branches, junctions, and/or varying coil pitches can be realized in certain sections as the pins emerge successively in course of the winding process.

With coil formers fixed onto an intermediate plate, gas pressure springs with different lengths are mechanically connected to the rotation of the winding table with an acme screw/trapezoidal threaded spindle. When the winding table is rotated, the intermediate support plate rises with each revolution (here 4 mm depending on the type of thread, nominal diameter, and pitch), until the coil former stands out at the required height from the winding table (e.g. HF-Litz wire diameter), and is stopped by slots in the winding table and a small flange at the lower end of the coil formers. The smaller gas pressure springs are still free of pressure, pushing the attached pins successively out of the base winding table. When the winding table rotates back in the other direction, the coil formers sink back to their initial position. Consequently, the position of the coil pins is directly and securely defined by the rotation of the base plate. These "coil formers" may

also be controlled by separate electric motors. However, such a solution to achieve precise sequential control is far more expensive and also prone to errors and problems.

To create more complex coil structures, one can also use kinematic concepts with stationary wire feeding on a base part that can move in all directions. This concept has the advantage that the HF-Litz wire enters the laying spot straight-on with a simpler wire feeding path and a reduced danger of wire twist. This works well for complex coils with several HF-Litz wires that have to be laid down simultaneously (see Fig. 90).

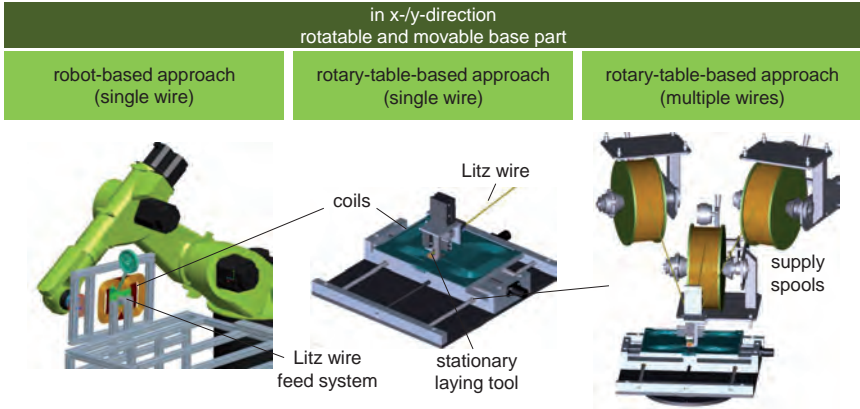


Fig. 90. Kinematic concepts with base part that is movable and rotatable in the x-/y-direction.

In addition, synchronization between laying tool guidance and winding table is less complex. The handling of the base, however, is more difficult, especially with complex coil designs. The advantage of easily programmable robot-systems with CAD-CAM chain thus becomes obvious. Moreover, robot-based systems can even create coil structures on both sides of the base frame in one winding process by simply turning the backside of the base frame to the wire laying point (e.g. for multi-coil pad designs like DDQ-pads). Afterwards, the base support structure can easily be transferred to the next process step. This requires stable base support structures with appropriate interfaces between the base part and the robot-system to avoid problems with winding tolerances. This concept can also be realized with winding tables that are rotatable and movable in x-/y-direction, as shown in Fig. 90, reducing process times.

An experimental test set-up was conducted in order to verify the winding tolerances of this approach with stationary wire nozzles and movable base part without expensive, grooved base plates, fixated on a plane plate with adhesive foil. Aside from the winding

tolerance, this test revealed the problem that individual bundles of HF-Litz wires without external insulation tend to fan out at insufficient radii (Fig. 91).

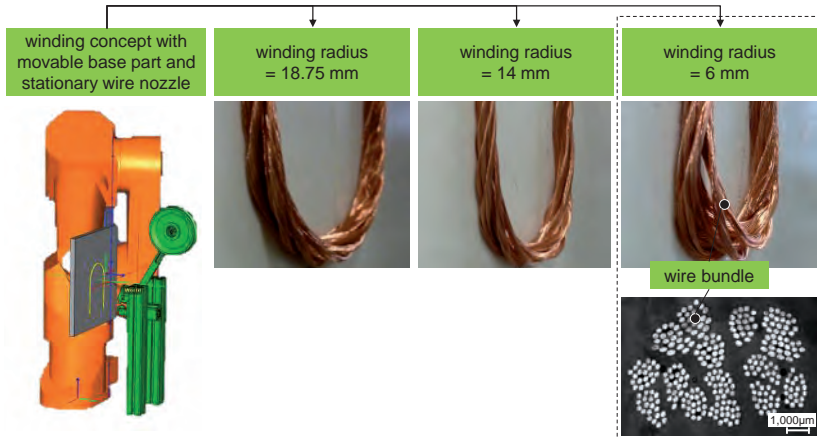


Fig. 91. Results of HF-Litz wire laying tests with a movable base part.

The microscopic image in Fig. 91 shows no insulation and wire damage. However, the cross-section is slightly elliptical, which reduces the number of strands that fit into a given area, and thus effectively increases resistance [143]. Moreover, the single wires are clearly separated, changing the proximity effect. These issues can be limited by using HF-Litz wires with external insulation (core-spun HF-Litz wire types). The fanning-out can also be reduced by adjusting the length of lay of the HF-Litz wire (the distance a single strand needs to complete a 360° turn). Moreover, the tests with movable base part and stationary wire nozzle also revealed problems with meeting desired winding tolerances. There were significant shifts, especially at the entry and exit points of the curves, which were even more substantial at smaller radii. As seen in Fig. 92, deviations depend mainly on the design of the wire nozzle and the pressure roller. If the inner radius of the wire nozzle is too big, it will cause problems, especially at smaller winding radii. At a radius of less than 10 mm, deviations amount to up to 2 mm. With larger radii about 14 mm, the deviation is no larger than 1 mm. HF-Litz wire without external insulation is more flexible and shows better winding tolerances except at the exit point. At this point, HF-Litz wire without external insulation is “too” flexible and loses contact to the guidance of the pressure roller (Fig. 92). To address this problem, the pressure roller needs a device such as a central groove to guide the HF-Litz wire properly.

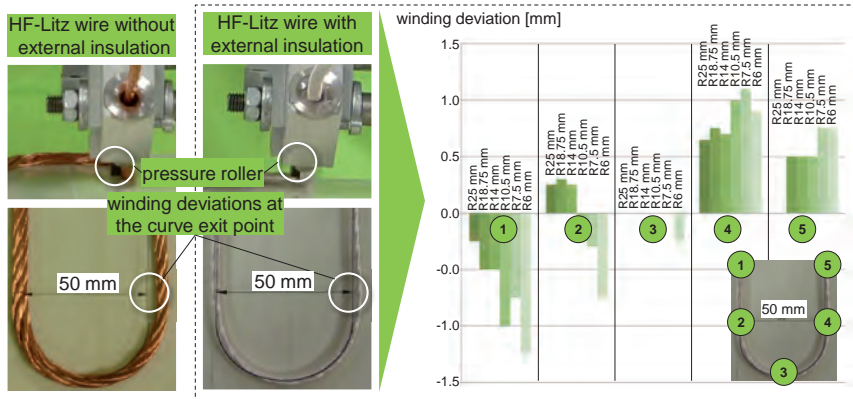


Fig. 92. Results of HF-Litz wire laying tests with a movable base part.

Combining the first two concepts yields a third kinematic approach (concept III, Fig. 78). A movable base part and a movable wire nozzle allow for complex motions with even more degrees of freedom.

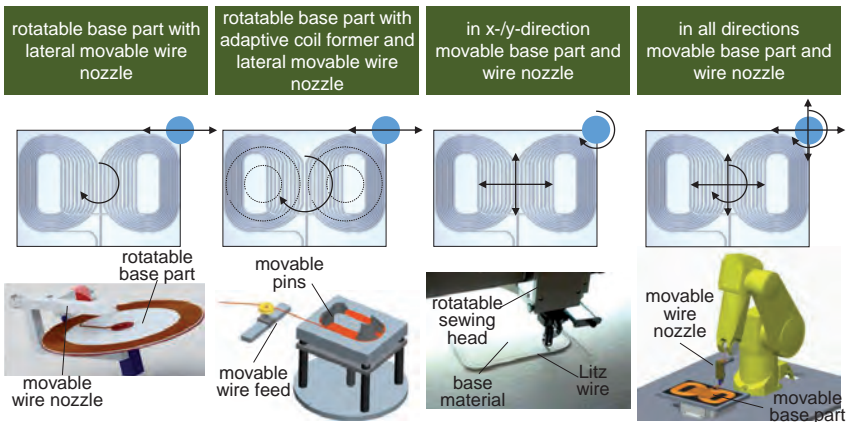


Fig. 93. Kinematic concepts with movable base part and movable wire nozzle.

A rotatable base part (with grooves) and a laterally movable wire nozzle allow for even higher winding speeds. The laying tool is fixed to a support structure that allows the tool to move from the inside to the outside at constant or even varying speeds depending on the coil concept, allowing for coil pitches. This approach can also be combined with

pressure rollers at the laying tool for a mechanical and/or adhesive fixation, as has already been described in chapter 5.2.3. Aside from simple two-dimensional coil forms, traditional coil-former-based techniques can also reliably and very quickly create solenoid designs with coils wound around a ferrite core in a tightly packed helix.

Coil pitches can also be achieved by adding adaptive emerging pins to the base part as already described above. The only difference to the afore-mentioned approach is the wire nozzle's additional lateral movement. This is the preferred solution, as the angle of the fed HF-Litz wires can be controlled more precisely, with even less wire stress (Fig. 94).

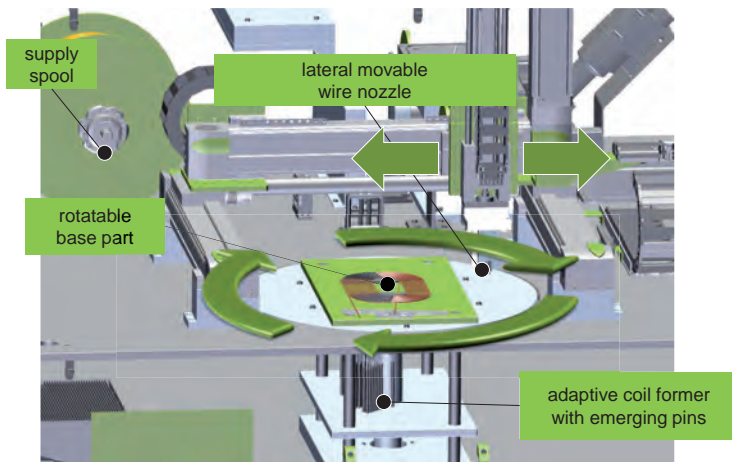


Fig. 94. Kinematic concept with rotatable base part, adaptive coil former, and laterally movable wire nozzle.

The wire nozzle is handled by a simple parallel jaw gripper fixed to a gantry system and moves laterally along the rotatable winding table and its emerging base pins during the winding process, which limits potential stress on the HF-Litz wire. Moreover, as the gripper that is attached to the gantry system also allows movements in the x-, y-, and z-direction, the winding process needs almost no manual preparation (e.g. for clamping wire ends to the winding table before each operation). This results in a fully automated winding station for even complex coil designs with coil pitches.

Aside from the above-described rotation-based concepts for base parts, winding structures can also be laid and fixed onto base material that moves horizontally underneath a rotatable wire nozzle, e.g. with industrial sewing machines. The base material is held in a machine frame which can move the material in the x- and y-directions [17], as shown

in Fig. 95. This concept allows HF-Litz wires to be placed and fixed with great freedom of design without expensive base plates with grooves etc. Developing an automatic "inter-changeable frame system" makes it possible to lay wires on an in theory endless stretch of base material. This concept can be used for any base material that can be penetrated by needle and thread, like textiles, foams, foils, or even more stable materials like glass-mat-reinforced plastic base parts for underbody systems. High productivity can be achieved with multiple guide units on the machine [204].

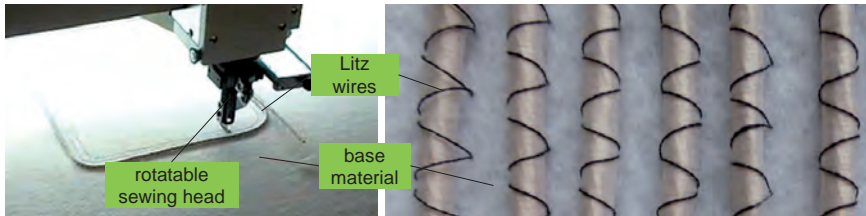


Fig. 95. Fixation of wire windings with industrial sewing machines [17].

To verify this concept, a DD winding structure with varying radii and coil pitches has been set up on a Filacon industrial sewing machine. These machines are commonly used to fix (non-insulated) Litz wires with small diameters of up to 1-2 mm, e.g. for seat heating systems in cars, but not for HF-Litz wires with diameters up to 4-6 mm. An optical multi-sensor coordinated measuring device (Video Check IP400 HA) was used to compare the attained installation accuracy to the intended target geometry. This revealed several issues as described in the following.

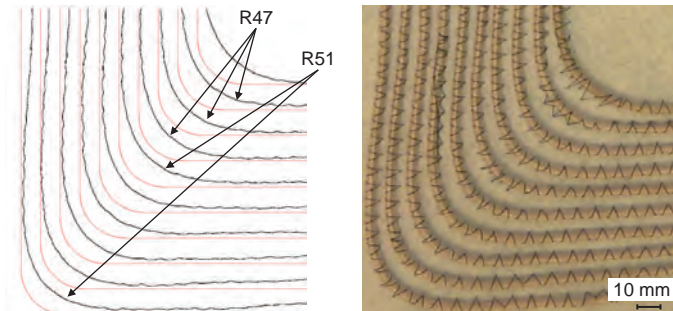


Fig. 96. Results of HF-Litz wires laying tests with a sewing machine (radii).

Fig. 96 reveals the low dimensional accuracy of this test coil with significant shifts and ripples. The radii in the actual layout differ starkly from the desired target layout. The discrepancies are caused by the rigidity and rebound force of the HF-Litz wires. Moreo-

ver, the limp base material shrinks when cut out. Aside from curves, parallel lines (which are, for example, needed for the coil pitches of a flux pipe for precise magnet field shaping) are also imperfect, as shown in Fig. 97.

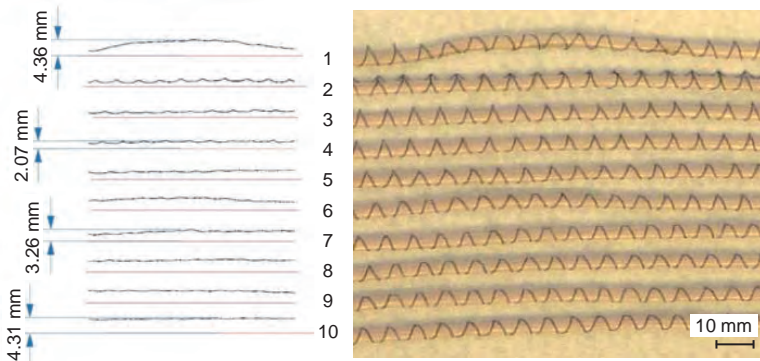


Fig. 97. Results of HF-Litz wire laying tests with a sewing machine (winding tolerances).

As seen in Fig. 97, discrepancies from the target geometry tend to worsen from the outside (winding number 2) to the inside (winding number 10) with the exception of the uppermost wire (winding number 1) which is irregular because of its close proximity to the starting point of the test coil. Overall, these deviations are once again due to the limpness of the base textile material. As the base material is clamped into a support frame and thereby stretched, the wires are sewed onto the base material with rather good accuracy to the target geometry. However, this accuracy is immediately lost when the base material is cut out of the support frame. Due to inner tension, the base material contracts significantly, especially when a complex winding structure with rigid HF-Litz wires is sewed to it. With the used wire types (diameters above 4 mm and added rigidity due to external insulation), it was also impossible to achieve the in theory possible laying speed of approximately 8 m/min that is commonly attained for smaller Litz wire diameters in seat heating systems (wire diameters of 1-2 mm without external insulation). Moreover, there is the danger of potential wire hits. Fig. 98 shows a microscopic picture of a cross-section of a hit Litz wire bundle (left) and a single wire that has been hit, resulting in significant deformations. Moreover, it can be seen that the needle scraped a portion of the wire, damaging the insulation. This has to be avoided at all cost.

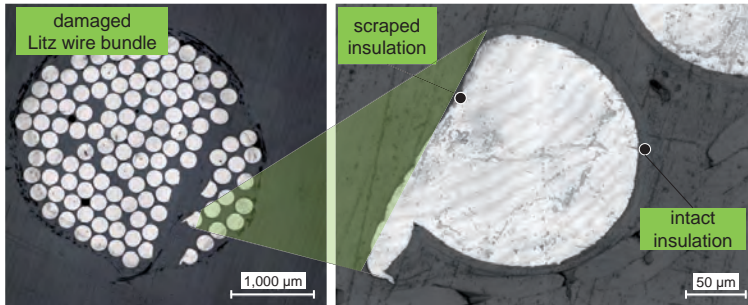


Fig. 98. Microscopic picture of a cross-section of damaged HF-Litz wires.

Despite all these problems, first prototypic attempts show quite some potential for this process. Stable base materials should be used for the fixation of the HF-Litz wires, as deviations became unacceptable especially after unloading limp textile base materials from the machine frame. In this context, it seems to make sense to fix HF-Litz wires directly onto stable underbody carriage modules that are made of Long-Fiber Reinforced Thermoplastics (LFRTs), with a porous and lightweight core that can be penetrated by needle and thread. In consequence, using more stable base part materials should result in higher process speed, and ideally eliminate wire hits due to higher dimensional accuracy. Moreover, as the used machine was inadequate to handle the needed HF-Litz wires, alternative, more stable sewing heads that feed HF-Litz wires appropriately should be considered. Even so, fixing a wire to a base material will still pose a critical process safety risk. Aside from adapting wire guidance, additional sensors will be needed to detect wire hits in the process.

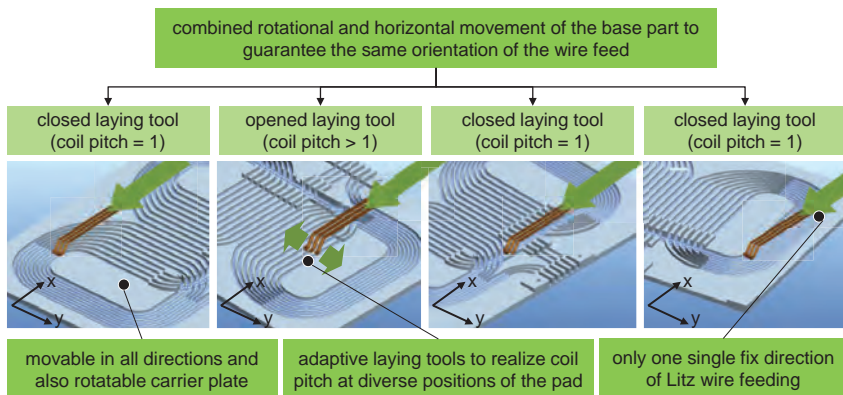


Fig. 99. Kinematic concept for “multi-Litz-wire multi-pole-coil” pad designs.

Adding more degrees of freedom to the base part (movable in all directions and also rotatable as already described by concept II), and to the wire nozzle results in a winding approach for HF-Litz wires that is highly capable and high-performing, but also complex, as the movements of wire nozzle and base part have to be synchronized. This is shown in Fig. 99 with a movable base part and an adaptive laying tool to attain a multi-Litz-wire multi-pole-coil pad design with three Litz wires and coil pitches at various pad positions. Therefore, a complex reference coil design has been set-up to verify the kinematic approach by simulation.

It can be shown that even the most sophisticated “multi-Litz-wire multi-pole-coil” designs can be achieved by combined rotational and horizontal movement of the base part on a winding table with an adaptive Litz wires laying tool to attain a coil pitch at various positions of the pad. Thereby, the complexity of the laying tool and Litz wire feeding can be reduced, as the laying tool only needs to cover the different coil pitches, as seen in Fig. 100.

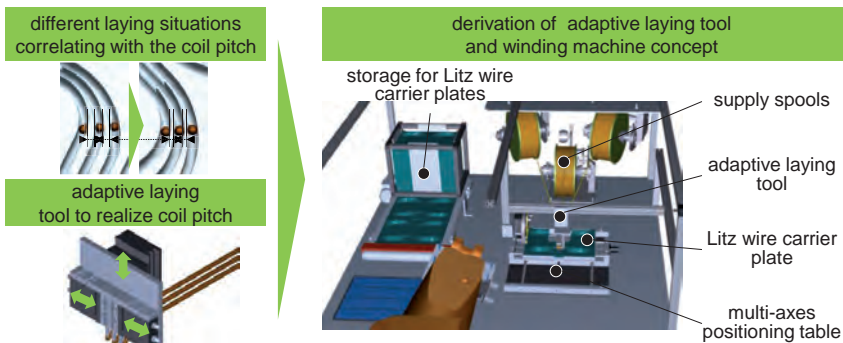


Fig. 100. Winding approach for “multi-Litz wire multi-pole” pad designs.

The concept that offers even more functionality features a base part movable in all directions and an adaptive laying tool for the wire nozzle, as can be seen in Fig. 101. Not only can you move and rotate the winding table horizontally, you can also tilt it, e.g. with a base part that is fixed to robot as described in Fig. 91 and a movable robot-guided wire nozzle. This is especially interesting for the use of ambidextrous robot concepts described in [205]. This allows for further coil concepts, like combined solenoid and circular pads [206] or DD-pads with sharp 3D corners at the coil edge to further reduce pad size [173].

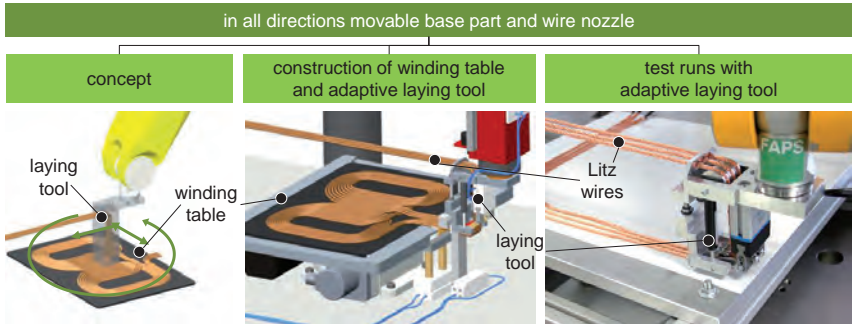



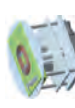







Fig. 101. Winding approach for “multi-Litz wire multi-pole” pad designs.

However, even if these coil designs are feasible, it must always be considered whether the production effort is really justified, or whether the desired CPT-pad functionalities can also be achieved with simpler coil designs and hence simpler winding techniques. The different kinematic approaches and their capability to create different desired coil parameters are summarized in Tab. 13.

Chapter 5 showed the principal production concepts that are possible to create even complex coil structures. In order to achieve high quality CPT systems, material behavior has to be taken into detailed account in addition to basic production concepts. Therefore, to reflect critical material behavior, selected production concepts have been implemented and reflected. Overall, the results described in this chapter show that self-bonding wires without external insulation can be processed more easily. However, HF-Litz wires without external insulation present the disadvantage of lower cohesion of individual strands and a lower degree of protection against mechanical damage. As shown, problems may arise in the winding process with tighter curves as the wires are being deformed. For complex coil designs, external insulation is needed to keep wires in shape and acting as a single conductive wire with a sufficient quality parameter λ_p [134] [203]. HF-Litz wires are thus insulated with adhesive tapes that provide good protection against mechanical and chemical impacts. However, inelastic adhesive tapes make HF-Litz wires very rigid and therefore difficult to wind, especially into tighter curves. Another disadvantage is the need to remove the adhesive tape before the contacting process to avoid residues and fumes. External insulation with silk offers the best compromise, providing high HF-Litz wire stability and good protection against mechanical damage while still offering certain flexibility, which is advantageous for winding. In addition, layers of silk may facilitate encapsulation [134]. A disadvantage is, once again, the need to strip the silk before the contacting process to avoid residues and fumes. Another decisive parameter is the length of lay of the HF-Litz wires.

Tab. 13. Classification of different winding technologies.

	concept I		concept II			concept III			
	movable wire nozzle, stationary base part		stationary wire nozzle, movable base part			movable wire nozzle, movable base part			
	flyer winding	wire laying	rotation-based concept with rigid coil former	rotation-based concept with adaptive coil former	base part movable and rotatable in x-y-direction	rotatable base part with laterally movable wire nozzle	rotatable base part with adaptive coil former and lateral movable wire nozzle	movable base part and rotatable wire nozzle in x-y-direction	base part and wire nozzle movable in all directions
									
3D contours	---	+	--	--	0	--	--	---	+
multi-coil systems	---	+	---	---	++	---	---	0	++
multi-pole coils	---	++	---	---	++	---	---	0	++
multi Litz wires coils	-	--	0	0	+	0	0	0	+
coil pitch	---	++	-	++	+	++	++	+	++
varying radii	---	++	--	++	+	++	++	+	++
precise winding tolerances	++	0	++	+	--	+	+	--	+
transitions/crossings	--	+	--	--	+	--	--	0	+
accurate positioning of Litz wires	0	++	0	0	+	+	++	0	++
comment	only of limited suitability for HF-Litz wire winding	suitable especially for prototypes	only for simple HF-Litz wire windings	for HF-Litz wire windings with coil pitch	for multi-coil, multi-pole HF-Litz wire windings	for HF-Litz wire windings with coil pitch	for HF-Litz wire windings with coil pitch	for HF-Litz wire windings with coil pitch	maximal functionality for HF-Litz wire winding

Longer length of lay is desirable from a production point of view, as it provides a better filling factor and high flexibility due to the lower rigidity of the individual wires. However, with a longer length of lay, dimensional stability and roundness decreases. In setting these parameters, it is important to consider the individual winding pattern, the generated (external/internal) proximity effect, and resulting varying resistances, as an individual strand in a twisted bundle travels a greater distance than a simple straight wire bundle [143]. The test results also highlight the challenges of using simple flat base materials to carry the coils compared to more expensive base parts with mechanical fixation elements such as grooves. Coil forms with grooves guarantee reliable wire positioning even for complex coil shapes. When fixing wires on simple flat base materials, limited positioning accuracy must be carefully considered as the main impeding factor.

In summary, the implemented tests shown above can identify production-relevant characteristics to assess the suitability of HF-Litz wires for winding and the winding/wire laying tools needed for this purpose.

6 Optimizing CPT Systems from a Process and Material Perspective

Optimized design results in considerable long-term cost and energy savings. The main objective of pad optimization is thus to identify the limitations of different pad designs and system behaviors, and to propose solutions to overcome them. So far, numerous pad models with various configurations dependent on many variables have been investigated to find improved charging pad designs [24]. This approach addressed system optimization mainly from a geometric (size, form and position of ferrites and coils) and functional perspective (power level, transmission frequency, control strategy, charging currents, protection measures) [120] [121].

But there is also a variety of other aspects from a material and production point of view. For practical application in an EV, power pads must meet strict automotive requirements (certification to ISO/TS 16949:2009). CPT systems have to function reliably from the first to the last day of the vehicle's product life. The power transfer rate or efficiency may not drop, total system failure is not acceptable. Failure modes and effects need to be identified ahead of time and assessed with a thorough material and process analysis. This has to be done for all production processes in the entire supply chain as early as possible, from early stages of product development (product- and process-FMEA³⁶). Winding resistances and ferrite core losses, for instance, are often ignored in system designs as they are considered to be significantly lower than mutual and leakage reactances at the resonant frequency [161]. This may be true for prototypical systems in the lab, where materials are chosen appropriately and the set-up is careful. However, this assumption also has to hold true for pads manufactured with less than perfect off-tool quality, less than premium (i.e. cost-sensitive) materials, processed at higher speeds on industrialized equipment designed for large-scale production, able to handle the stress profiles that arise over the entire product life.

Fig. 102 shows the cause-and-effect diagram of possible issues with CPT systems. Very significant potential failure modes, e.g. due to radiated emissions (EMC issues with keyless entry systems, control systems, LOP, FOD, exceeding permissible exposure limits, etc.) have to be carefully considered with suitable design approaches and substantial analyzes in special anechoic RF chambers. Aside from EMC compliance profiles, further problems induced by production, material and operational influences may also significantly impact CPT system performance. The fact that CPT devices operate inside vehicles (underbody, front, rear bumpers) and in the ground poses additional challenges. The introduction of contactless charging technology and the integration of secondary charging pads in the underbody means that underbody trim parts must serve an even broader range of functionality and requirements [27].

³⁶ Failure Mode and Effects Analysis

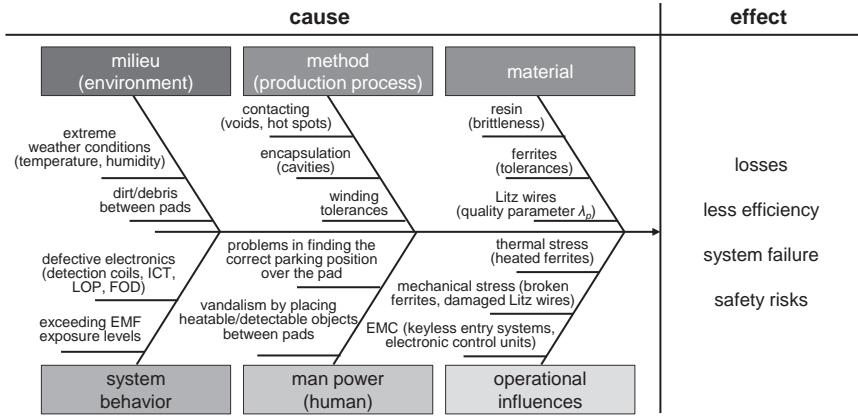


Fig. 102. Cause-and-effect diagram for CPT systems during production and product life.

The materials qualification is commonly done or assisted by the materials supplier. However, it is significantly more complex to validate processing effects on materials like HF-Litz wires in winding and contacting or under mechanical (see chapter 6.1) and thermal stress (see chapter 6.2) during operation. Testing methods need to be found to determine how such stress profiles impact pad performance. This impact analysis ideally always has to be conducted in relation to individual underbody and powertrain concepts (PHEV, REEV, BEV). As of today, several test bench concepts have been presented that directly compare the properties of different pad topologies according to their main parameters, such as achieved power P_{out} , efficiency η , magnetic coupling coefficient k , safety (EMF exposure levels), and temperature ϑ_{max} [41] [167] [207]. In addition, approaches have been developed to test the inter-operability of different magnetic designs, especially considering different misalignment scenarios. To do this, the pads are usually fixed to a simple support structure made of non-conductive material (e.g. fiberglass strut support systems). These support struts commonly allow multi-axes positioning of the secondary and/or primary pad for a precise study of parameters like power and efficiency [167]. However, the tools to measure magnetic field exposure and temperature and secondary coils are usually installed at a fixed position or manually adjusted with limited measurement capabilities, especially for pad designs that show complex behaviors with varying environmental circumstances (misalignment scenarios in x-, y-, and z-directions, rotation and tilt, temperature influences, etc.).

To measure the impact of manufacturing and material parameters on pad performance, an automated test bench concept based on a linear x-, y-, z-gantry system has been developed, as shown in Fig. 103.

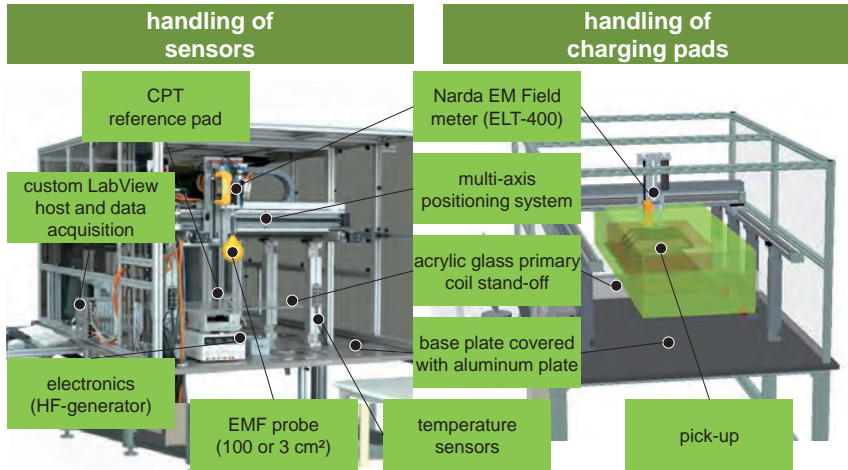


Fig. 103. Test-bench approach to evaluate contactless power transfer systems from a process and material perspective.

The test bench should be made of non-conductive, non-permeable materials like wood or plastic in order not to affect the magnetic field and examined parameters. The prototype test bench concept shown in Fig. 103 uses acrylic glass support structures with appropriate distances to the metallic base structure of the test system and an additional aluminum shielding plate that covers the base plate to avoid disturbances. The developed test bench presents the main advantage that, independent of measuring techniques, diverse objects (secondary or primary pad, EMF- and temperature sensors, infrared camera, etc.) can be handled in a precisely reproducible manner. The set-up can produce detailed images of magnetic field disturbance as well as temperature and power profiles for misalignments in all x-, y-, and z-axes, limited only by the resolution of the testing equipment (*"handling of sensors"*). In this context, production processes and materials for CPT systems with different potential failure modes of the processed materials during the pads' lifetime (from the production phase to potential failures during pad operation) can be analyzed. By rotating the investigated primary and secondary pad by 90° in the test set-up, one single test run can measure magnetic field exposures and temperature profiles below (e.g. impact on supply cables in the sub-floor area) and above the primary and secondary pad (e.g. impact on vehicle subfloor, vehicle interior, engine-compartment, etc.). Another promising aspect of the test bench concept is its precise and flexible orientation between source and capture device (*"handling of pads"*). This feature allows e.g. for an exact evaluation of RPEV CPT systems by placing several primary CPT systems on the ground and precisely positioning the secondary sys-

tem above the pads with different test profiles (varying air gaps, lateral tolerance, etc.). Fig. 104 summarizes the features of the kinematic concept of the developed test bench.

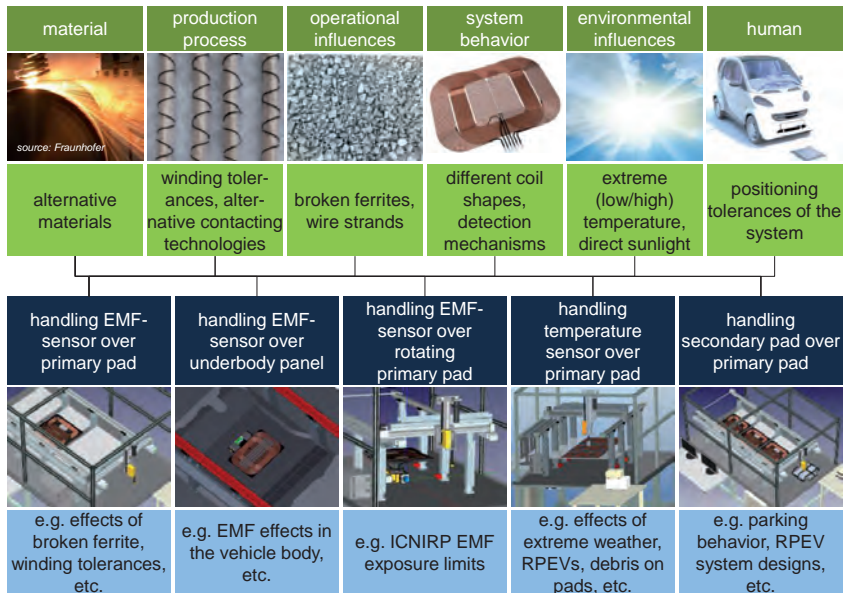


Fig. 104. Kinematic concept of the developed test bench for CPT systems.

In the following, mechanical (see chapter 6.1) and thermal (see chapter 6.2) stress profiles are reflected to derive the impact on pad performance.

6.1 Mechanical stress profiles

There are extreme mechanical stress profiles that may occur on the underside of a vehicle during its lifetime (e.g. when electric vehicles are driven on rough unpaved roads etc.), from which its sensitive pads have to be protected, in particular. They include massive shocks to the vehicle body in different crash situations (especially underbody parts close to the edges of the vehicle). Fig. 105 shows a heat map³⁷, highlighting currently used locations of contactless power transfer systems in prototypic vehicles and how different areas of the vehicle might be impacted in a crash, by severity (zones A-C) [18].

³⁷ The name "heat map" originally derives from the fact that some colors are associated with temperatures. In this case, however, a "heat map" is not a visual color-coded representation of temperatures in certain areas of the vehicle underbody, but the density of pads in a certain area.

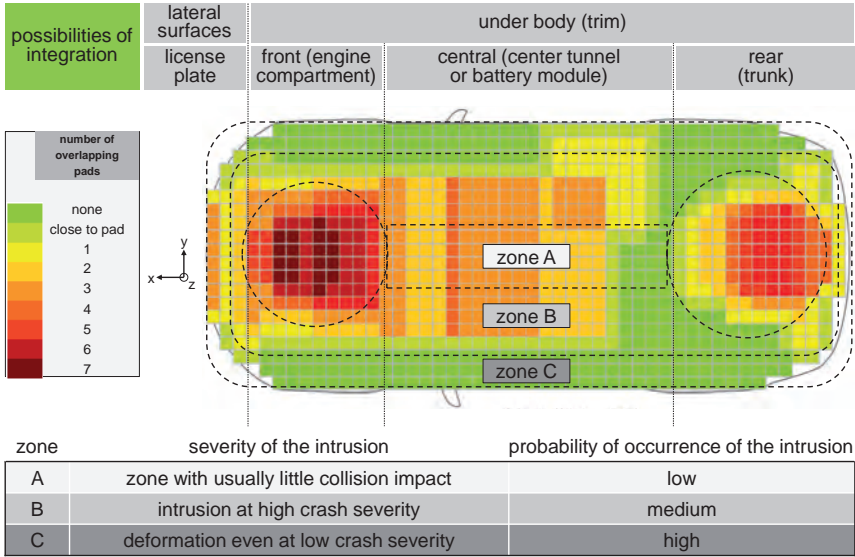


Fig. 105. Schematic illustration of different charging pad positions in the form of a heat map.

Dark-red areas show where the most pads are likely to be located, green areas show zones of lesser interest. It illustrates the large number of possible integration variants, which significantly differ in size and integration type. The position of charging pads in the vehicles mainly depends on the vehicle type and the electrification of the power train. The map shows that virtually all pads are integrated along the axial symmetry of the vehicle. These most commonly used positions are thus at the side (license plate at the front or the rear) and at the underbody of the vehicle (front, rear, or central part).

License plate systems are frequently proposed. A primary infrastructure-sided coil is mounted, for example, to the wall of a garage, and a secondary coil is integrated in the front of the vehicle behind the license plate [60] [130] [131]. Integrating the secondary side in the front license plate has benefits in terms of weight, space, and cost. However, this form of integration poses a greater risk in crash scenarios, especially in accidents that involve pedestrians. The hard structure of the pads with ferrites undermine the ideal of a well-defined and smooth vehicle front. The risk of injury to pedestrians increases. Early CPT systems with U-shaped half transformer cores caused even more problems as they took away space for deformation elements between the bumper and the passenger compartment [208]. Recent approaches [129] therefore try to reduce this problem with thin flat coils in the secondary sides, also equipped with foam materials and

pre-determined deformation elements between the ferrite blocks to minimize the risk of injury to pedestrians. This way, the usually hard secondary ferrite core can deform in an accident with a pedestrian, whose impact energy is better absorbed. The same goes for the impact energy of the primary pad in the event of a parking collision. Ideally, these pre-determined deformation elements will be made of a mixture of plastics such as PE, PP, or rubber and contain a fine powder of soft magnetic material (ferrite powder) [129].

New CPT systems that can handle power transmission over larger air gaps avoid the disadvantages of license plate systems. Thus, most recent projects focus on pad systems that are fixed to the underbody near the front axle. In this area, especially smaller pads can be integrated relatively easily into existing vehicle concepts [27], e.g. into the engine sub-frame, as shown in Fig. 106.

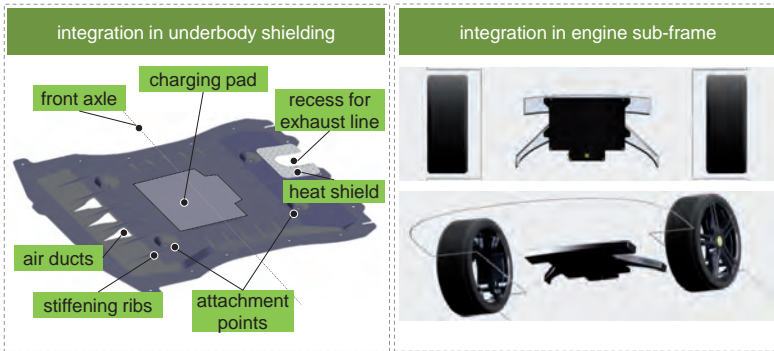


Fig. 106. Underbody systems in the front area of the vehicle.

Moreover, the area of the front axle works well as a pad location, as CPT systems must work simply and intuitively, without tedious parking maneuvers. As the driver can keep visual contact with the pad for a relatively long time, the driver can easily correct the vehicle's position with a few maneuvers. However, Japanese companies like Toyota and Nissan have presented several prototypes with CPT systems integrated in the rear part of the vehicle underbody [14] [64], most likely due to the Japanese practice of parking cars backwards. Considerations of system integration, thermal stress, and space requirements also favor positioning the pad under the trunk in the back of the car. However, this position requires the system to handle air gap variations, as activities like loading/unloading cargo to/from the trunk result in varying weight distribution along the vehicle.

Taking into account safety (crash and EMC requirements), culture-related parking behaviors (permitting forward and reverse parking), and inter-operability, it makes sense to position the pick-up near the center of the vehicle [134] [170]. In principle, integrating

CPT systems in the battery modules is also an attractive option, as especially larger batteries for PHEV or BEV are usually installed close to the car's center of gravity for better driving dynamics, as low as possible in the central part [188] [195]. This also has the benefit of safe and compact integration of charging pad and electronics in the battery structures, which reduces the need for high-voltage cabling and cooling, especially for systems in higher power classes. Moreover, the central underbody position also lends itself to RPEVs and the option of dynamic charging.

Aside from crash zones, there are other mechanical impacts that have to be considered, such as curbs, speed bumps, driving through standing water, rocks, or even road debris like metal parts on the street resulting in abrasion damage to single components or even complete shifts of parts inside the pad. Especially road curbs and driving through water present significant failure potential for the pads. The probability that heavy rocks might chip the pads is highest in the wheel arches, because tires throw up rocks while driving. Damaged electronics, ferrites, and/or HF-Litz wires may lead to failures like poor performance, complete system shut-down, or even intense damage endangering the entire integrity of the system with severe safety risks (wires sticking out of the pad, losing the pad while driving, etc.). In addition, there are several other forms of potential long-term damage, e.g. in hybrid concepts when pads are integrated in engine underbody carriages, as engine vibrations result in vehicle body vibrations.

While the protection of the secondary side has to be designed strong, robust, and capable of withstanding surface loads or vibrations, the base power device positioned on the ground pads need special reinforcement against distributed loads (e.g. truck wheels) and point loads (e.g. heeled shoe) [41] [71]. To withstand such pressures, [71] propose installing pillars in the base power device, made of plastics like polyethylene which are elastically deformable under compression, thus absorbing a large amount of the impact energy. [83] propose to cover the base pad with polymer concrete.

In this context of mechanical stress profiles, fragile and brittle ferrites have to be carefully considered, in particular. Ferrites can break not only if handled roughly during logistics and assembly operations, but also by mechanical impacts or vibration-induced abrasion during the vehicle lifetime. Ferrites in CPT systems should always be positioned in the pad safely and with several protective measures. Early CPT systems still used large pot core plates [209], which are specifically prone to breakage. Recent pads use smaller I-core ferrites covering the entire pad area [157] [210] or positioned as single strips in cavities. Cracks in ferrites may deteriorate pad characteristics and cause heating with local "hot spots". The higher the power level and magnetic field, and the more directed the flux lines, the more critical failures may occur in the material due to increased (thermal) loss effects (see also measurements in chapter 6.2). The situation is particularly critical as the high relative permeability of the ferrite in the order of 2,000 means that a crack with a width of 10 μm is equivalent to 20 mm of ferrite [41]. Moreo-

ver, mechanical impact can dislodge the ferrites in the pad, changing the distances between adjacent ferrite blocks, shielding material, or coils, resulting in leakage flux with additional gap losses. This creates localized areas of increased flux density, resulting in higher losses at those points that can drastically increase overall losses. However, these aspects always strongly depend on the individual magnetic design. Preliminary experiments in research projects with larger circular pads showed that small cracks in and minor damage to the ferrite have hardly any negative effects on the quality of power transmission [56].

To verify mechanical impacts and compressive forces, sample FEM-based mechanical simulations have been conducted to determine stress profiles caused by hitting curbs and driving through water on the secondary pad and the underbody panel. Under such stress profiles, a large proportion of the vehicle weight impacts with a narrow portion of the bottom surface of the UBV. Several assumptions were made to simplify the model for FEM simulation in ANSYS Workbench, limit system boundaries and thus reduce complexity. The CAD models of the pad and underbody shielding were simplified by suppressing small details such as radii, chamfers, and ribs. In addition, all components in the housing except ferrites were replaced by a volume representing the encapsulation that fills the entire housing. This approach is applicable when the electrical components are completely impregnated by resin and, as a consequence, impact forces are more evenly distributed throughout the pad [134].

To determine the effect of a mechanical impact, a proportionate vehicle-weight-caused force is applied to a contact surface. Total load surfaces P_{load} can be distributed to quite a low level, avoiding point loads. Depending on the impact surface ($A_{impact_surface} = width_{impact} \times length_{impact}$) and the portion of vehicle $weight_{load}$, the following equation applies:

$$P_{load} [MPa] = \frac{weight_{load} \times 9.81 \frac{m}{s^2}}{width_{impact} \times length_{impact}} \quad (6.1)$$

Due to the significantly higher ductility of copper alloys in comparison to soft magnetic materials, coil windings are not considered in the simulation model. The calculation model thus includes only the gross geometry of the underbody panel, the pad housing with the cover, and the encapsulated ferrites. With this simplified CAD model, a fast calculation with fewer elements and nodes as well as a lower number of possible failure causes provides a first rough assessment of stress profiles (Fig. 107).

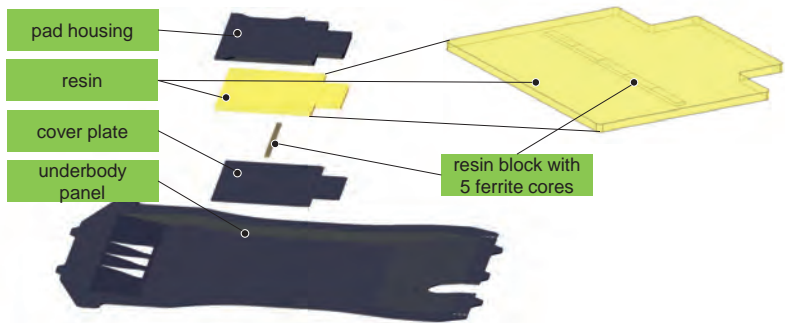


Fig. 107. CAD design of the underbody panel and pad for the FEM analysis.

In preparing the simulation model, initial materials data was defined in ANSYS Workbench for the respective components. In the simulation, the underbody panel, pad housing, and cover consisted of glass-fiber-reinforced polypropylene with a fiber content of 40%. The mechanical characteristics of Aratherm® XB 2710/2711 were used for the epoxy resin, Tridelta Manifer® 106 for the MnZn ferrite.

Fig. 108 shows the difference between curb test and driving through water with abrupt surface loads (bending loads) that are distributed over specific areas of the underbody panel. Especially the curb test is of significant importance, as this is a scenario that is very likely to occur during a vehicle's life cycle.

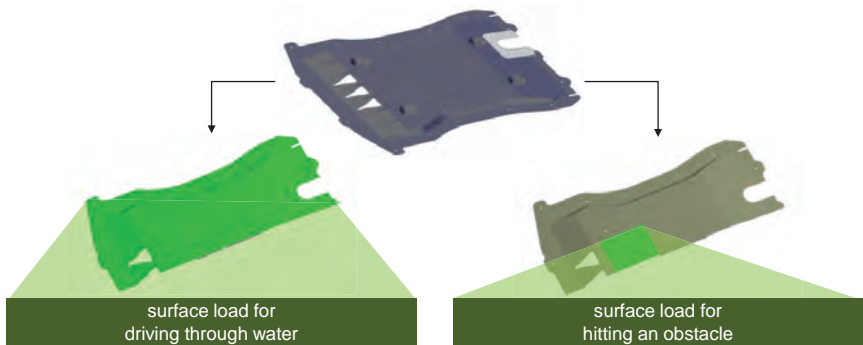


Fig. 108. Surface loads while driving through water and hitting obstacles.

In [56], the abrupt surface load amounts to approximately half the weight of the vehicle for driving through water and to one third of the vehicle weight for the curb test.

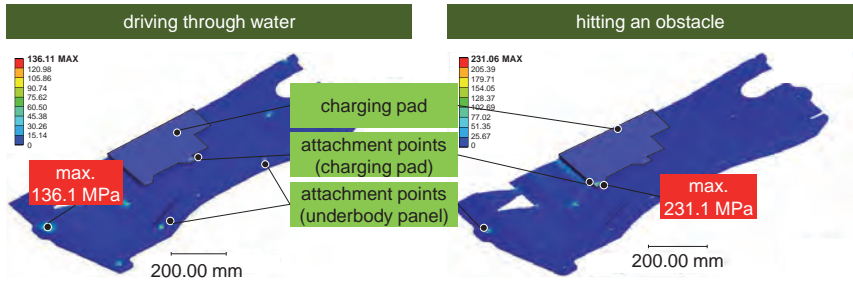


Fig. 109. Distribution of equivalent stress while driving through water (left) and hitting an obstacle (right).

As seen in Fig. 109, PP-GF40 for the underbody panel ensures sufficient mechanical strength in both mechanical impact situations. The underbody panels in both tests only deform in the elastic range, with sufficient rigidity and mechanical strength in the underbody panel. However, underbody panels with integrated CPT systems may be critical as the mechanical stress is not evenly distributed, due to the basic construction of the underbody panel. Especially at points where the underbody panel and CPT pad are fixed to the vehicle structure, high mechanical bending stress was determined.

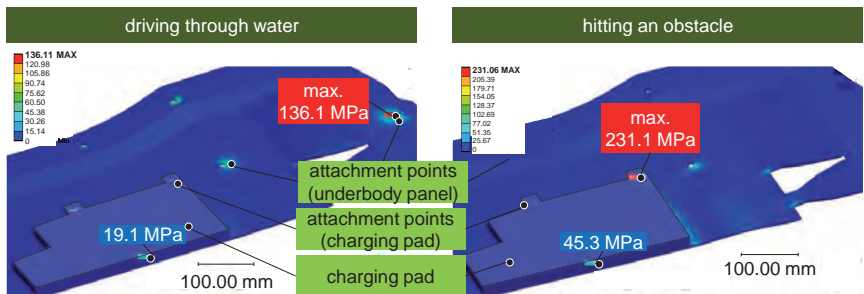


Fig. 110. Sample of mechanical impact on ferrite while driving through water (left) and when hitting an obstacle (right).

In the curb tests, the simplified simulation detected a maximum equivalent stress of 231 MPa at the attachment points of the pad housing, which would be higher than the tolerated mechanical strength level of PP40GF of 190 MPa. This could break the fixing points and eventually risk losing the underbody panel. In this case, it will be necessary to take further measures, like adjusting the geometry of the fixation bolts (differently positioned and/or more attachment points), increasing plate thickness, or choosing a dif-

ferent material with better mechanical properties. Special attention must be paid to air vents that effectively perforate the panel, as they could present weak points in the underbody panel, as well.

Fig. 110 shows stress in a ferrite core in the simulated example. Due to the brittle material behavior and thus low ductility, ferrites are very vulnerable under bending stress. Ferrite bending strength amounts to only 20 to 50 MPa. A sample of ferrite in the simulation results in an equivalent stress of 19 MPa while driving through water and 45 MPa when hitting an obstacle like a curb. In this case, with simplified assumptions, ferrite cores show barely adequate bending strength. In addition, due to complex material behavior (fine cracks, pre-damaged materials, etc.), the large variety of possible pad designs, materials, impact situations (when hitting a curb, the load profile may occur in the middle, in the front or rear of the vehicle), etc., any statement has to be considered in its specific context situation.

In order to verify both the effects of damaged ferrites and the approach of an automated CPT test bench, small circular reference pad design³⁸ with several different degrees of ferrite damage were set up (Fig. 111).

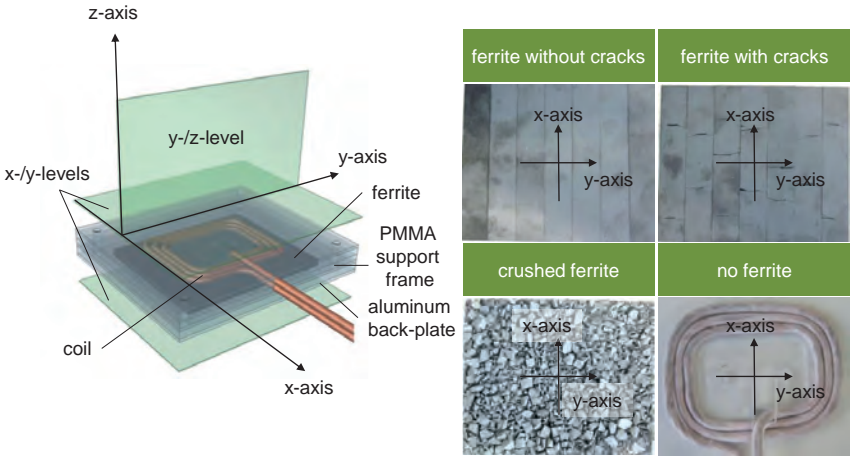


Fig. 111. Test-set-up to verify the consequences of damaged ferrites in CPT-systems.

As can be seen in Fig. 111, damage is purposefully introduced into the MnZn-ferrites. First, seven undamaged ferrite I-cores are arranged side by side in an acrylic glass frame. The second picture shows broken ferrite at – in a first test set-up – randomly se-

³⁸ Variable intermediate circuit voltage, constant intermediate circuit current $I=1$ A, excitation frequency $f=250$ kHz, Litz wire (Cu): 300×0.2 mm, $\mu_{\text{ferrite (MnZn)}}=2,500$, EMF probe $A=3$ cm².

lected locations (referred to as "ferrite with cracks"). The third picture shows ferrites broken into small fragments with an edge length of no more than 2-3 mm (referred as "crushed ferrite"). This results in numerous air pockets between the fragments. It must be noted that the mounting frame can hold only the amount of six rather than seven crushed ferrite I-cores.

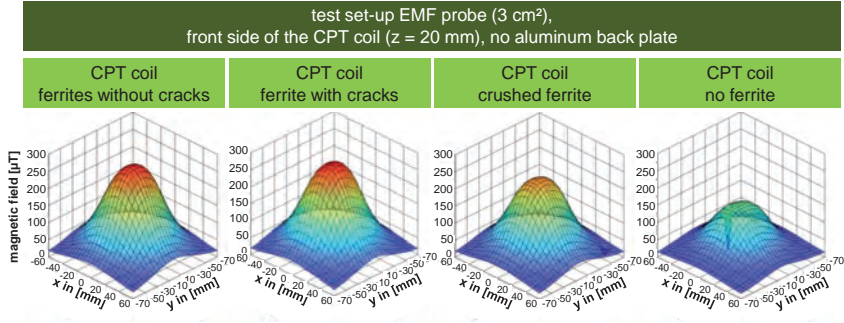


Fig. 112. Results of the test set-up with different conditions of the ferrite (front side, without aluminum back-plate).

As can be seen in Fig. 112 and Fig. 113, the presence of cracks in the ferrite has hardly any effect on magnetic field exposure of the CPT system. However, with crushed ferrite, the field exposure is significantly reduced.

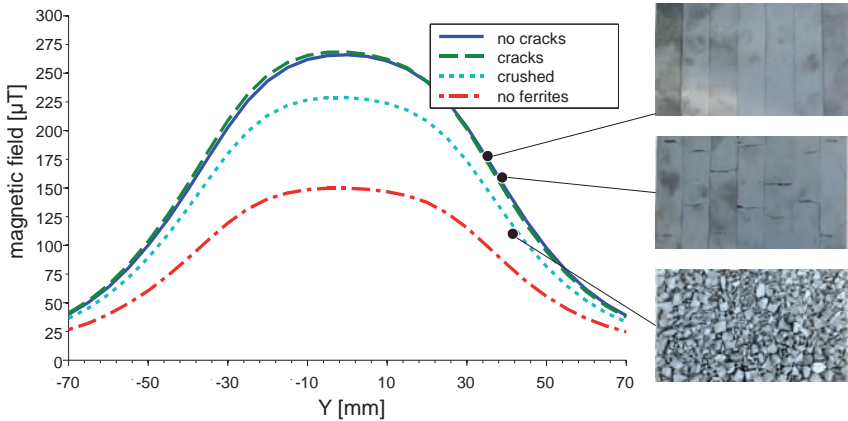


Fig. 113. Comparison of different ferrite structures (front side of the pad, $x=0 \text{ mm}$, $z=20 \text{ mm}$).

Fig. 113 shows the measurements of the y-plane located on the winding side (front side of the pad). All samples show a bell-shaped curve of the field distribution as is typical for circular pads. The magnetic fields for the samples with undamaged ferrite and ferrite with cracks evolve nearly congruently. However, the latter graph shows a gentle rise toward the center of the winding. In contrast, the sample with crushed ferrite shows a significant decrease in the maximum at about $40 \mu\text{T}$. It must still be clarified to what extent the decrease is caused by additional loss effects and to what extent to the reduced amount of material (only six I-cores instead of seven). As a further reference for the change in field exposure, the diagram also shows another measurement with an air coil without any ferrite. The absence of the ferrites' flux-guiding effect causes a drastic drop in the evolution of the flux density.

In Fig. 114, measurements of the xy-plane are shown on the rear side of the pad. The effects of crushed ferrite on the back side of the CPT system can be seen. The magnetic field from the transmitting coil is shielded to the back side of the pad by the ferrite by far less. Logically, the evolution of flux density for the air-core coil is largely identical. The maximum is slightly lower because the distance to the coil is slightly greater due to the thickness of the pad (4 mm). Again, the undamaged ferrite and ferrite with cracks behave almost identically.

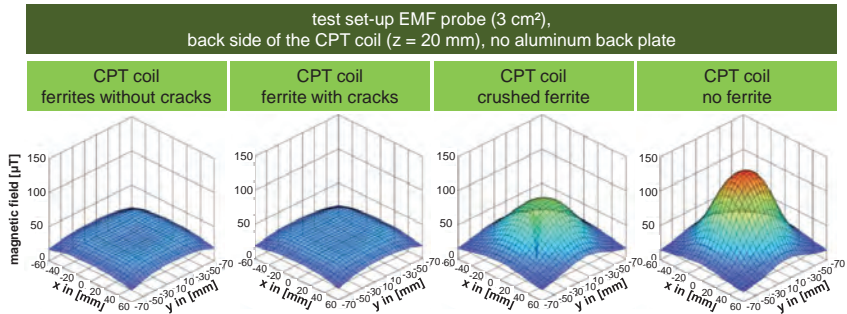


Fig. 114. Results of the test set-up with different conditions of the ferrite (back side, without aluminum back-plate).

However, in the range around the zero point, the latter shows a minimal increase in flux density (see also Fig. 115).

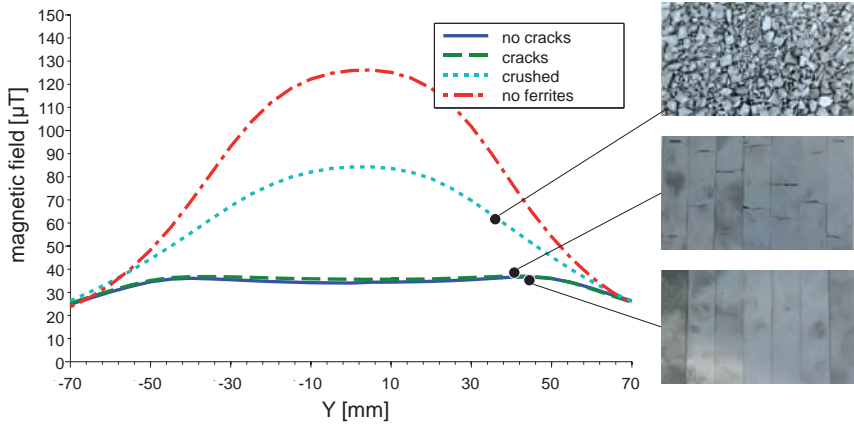


Fig. 115. Comparison of the different ferrite structures (rear side of the pad, $x=0$ mm, $z=20$ mm).

The crushed ferrite shows a significant loss, not only of its field-guiding but also of its field-shielding property. In consequence, higher losses can be expected and the field may even penetrate into the vehicle underbody and potentially breach magnetic field exposure limits. In consequence, higher losses can be expected and the field may even penetrate into the vehicle underbody with potentially negative effects in regard of the magnetic field exposure limits (see safety zones according to the application guideline VDE-AR-E 2122-4-2 [48] in chapter 2.3.1).

The shown testing diagrams confirm the potential of the test bench with its automated and precise handling of the probes. Even small differences can be observed, e.g. the small but detectable influence of minor fractures on the intensity of the magnetic field. Beyond a certain degree of damage, as shown here with ferrite powder, there is a clear effect on the field profile and thus the field-leading features. It should be noted that the input power is relatively small. At a larger power rate, effects are likely to be larger. However, the used measurement equipment (here Narda ELT-400 EM Field meter with 100 cm^2 and 3 cm^2 probes) is limited for such larger power levels with regard to spatial resolution of the probe size and limited measuring range, which strongly depends on the operating frequency of the CPT system. Magnetic fields in the frequency range between 1 Hz - 400 kHz can be detected, which would be enough for CPT systems for EVs (discussions about the frequency are in the range of ~ 20 - 140 kHz). At higher power levels and higher frequencies, the frequency-dependent overload limit must be observed, as the test probes might be damaged, especially when positioned between/above the power pads [211]. The destruction/overload limit for the two probe sizes is shown in Fig.

116 in correlation to the frequency in double logarithmic form. The destruction limit of the 3 cm² probe is 1,500 mT, which decreases with increasing frequency above 30 Hz. For the 100 cm² probe, the destruction limit starts as low as 160 mT and decreases at 1/f above 77.5 Hz.

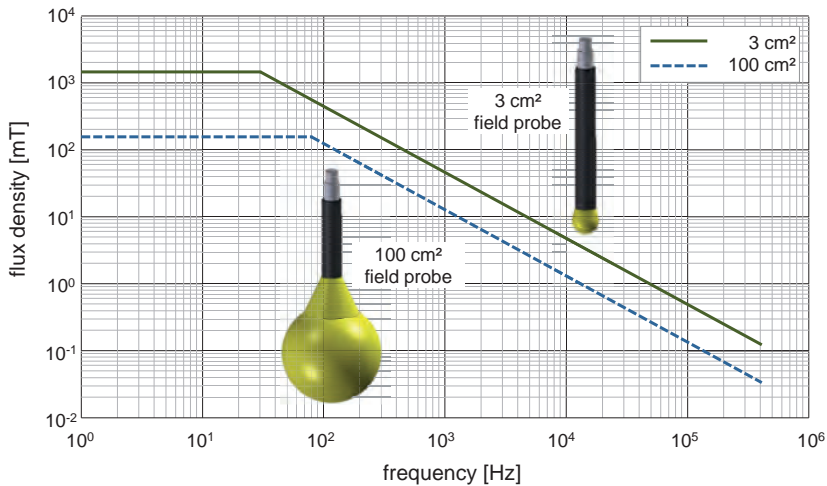


Fig. 116. Destruction limit of the probes as a function of the frequency [211].

It can be seen that the possible measurement range is drastically limited towards higher frequencies (e.g. 550 μ T at 85 kHz for the 3 cm² probe). It is therefore impossible to measure directly above CPT pads at higher power levels with this type of field measuring equipment. This will become even more critical in the future as power levels will increase further to the two-digit kW range and there is a trend towards ever smaller charging pads (from 800x800 mm to 300x300 mm and now even 250x250 mm) with field strengths well in the mT-range between the pads.

The limitation of today's EMF testing equipment shows further future need for research, in particular, regarding the development and implementation of arrays with robust magnetic field sensor with enhanced spatial resolution ($\sim\mu$ m-range), sensing ($>$ mT-range), detectability ($<$ μ T-range), response time (\sim ms-range), and reduced size ($<$ cm²-range). Promising field detection sensors based on magneto-resistive effect (MR effect) are available on the market to develop highly accurate PCB-based sensor arrays. This MR-effect causes a change in resistance as a function of the magnetic field. These field detection sensors have a measuring range independent of frequency of up to 3 mT, a spatial resolution of only 0.8 mm, and a low response time of just \sim 1 ms. The low response

time allows to collect measurements even while the gantry is moving the sensor, with no need to stop at each measurement point.

There are several protective measures to avoid such negative effects caused by damaged ferrites as described above. Ferrites can be protected by soft cavities or predetermined breaking points [129], additional protection layers [14] [51], or impregnation with resin. Cores of greater mechanical strength can be achieved by adapting grain size [209] or even by using polymer-based soft magnetics compounds. Air gaps between ferrites inside a pad are especially critical in polarized systems (e.g. solenoids or DDs with a strong flux pipe). Ferrite blocks only work loss-free if placed end-to-end and vertical to the winding axis, ideally without any air gaps, as the coupling between adjacent ferrites is one major factor affecting variations in permeability. The presence of an air gap reduces the magnitude of the electromagnetic field in the flux pipe and eventually results in inefficient power transfer due to reduced coupling. To avoid air gaps between the ferrites, [188] propose DD pads with pressure applied to the ends of the ferrites in the cavities of the flux pipe. [212] uses solenoid pads with single core pieces long enough to reach from one pole end to the other. Thinner ferrite bars are in the interest of lightweight construction, however, they have to be even more carefully protected, as they are more likely to break [41]. Thinner ferrites can be used without any harm to coupling as long as saturation effects in the core materials are avoided and fundamental flux paths are unaffected [120]. Any such measures must, however, be taken in full consideration of all the parameters they might affect, such as permeability μ (especially by polymer-based soft magnetics), coercivity H_c , saturation B_s , etc.

In an environment that is susceptible to strong vibration, such as a vehicle, the ferrites are not the only components that are delicate and prone to mechanical impact damage. HF-Litz wires can suffer abrasions, particularly at a number of locations within a pad that are under external vibration during normal use or normal assembly, especially at bends. The spots at risk of abrasion include exposed exit/entry points, wire crossings, coil overlaps, corners, contacts, and areas with sharp edges, e.g. close to ferrites. Exit and entry points are at risk and are typically protected by heat shrinkable tubes. Especially HF-Litz wire connections may be weak points which vibration can cause to fail [6]. Due to the heat that is applied during contacting, the enamel coating on the individual strands may be stiff in certain sections. In these sections, HF-Litz wires are more brittle and thus more susceptible to damage if the wire is bent [134]. Therefore, the hot crimping connections from chapter 5.1.3 were tested for vibration strength, a test that is indispensable in view of the planned vehicle underbody integration. DIN EN 60068-2-64 proposes four categories of installation locations in motor vehicles: chassis, engine compartment, engine block, and radiator. When a contactless charging pad is installed in the underbody of a vehicle, the chassis appears to be the best suited spot. The test items are put under stress in all three dimensions for eight hours respectively. A support

structure was built that represents the external terminal connections of a fully impregnated charging pad, as shown in Fig. 117. The HF-Litz wires cannot swing freely and remain in a clearly fixed position. In consequence, only the cable socket is affected by vibration during operation.

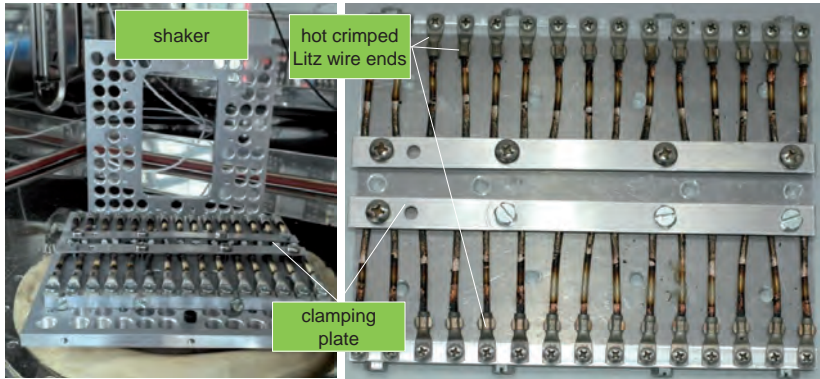


Fig. 117. Clamping plate for vibration test samples, results after the test.

None of the test samples showed any sign of damage after the vibration test. There were neither broken HF-Litz wires nor damaged cable sockets. The same goes for the correlations with crimping pressure, pause time, crimping pulse duration, number of pulses, and crimping current. Since no deterioration in the pull-out force is detectable, all hot-crimped samples proved to have a very good resistance to vibration with the chosen process parameters, HF-Litz wire types and cable sockets.

Abrasive forces or even a shifting of coils under massive mechanical shock on the conductive filaments at critical points inside the pad can be countered by applying additional abrasion- and impact-resistant layers with sufficient tensile strength to selected areas on the conductive filaments, such as Kapton® tape or Mylar® (high tensile strength with a Young's modulus of about 3-4 GPa and a tensile strength of 55-75 MPa), or by impregnating the spaces around the individual strands that make up the HF-Litz wire with epoxy/PU filling [134]. Especially impregnating fragile filaments like HF-Litz wire and ferrites in a settable fluid such as epoxy can provide a structural matrix which is highly impact-resistant and securely holds the parts in position [134]. Furthermore, the matrix creates additional voltage isolation, stops ferrites, and strands from rubbing against each other under vibration in the pad (such as those caused by the repeated compression and decompression of magnetic domains in the ferrite) as well as creates a lattice of bonded wires, which significantly enhances the mechanical strength of the pad.

Aside from mechanical impacts on the pad interior, the entire pad housing may be damaged. This leads to severe risks, e.g. losing the pad while driving or open wires sticking out of the pad. The pads have to be protected by strong durable housing with defined stiffening ribs, support pillars, increased material thickness, or additional fixing points, adding strength to the pad as well as assisting in the positioning of other components within the casing to withstand impact and distribute impact forces more evenly. All this has to be done while still maintaining the electrical integrity of the components [134]. Thick metal structures to protect the coils have to be avoided, because they would shield the magnetic field, adding unnecessary weight to the vehicle. On the other hand, non-metallic material on the underside of a motor vehicle can be easily damaged, which poses a safety hazard. Safety systems must detect and act upon any mechanical impact immediately by interrupting the charging operation. [213] proposes to place optical waveguides in the underside of the housing of secondary systems to detect mechanical impacts on the pad. Thereby, a meander-shaped optical waveguide forms a fine-mesh net which virtually covers the entire bottom of the housing and also extends into the side walls. As long as a sensor element receives light from a light source, the system assumes that the pad is not damaged. In case of damage, the optical waveguide is interrupted, the opto-electric sensor element no longer receives light in the expected intensity. This enables damage detection that disables charging to avoid hazards to persons.

6.2 Thermal stress profiles

Apart from mechanical requirements, there are also thermal requirements during production and product lifetime that have to be discussed, as heat losses are an important limiting factor for transferable power and CPT system efficiency.

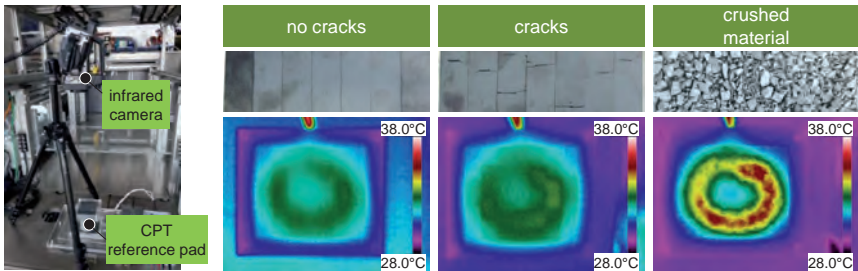


Fig. 118. Temperature profile of ferrites at different degrees of structural damage (rear side of the pad).

The close correlation between mechanical (chapter 6.1) and thermal stress profiles (chapter 6.2) and its importance with regard to power transfer efficiency can be seen in the temperature profile of the ferrites. Fig. 118 shows a significant increase in tempera-

ture for the crushed ferrite material. Heating by thermal conduction between the winding and the ferrites can be ruled out, since they are separated by a 2 mm PMMA plate with poor heat conduction. The difference in temperature can therefore be attributed to hysteresis losses in the material. Even though this test set-up was conducted with a low-power CPT reference pad with moderate max. temperature levels, the rise in temperature emphasizes the importance of safely integrating the ferrites into the pads to avoid additional heat problems due to damaged pad structures.

In first prototypical EV charging CPT systems in the kW-range (3.7 kW, large pad dimensions ~800x800 mm on both primary and secondary side and without damaged ferrites), the stationary measured operating temperatures did not exceed 100°C in the CPT systems, as documented in the final reports, with no further need for thermal heat dissipation [56] [69] [214]. However, thermal issues occur in CPT systems, especially when pad size is further reduced and/or with high power pad systems of several dozen kW. A fast chargeable CPT system of 22 kW inevitably presents thermal problems as generated losses (e.g. P_{losses} = of 2,200 W with $\eta_{\text{static}} = 90\%$) have to be quickly and effectively transferred away from the charging equipment to ensure optimal operation of the CPT system (transmitter pad, electronics, etc. - see loss model of CPT systems in chapter 4.1) [84]. The smaller the pad area, the lower the heat capacity, especially of secondary charging pads. Thus, small systems dissipate substantially smaller amounts of heat via convection and radiation and generate considerably higher temperatures during the charging process (comparison of surface areas: 1,000 mm x 1,000 mm = 1 m² versus 300 mm x 300 mm = 0.09 m²). Thermal issues arise especially with smaller secondary high-power double-sided solenoid systems, due to poor heat dissipation per unit of space that is related to their magnetic design [161].

Moreover, intelligent heat dissipation concepts are needed especially for pads that are mounted to the undercarriage of plug-in and range-extender vehicles with internal combustion engine and exhaust systems. The exhaust line and catalytic converter are the largest sources of heat in a conventional or hybrid-powered vehicle, whose temperature can exceed 500°C (T_{max} ~900°C). To integrate pads in the front, they may have to be installed close to components such as the gearbox that may also reach temperatures of over 100°C after driving. Together with seasonal differences between winter and summer, the heat of surrounding components may negatively affect charging, e.g. heat in the underbody engine compartment immediately after a highway trip at a rest area (Fig. 119).

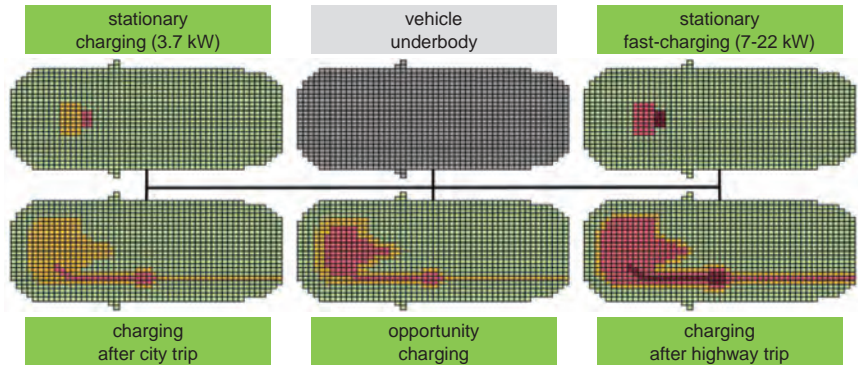


Fig. 119. Thermal stress profiles in the vehicle underbody.

Such scenarios are especially important for vehicles that frequently have to use fast charging stations during their day-long operation, such as taxis, buses, or vans (opportunity charging, see chapter 2.3), and need instantly “ready-to-charge” CPT systems. In addition, cooling strategies have to be considered for the vision of (Hybrid-)RPEVs with higher power levels.

High temperature may also have negative effects on pad systems due to joule heating with increased electrical resistivity of copper and higher losses. Moreover, the permeability of ferrites strongly depends on temperature. The secondary permeability maximum of MnZn ferrite is located at 80-120°C (temperature of minimum loss) [215]. In this temperature range, ferrite cores have higher magnetic conductivity, whereby specific power dissipation decreases. Above this temperature range, the core losses of ferrite materials increase.

Materials in pads also have to be considered in terms of their coefficients of thermal expansion (CTE) in order to avoid thermal cycles with thermo-mechanical stress and thus premature materials fatigue [216]. In worst cases (driving through a cold mountain river in summer with a heated engine compartment), the ferrites are subject to rapid temperature changes (heat shock) and may get damaged/permanently deformed, especially due to the different CTEs of the materials/layers in a pad. Specifically when resin, adhesives for the carrier plates etc. expand or contract more quickly under temperature changes than the ferrites on which they are fixed, ferrite cracks may occur that will degrade core properties³⁹. To avoid cracks in the pad due to different thermal expansion coefficients, ferrites could be fixed to the carrier plate with permanently elastic two-sided adhesive tape and defined small gaps between the ferrites, e.g. 0.2 mm [157]. This configuration

³⁹ CTE of ferrite $10 \text{ K}^{-1} \times 10^{-6}$ versus CTE of epoxy/PU $146 \text{ K}^{-1} \times 10^{-6}$, insulation foils $110 \text{ K}^{-1} \times 10^{-6}$.

enables the ferrite to withstand mechanical stresses that are caused by different expansion coefficients of carrier plate material and ferrite under temperature changes. However, as the small air gaps provide paths of magnetic reluctance, this configuration may weaken power transmission properties [188]. Special membranes (Goretex) can be integrated in the pad to equalize pressure between the interior of the housing and the surrounding atmosphere in the event of temperature changes or air pressure fluctuations [157]. In addition, [69] reported that overlapping HF-Litz wires caused heating problems with a local maximum in the temperature range. This calls for corresponding countermeasures such as flexible cavities/avoiding fix-bonding of materials with extremely different CTEs, like ferrites and insulation foils, and avoiding coil crossings in the pads [170], along with appropriate cooling measures. Based on the calculated power loss and coil geometry as well as heat-flow analysis, cooling measures have to be considered for maximum system efficiency as early as in the design phase of coil geometries [121].

Passive and/or active cooling devices in combination with aerodynamic approaches are needed to deal with increasing heat losses. Selecting a cooling concept for electric vehicle components to reduce the operating temperature is a compromise between efficiency, cooling efficiency, footprint/volume, weight, and complexity. It is possible to passively cool without any additional devices via convection to the ambient air, e.g. by air vents, cooling channels, etc. in the pads or adjacent underbody parts. This effect can be reinforced by increasing the surface of the components that serve convection/air exchange, e.g. once again by defined gaps between the HF-Litz wire windings or ferrites [24] [60]. Such gaps between windings and/or ferrites increases the surface through which heat can dissipate away from the coil/ferrites [51]. This can also be achieved by adding cooling plates to coarse-textured surfaces, plate fins, pin fins, open-celled metal foam, etc. made of material with high thermal conductivity ($\lambda_{\text{copper}} = 401 \text{ W/mK}$, $\lambda_{\text{aluminum}} = 236 \text{ W/mK}$) [51] [216] [217] (Fig. 120).

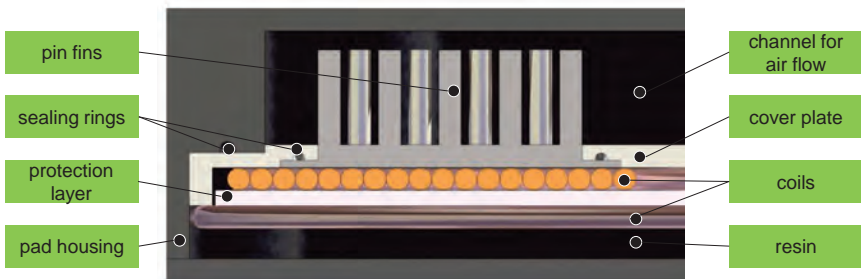


Fig. 120. Pad housing structured with cooling fins.

Another way to improve heat dissipation is to integrate copper elements between heat-conducting foils in the coil system and the housing wall. This is particularly useful when the heat source is located centrally in the housing [51]. In addition, the resin or silicone pastes between the pad components (coils, electronics) can be dispersed with fine thermally conductive particles and a heat sink can be created (e.g. using the aluminum backing of solenoids, as described in [155]). However, these approaches must always be considered in the context of induced eddy currents in the aluminum shielding.

If necessary, air vents can be integrated into the underbody panels close to the charging pad. The shape of these vents could be based on what is called the NACA⁴⁰ profile, which is a flow-optimized design to minimize air turbulence (Fig. 121).

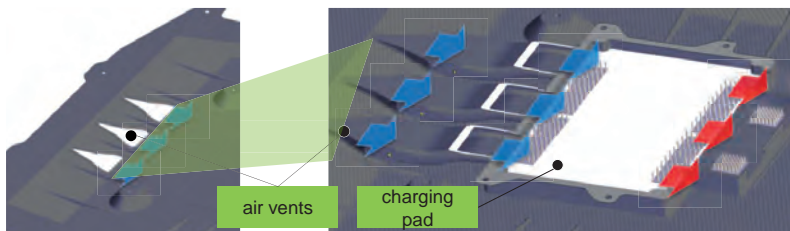


Fig. 121. Air vents in the underbody panel.

Furthermore, controllable air flap systems with a sophisticated actuator system can attain an even higher functional integration that combines improved aerodynamics (reducing the air drag coefficient/ C_d -value) with a cooling function. This may be of special interest to RPEVs that drive with higher levels of power transfer. The cooling flaps open when more cooling is needed or desired, and otherwise remain closed to reduce air resistance. A filter system is needed to prevent roadway dirt etc. from entering the air vents. To avoid this problem, air vents can also be integrated in the lower part of the front bumper, as shown in Fig. 122.

In stationary charging, air flow can be maintained by using engine-off cooling (EOC) feature of the vehicle's air conditioning system. However, space constraints make it challenging to integrate additional air channels in the area of the engine compartment (e.g. under the oil pan).

⁴⁰ National Advisory Committee for Aeronautics

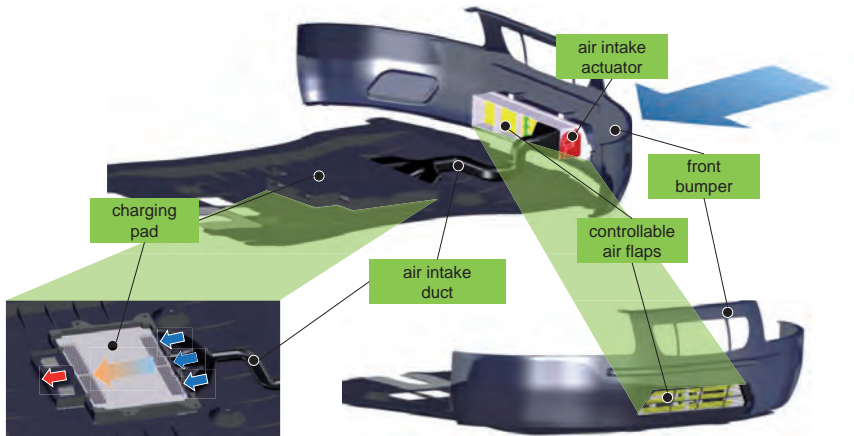


Fig. 122. Air supply through the front bumper grill.

In addition, active, higher-performing cooling measures may be needed if the cooling capacity of passive systems is not sufficient to guarantee efficient operation of the CPT system. Auxiliary equipment like ventilation fans and/or connections to the vehicle's water⁴¹ or oil cooling circuit must be used to dissipate the heat. Fluid-cooling systems have significantly higher heat transfer coefficients compared to air/air-heat-exchange approaches.

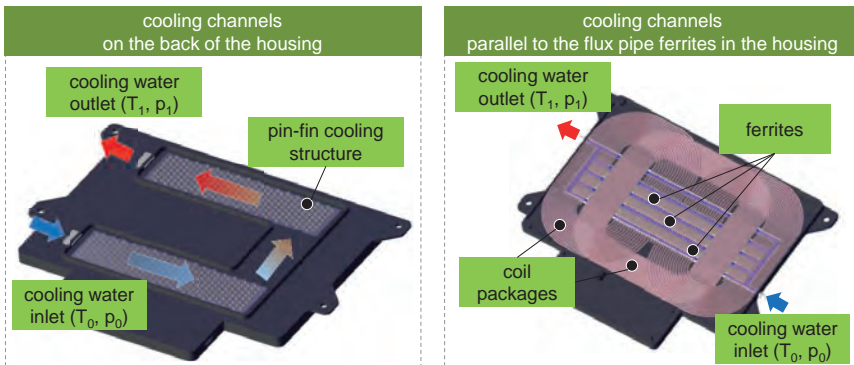


Fig. 123. Integration of a cooling channel into the housing (left) and between the ferrite blocks in the CPT pad (right).

⁴¹ e.g. water-glycol-mixture.

A cooling channel system can be added to the housing, as shown in Fig. 123 (left), or may even be integrated in existing pad arrangements in a space-saving manner, if HF-Litz wires and ferrites can be spaced apart from each other (without disturbing the magnetic flux path), as shown in Fig. 123 (right). The core geometry of solenoids, which may contain a number of spaced-apart core pieces, and cavities between the core pieces vertical to the winding axis, also allows for an easy integration of cooling channels to further reduce power losses [214]. It would be even better to integrate cooling channels directly on top of the HF-Litz wires, as shown in Fig. 124. However, this option reduces ground clearance and may need additional protection against potential mechanical impacts, as described in chapter 6.1.

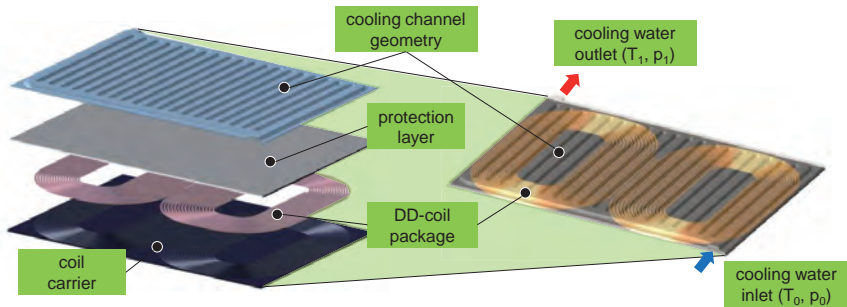


Fig. 124. Arrangement of cooling channels directly on top of the windings.

As the existing cause-effect relationships in the vehicle underbody are complex, thermal and mechanical impacts always have to be tested when added to a real vehicle underbody. This chapter has shown which efforts are needed for a proper homologation and integration of thermal and mechanical stress protection into the vehicle body. This will be even more important in the future as higher power levels and even more so, the vision of high-power RPEV applications will demand safe and unattended operation.

7 Summary and Outlook

Contactless power transfer in electric vehicles is technically feasible for both stationary vehicles and in-motion [3] and can help popularize EVs by enhancing their capability and convenience. Renowned OEMs are developing CPT charging pads in cooperation with suppliers and presenting more and more concepts and prototypes [16]. However, the market introduction of contactless power transfer systems still faces some uncertainties.

Therefore, this thesis presents and discusses different fields of application for static and dynamic CPT approaches with their advantages and possibilities in chapter 2. For a detailed evaluation of the benefits of different fields of application and to improve planning security, a simulation-based approach (ETEV|SIM) has been developed and successfully verified by adapting a production and logistics event-discrete simulation tool in chapter 3. This allowed for a thorough verification of the scenarios approach with a significant number of simulation runs, and has shown promising results. Thus, this approach enables potential customers of CPT systems to reliably simulate and calculate even complex scenarios with the help of Digital Factory planning tools in an early planning phase. However, the output of these models is only as accurate as the input variables. This is specifically true for system cost and battery systems behavior, as they have complex correlations especially at different charging levels. A critical review of results and assumptions is therefore always necessary. As deterministic assumptions and given settings may not perfectly reflect actual vehicle operation under all possible circumstances (e.g. cold weather, mass event in a city, traffic jam), more detailed technical performance parameters and cost data need to be collected and confirmed in future demonstration projects for all CPT scenarios, so that ultimately, reliable operation can be guaranteed in almost any conceivable operation scenario. Particularly for RPEV approaches, further tests are pending to show the systems' technical and economic performance. In order to convince governments and other authorities, there has to be independent verification of safety levels, efficiency rates, and construction cost for systems that may be on the road for decades as technology continues to change [41], in harsh environmental conditions, and at higher speeds with different vehicle types. Therefore, the developed simulation tool can easily be adapted and expanded as soon as more detailed data becomes available in the ongoing technological development of CPT and battery systems. Thus reducing uncertainty in the planning of CPT systems for fleet-operated electric vehicle scenarios will further promote future acceptance and spread of this technology.

To further support this development with reduced costs, production approaches for CPT systems have been developed and implemented in the scope of this thesis. In chapter 4 it could be shown that the developed pads, and especially the coil systems become in-

creasingly complex, as does a detailed understanding of their correlations. These correlations have yet to be reflected in detail from a process and material perspective. Based on these considerations, chapter 5 showed production technologies with a focus on producing a finished coil package, as most complex part of a charging pad. Winding processes for HF-Litz wires have been developed to attain complex pad designs. Flexible robot-based assembly and handling technologies work best in the early stages of market development when different coil designs are being considered. This robot-based approach allows for the creation of prototype systems, an analysis of their suitability for manufacturing, and setting design rules. These approaches (kinematic models, material reflection, and design rules) lay another cornerstone that will make it easier to analyze newly developed coil designs for their viability in high-quality and high-performance systems with steady cost reduction potentials.

Chapter 6 revealed the importance of a detailed study of materials- and process-related aspects over the entire product-life, showing potential failure modes but also further opportunities for improvement from a material and production perspective. The study of production and material parameters during the entire product-life, with appropriate measures against mechanical and thermal stress, shows the variety of challenges that come with CPT systems that are integrated in the underbody of a vehicle. Although there are retro-fitted CPT systems on the market already⁴², the integration of a contactless power transfer system is by far more complex than just adding a socket and plug system. It will take well designed, well produced, vehicle-integrated, and tested contactless power transfer systems with high efficiency rates to meet safety and environmental standards. Therefore, in the interest of greater market penetration, the industry will move from retro-fitting vehicles to a properly integrated and homologated OEM option with comprehensively adapted and safety-tested body structures. OEMs that gain a thorough understanding of CPT systems, which can, for instance, predict in detail where stray fields go in the underbody of a given vehicle, which can determine safety levels all around the car, which are ready for yet higher power levels, or even for RPEV vehicle concepts with all their mechanical, thermal, and EMC challenges - those OEMs will have a distinct competitive advantage. In order to support this approach from a production and material perspective, an automated test concept has been developed to examine the impact of different materials, varying tolerances, and alternative production processes on the efficiency of the power transfer system. This allows for a thorough analysis of the relevant automated production processes with a suitable material characterization to reduce production cost, weight, and volume of the charging pads. Thorough and expensive material test set-ups are therefore inevitable to understand material behavior and potential failures in the different processes in detail, especially for the development of large-scale automated production processes.

⁴² 3.3 kW-CPT systems (240V, Level 2) from Evatran Plugless Power and Bosch SPX Service Solutions to retro-fit Chevrolet Volt and Nissan Leaf [167].

In the future, as test set-ups are expensive, it would make sense to have appropriate simulation techniques for a virtual process validation to simplify validation (time and equipment costs) rather than running several iterations with only slight pad modifications [67]. It is conceivable to link production- and material-related parameters with simulations of magnetic field exposure to check and simulate different production variations, their manufacturability and potential material stress with its impacts on pad functionality in a very early design phase. This can be achieved by developing a CAD-CAM chain process validation with realistically-imaged HF-Litz wire strands that simulates the mechanics of the materials, but also includes a virtual validation of electrical parameters.

Moreover, in the future, assessment of new materials, production technologies, and intelligent integration of electronics (communication and surveillances systems - built-in temperature sensing, LOP, FOD, etc.) has to be expanded consistently. New materials could be used, such as innovative magnetic materials (amorphous iron alloys/nano-crystalline iron foils in the form of multi-layer stacks with intermediate layers of polyethylene) [218], or alternative conductor materials, like wires with wire-cladding techniques. In addition, Litz wire inductor arrangements can directly be integrated into a stack of multi-layer Printed Circuit Boards (PCBs), which are already being investigated for domestic induction heating applications (20-150 kHz, $P_{out}=500$ W) [219] or 3D additive spray-coating methods, which are already being investigated for MRI gradient coils [220], but which have to perform under more demanding AC performance requirements for EV charging (especially when considered for loosely coupled EV CPT systems). Such new technologies would immensely increase freedom of design and facilitate manufacturing. The automated test bench concept from chapter 6, together with further developed AC magnetic field sensor technologies and combined with flexible automated production cells, offers a promising approach to verify such alternative materials and production processes for different pad designs (see Fig. 125).

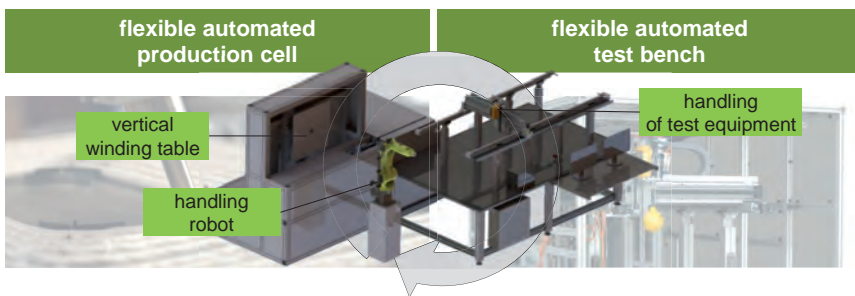


Fig. 125. Automated test bench combined with automated production cell.

Detailed process knowledge and experience yields positive effects on functionality, quality, and cost structure. It is this sort of process mastery that will eventually differentiate global competition. The approaches presented in this thesis thus deliver a basis to achieve future high-performance CPT systems for challenging automotive applications.

8 Zusammenfassung

Die Technologie der kontaktlosen Energieübertragung bietet eine attraktive Alternative zu kabelgebundenen Ladesystemen. Die kontaktlose Energieübertragung wird dabei in der Konsumelektronik, der Medizintechnik und auch bei Industrielösungen bereits vielfach eingesetzt. Durch die stetige Weiterentwicklung dieser Technologie werden Übertragungsleistungen in einer Höhe erreicht, die auch für den Einsatz in Fahrzeugen mit elektrifiziertem Antriebsstrang wegweisend sein werden. Die meisten OEMs haben die potentielle Schlüsselrolle der kontaktlosen Ladetechnik erkannt und entwickeln zusammen mit ihren Lieferanten erste Lösungsansätze mit dem Ziel in den nächsten Jahren serienreife Produkte auf den Markt zu bringen. Bis 2020 werden dabei von Marktforschungsinstituten bereits signifikante Stückzahlen für CPT Systeme vorausgesagt. Für eine umfassende Markteinführung von kontaktlosen Energieübertragungssystemen existieren allerdings noch Barrieren, die es zu überwinden gilt. Diese betreffen neben den Herausforderungen in der Standardisierung und Interoperabilität insbesondere die hohe Unsicherheit hinsichtlich der Auswahl geeigneter Anwendungsfelder sowie die zunächst noch hohen Kosten der CPT Systeme. Ziel der vorliegenden Arbeit ist es daher zum einen die Planungsunsicherheit durch die Entwicklung geeigneter simulations-basierter Planungsmethoden zu reduzieren und zum anderen die Realisierung kosten-effizienter und zuverlässiger CPT Systeme durch die Entwicklung geeigneter Produktions- und Prüfverfahren zu fördern.

Dazu werden zunächst die verschiedenen Anwendungsbereiche für statische und dynamische CPT Systeme mit ihren Vorteilen und Möglichkeiten präsentiert und diskutiert. Für eine detaillierte Bewertung verschiedener Anwendungsbereiche wurde ein simulations-basierter Ansatz (ETEV|SIM) auf Basis von Methoden der Digitalen Fabrik entwickelt und erfolgreich verifiziert. Dieser Ansatz ermöglicht vorab eine fundierte Analyse unterschiedlicher Einsatzfelder für die kontaktlose Energieübertragung. Der entwickelte Lösungsansatz basiert auf der automatisierten Durchführung zahlreicher Simulationsläufe und liefert potentiellen Anwendern von CPT Systemen die Grundlage in einer frühen Planungsphase auch komplexe Szenarien zuverlässig simulieren und berechnen zu können. Die Unsicherheit bei der Planung von CPT Systemen kann dadurch insbesondere für flottenbetriebene Elektrofahrzeug-Szenarien reduziert werden, was die Akzeptanz und zukünftige Verbreitung dieser Technologie fördert.

Inwiefern sich die kontaktlose Ladetechnologie am Markt durchsetzen kann, hängt zudem von den realisierbaren Kosten für die Systeme ab. Im Wettbewerb zwischen potentiellen Lieferanten der CPT Systeme sind insofern neben produktseitigen Entwicklungskompetenzen vor allem detaillierte Prozesskenntnisse zur Erreichung der angestrebten Funktionalität, Qualität und Kostenstruktur erforderlich. Dazu wurden im Rahmen der vorliegenden Arbeit Produktionsansätze für CPT Systeme basierend auf flexiblen robo-

tergestützten Montage- und Handhabungs-Technologien entwickelt und implementiert. Die Ansätze erlauben die umfassende Reflektion derzeit diskutierter komplexer Spulen-Geometrien aus Prozess- und Material-Perspektive. Zudem werden die speziellen Herausforderungen adressiert, die bei der Integration von CPT Systemen im Fahrzeugunterboden entstehen (insbesondere thermische und mechanische). Ein automatisierter Prüfstand zur detaillierten Untersuchung material- und prozessbezogener Aspekte über den gesamten Produktlebenszyklus wurde entwickelt und realisiert. Dieser ermöglicht die fundierte Analyse der vielfältigen Wechselwirkungen in komplexen Pad-Systemen (Mehrspulen-Systeme, integrierte Elektronik, etc.) und Unterbodenkonfigurationen. Zudem ermöglicht der Ansatz die systematische Analyse alternativer Fertigungsverfahren bzw. alternativer Materialien, sowie möglicher Fehlerzustände im Fahrzeuglebenszyklus, um Verbesserungsmöglichkeiten für eine kontinuierliche Reduktion von Produktionskosten, Gewicht und Volumen ableiten zu können. Die in dieser Arbeit vorgestellten Ansätze liefern somit eine Basis zur Entwicklung leistungsgesteigerter CPT Systeme für anspruchsvolle Automotive-Anwendungen.

9 List of Abbreviations

A4WP	Alliance for Wireless Power
AC	Alternating Current
ADD	Animal Deterrent Device
AGV	Automated Guided Vehicle
B-AGV	Battery Swapping-Automated Guided Vehicle
BCU	Base Charging Unit
BEV	Battery Electric Vehicle
BMS	Battery Management System
CAD	Computer-Aided Design
CAM	Computer-Aided Manufacturing
CCA	Copper Cladded Aluminum
CPT	Contactless Power Transfer
CT	Computed Tomography
CTE	Coefficient of Thermal Expansion
DC	Direct Current
DIN	Deutsches Institut für Normung
EOC	Engine-Off Cooling
EMC	Electromagnetic compatibility
EMF	Electromagnetic Field
ETEV SIM	Energy Transfer for Electric Vehicles Simulation Tool
EV	Electric Vehicle
FIA	Fédération Internationale de l'Automobile
FEH	Formula E Holdings
FEM	Finite Element Method
FMEA	Failure Mode and Effects Analysis
FOD	Foreign Object Detection
GFRP	Glas-Fiber Reinforced Plastic
HD	High-Definition
HF	High Frequency
ICE	Internal Combustion Engine
ICNIRP	International Commission in Non-Ionizing Radiation Protection
ICT	Information and Communications Technology
IDC	Insulation Displacement Connectors

IEC	International Electrotechnical Commission
ISO	International Organization for Standardization
LASER.....	Light Amplification by Stimulated Emission of Radiation
LED	Light-Emitting Diode
LFRT	Long-Fiber Reinforced Thermoplastics
LOP	Living Object Protection
LVAD	Left Ventricular Assist Device
MF	Medium Frequency
MIT	Massachusetts Institute of Technology
MnZn	Manganese-Zinc
MRI	Magnetic Resonance Imaging
NACA	National Advisory Committee for Aeronautics
NPE	Nationale Plattform Elektromobilität
OEM	Original Equipment Manufacturer
PATH	Partner for Advanced Transit and Highways
PCB	Printed Circuit Board
PE.....	Polyethylene
PHEV.....	Plug-In Hybrid Electric Vehicle
PMA.....	Power Matters Alliance
PMMA.....	Poly-Methyl-Methacrylate
PP	Polypropylene
PU	Polyurethane
R&D	Research and Development
REEV.....	Range Extended Electric Vehicle
RF	Radio Frequency
RFID	Radio Frequency Identification
RPEV.....	Roadway Powered Electric Vehicle
SAE	Society of Automotive Engineers
SCARA	Selective Compliance Assembly Robot Arm
SEA	Swedish Energy Agency
SOC.....	State of Charge
SUMO.....	Simulation of Urban Mobility
TCO	Total Cost of Ownership
TS.....	Technical Specification
U.S.	United States

US	Ultra-Sonic
V2G	Vehicle-to-Grid
VBA	Visual Basic for Applications
VCU.....	Vehicle Charging Unit
VDE	Verband der Elektrotechnik Elektronik Informationstechnik
VDI	Verein Deutscher Ingenieure
VHF	Very High Frequency
VISSIM	Verkehr In Städten - SimulationsModell
WPC	Wireless Power Consortium

10 Literature

- [1] BROOKER, A.; THORNTON, M.; RUGH, J.: *Technology Improvement Pathways to Cost-Effective Vehicle Electrification*. SAE 2010 World Congress, Detroit, Michigan, USA (2010), p. 1–15
- [2] N. N.: *Roadway Powered Electric Vehicle Project Track Construction And Testing Program Phase 3D*. Palo Alto, California, USA, 1994
- [3] COVIC, G. A.; BOYS, J. T.; BUDHIA, M.; HUANG, C.-Y.: *Electric Vehicles – Personal transportation for the future*. In: *EVS25 World Battery, Hybrid and Fuel Cell Electric Vehicle Symposium, Shenzhen, China* (2010), p. 693–704
- [4] KAHL, M.: *Wireless charging: the Holy Grail of the EV*. In: *Automotive World megatrends magazine*, Q1 2013, p. 27–31
- [5] PANTIC, Z.: *Inductive Power Transfer Systems for Charging of Electric Vehicles*. Raleigh, North Carolina, North Carolina State University, Electrical Engineering. PhD thesis. 2013
- [6] COVIC, G. A.; BOYS, J. T.; VAN BOHEEMEN, E.; KISSIN, M.; KEELING, N. A.; BEAVER, J.: *A Wiring Harness and Wireless Power Transfer System*. 26.09.2013. Publication nr. WO2013/141717A1
- [7] WESSNER, K.; RISCH, F.; MEINDL, P.; FITZEK, M.: *Marktpotenziale von induktivem Laden als Aufladetechnologie von Elektrofahrzeugen*. 1. Aufl. Schwaig bei Nürnberg, 2011
- [8] LORICO, A.; TAIBER, J.; YANNI, T.: *Inductive Power Transfer System Integration for Battery-Electric Vehicles*. In: *3rd International Conference of Sustainable Automotive Technologies* (2011), p. 75–83
- [9] FRANKE, J.; RISCH, F.: *Unternehmensübergreifende Planung komplexer Technologieszenarien am Beispiel des kontaktlosen Ladens von Elektrofahrzeugen über eine elektrifizierte Straße (E|ROAD)*. In: 6. Symposium für Vorausschau und Technologieplanung (2010), p. 255–271
- [10] COVIC, G. A.; KISSIN, M.; KACPRZAK, D.; CLAUSEN, N.; HAO HAO: *A bipolar primary pad topology for EV stationary charging and highway power by inductive coupling*. In: *Energy Conversion Congress and Exposition (ECCE), IEEE* (2011), p. 1832–1838
- [11] MARTIN, R.: *Wireless Charging for EVs: Forecasts, Market Issues and Technological Issues* (International Forum on Electric Vehicle). Daejeon, Korea, 18.11.2011
- [12] NIETSCHKE, W.; FICKEL, F.; KÜMMELL, S.: *Induktive Energieübertragung für Elektrofahrzeuge*. In: *ATZ* 113 (2011), no. 04, p. 280–285
- [13] PERRIN, J.: *Inductive Charging of Electric Vehicles: a European Perspective* (Conference on Electric Roads & Vehicles (CERV)). Park City, Utah, USA, 04.02.2013

- [14] TANAKA, J.; YOSHI, S.: *Vehicle capable of contact-free power reception*. Toyota Jidosha Kabushiki Kaisha. 14.11.2013. Publication nr. WO2013168239 A1
- [15] WEBB, A.: *Coming Soon: Standards for Wireless Electric Car Charging*. URL <http://www.pluginrcars.com/coming-soon-standards-wireless-electric-car-charging-128975.html> – last checked on 2014-03-02
- [16] N. N.: *Wireless EV Charging System Sales to Surpass 280,000 by 2020*. URL <http://electriccarsreport.com/2012/12/wireless-ev-charging-system-sales-to-surpass-280000-by-2020/> – last checked on 2014-01-20
- [17] RISCH, F.; GÜNTHER, S.; BICKEL, B.; FRANKE, J.: *Flexible Automation for the Production of Contactless Power Transfer Systems for Electric Vehicles*. In: *3rd International Electric Drives Production Conference (EDPC)*, Nuremberg, Germany (2013)
- [18] RISCH, F.; GÜNTHER, S.; FRANKE, J.: *Production Concepts for Inductive Power Transfer Systems for Electric Vehicles*. In: *2nd International Electric Drives Production Conference (EDPC)*, Nuremberg, Germany (2012)
- [19] HUTIN, M.; LEBLANC, M.: *Transformer system for electric railways*. 23.10.1894. Publication nr. US527857
- [20] KESLER, M.: *Highly Resonant Wireless Power Transfer: Safe, Efficient, and over Distance*. Watertown, Mass., USA, 2013
- [21] RAABE, S.: *Inductive Power Transfer Pickups for High Demand Applications*. University of Auckland. PhD thesis. 2011
- [22] TESLA, N.: *Apparatus for Transmission of Electrical Energy*. Publication nr. US649621A
- [23] RAABE, S.; COVIC, G. A.: *Practical Design Considerations for Contactless Power Transfer Quadrature Pick-Ups*. In: *IEEE Transactions on Industrial Electronics* (2013), p. 400–409
- [24] BUDHIA, M.; BOYS, J. T.; COVIC, G. A.; HUANG, C.-Y.: *Development of a Single-Sided Flux Magnetic Coupler for Electric Vehicle IPT Charging Systems*. In: *IEEE Transactions on Industrial Electronics* (2011), p. 318–328
- [25] AHN, D.; HONG, S.: *Wireless Power Transmission With Self-Regulated Output Voltage for Biomedical Implant*. In: *IEEE Transactions on Industrial Electronics*, vol. 61, issue 5 (2014), p. 2225–2235
- [26] JOUNG, G. B.; CHO, B. H.: *An Energy Transmission System for an Artificial Heart Using Leakage Inductance Compensation of Transcutaneous Transformer*. In: *IEEE Transactions on Power Electronics*, vol. 13, no. 6 (1998), p. 1013–1022
- [27] HERNANDEZ, G.; HIRSCH, O.: *Inductive Power Transfer: From the laboratory to the real world* (Conference on Electric Roads & Vehicles (CERV)). Park City, Utah, USA, 17.02.2012

-
- [28] ZAHEER, A.; COVIC, G. A.; KACPRZAK, D.: *A Bipolar Pad in a 10-kHz 300-W Distributed IPT System for AGV Applications*. In: *IEEE Transactions on Industrial Electronics*, vol. 61, issue 7 (2014), p. 3288–3301
 - [29] KANEKO, Y.; ABE, S.: *Technology trends of wireless power transfer systems for electric vehicle and plug-in hybrid electric vehicle*. In: *IEEE 10th International Conference on Power Electronics and Drive Systems (PEDS)* (2013), p. 1009–1014
 - [30] COVIC, G. A.; BOYS, J. T.: *Inductive Power Transfer*. In: *Proceedings of the IEEE, Invited Paper*, vol. 101, no. 6 (2013), p. 1276–1289
 - [31] N. N.: *SAE International Task Force Announces Agreement on Frequency of Operation and Power Classes for Wireless Power Transfer for its Electric and Plug-In Electric Vehicle Guideline*. URL http://www.sae.org/servlets/pressRoom?OBJECT_TYPE=PressReleases&PAGE=showRelease&RELEASE_ID=2296 – last checked on 2014-02-22
 - [32] N. N.: *Zwischenbericht der Nationalen Plattform Elektromobilität (NPE)*. Berlin, November 2010
 - [33] GUSTAVSSON, H.: *Slide-in Electric Road System, Inductive project report*. Gothenburg, Sweden, 18.10.2013
 - [34] KÖBEL, C.: *Primove - inductive charging for electric mobility* (3rd International Electric Drives Production Conference (EDPC)). Nuremberg, Germany, 29.10.2013
 - [35] SCHUDER, J. C.: *Powering an Artificial Heart: Birth of the Inductively Coupled-Radio Frequency System in 1960*. In: *Artificial Organs*, vol. 26, issue 11 (2002), p. 909–915
 - [36] ROSZYK, L.; BARNAS, L.: *Hand held battery operated device and charging means therefor*. Sunbeam Corp. 08.10.1974. Publication nr. US3840795 A
 - [37] KIM, C.-G.; SEO, D.-H.; YOU, J.-S.; PARK, J.-H.; CHO, B.-H.: *Design of a Contactless Battery Charger for Cellular Phone*. In: *Applied Power Electronics Conference and Exposition (APEC)*, vol. 2 (2000), p. 769–773
 - [38] HUI, S. Y. R.; HO, W. C.: *A New Generation of Universal Contactless Battery Charging Platform for Portable Consumer Electronic Equipment*. In: *35th Annual IEEE Power Electronics Specialists Conference (PESC)* (2004), p. 638–644
 - [39] FRIEDMAN, J.: *Companies, public connect with wireless smartphone chargers*. In: *USA TODAY* (2013-08-02)
 - [40] TSENG, R.; VON NOVAK, B.; SHEVDE, S.; GRAJSKI, K. A.: *Introduction to the Alliance for Wireless Power Loosely-Coupled Wireless Power Transfer System Specification Version 1.0*. In: *IEEE Wireless Power Transfer (WPT)* (2013), p. 79–83

- [41] COVIC, G. A.; BOYS, J. T.: *Modern Trends in Inductive Power Transfer for Transportation Applications*. In: *IEEE Journal of Emerging and Selected Topics in Power Electronics* (2013), p. 28–41
- [42] SHLADOVER, S. E.: *PATH at 20-History and Major Milestones*. In: *IEEE Transactions in Intelligent Transportation Systems*, vol. 8, no. 4, December 2007 (2007), p. 584–592
- [43] MASSOT, M.-H.; LAPIERRE, E.: *Praxitele: The Missing Link*. In: *Association for European Transport Conference, Cambridge* (1999), p. 91–100
- [44] COVIC, G. A.; ELLIOTT, G.; STIELAU, O. H.; GREEN, R. M.; BOYS, J. T.: *The design of a contact-less energy transfer system for a people mover system*. In: *International Conference on Power System Technology (PowerCon)* (2000), p. 79–84
- [45] WU, H.; BOYS, J. T.; COVIC, G. A.; RIM, C.-T.; RISCH, F.: *Pre-Conference-Tutorial* (Conference on Electric Roadway and Vehicles (CERV)). Park City, Utah, USA, 16.02.2012
- [46] KIEFER, S.: *Verbundvorhaben InterOp - Inductive Norm Test by Exchange in Real Operation: Auslegungskriterien Interoperabilität: Kostenstruktur und -ziele, Geschäftsmodelle* (8. Fachveranstaltung Kontaktlose Energieübertragung Stand der Technik (Haus der Technik)). Stuttgart, 11.06.2013
- [47] N. N.: *ICNIRP: Guidelines for limiting exposure to time-varying electric, magnetic, and electromagnetic fields (up to 300 GHz)*. In: *Health Physics*, vol. 74, no. 4 (1998), p. 494–522
- [48] N. N.: *Elektrische Ausrüstung von Elektro-Straßenfahrzeugen - Induktive Ladung von Elektrofahrzeugen - Teil 4-2: Niedriger Leistungsbereich (Electric equipment of electric road vehicles - Electric vehicle inductive charging systems - Part 4-2: Low power range)*. 01.03.2011 (VDE-AR-E 2122-4-2)
- [49] N. N.: *ICNIRP: Guidelines for limiting exposure to time-varying electric and magnetic fields (1 Hz to 100 kHz)*. In: *Health Physics*, vol. 99, no. 6 (2010), p. 818–836
- [50] ELIAS, B.; SCHMIDT, F.: *Measuring a Temperature During Contactless Transmission of Energy*. AUDI AG. 12.01.2012. Publication nr. WO2012003957A2
- [51] HICKOX, J. M.: *Coil apparatus having coil arrangement that includes a ferrite layer and a thermally-conductive silicone layer*. Delphi Technologies, Inc. 24.07.2013. Publication nr. EP2618344A1
- [52] MAHLEIN, J.; EGGER, B.: *Anordnung zur berührungslosen Energieübertragung*. SEW-EURODRIVE GmbH & Co. KG. 10.11.2011. Publication nr. DE102010020122A1
- [53] KRONWITTER, M.; BAIER, K.; WEBER, T.: *Motor Vehicle Charging and/or Motor Vehicle Discharging Device*. Daimler AG. 21.06.2012. Publication nr. DE102010055369A1

-
- [54] BUDHIA, M.; COVIC, G. A.; BOYS, J. T.: *A New IPT Magnetic Coupler for Electric Vehicle Charging Systems*. In: *36th Annual Conference on IEEE Industrial Electronics Society (IECON)* (2010), p. 2487–2492
 - [55] BARTH, H.; BRAUN, M.; JUNG, M.; ELIAS, B.; PEER, R.; REKER, U.; SCHMÜLLING, B.; TURKI, F.; SCHULZE, E.: *Abschlussbericht zum Verbundvorhaben Kontaktloses Laden von Elektrofahrzeugen (W-Charge)*. Kassel, October 2011
 - [56] N. N.: *Abschlussbericht zum Verbundvorhaben Kabelloses Laden von Elektrofahrzeugen (Conductix)*. Weil am Rhein, Oktober 2011
 - [57] N. N.: *WiTricity: WiT-3300 Deployment Kit Data Sheet*. Watertown, Mass., USA, 2011
 - [58] N. N.: *Data Sheet ICS - Inductive Charging System (Brusa Elektronik AG)*. Sennwald, Switzerland, 2013
 - [59] GÖTZMANN, T.: *Urban Infrastructure: Inductive Charging Technology* (2nd International Electric Drives Production Conference (EDPC)). Nuremberg, Germany, 17.10.2012
 - [60] TURKI, F.; SCHMÜLLING, B.; PAVLIDIS, M.: *Coil Design of Electric Vehicle Inductive Chargers with Homogeneous Low Magnetic Flux Density* (3rd International Electric Drives Production Conference (EDPC)). Nuremberg, Germany, 29.10.2013
 - [61] PRESTL, W.; HÄSE, K.; NIEDERBERGER, D.: *Abschlussbericht zum Verbundvorhaben Kontaktloses Laden von batterieelektrischen Fahrzeugen (IndiOn)*. München, Oktober 2011
 - [62] ODACHI, Y.; TAKASAN, M.; MINOSHIMA, N.: *Non-Contact Electric Power Supplying System For Vehicle*. Toyota Automatic Loom Works. 05.01.1999. Publication nr. US5855261A
 - [63] OGURI, K.: *Charging paddle*. Toyota Motor Co. Ltd. 16.01.2001. Publication nr. US6175212B1
 - [64] ICHIKAWA, S.; TAKURA, T.; MATSUKI, H.; SATO, F.: *Contactless power transmitting device, contactless power receiving device, and contactless power transfer system*. Toyota Jidosha Kabushiki Kaisha. 19.12.2013. Publication nr. US20130335015 A1
 - [65] GARDNER, M.; SCHATZ, D.: *Toyota Licenses WiTricity Patent Portfolio for Wireless Power*. URL <http://www.businesswire.com/news/home/20131205005161/en/Toyota-Licenses-WiTricity-Patent-Portfolio-Wireless-Power#>. Uv91IIX6QnU – last checked on 2014-02-15
 - [66] N. N.: *Fun Vii Concept Car*. URL <http://www.toyota.com/letsgoplaces/fun-vii-concept-car/> – last checked on 2014-02-04

- [67] BUDHIA, M.; COVIC, G. A.; BOYS, J. T.; HUANG, C.-Y.: *Development and evaluation of single sided flux couplers for contactless electric vehicle charging*. In: *IEEE Energy Conversion Congress and Exposition (ECCE)* (2011), p. 614–621
- [68] FRANKE, J.; RISCH, F.: *Forschungsbericht - Geschäftspotenziale durch kontaktlose Energieübertragung in Elektromobile*. October 2011
- [69] MATHAR, S.: *Konzeption und Entwicklung eines Systems zur kontaktlosen Energieübertragung für Elektrofahrzeuge*. Aachen, RWTH Aachen, Fakultät für Maschinenwesen. PhD thesis. 20.08.2012
- [70] MAGGETTO, G.; VAN DEN BOSSCHE, P.: *Inductive Automatic Charging: The Way to Safe, Efficient and User-Friendly Electric Vehicle Infrastructure*. In: *Electric Vehicle Symposium EVS-18* (2001)
- [71] KEELING, N. A.; VAN BOHEEMEN, E.; KISSIN, M.; BEAVER, J.: *Wireless power transfer apparatus and method of manufacture*. Qualcomm Inc. 26.09.2013. Publication nr. WO2013142064A1
- [72] DIXON, J.: *Energy Storage for Electric Vehicles*. In: *IEEE International Conference on Industrial Technology (ICIT)* (2010), p. 20–26
- [73] N. N.: *Abschlussbericht zum Verbundvorhaben Begleitforschung zum kabellosen Laden von Elektrofahrzeugen: Chancen und Risiken beim kabellosen Laden von Elektrofahrzeugen, Technologiefolgenabschätzung für eine Schlüsseltechnologie in der Durchbruchphase der Elektromobilität (JustPark)*. October 2011
- [74] FASUGBA, M. A.; KREIN, P. T.: *Gaining Vehicle-to-Grid Benefits with Unidirectional Electric and Plug-In Hybrid Vehicle Chargers*. In: *IEEE Vehicle Power and Propulsion Conference (VPPC)* (2011), p. 1–6
- [75] FASUGBA, M. A.; KREIN, P. T.: *Cost Benefits and Vehicle-to-Grid Regulation Services of Unidirectional Charging of Electric Vehicles*. In: *IEEE Energy Conversion Congress and Exposition (ECCE)* (2011), p. 827–834
- [76] N. N.: *Mobilität in Deutschland 2008 (MiD): Ergebnisbericht: Struktur – Aufkommen – Emissionen – Trends*. Bonn und Berlin, February 2010
- [77] VALØENA, L. O.; SHOESMITH, M. I.: *The Effect of PHEV and HEV Duty Cycles on Battery and Battery Pack Performance*. In: *Plugin Highway Conference* (2007), p. 1–9
- [78] SAMMER, G.; BERGER, W. J.; MATIASEK, F.: *Travel Behaviour Patterns in the USA and Austria in Comparison: An Instructive Lesson for Transport Policy*. In: *European Transport Conference, Homerton College, Cambridge* (2002)
- [79] BIERE, D.; DALLINGER, D.; WIETSCHER, M.: *Ökonomische Analyse der Erstnutzer von Elektrofahrzeugen*. In: *ZfE Zeitschrift für Energiewirtschaft* 02 | 173 (2009), no. 02, p. 173–181

-
- [80] EVANSON, J.: *Tesla Motors Investor Presentation*. January 2014. URL <http://files.shareholder.com/downloads/ABEA-4CW8X0/2921970389x0x720221/5647bed2-1c27-4b40-abd3-dd11f8bc474e/Investor%20Presentation%20-%20Jan%202014.pdf> – last checked on 2014-02-16
 - [81] N. N.: *DIN 1998: Placing of service conduits in public areas; directives for planning*. 1978-05
 - [82] WECHLIN, M.: *Device for Inductive Power Transfer of Electrical Energy*. Conductix-Wampfler GmbH. 28.11.2013. Publication nr. WO2013174527A1
 - [83] SLISKOVIC, M.; HUA, Z.; EGGER, B.: *System zum berührungslosen Übertragen von Energie an ein Fahrzeug*. SEW-EURODRIVE GmbH & Co. KG. 13.09.2012. Publication nr. WO2012119688 A2
 - [84] BORRMANN, D.; ROTHFUSS, F.; DANGELMAIER, M.: *Charging infrastructure for shared use of electric vehicles in an urban area*. In: *3rd International Electric Drives Production Conference (EDPC)*, Nuremberg, Germany (2013)
 - [85] GANDULFO, M.; BYRNS, J.: *Branché -Self-Service Electric Car and Bicycle Project in the Metropolitan Region of Montréal*. Montréal, Québec, Canada, 2003
 - [86] SUH, I.-S.: *Innovative EV Charging with OLEV Technology and its Practical Applicability* (2nd International Electric Drives Production Conference (EDPC)). Nuremberg, Germany, 16.10.2012
 - [87] BUDHIA, M.; COVIC, G. A.; BOYS, J. T.: *Magnetic Design of a Three-Phase Inductive Power Transfer System for Roadway Powered Electric Vehicles*. In: *IEEE Vehicle Power and Propulsion Conference (VPPC)* (2010)
 - [88] KISZKA, J.: *System zur kurzfristigen Ladung von elektrisch betriebenen Fahrzeugen*. Siemens AG. 27.09.2012. Publication nr. DE102011005915A1
 - [89] BOLGER, J. G.; KIRSTEN, F. A.; NG, L. S.: *Inductive Power Coupling for an Electric Highway System*. In: *IEEE Vehicular Technology Conference*, vol. 28 (1978), p. 137–144
 - [90] BOLGER, J. G.; NG, L. S.; TURNER, D. B.; WALLACE, R. I.: *Testing a Prototype Inductive Power Coupling for an Electric Highway System*. In: *IEEE Vehicular Technology Conference*, vol. 29 (1979), p. 48–56
 - [91] BOLGER, J. G.: *Urban Electric Transportation Systems: The Role of Magnetic Power Transfer*. In: *WESCON/94. Idea/Microelectronics. Conference Record* (1994), p. 41–45
 - [92] BROOKER, A.; WU, H.; EARLEYWINE, M.; GONDER, J.: *Evaluation of the Costs, Benefits, and Feasibility of Electric Roadway Technologies and Travel Scenarios* (Conference on Electric Roads & Vehicles (CERV)). Park City, Utah, USA, 17.02.2012

- [93] PANTIC, Z.; BAI, S.; LUKIC, S. M.: *Inductively Coupled Power Transfer for Continuously Powered Electric Vehicles*. In: *IEEE Vehicle Power and Propulsion Conference (VPPC)* (2009), p. 1271–1278
- [94] GARCIA, F.; PÉREZ, S.; CURRAN, É.: *Cable Support for Supporting a Conductor Arrangement Producing an Electromagnetic Field, Conductor Arrangement, and Route for Vehicles Comprising the Conductor Arrangement*. Bombardier Transportation GmbH. 30.01.2014. Publication nr. WO2014/016365A2
- [95] PERIK, H.: *Practical EV Integration Cases for Static and Dynamic Wireless Power Transfer* (3rd International Electric Drives Production Conference (EDPC)). Nuremberg, Germany, 30.10.2013
- [96] N. N.: *FIA Formula E Championship Technical Regulations*. Paris, France, 05.12.2013
- [97] HARRIS, S.: *Your questions answered: inductive charging for road vehicles*. URL <http://www.theengineer.co.uk/automotive/in-depth/your-questions-answered-inductive-charging-for-road-vehicles/1015724.article#ixzz2Zzf184z8> – last checked on 2013-02-16
- [98] SEBESTYÉN, R.: *Slide-in Electric Road System, Conductive project report*. Gothenburg, 18.10.2013
- [99] SHINOHARA, N.; KUBO, Y.; TONOMURA, H.: *Mid-Distance Wireless Power Transmission for Electric Truck via Microwaves*. In: *Proceedings of URSI International Symposium on Electromagnetic Theory (EMTS)* (2013), p. 841–843
- [100] GERSTENBERG, F.; LEHMANN, M.; ZAUNER, F.: *Elektromobilität bei schweren Nutzfahrzeugen*. In: *eb - Elektrische Bahnen* 110 (2012), 8-9, p. 452–460
- [101] ALAKÜLA, M.: *Electric Road Systems* (Conference on Electric Roads & Vehicles (CERV)). Park City, Utah, USA, 17.02.2012
- [102] N. N.: *DIW Tabellenblatt - Gütertransportleistung in Deutschland in Mrd. tkm 1991 - 2006*. URL http://www.bmub.bund.de/fileadmin/bmu-import/files/pdfs/allgemein/application/pdf/verk_guetertransport.pdf – last checked on 2014-02-16
- [103] WINTER, J.; MAYER, S.; KAIMER, S.; SEITZ, P.; PAGENKOPF, J.; STREIT, S.: *Inductive Power Supply for Heavy Rail Vehicles*. In: *3rd International Electric Drives Production Conference (EDPC)*, Nuremberg, Germany (2013)
- [104] SCHENK, M.; SEIDEL, H.; EBERT, R.: *Konfiguration einer Ladeinfrastruktur für Elektrofahrzeuge*. In: *Industrie-Management* 26 (2010), no. 6, p. 53–56
- [105] WAHLSTEDT, J.: *Evaluation of the two self-optimising traffic signal systems Utopia/Spot and ImFlow, and comparison with existing signal control in Stockholm, Sweden*. In: *16th International IEEE Conference on Intelligent Transportation Systems (ITSC)* (2013), p. 1541–1546

- [106] KRAJZEWICZ, D.; BONERT, M.; WAGNER, P.: *The Open Source Traffic Simulation Package SUMO*. In: *RoboCup 2006 Infrastructure Simulation Competition* (2006)
- [107] MASALKINA, E.; ECKHOFF, D.; BERNDT, R.; GERMAN, R.: *Towards the City-scale Simulation and Performance Assessment of Electric Vehicles*. In: *Proceedings of 2nd GI/ITG KuVS Fachgespräch Inter-Vehicle Communication (FG-IVC 2014)*.
- [108] KURCZVEIL, T.; SCHNIEDER, E.: *Extending a Traffic Simulation Tool for the Evaluation of novel Charging Infrastructures*. In: *3rd International Electric Drives Production Conference (EDPC), Nuremberg, Germany* (2013)
- [109] KÜHN, W.: *Digitale Fabrik - Fabriksimulation für Produktionsplaner*: Carl Hanser Verlag GmbH & Co. KG, 2006
- [110] N. N.: *Type sheets for industrial trucks*, VDI 2198, Düsseldorf, Germany. 2012-12
- [111] JAE JANG, Y.; DAE KO, Y.; JEONG, S.: *Optimal Design of the Wireless Charging Electric Vehicle*. In: *IEEE International Electric Vehicle Conference (IEVC)* (2012)
- [112] ROSS, H. R.: *Roadway-Powered Electric Vehicle System*. H. R. Industries, Inc. 23.09.1997. Publication nr. US5669470
- [113] ANDERSON, H. L.: *Metropolis, Monte Carlo, and the MANIAC*. In: *Los Alamos Science* (1986), no. 14, p. 96–108
- [114] N. N.: *B-AGV: Forschung und Entwicklung batteriebetriebener Schwerlastfahrzeuge (AGV) und deren Erprobung in einem Feldversuch im Container-Terminal Altenwerder in Hamburg*. Düsseldorf, 10/2011
- [115] LUKIC, S. M.; SAUNDERS, M.; PANTIC, Z.; HUNG, S.; TAIBER, J.: *Use of Inductive Power Transfer for Electric Vehicles*. In: *IEEE Power and Energy Society General Meeting* (2010), p. 1–6
- [116] STUCHLY, M. A.: *Health Effects of Exposure to Electromagnetic Fields*. In: *IEEE Aerospace Applications Conference*, vol. 1 (1995), p. 351–368
- [117] KIM, J.; HOANG, H.; BIEN, F.: *Feasibility of Electric-Field Coupling Scheme for Wireless Power Transfer of Electric Vehicles* (International Forum on Electric Vehicle). Daejeon, Korea, 18.11.2011
- [118] KLINE, M.; IZYUMIN, I.; BOSER, B.; SANDERS, S.: *Capacitive Power Transfer for Contactless Charging*. In: *26th IEEE Applied Power Electronics Conference and Exposition (APEC)* (2011), p. 1398–1404
- [119] KURS, A.; KARALIS, A.; MOFFATT, R.; JOANNOPOULOS, J. D.; FISHER, P.; SOLJACIC, M.: *Wireless Power Transfer via Strongly Coupled Magnetic Resonances*. In: *Science* (2007), no. 317, p. 83–86
- [120] BUDHIA, M.; COVIC, G. A.; BOYS, J. T.: *Design and Optimization of Circular Magnetic Structures for Lumped Inductive Power Transfer Systems*. In: *IEEE Transactions on Power Electronics*, vol. 26, issue 11 (2011), p. 3096–3108

- [121] KÜRSCHNER, D.; RATHGE, C.; JUMAR, U.: *Design Methodology for High Efficient Inductive Power Transfer Systems With High Coil Positioning Flexibility*. In: *IEEE Transactions on Industrial Electronics*, vol. 60, issue 1 (2013), p. 372–381
- [122] VAN SCHUYLENBERGH, K.; PUERS, R.: *Inductive Powering: Basic Theory and Application to Biomedical Systems* : Springer, 2009
- [123] ZAHEER, A.; KACPRZAK, D.; COVIC, G. A.: *A Bipolar Receiver Pad in a Lumped IPT System for Electric Vehicle Charging Applications*. In: *IEEE Energy Conversion Congress and Exposition (ECCE)* (2012), p. 283–290
- [124] MCLEAN, J.; MEDINA, A.; SUTTON, R.: *Magnetostimulation by Inductive Power Transfer Systems*. In: *IEEE Topical Conference on Power Amplifiers for Wireless and Radio Applications (PAWR)* (2013), p. 127–129
- [125] PETERSEN, M.; FUCHS, F. W.: *Comparative Study on Optimal Core Design for Maximizing the Coupling Coefficient in Electric Vehicle Inductive Power Transfer System*. In: *PCIM Europe* , 14-16 May 2013, Nuremberg, Germany (2013), p. 1525–1530
- [126] SAKAMOTO, H.; HARADA, K.; WASHIMIYA, S.; TAKEHARA, K.: *Large air-gap coupler for inductive charger*. In: *IEEE Transactions on Magnetics*, Vol. 35, Issue 5 (1999), p. 3526–3528
- [127] N. N.: *WM7200 Inductive Charger, Owner's Manual: WM7200 Inductive Charger, Owner's Manual*. 1998
- [128] SEVERNS, R.; YEOW, E.; WOODY, G.; HALL, J.; HAYES, J.: *An ultra-compact transformer for a 100 W to 120 kW inductive coupler for electric vehicle battery charging*. In: *11th Applied Power Electronics Conference and Exposition (APEC)*, vol. 1 (1996), p. 32–38
- [129] ELIAS, B.; EBNER, A.; OHLEN, C.: *Sekundärtransformatoreinheit zur Anbringung an einem Fahrzeug mit Elektroantrieb und Fahrzeug mit Elektroantrieb*. AUDI AG. 25.04.2013. Publication nr. WO2013056799
- [130] JOFFE, C.; DITZE, S.; ROßKOPF, A.: *A novel positioning tolerant inductive power transfer system*. In: *3rd International Electric Drives Production Conference (EDPC)*, Nuremberg, Germany (2013)
- [131] SCHERBAUER, B.; SCHNEIDER, U.: *Energieübertragungsvorrichtung für ein Kraftfahrzeug, mit zumindest einem induktiven Energieübertragungsmodul*. Daimler AG, DE. 23.01.2014. Publication nr. DE102012014185A1
- [132] KELLERMANN, M.; RITZINGER, R.; VANA, C.: *Verfahren zur induktiven Energieerzeugung für ein Fahrzeug sowie Vorrichtung zur induktiven Energieerzeugung für ein Fahrzeug*. Viseon Bus GmbH. 02.01.2014. Publication nr. DE102012105687A1
- [133] SEELIG, A.: *Verfahren und Anordnung zum automatischen berührungslosen Laden*. Daimler AG. 05.05.1994. Publication nr. DE4236286A1

- [134] KEELING, N. A.; VAN BOHEEMEN, E.; KISSIN, M.; BEAVER, J.: *Wireless power charging pad and method of construction*. Qualcomm Inc. 26.09.2013. Publication nr. WO2013142056A1
- [135] ELIAS, B.; PEER, R.: *Verfahren zum Aufladen einer Traktionsbatterie, Vorrichtung zum Übertragen von Energie an ein Elektrofahrzeug und Kraftwagen*. AUDI AG. 24.01.2013. Publication nr. DE102011108386A1
- [136] HEINRICH, J.: *Positionierungstolerante, bidirektionale Ladestation für Elektrofahrzeuge* (8. Fachveranstaltung Kontaktlose Energieübertragung Stand der Technik (Haus der Technik)). Stuttgart, 10.06.2013
- [137] TURKI, F.; REKER, U.: *Further Design Approaches of the Standardization: Inductive Charging of Electric Vehicles*. In: *2nd International Electric Drives Production Conference (EDPC)*, Nuremberg, Germany (2012)
- [138] PARSPOUR, N.: *Einführung in die kontaktlose Energieübertragung* (8. Fachveranstaltung Kontaktlose Energieübertragung Stand der Technik (Haus der Technik)). Stuttgart, 10.06.2013
- [139] MAYER, A.; BÖLLING, F.: *Some Physical and Metallurgical Fundamentals of the Electrical Sheet Production*. In: *Journal of Magnetism and Magnetic Materials* 2 2 (1976), p. 151–161
- [140] DE LEÓN, F.; SEMLYEN, A.: *A Simple Representation of Dynamic Hysteresis Losses in Power Transformers*. In: *IEEE Transactions on Power Delivery* 10 (1995), no. 1, p. 315–321
- [141] BIELA, J.: *Wirbelstromverluste in Wicklungen induktiver Bauelemente: Skriptum Professur für Hochleistungselektronik, ETH Zürich*. 2012
- [142] DREIKORN, J.: *Gefügebildung und Verdichtungsvorgänge bei weichmagnetischen Ferriten*. Göttingen, Georg-August-Universität. PhD thesis. 2005
- [143] SULLIVAN, C. R.: *Optimal Choice for Number of Strands in a Litz-Wire Transformer Winding*. In: *IEEE Transactions on Power Electronics*, vol. 14, no. 2 1999, p. 283–291
- [144] BÜHLER, G.: *Wirbelstromverluste in Litzenleitern*. Braunschweig, 2008 (Jahresbericht)
- [145] N. N.: *ELEKTRISOLA: Hochfrequenz-Litzen*. URL <http://www.elektrisola.com/de/hochfrequenz-litzen.html> – last checked on 2014-02-23
- [146] REINOLD, S.: *Aluminium Verbindungstechnologie bei kleinen und mittleren Querschnitten* (Fachkongress Bordnetze im Automobil). Ludwigsburg, Germany, 12.04.2013

- [147] BÜHLER, G.; CZAINSKI, R.: *CPS für die Magnetschnellbahn Transrapid*. TU Braunschweig, 2005 (Jahresbericht)
- [148] BARTOLI, M.; NOFERI, N.; REATTI, A.; KAZIMIERCZUK, M. K.: *Modeling Litz-wire winding losses in high-frequency power inductors*. In: *27th Annual IEEE Power Electronics Specialists Conference (PESC)*, vol. 2 (1996), p. 1690–1696
- [149] WAMBSGANSS, P.; PARSPOUR, N.: *Kontaktlose Energieübertragung*. URL http://www.rrc-wireless-power.de/fileadmin/website_wireless_power/Dokumente/Whitepapers/RRC_WirelessPower_Kontaktlose_Energieuebertragung.pdf – last checked on 2014-02-19
- [150] MATSUO, Y.; OTOBE, S.; NAKAO, F.; SAKAMOTO, H.: *Development of a Ferrite Material for Inductive Chargers*. In: *International Electric Vehicle Symposium (EVS)*, vol. 16, Beijing, China (1999)
- [151] MATSUO, Y.; MOCHIZUKI, T.; ISHIKURA, M.; SASAKI, I.: *Decreasing core loss of Mn-Zn ferrite*. In: *Magn. Soc. Jpn.*, vol. 20, no. 2, 429 (1996)
- [152] YOSHIZAWA, K.: *Nano-structure Control and Soft Magnetic Properties of Rapidly Quenched Metal Ribbons*. In: *Magn. Soc. Jpn.*, vol. 91st, 15 (1995)
- [153] MAKINO, A.; HATANAI, T.; AKIHISA, I.; MASUMOTO, T.: *Development of Nanocrystalline Soft Magnetic Alloys "Nanoperm" with High Saturation Magnetization*. In: *Materia Japan*, vol. 34, no. 5 (1995)
- [154] ASSELIN, P.; GREEN, A.; WECHLIN, M.: *Apparatus for Inductively Transmitting Electrical Energy*. Conductix-Wampfler GmbH. 25.04.2013. Publication nr. WO2013056879A1
- [155] YASUDA, T.; KISHI, H.; ABE, S.; SUZUKI, A.: *Contactless Power Transfer System*. Technova Inc. 27.11.2013. Publication nr. EP2667390A1
- [156] GIMM, Y.-M.; JU, Y.-J.; LEE, D.-Y.; LEE, Y.-R.: *Magnetic Field Shielding Materials of 20 kHz for Roadbed Recharging Vehicle* (International Forum on Electric Vehicle (IFEV)). Daejeon, Korea, 18.11.2011
- [157] ELLINGER, G.; KOMMA, T.; PÖBL, M.; WÜNSCHE, H.: *Vorrichtung zur kontaktlosen Übertragung von Energie auf eine korrespondierende Vorrichtung*. Siemens AG. 22.08.2013. Publication nr. DE102012202472 A1
- [158] KOMMA, T.: *Arrangement for the inductive wireless delivery of energy*. Siemens AG. 19.12.2013. Publication nr. US20130334891 A1
- [159] NAGATSUKA, Y.; EHARA, N.; KANEKO, Y.; ABE, S.; YASUDA, T.: *Compact contactless power transfer system for electric vehicles*. In: *International Power Electronics Conference (IPEC)* (2010), p. 807–813
- [160] MEINS, J.: *Berührungslose Energieübertragung für mobile Anwendungen: Grundlagen der Induktiven Energieübertragung - Grundlagen, Designoptimierung und*

- Anwendung* (8. Fachveranstaltung Kontaktlose Energieübertragung Stand der Technik (Haus der Technik)). Stuttgart, 10.06.2013
- [161] YAMANAKA, T.; KANEKO, Y.; ABE, S.; YASUDA, T.: *10 kW Contactless Power Transfer System for Rapid Charger of Electric Vehicle*. In: *EVS26 International Battery, Hybrid and Fuel Cell Electric Vehicle Symposium*, Los Angeles, CA, USA (2012)
- [162] OMBACH, G.: *Wireless EV Charging, optimum operating frequency selection for power range 3.3 and 6.6kW* (IEEE Energy Conversion Congress & Expo). Denver, Colorado, USA, September 2013
- [163] CHIGIRA, M.; NAGATSUKA, Y.; KANEKO, Y.; ABE, S.; YASUDA, T.; SUZUKI, A.: *Small-size light-weight transformer with new core structure for contactless electric vehicle power transfer system*. In: *IEEE Energy Conversion Congress and Exposition (ECCE)* (2011), p. 260–266
- [164] CHEN, Y.; YU, R. R.; DE LA PARRA, H. Z.: *Standardization Progress Investigation on Electric Vehicle Charging Infrastructure in China*. In: *IET Hybrid and Electric Vehicles Conference (HEVC)* (2013), p. 1–6
- [165] ERDLE, F.: *Smartphones ohne Ladehemmung*. In: *VDI Nachrichten, Düsseldorf, Germany 2012* (2012-12-14), Nr. 50
- [166] SHIMIZU, R.; KANEKO, Y.; ABE, S.: *A New Hc-Core Transmitter of a Contactless Power Transfer System that is Compatible with Circular Core Receivers and H-Shaped Core Receivers*. In: *3rd International Electric Drives Production Conference (EDPC)*, Nuremberg, Germany (2013), p. 1–7
- [167] FRANCFORT, J.: *Testing Results: PLUGLESS™ Wireless Charging System by Evatran Group Inc.* (IWC meeting). Franklin, TN, December 2013
- [168] TAKANASHI, H.; SATO, Y.; KANEKO, Y.; ABE, S.; YASUDA, T.: *A large air gap 3 kW wireless power transfer system for electric vehicles*. In: *IEEE Energy Conversion Congress and Exposition (ECCE)* (2012), p. 269–274
- [169] BOYS, J. T.; COVIC, G. A.; BUDDHIA, M.: *Inductive Power Transfer Apparatus*. Auckland Uniservices Ltd. 17.10.2013. Publication nr. US2013270921A1
- [170] COVIC, G. A.; BOYS, J. T.; KEELING, N. A.; VAN BOHEEMEN, E.; KISSIN, M.; BEAVER, J.; BUDHIA, M. B.; HUANG, C.-Y.: *Winding Arrangements in Wireless Power Transfer Systems*. Auckland Uniservices Limited. 26.09.2013. Publication nr. WO2013141718A1
- [171] ELLIOTT, G.; RAABE, S.; COVIC, G. A.; BOYS, J. T.: *Multiphase Pickups for Large Lateral Tolerance Contactless Power-Transfer Systems*. In: *IEEE Transactions on Industrial Electronics*, vol. 57, issue 5 (2010), p. 1590–1598
- [172] RAABE, S.; ELLIOTT, G.; COVIC, G. A.; BOYS, J. T.: *A Quadrature Pickup for Inductive Power Transfer Systems*. In: *2nd IEEE Conference on Industrial Electronics and Applications (ICIEA)* (2007), p. 68–73

- [173] NINDL, T.: *Qualcomm Halo™ WEVC Interoperability: Multi-coil resonant magnetic induction* (eMonday). Munich, 21.07.2014
- [174] ELIAS, B.; PEER, R.: *Vorrichtung zur induktiven Übertragung elektrischer Energie an ein Fahrzeug*. AUDI AG. 17.01.2013. Publication nr. DE102012013498 B3
- [175] MEINS, J.; SCHMÜLLING, B.; TURKI, F.; VOSSHAGEN, T.: *Flat Coil for a Contactless Inductive Energy Transmission*. Paul Vahle GmbH & Co. KG. 22.08.2013. Publication nr. US20130328412A1
- [176] BOLGER, J. G.: *Power control system for electrically driven vehicle*. 25.05.1982. Publication nr. US4331225
- [177] BOLGER, J. G.: *Roadway power and control system for inductively coupled transportation system*. Inductran Corp. 06.06.1989. Publication nr. US4836344
- [178] MUHS, J. D.: *An Analysis of the Potential of Roadway Electrification and Vehicle Automation in the United States and Preliminary Results on Energy and Transportation Impacts* (2nd International Electric Drives Production Conference (EDPC)). Nuremberg, Germany, 16.10.2012
- [179] KRAUSE, A.: *Vorrichtung zum induktiven Laden zumindest eines elektrischen Energiespeichers eines Elektrofahrzeuges*. Brusa Elektronik AG. 21.11.2012. Publication nr. EP2524834 A1
- [180] COVIC, G. A.; BOYS, J. T.; KISSIN, M.; LU, H. G.: *A Three-Phase Inductive Power Transfer System for Roadway-Powered Vehicles*. In: *IEEE Transactions on Industrial Electronics*, vol. 54, issue 6 2007, p. 3370–3378
- [181] HUH, J.; LEE, S.; PARK, C.; CHO, G.-H.; RIM, C.-T.: *High performance inductive power transfer system with narrow rail width for On-Line Electric Vehicles*. In: *IEEE Energy Conversion Congress and Exposition (ECCE)* (2010), p. 647–651
- [182] LEE, S.; HUH, J.; PARK, C.; CHOI, N.-S.; CHO, G.-H.; RIM, C.-T.: *On-Line Electric Vehicle using Inductive Power Transfer System*. In: *IEEE Energy Conversion Congress and Exposition (ECCE)* (2010), p. 1598–1601
- [183] WU, H.; GILCHRIST, A.; SEALY, K.; ISRAELSEN, P.; MUHS, J.: *A Review on Inductive Charging for Electric Vehicles*. In: *IEEE International Electric Machines & Drives Conference (IEMDC)* (2011), p. 143–147
- [184] SCHULTE, J.; SNIEDERS, G.: *Primärleitersystem und Energieübertragungsvorrichtung*. IABG mbh. 13.02.2014. Publication nr. DE102012107358A1
- [185] YILMAZ, M.; BUYUKDEGIRMENCI, V. T.; KREIN, P. T.: *General design requirements and analysis of roadbed inductive power transfer system for dynamic electric vehicle charging*. In: *IEEE Transportation Electrification Conference and Expo (ITEC)* (2012), p. 1–6

- [186] FRANKE, J.; RISCH, F.; KÜHL, A.: *Produktionsprozesse für kontaktlose Ladeinfrastrukturen: Kosteneffiziente Produktion und Integration von Systemen zur kontaktlosen Übertragung von Energie in stationäre und bewegte Elektrofahrzeuge*. In: ZWF 106 (2011), no. 5, p. 361–365
- [187] BOYS, J. T.; COVIC, G. A.: *Roadway Powered Electric Vehicle*. Auckland Uniservices Lim. 10.02.2011. Publication nr. WO2011016736A2
- [188] KEELING, N. A.; VAN BOHEEMEN, E.; KISSIN, M.; BEAVER, J.: *Magnetically Permeable Structures*. Qualcomm Inc. 26.09.2013. Publication nr. US2013249303A1
- [189] MARYNIAK, B.; SAATHOFF, T.; FLEISCHER, M.; CLAßEN, T.; WAGENAAR, C.: *Device for Inductively Removing the Insulation from Wires and/or Profiles*. Wobben Properties GmbH. 23.08.2012. Publication nr. WO2012110475 A2
- [190] BUCHHALLA, H.; MEYER, C.: *Process for Electric Bonding of an Aluminum Wire*. Hanning Elektro Werke GmbH & Co. KG. 12.12.2013. Publication nr. US2013327814 A1
- [191] TSUJINO, J.; IHARA, S.; HARADA, Y.; KASAHARA, K.; SAKAMAKI, N.: *Characteristics of coated copper wire specimens using high frequency ultrasonic complex vibration welding equipments*. In: *Ultrasonics*, vol. 42, issue 1-9 (2004), p. 121–124
- [192] BUCHALLA, H.; MEYER, C.: *Process for Electric Bonding of an Aluminum Wire*. Hanning Elektro Werke GmbH & Co. KG. 12.12.2013. Publication nr. US2013327814A1
- [193] ROßKOPF, A.; BÄR, E.; JOFFE, C.: *Influence of Inner Skin- and Proximity Effects on Conduction in Litz Wires*. In: *IEEE Transactions on Power Electronics*, Vol. 29, Issue 10 (2014), p. 5454–5461
- [194] N. N.: *Plugless L2 EV Charging System (Evatran Group, Inc.)*. URL <http://www.pluglesspower.com/order/> – last checked on 2014-04-02
- [195] WECHLIN, M.; GREEN, A.: *Energieversorgungseinheit, Landfahrzeug, Austauschstation und Verfahren zum Austausch einer in einem Landfahrzeug enthaltenen Energieversorgungseinheit*. Conductix-Wampfler. 20.01.2011. Publication nr. DE102009033235A1
- [196] RISCH, F.; GÜNTHER, S.; FRANKE, J.: *Wertschöpfungsketten für kontaktlose Ladesysteme: Konsequenzen der kontaktlosen Energieübertragung in Elektrofahrzeuge für automobile Wertschöpfungsketten*. In: *Industrie Management* 28 (2012), no. 5, p. 45–48
- [197] MICHALK, M.: *Spulenordnung und Verfahren zu ihrer Herstellung*. Cubit Electronics GmbH. 18.06.2003. Publication nr. DE10160390A1
- [198] WENGER, U.: *Prozessoptimierung in der Wickeltechnik durch innovative maschinenbauliche und regelungstechnische Ansätze*. Erlangen-Nürnberg, Friedrich-

- Alexander-Universität, Lehrstuhl für Fertigungsautomatisierung und Produktionssystematik. PhD thesis. 2004
- [199] KUNZE, A.: *Automatisierte Montage von makromechatronischen Modulen zur flexiblen Integration in hybride Pkw-Bordnetzsysteme*. Erlangen-Nürnberg, Friedrich-Alexander-Universität, Lehrstuhl für Fertigungsautomatisierung und Produktionssystematik. PhD thesis. 2008
- [200] WOLF, K.-U.: *Verbesserte Prozessführung und Prozessplanung zur Leistungs- und Qualitätssteigerung beim Spulenwickeln*. Erlangen-Nürnberg, Friedrich-Alexander-Universität, Fertigungsautomatisierung und Produktionssystematik. PhD thesis. 1997
- [201] TREMEL, J.; RISCH, F.: *Method and device for producing flat coils*. Friedrich-Alexander-Universität Erlangen-Nürnberg. 28.02.2013. Publication nr. WO2013/026531A2
- [202] DOBROSCHKE, A.: *Flexible Automatisierungslösungen für die Fertigung wickeltechnischer Produkte*. Erlangen-Nürnberg, Friedrich-Alexander-Universität, Lehrstuhl für Fertigungsautomatisierung und Produktionssystematik. PhD thesis. 2011
- [203] ALBACH, M.; PATZ, J.; ROßMANITH, H.; EXNER, D.; STADLER, A.: *Optimale Wicklung = optimaler Wirkungsgrad: Vergleich der Verluste in Litzen und Runddrähten*. In: *Elektronik power* (2010), p. 38–47
- [204] N. N.: *Draht und Kabel auf dünnem Stoff fixiert*. In: *Draht* (2014), no. 1, p. 28
- [205] KÜHL, A.; HÖFT, A.; FRANKE, J.: *Roboterassistierte Montage von Elektromotorstatoren: Methoden und Werkzeuge zur Montage von Wicklungen und Deckschiebern*. In: *ZWF* (2014), no. 05, p. 310–313
- [206] ICHIKAWA, S.; KOMATSU, M.; MATSUKI, H.; SATO, F.; TAKURA, T.; YAMAGUCHI, H.: *Parking Assist System for Vehicle, Contactless Power Transmitting Device, and Contactless Power Receiving Device*. Toyota Jidosha Kabushiki Kaisha. Publication nr. WO2014/68384A2
- [207] SUH, N. P.; CHANG, S. H.; CHO, D.; YIM, J.; KANG, S.: *Energy consumption efficiency measuring apparatus and method for on-line electric vehicle*. Korea Advanced Institute Of Science And Technology (KAIST). 09.09.2011. Publication nr. WO2011046408 A3
- [208] KÖPPL, J.; NIRSCHL, J.: *System zur elektrischen Energieübertragung*. Rohde & Schwarz GmbH & Co. KG. 09.12.2010. Publication nr. DE102009023409 A1
- [209] MATSUO, Y.; ONO, K.; HASHIMOTO, T.; NAKAO, F.: *Magnetic Properties and Mechanical Strength of MnZn Ferrite*. In: *IEEE Transactions on Magnetics*, Vol. 37, Issue 4 (2001), p. 2369–2372

- [210] DEGEN, D.; MAHLEIN, J.; PODBIELSKI, L.; SCHWESINGER, K.: *Vorrichtung zur berührungslosen Energieübertragung*. SEW-EURODRIVE GmbH & Co. KG. 29.09.2011. Publication nr. DE102010050935A1
- [211] N. N.: *ELT-400 - Exposure Level Tester (Narda Safety Test Solutions GmbH): Operating Manual*. Pfullingen, Germany, 2004 (BN 2300/98.11)
- [212] ICHIKAWA, S.: *Vehicle*. 14.11.2013. Publication nr. WO2013168241 A1
- [213] ELIAS, B.; PEER, R.: *Motor Vehicle having a Store for Electrical Energy*. AUDI AG. 13.12.2012. Publication nr. WO2012167851 A2
- [214] FUJITA, I.; YAMANAKA, T.; KANEKO, Y.; ABE, S.; YASUDA, T.: *A 10kW Transformer with A Novel Cooling Structure of A Contactless Power Transfer System for Electric Vehicles*. In: *IEEE Energy Conversion Congress and Exposition (ECCE)*, Denver, CO, USA (2013), p. 3643–3650
- [215] WINKLER, J.: *Materialen für ein effizientes Magnetic Design zur kontaktlosen Energieübertragung* (bayme vbm F+E Tagung Elektrofahrzeuge kontaktlos laden). Augsburg, Germany, 25.10.2011
- [216] MÄRZ, M.; SCHLETZ, A.; ECKARDT, B.; EGELKRAUT, S.; RAUH, H.: *Power electronics system integration for electric and hybrid vehicles*. In: *Conference on Integrated Power Electronics Systems (CIPS)*, vol. 6, Nuremberg, Germany (2010)
- [217] YASUDA, T.; KISHI, H.; ABE, S.; SUZUKI, A.: *Contactless Power Transfer System*. Technova Inc. 26.07.2012. Publication nr. WO2012099170A1
- [218] VANAUD, S.: *Coil Arrangement for a System for Inductive Energy Transmission*. SEW-EURODRIVE GmbH & Co. KG. 25.07.2013. Publication nr. WO2013107620 A1
- [219] LOPE, I.; ACERO, J.; BURDIO, J. M.; ALONSO, R.: *Printed Circuit Board Implementation of Small Inductors for Domestic Induction Heating Applications Using a Planar Litz Wire Structure*. In: *IEEE Applied Power Electronics Conference and Exposition (APEC)*, vol. 28, Long Beach, CA, USA (2013), p. 2402–2407
- [220] URDANETA, M. G.; PROBST, R.; STEPANOV, P. Y.; WEINBERG, I. N.; FRICKE, S. T.: *Goodbye Wires and Formers: 3-D Additive Manufacturing and Fractal Cooling Applied to Construction of MRI Gradient Coils*. In: *IEEE Nuclear Science Symposium and Medical Imaging Conference (NSS/MIC)*, Valencia, Spain (2011), p. 2479–2482

Reihe Fertigungstechnik - Erlangen

www.mb.uni-erlangen.de/diss

Band 1 - 52
Carl Hanser Verlag, München

ab Band 53
Meisenbach Verlag, Bamberg
45,-- Euro

Band 1: Andreas Hemberger
**Innovationspotentiale in der rechnerintegrierten Produktion
durch wissensbasierte Systeme**
208 Seiten, 107 Bilder. 1988.

Band 2: Detlef Classe
**Beitrag zur Steigerung der Flexibilität automatisierter Montagesysteme
durch Sensorintegration und erweiterte Steuerungskonzepte**
194 Seiten, 70 Bilder. 1988.

Band 3: Friedrich-Wilhelm Nolting
Projektierung von Montagesystemen
201 Seiten, 107 Bilder, 1 Tabelle. 1989.

Band 4: Karsten Schlüter
**Nutzungsgradsteigerung von Montagesystemen
durch den Einsatz der Simulationstechnik**
177 Seiten, 97 Bilder. 1989.

Band 5: Shir-Kuan Lin
Aufbau von Modellen zur Lageregelung von Industrierobotern
168 Seiten, 46 Bilder. 1989.

Band 6: Rudolf Nuss
**Untersuchungen zur Bearbeitungsqualität
im Fertigungssystem Laserstrahlschneiden**
206 Seiten, 115 Bilder, 6 Tabellen. 1989.

Band 7: Wolfgang Scholz
**Modell zur datenbankgestützten Planung
automatisierter Montageanlagen**
194 Seiten, 89 Bilder. 1989.

Band 8: Hans-Jürgen Wißmeier
**Beitrag zur Beurteilung des Bruchverhaltens
von Hartmetall-Fließpreßmatrizen**
179 Seiten, 99 Bilder, 9 Tabellen. 1989.

Band 9: Rainer Eisele
**Konzeption und Wirtschaftlichkeit
von Planungssystemen in der Produktion**
183 Seiten, 86 Bilder. 1990.

Band 10: Rolf Pfeiffer
**Technologisch orientierte Montageplanung
am Beispiel der Schraubtechnik**
216 Seiten, 102 Bilder, 16 Tabellen. 1990.

Band 11: Herbert Fischer
**Verteilte Planungssysteme zur Flexibilitätssteigerung
der rechnerintegrierten Teilefertigung**
201 Seiten, 82 Bilder. 1990.

Band 12: Gerhard Kleineidam
CAD/CAP: Rechnergestützte Montagefeinplanung
203 Seiten, 107 Bilder. 1990.

Band 13: Frank Vollertsen
**Pulvermetallurgische Verarbeitung
eines übereutektoiden verschleißfesten Stahls**
XIII u. 217 Seiten, 67 Bilder, 34 Tabellen. 1990.

Band 14: Stephan Biermann
**Untersuchungen zur Anlagen- und Prozeßdiagnostik
für das Schneiden mit CO₂-Hochleistungslasern**
VIII u. 170 Seiten, 93 Bilder, 4 Tabellen. 1991.

Band 15: Uwe Geißler
**Material- und Datenfluß
in einer flexiblen Blechbearbeitungszelle**
124 Seiten, 41 Bilder, 7 Tabellen. 1991.

Band 16: Frank Oswald Hake
**Entwicklung eines rechnergestützten Diagnosesystems
für automatisierte Montagezellen**
XIV u. 166 Seiten, 77 Bilder. 1991.

Band 17: Herbert Reichel
**Optimierung der Werkzeugbereitstellung
durch rechnergestützte Arbeitsfolgenbestimmung**
198 Seiten, 73 Bilder, 2 Tabellen. 1991.

Band 18: Josef Scheller
**Modellierung und Einsatz von Softwaresystemen
für rechnergeführte Montagezellen**
198 Seiten, 65 Bilder. 1991.

Band 19: Arnold vom Ende
Untersuchungen zum Biegeumformen mit elastischer Matrizie
166 Seiten, 55 Bilder, 13 Tabellen. 1991.

Band 20: Joachim Schmid
**Beitrag zum automatisierten Bearbeiten
von Keramikguß mit Industrierobotern**
XIV u. 176 Seiten, 111 Bilder, 6 Tabellen. 1991.

Band 21: Egon Sommer
**Multiprozessorsteuerung für kooperierende
Industrieroboter in Montagezellen**
188 Seiten, 102 Bilder. 1991.

Band 22: Georg Geyer
**Entwicklung problemspezifischer Verfahrensketten
in der Montage**
192 Seiten, 112 Bilder. 1991.

Band 23: Rainer Flohr
**Beitrag zur optimalen Verbindungstechnik
in der Oberflächenmontage (SMT)**
186 Seiten, 79 Bilder. 1991.

Band 24: Alfons Rief
**Untersuchungen zur Verfahrensfolge Laserstrahlschneiden
und -schweißen in der Rohkarosseriefertigung**
VI u. 145 Seiten, 58 Bilder, 5 Tabellen. 1991.

Band 25: Christoph Thim
**Rechnerunterstützte Optimierung von Materialflußstrukturen
in der Elektronikmontage durch Simulation**
188 Seiten, 74 Bilder. 1992.

Band 26: Roland Müller
**CO₂-Laserstrahlschneiden
von kurzglasverstärkten Verbundwerkstoffen**
141 Seiten, 107 Bilder, 4 Tabellen. 1992.

Band 27: Günther Schäfer
Integrierte Informationsverarbeitung bei der Montageplanung
195 Seiten, 76 Bilder. 1992.

Band 28: Martin Hoffmann
**Entwicklung einer CAD/CAM-Prozeßkette
für die Herstellung von Blechbiegeteilen**
149 Seiten, 89 Bilder. 1992.

Band 29: Peter Hoffmann
**Verfahrensfolge Laserstrahlschneiden und –schweißen :
Prozeßführung und Systemtechnik in der 3D–Laserstrahlbearbeitung
von Blechformteilen**
186 Seiten, 92 Bilder, 10 Tabellen. 1992.

Band 30: Olaf Schrödel
Flexible Werkstattsteuerung mit objektorientierten Softwarestrukturen
180 Seiten, 84 Bilder. 1992.

Band 31: Hubert Reinisch
**Planungs– und Steuerungswerkzeuge
zur impliziten Geräteprogrammierung in Roboterzellen**
XI u. 212 Seiten, 112 Bilder. 1992.

Band 32: Brigitte Bärnreuther
**Ein Beitrag zur Bewertung des Kommunikationsverhaltens
von Automatisierungsgeräten in flexiblen Produktionszellen**
XI u. 179 Seiten, 71 Bilder. 1992.

Band 33: Joachim Hutfless
**Laserstrahlregelung und Optikdiagnostik
in der Strahlführung einer CO₂-Hochleistungslaseranlage**
175 Seiten, 70 Bilder, 17 Tabellen. 1993.

Band 34: Uwe Günzel
**Entwicklung und Einsatz eines Simulationsverfahrens für operative
und strategische Probleme der Produktionsplanung und –steuerung**
XIV u. 170 Seiten, 66 Bilder, 5 Tabellen. 1993.

Band 35: Bertram Ehmann
**Operatives Fertigungscontrolling durch Optimierung
auftragsbezogener Bearbeitungsabläufe in der Elektronikfertigung**
XV u. 167 Seiten, 114 Bilder. 1993.

Band 36: Harald Kolléra
**Entwicklung eines benutzerorientierten Werkstattprogrammiersystems
für das Laserstrahlschneiden**
129 Seiten, 66 Bilder, 1 Tabelle. 1993.

Band 37: Stephanie Abels
**Modellierung und Optimierung von Montageanlagen
in einem integrierten Simulationssystem**
188 Seiten, 88 Bilder. 1993.

Band 38: Robert Schmidt–Hebbel
Laserstrahlbohren durchflußbestimmender Durchgangslöcher
145 Seiten, 63 Bilder, 11 Tabellen. 1993.

Band 39: Norbert Lutz
**Oberflächenfeinbearbeitung keramischer Werkstoffe
mit XeCl–Excimerlaserstrahlung**
187 Seiten, 98 Bilder, 29 Tabellen. 1994.

Band 40: Konrad Grampp
**Rechnerunterstützung bei Test und Schulung
an Steuerungssoftware von SMD–Bestücklinien**
178 Seiten, 88 Bilder. 1995.

Band 41: Martin Koch
**Wissensbasierte Unterstützung der Angebotsbearbeitung
in der Investitionsgüterindustrie**
169 Seiten, 68 Bilder. 1995.

Band 42: Armin Gropp
**Anlagen– und Prozeßdiagnostik
beim Schneiden mit einem gepulsten Nd:YAG–Laser**
160 Seiten, 88 Bilder, 7 Tabellen. 1995.

Band 43: Werner Heckel
**Optische 3D-Konturerfassung und on-line Biegewinkelmessung
mit dem Lichtschnittverfahren**
149 Seiten, 43 Bilder, 11 Tabellen. 1995.

Band 44: Armin Rothhaupt
**Modulares Planungssystem
zur Optimierung der Elektronikfertigung**
180 Seiten, 101 Bilder. 1995.

Band 45: Bernd Zöllner
Adaptive Diagnose in der Elektronikproduktion
195 Seiten, 74 Bilder, 3 Tabellen. 1995.

Band 46: Bodo Vormann
**Beitrag zur automatisierten Handhabungsplanung
komplexer Blechbiegeteile**
126 Seiten, 89 Bilder, 3 Tabellen. 1995.

Band 47: Peter Schnepf
Zielkostenorientierte Montageplanung
144 Seiten, 75 Bilder. 1995.

Band 48: Rainer Klotzbücher
**Konzept zur rechnerintegrierten Materialversorgung
in flexiblen Fertigungssystemen**
156 Seiten, 62 Bilder. 1995.

Band 49: Wolfgang Greska
Wissensbasierte Analyse und Klassifizierung von Blechteilen
144 Seiten, 96 Bilder. 1995.

Band 50: Jörg Franke
**Integrierte Entwicklung neuer Produkt- und Produktionstechnologien
für räumliche spritzgegossene Schaltungsträger (3-D MID)**
196 Seiten, 86 Bilder, 4 Tabellen. 1995.

Band 51: Franz-Josef Zeller
Sensorplanung und schnelle Sensorregelung für Industrieroboter
190 Seiten, 102 Bilder, 9 Tabellen. 1995.

Band 52: Michael Solvie
**Zeitbehandlung und Multimedia-Unterstützung
in Feldkommunikationssystemen**
200 Seiten, 87 Bilder, 35 Tabellen. 1996.

Band 53: Robert Hopperdietzel
Reengineering in der Elektro- und Elektronikindustrie
180 Seiten, 109 Bilder, 1 Tabelle. 1996.
ISBN 3-87525-070-2

Band 54: Thomas Rebhan
**Beitrag zur Mikromaterialbearbeitung mit Excimerlasern –
Systemkomponenten und Verfahrensoptimierungen**
148 Seiten, 61 Bilder, 10 Tabellen. 1996.
ISBN 3-87525-075-3

Band 55: Henning Hanebuth
Laserstrahlhartlöten mit Zweistrahltechnik
157 Seiten, 58 Bilder, 11 Tabellen. 1996.
ISBN 3-87525-074-5

Band 56: Uwe Schönherr
**Steuerung und Sensordatenintegration für flexible Fertigungszellen
mit kooperierenden Robotern**
188 Seiten, 116 Bilder, 3 Tabellen. 1996.
ISBN 3-87525-076-1

Band 57: Stefan Holzer
Berührungslose Formgebung mit Laserstrahlung
162 Seiten, 69 Bilder, 11 Tabellen. 1996.
ISBN 3-87525-079-6

Band 58: Markus Schultze
**Fertigungsqualität beim 3D–Laserstrahlschweißen
von Blechformteilen**
165 Seiten, 88 Bilder, 9 Tabellen. 1997.
ISBN 3-87525-080-X

Band 59: Thomas Krebs
**Integration elektromechanischer CA–Anwendungen
über einem STEP–Produktmodell**
198 Seiten, 58 Bilder, 8 Tabellen. 1997.
ISBN 3-87525-081-8

Band 60: Jürgen Sturm
**Prozeßintegrierte Qualitätssicherung
in der Elektronikproduktion**
167 Seiten, 112 Bilder, 5 Tabellen. 1997.
ISBN 3-87525-082-6

Band 61: Andreas Brand
**Prozesse und Systeme zur Bestückung
räumlicher elektronischer Baugruppen (3D-MID)**
182 Seiten, 100 Bilder. 1997.
ISBN 3-87525-087-7

Band 62: Michael Kauf
**Regelung der Laserstrahlleistung und der Fokusparameter
einer CO₂-Hochleistungslaseranlage**
140 Seiten, 70 Bilder, 5 Tabellen. 1997.
ISBN 3-87525-083-4

Band 63: Peter Steinwässer
**Modulares Informationsmanagement
in der integrierten Produkt– und Prozeßplanung**
190 Seiten, 87 Bilder. 1997.
ISBN 3-87525-084-2

Band 64: Georg Liedl
**Integriertes Automatisierungskonzept
für den flexiblen Materialfluß in der Elektronikproduktion**
196 Seiten, 96 Bilder, 3 Tabellen. 1997.
ISBN 3-87525-086-9

Band 65: Andreas Otto
Transiente Prozesse beim Laserstrahlschweißen
132 Seiten, 62 Bilder, 1 Tabelle. 1997.
ISBN 3-87525-089-3

Band 66: Wolfgang Blöchl
**Erweiterte Informationsbereitstellung an offenen CNC–Steuerungen
zur Prozeß– und Programmoptimierung**
168 Seiten, 96 Bilder. 1997.
ISBN 3-87525-091-5

Band 67: Klaus–Uwe Wolf
**Verbesserte Prozeßführung und Prozeßplanung
zur Leistungs– und Qualitätssteigerung beim Spulenwickeln**
186 Seiten, 125 Bilder. 1997.
ISBN 3-87525-092-3

Band 68: Frank Backes
Technologieorientierte Bahnplanung für die 3D–Laserstrahlbearbeitung
138 Seiten, 71 Bilder, 2 Tabellen. 1997.
ISBN 3-87525-093-1

Band 69: Jürgen Kraus
Laserstrahlumformen von Profilen
137 Seiten, 72 Bilder, 8 Tabellen. 1997.
ISBN 3-87525-094-X

Band 70: Norbert Neubauer
Adaptive Strahlführungen für CO₂-Laseranlagen
120 Seiten, 50 Bilder, 3 Tabellen. 1997.
ISBN 3-87525-095-8

Band 71: Michael Steber
**Prozeßoptimierter Betrieb flexibler Schraubstationen
in der automatisierten Montage**
168 Seiten, 78 Bilder, 3 Tabellen. 1997.
ISBN 3-87525-096-6

Band 72: Markus Pfestorf
Funktionale 3D-Oberflächenkenngrößen in der Umformtechnik
162 Seiten, 84 Bilder, 15 Tabellen. 1997.
ISBN 3-87525-097-4

Band 73: Volker Franke
**Integrierte Planung und Konstruktion
von Werkzeugen für die Biegebearbeitung**
143 Seiten, 81 Bilder. 1998.
ISBN 3-87525-098-2

Band 74: Herbert Scheller
**Automatisierte Demontagesysteme und recyclinggerechte
Produktgestaltung elektronischer Baugruppen**
184 Seiten, 104 Bilder, 17 Tabellen. 1998.
ISBN 3-87525-099-0

Band 75: Arthur Meßner
**Kaltmassivumformung metallischer Kleinstteile
– Werkstoffverhalten, Wirkflächenreibung, Prozeßauslegung**
164 Seiten, 92 Bilder, 14 Tabellen. 1998.
ISBN 3-87525-100-8

Band 76: Mathias Glasmacher
Prozeß- und Systemtechnik zum Laserstrahl-Mikroschweißen
184 Seiten, 104 Bilder, 12 Tabellen. 1998.
ISBN 3-87525-101-6

Band 77: Michael Schwind
**Zerstörungsfreie Ermittlung mechanischer Eigenschaften
von Feinblechen mit dem Wirbelstromverfahren**
124 Seiten, 68 Bilder, 8 Tabellen. 1998.
ISBN 3-87525-102-4

Band 78: Manfred Gerhard
**Qualitätssteigerung in der Elektronikproduktion durch Optimierung
der Prozeßführung beim Löten komplexer Baugruppen**
179 Seiten, 113 Bilder, 7 Tabellen. 1998.
ISBN 3-87525-103-2

Band 79: Elke Rauh
**Methodische Einbindung der Simulation
in die betrieblichen Planungs- und Entscheidungsabläufe**
192 Seiten, 114 Bilder, 4 Tabellen. 1998.
ISBN 3-87525-104-0

Band 80: Sorin Niederkorn
**Meßeinrichtung zur Untersuchung der Wirkflächenreibung
bei umformtechnischen Prozessen**
99 Seiten, 46 Bilder, 6 Tabellen. 1998.
ISBN 3-87525-105-9

Band 81: Stefan Schubert
**Regelung der Fokusslage beim Schweißen mit CO₂-Hochleistungslasern
unter Einsatz von adaptiven Optiken**
140 Seiten, 64 Bilder, 3 Tabellen. 1998.
ISBN 3-87525-106-7

Band 82: Armando Walter Colombo
**Development and Implementation of Hierarchical Control Structures
of Flexible Production Systems Using High Level Petri Nets**
216 Seiten, 86 Bilder. 1998.
ISBN 3-87525-109-1

Band 83: Otto Meedt
**Effizienzsteigerung bei Demontage und Recycling
durch flexible Demontagetechnologien und optimierte Produktgestaltung**
186 Seiten, 103 Bilder. 1998.
ISBN 3-87525-108-3

Band 84: Knuth Götz
**Modelle und effiziente Modellbildung
zur Qualitätssicherung in der Elektronikproduktion**
212 Seiten, 129 Bilder, 24 Tabellen. 1998.
ISBN 3-87525-112-1

Band 85: Ralf Luchs
**Einsatzmöglichkeiten leitender Klebstoffe
zur zuverlässigen Kontaktierung elektronischer Bauelemente in der SMT**
176 Seiten, 126 Bilder, 30 Tabellen. 1998.
ISBN 3-87525-113-7

Band 86: Frank Pöhlau
**Entscheidungsgrundlagen zur Einführung
räumlicher spritzgegossener Schaltungsträger (3-D MID)**
144 Seiten, 99 Bilder. 1999.
ISBN 3-87525-114-8

Band 87: Roland T. A. Kals
Fundamentals on the miniaturization of sheet metal working processes
128 Seiten, 58 Bilder, 11 Tabellen. 1999.
ISBN 3-87525-115-6

Band 88: Gerhard Luhn
**Implizites Wissen und technisches Handeln
am Beispiel der Elektronikproduktion**
252 Seiten, 61 Bilder, 1 Tabelle. 1999.
ISBN 3-87525-116-4

Band 89: Axel Sprenger
Adaptives Streckbiegen von Aluminium-Strangpreßprofilen
114 Seiten, 63 Bilder, 4 Tabellen. 1999.
ISBN 3-87525-117-2

Band 90: Hans-Jörg Pucher
**Untersuchungen zur Prozeßfolge Umformen, Bestücken
und Laserstrahllöten von Mikrokontakten**
158 Seiten, 69 Bilder, 9 Tabellen. 1999.
ISBN 3-87525-119-9

Band 91: Horst Arnet
Profilbiegen mit kinematischer Gestalterzeugung
128 Seiten, 67 Bilder, 7 Tabellen. 1999.
ISBN 3-87525-120-2

Band 92: Doris Schubart
**Prozeßmodellierung und Technologieentwicklung
beim Abtragen mit CO₂-Laserstrahlung**
133 Seiten, 57 Bilder, 13 Tabellen. 1999.
ISBN 3-87525-122-9

Band 93: Adrianus L. P. Coremans
**Laserstrahlintern von Metallpulver – Prozeßmodellierung,
Systemtechnik, Eigenschaften laserstrahlgesinterter Metallkörper**
184 Seiten, 108 Bilder, 12 Tabellen. 1999.
ISBN 3-87525-124-5

Band 94: Hans-Martin Biehler
**Optimierungskonzepte für Qualitätsdatenverarbeitung
und Informationsbereitstellung in der Elektronikfertigung**
194 Seiten, 105 Bilder. 1999.
ISBN 3-87525-126-1

Band 95: Wolfgang Becker
**Oberflächenausbildung und tribologische Eigenschaften
excimerlaserstrahlbearbeiteter Hochleistungskeramiken**
175 Seiten, 71 Bilder, 3 Tabellen. 1999.
ISBN 3-87525-127-X

Band 96: Philipp Hein
**Innenhochdruck-Umformen von Blechpaaren:
Modellierung, Prozeßauslegung und Prozeßführung**
129 Seiten, 57 Bilder, 7 Tabellen. 1999.
ISBN 3-87525-128-8

Band 97: Gunter Beitinger
**Herstellungs- und Prüfverfahren
für thermoplastische Schaltungsträger**
169 Seiten, 92 Bilder, 20 Tabellen. 1999.
ISBN 3-87525-129-6

Band 98: Jürgen Knoblach
**Beitrag zur rechnerunterstützten verursachungsgerechten Angebotskalkulation von
Blechteilen mit Hilfe wissensbasierter Methoden**
155 Seiten, 53 Bilder, 26 Tabellen. 1999.
ISBN 3-87525-130-X

Band 99: Frank Breitenbach
**Bildverarbeitungssystem zur Erfassung der Anschlußgeometrie
elektronischer SMT-Bauelemente**
147 Seiten, 92 Bilder, 12 Tabellen. 2000.
ISBN 3-87525-131-8

Band 100: Bernd Falk
**Simulationsbasierte Lebensdauervorhersage
für Werkzeuge der Kaltmassivumformung**
134 Seiten, 44 Bilder, 15 Tabellen. 2000.
ISBN 3-87525-136-9

Band 101: Wolfgang Schlögl
**Integriertes Simulationsdaten-Management
für Maschinenentwicklung und Anlagenplanung**
169 Seiten, 101 Bilder, 20 Tabellen. 2000.
ISBN 3-87525-137-7

Band 102: Christian Hinsel
**Ermüdungsbruchversagen hartstoffbeschichteter
Werkzeugstähle in der Kaltmassivumformung**
130 Seiten, 80 Bilder, 14 Tabellen. 2000.
ISBN 3-87525-138-5

Band 103: Stefan Bobbert
**Simulationsgestützte Prozessauslegung
für das Innenhochdruck-Umformen von Blechpaaren**
123 Seiten, 77 Bilder. 2000.
ISBN 3-87525-145-8

Band 104: Harald Rottbauer
**Modulares Planungswerkzeug
zum Produktionsmanagement in der Elektronikproduktion**
166 Seiten, 106 Bilder. 2001.
ISBN 3-87525-139-3

Band 105: Thomas Hennige
Flexible Formgebung von Blechen durch Laserstrahlumformen
119 Seiten, 50 Bilder. 2001.
ISBN 3-87525-140-7

Band 106: Thomas Menzel
**Wissensbasierte Methoden für die rechnergestützte Charakterisierung
und Bewertung innovativer Fertigungsprozesse**
152 Seiten, 71 Bilder. 2001.
ISBN 3-87525-142-3

Band 107: Thomas Stöckel
**Kommunikationstechnische Integration der Prozeßebene
in Produktionssysteme durch Middleware-Frameworks**
147 Seiten, 65 Bilder, 5 Tabellen. 2001.
ISBN 3-87525-143-1

Band 108: Frank Pitter
**Verfügbarkeitssteigerung von Werkzeugmaschinen
durch Einsatz mechatronischer Sensorlösungen**
158 Seiten, 131 Bilder, 8 Tabellen. 2001.
ISBN 3-87525-144-X

Band 109: Markus Korneli
**Integration lokaler CAP-Systeme
in einen globalen Fertigungsdatenverbund**
121 Seiten, 53 Bilder, 11 Tabellen. 2001.
ISBN 3-87525-146-6

Band 110: Burkhard Müller

Laserstrahljustieren mit Excimer-Lasern – Prozeßparameter und Modelle zur Aktorkonstruktion

128 Seiten, 36 Bilder, 9 Tabellen. 2001
ISBN 3-87525-159-8

Band 111: Jürgen Göhringer

**Integrierte Telediagnose via Internet
zum effizienten Service von Produktionssystemen**

178 Seiten, 98 Bilder, 5 Tabellen. 2001.
ISBN 3-87525-147-4

Band 112: Robert Feuerstein

**Qualitäts- und kosteneffiziente Integration
neuer Bauelementetechnologien
in die Flachbaugruppenfertigung**

161 Seiten, 99 Bilder, 10 Tabellen. 2001.
ISBN 3-87525-151-2

Band 113: Marcus Reichenberger

**Eigenschaften und Einsatzmöglichkeiten
alternativer Elektroniklote
in der Oberflächenmontage (SMT)**

165 Seiten, 97 Bilder, 18 Tabellen. 2001.
ISBN 3-87525-152-0

Band 114: Alexander Huber

**Justieren vormontierter Systeme mit dem Nd:YAG-Laser
unter Einsatz von Aktoren**

122 Seiten, 58 Bilder, 5 Tabellen. 2001.
ISBN 3-87525-153-9

Band 115: Sami Krimi

**Analyse und Optimierung von Montagesystemen
in der Elektronikproduktion**

155 Seiten, 88 Bilder, 3 Tabellen. 2001.
ISBN 3-87525-157-1

Band 116: Marion Merklein

**Laserstrahlumformen von Aluminiumwerkstoffen -
Beeinflussung der Mikrostruktur und der mechanischen Eigenschaften**

122 Seiten, 65 Bilder, 15 Tabellen. 2001.
ISBN 3-87525-156-3

Band 117: Thomas Collisi

**Ein informationslogistisches Architekturkonzept
zur Akquisition simulationsrelevanter Daten**

181 Seiten, 105 Bilder, 7 Tabellen. 2002.
ISBN 3-87525-164-4

Band 118: Markus Koch

**Rationalisierung und ergonomische Optimierung im Innenausbau
durch den Einsatz moderner Automatisierungstechnik**

176 Seiten, 98 Bilder, 9 Tabellen. 2002.
ISBN 3-87525-165-2

Band 119: Michael Schmidt

**Prozeßregelung für das Laserstrahl-Punktschweißen
in der Elektronikproduktion**

152 Seiten, 71 Bilder, 3 Tabellen. 2002.
ISBN 3-87525-166-0

Band 120: Nicolas Tiesler

Grundlegende Untersuchungen zum Fließpressen metallischer Kleinteile

126 Seiten, 78 Bilder, 12 Tabellen. 2002.
ISBN 3-87525-175-X

Band 121: Lars Pursche

**Methoden zur technologieorientierten Programmierung für die
3D-Lasermikrobearbeitung**

111 Seiten, 39 Bilder, 0 Tabellen. 2002.
ISBN 3-87525-183-0

Band 122: Jan-Oliver Brassel

Prozeßkontrolle beim Laserstrahl-Mikroschweißen

148 Seiten, 72 Bilder, 12 Tabellen. 2002.
ISBN 3-87525-181-4

Band 123: Mark Geisel

**Prozeßkontrolle und –steuerung beim Laserstrahlschweißen
mit den Methoden der nichtlinearen Dynamik**

135 Seiten, 46 Bilder, 2 Tabellen. 2002.

ISBN 3-87525-180-6

Band 124: Gerd Eßer

**Laserstrahlunterstützte Erzeugung metallischer Leiterstrukturen auf
Thermoplastsubstraten für die MID-Technik**

148 Seiten, 60 Bilder, 6 Tabellen. 2002.

ISBN 3-87525-171-7

Band 125: Marc Fleckenstein

**Qualität laserstrahl-gefügter Mikroverbindungen
elektronischer Kontakte**

159 Seiten, 77 Bilder, 7 Tabellen. 2002.

ISBN 3-87525-170-9

Band 126: Stefan Kaufmann

**Grundlegende Untersuchungen zum Nd:YAG- Laserstrahlfügen
von Silizium für Komponenten der Optoelektronik**

159 Seiten, 100 Bilder, 6 Tabellen. 2002.

ISBN 3-87525-172-5

Band 127: Thomas Fröhlich

**Simultanes Löten von Anschlußkontakten elektronischer Bauelemente
mit Diodenlaserstrahlung**

143 Seiten, 75 Bilder, 6 Tabellen. 2002.

ISBN 3-87525-186-5

Band 128: Achim Hofmann

**Erweiterung der Formgebungsgrenzen beim Umformen von
Aluminiumwerkstoffen durch den Einsatz prozessangepasster Platinen**

113 Seiten, 58 Bilder, 4 Tabellen

ISBN 3-87525-182-2

Band 129: Ingo Kriebitzsch

3 - D MID Technologie in der Automobilelektronik

129 Seiten, 102 Bilder, 10 Tabellen. 2002.

ISBN 3-87525-169-5

Band 130: Thomas Pohl

**Fertigungsqualität und Umformbarkeit laserstrahlgeschweißter
Formplatinen aus Aluminiumlegierungen**

133 Seiten, 93 Bilder, 12 Tabellen. 2002

ISBN 3-87525-173-3

Band 131: Matthias Wenk

**Entwicklung eines konfigurierbaren Steuerungssystems für die
flexible Sensorführung von Industrierobotern**

167 Seiten, 85 Bilder, 1 Tabelle. 2002.

ISBN 3-87525-174-1

Band 132: Matthias Negendanck

**Neue Sensorik und Aktorik für Bearbeitungsköpfe
zum Laserstrahlschweißen**

116 Seiten, 60 Bilder, 14 Tabellen

ISBN 3-87525-184-9

Band 133: Oliver Kreis

Integrierte Fertigung –

**Verfahrensintegration durch Innenhochdruck-Umformen, Trennen und
Laserstrahlschweißen in einem Werkzeug sowie ihre tele- und multimediale Präsentation**

167 Seiten, 90 Bilder, 43 Tabellen

ISBN 3-87525-176-8

Band 134: Stefan Trautner

**Technische Umsetzung produktbezogener Instrumente der
Umweltpolitik bei Elektro- und Elektronikgeräten**

179 Seiten, 92 Bilder, 11 Tabellen. 2002.

ISBN 3-87525-177-6

Band 135: Roland Meier

**Strategien für einen produktorientierten Einsatz räumlicher
spritzgegossener Schaltungsträger (3-D MID)**

155 Seiten, 88 Bilder, 14 Tabellen. 2002.

ISBN 3-87525-178-4

Band 136: Jürgen Wunderlich

**Kostensimulation – Simulationsbasierte Wirtschaftlichkeitsregelung
komplexer Produktionssysteme**

202 Seiten, 119 Bilder, 17 Tabellen. 2002.

ISBN 3-87525-179-2

Band 137: Stefan Novotny

**Innenhochdruck-Umformen von Blechen aus Aluminium- und
Magnesiumlegierungen bei erhöhter Temperatur**

132 Seiten, 82 Bilder, 6 Tabellen. 2002.

ISBN 3-87525-185-7

Band 138: Andreas Licha

**Flexible Montageautomatisierung zur Komplettmontage flächenhafter
Produktstrukturen durch kooperierende Industrieroboter**

158 Seiten, 87 Bilder, 8 Tabellen. 2003.

ISBN 3-87525-189-X

Band 139: Michael Eisenbarth

**Beitrag zur Optimierung der Aufbau- und Verbindungstechnik
für mechatronische Baugruppen**

207 Seiten, 141 Bilder, 9 Tabellen. 2003.

ISBN 3-87525-190-3

Band 140: Frank Christoph

**Durchgängige simulationsgestützte Planung von
Fertigungseinrichtungen der Elektronikproduktion**

187 Seiten, 107 Bilder, 9 Tabellen. 2003.

ISBN 3-87525-191-1

Band 141: Hinnerk Hagenah

**Simulationsbasierte Bestimmung der zu erwartenden
Maßhaltigkeit für das Blechbiegen**

131 Seiten, 36 Bilder, 26 Tabellen. 2003.

ISBN 3-87525-192-X

Band 142: Ralf Eckstein

**Scherschneiden und Biegen metallischer Kleinstteile –
Materialeinfluss und Materialverhalten**

148 Seiten, 71 Bilder, 19 Tabellen. 2003.

ISBN 3-87525-193-8

Band 143: Frank H. Meyer-Pittroff

**Excimerlaserstrahlbiegen dünner metallischer Folien
mit homogener Lichtlinie**

138 Seiten, 60 Bilder, 16 Tabellen. 2003.

ISBN 3-87525-196-2

Band 144: Andreas Kach

**Rechnergestützte Anpassung von Laserstrahlschneidbahnen
an Bauteilabweichungen**

139 Seiten, 69 Bilder, 11 Tabellen. 2004.

ISBN 3-87525-197-0

Band 145: Stefan Hierl

**System- und Prozeßtechnik für das simultane Löten mit
Diodenlaserstrahlung von elektronischen Bauelementen**

124 Seiten, 66 Bilder, 4 Tabellen. 2004.

ISBN 3-87525-198-9

Band 146: Thomas Neudecker

**Tribologische Eigenschaften keramischer Blechumformwerkzeuge-
Einfluss einer Oberflächenendbearbeitung mittels Excimerlaserstrahlung**

166 Seiten, 75 Bilder, 26 Tabellen. 2004.

ISBN 3-87525-200-4

Band 147: Ulrich Wenger

Prozessoptimierung in der Wickeltechnik durch innovative maschinenbauliche und regelungstechnische Ansätze

132 Seiten, 88 Bilder, 0 Tabellen. 2004.

ISBN 3-87525-203-9

Band 148: Stefan Slama

Effizienzsteigerung in der Montage durch marktorientierte Montagestrukturen und erweiterte Mitarbeiterkompetenz

188 Seiten, 125 Bilder, 0 Tabellen. 2004.

ISBN 3-87525-204-7

Band 149: Thomas Wurm

**Laserstrahljustieren mittels Aktoren –
Entwicklung von Konzepten und Methoden für die rechnerunterstützte Modellierung
und Optimierung von komplexen Aktorsystemen in der Mikrotechnik**

122 Seiten, 51 Bilder, 9 Tabellen. 2004.

ISBN 3-87525-206-3

Band 150: Martino Celeghini

**Wirkmedienbasierte Blechumformung:
Grundlagenuntersuchungen zum Einfluss von Werkstoff und Bauteilgeometrie**

146 Seiten, 77 Bilder, 6 Tabellen. 2004.

ISBN 3-87525-207-1

Band 151: Ralph Hohenstein

**Entwurf hochdynamischer Sensor- und Regelsysteme
für die adaptive Laserbearbeitung**

282 Seiten, 63 Bilder, 16 Tabellen. 2004.

ISBN 3-87525-210-1

Band 152: Angelika Hutterer

**Entwicklung prozessüberwachender Regelkreise
für flexible Formgebungsprozesse**

149 Seiten, 57 Bilder, 2 Tabellen. 2005.

ISBN 3-87525-212-8

Band 153: Emil Egerer

**Massivumformen metallischer Kleinstteile
bei erhöhter Prozesstemperatur**

158 Seiten, 87 Bilder, 10 Tabellen. 2005.

ISBN 3-87525-213-6

Band 154: Rüdiger Holzmann

**Strategien zur nachhaltigen Optimierung von Qualität und Zuverlässigkeit
in der Fertigung hochintegrierter Flachbaugruppen**

186 Seiten, 99 Bilder, 19 Tabellen. 2005.

ISBN 3-87525-217-9

Band 155: Marco Nock

Biegeumformen mit Elastomerwerkzeugen

Modellierung, Prozessauslegung und Abgrenzung
des Verfahrens am Beispiel des Rohrbiegens

164 Seiten, 85 Bilder, 13 Tabellen. 2005.

ISBN 3-87525-218-7

Band 156: Frank Niebling

**Qualifizierung einer Prozesskette zum
Laserstrahlsintern metallischer Bauteile**

148 Seiten, 89 Bilder, 3 Tabellen. 2005.

ISBN 3-87525-219-5

Band 157: Markus Meiler

**Großserientauglichkeit
trockenschmierstoffbeschichteter
Aluminiumbleche im Presswerk**

Grundlegende Untersuchungen zur Tribologie,
zum Umformverhalten und Bauteilversuche

104 Seiten, 57 Bilder, 21 Tabellen. 2005.

ISBN 3-87525-221-7

Band 158: Agus Sutanto

**Solution Approaches for Planning of Assembly Systems
in Three-Dimensional Virtual Environments**

169 Seiten, 98 Bilder, 3 Tabellen. 2005.
ISBN 3-87525-220-9

Band 159: Matthias Boiger

**Hochleistungssysteme für die Fertigung elektronischer Baugruppen
auf der Basis flexibler Schaltungsträger**

175 Seiten, 111 Bilder, 8 Tabellen. 2005.
ISBN 3-87525-222-5

Band 160: Matthias Pitz

Laserunterstütztes Biegen höchstfester Mehrphasenstähle

120 Seiten, 18 Bilder, 11 Tabellen. 2005.
ISBN 3-87525-223-3

Band 161: Meik Vahl

**Beitrag zur gezielten Beeinflussung des Werkstoffflusses
beim Innenhochdruck-Umformen von Blechen**

165 Seiten, 94 Bilder, 15 Tabellen. 2005.
ISBN 3-87525-224-1

Band 162: Peter K. Kraus

**Plattformstrategien – Realisierung einer varianz- und
kostenoptimierten Wertschöpfung**

181 Seiten, 95 Bilder, 0 Tabellen. 2005.
ISBN 3-87525-226-8

Band 163: Adrienn Cser

Laserstrahlschmelzabtrag – Prozessanalyse und -modellierung

146 Seiten, 79 Bilder, 3 Tabellen. 2005.
ISBN 3-87525-227-6

Band 164: Markus C. Hahn

**Grundlegende Untersuchungen zur Herstellung von
Leichtbauverbundstrukturen mit Aluminiumschaumkern**

143 Seiten, 60 Bilder, 16 Tabellen. 2005.
ISBN 3-87525-228-4

Band 165: Gordana Michos

Mechatronische Ansätze zur Optimierung von Vorschubachsen

146 Seiten, 87 Bilder, 17 Tabellen. 2005.
ISBN 3-87525-230-6

Band 166: Markus Stark

Auslegung und Fertigung hochpräziser Faser-Kollimator-Arrays

158 Seiten, 115 Bilder, 11 Tabellen. 2005.
ISBN 3-87525-231-4

Band 167: Yurong Zhou

**Kollaboratives Engineering Management in der integrierten virtuellen
Entwicklung der Anlagen für die Elektronikproduktion**

156 Seiten, 84 Bilder, 6 Tabellen. 2005.
ISBN 3-87525-232-2

Band 168: Werner Enser

**Neue Formen permanenter und lösbarer elektrischer
Kontaktierungen für mechatronische Baugruppen**

190 Seiten, 112 Bilder, 5 Tabellen. 2005.
ISBN 3-87525-233-0

Band 169: Katrin Melzer

**Integrierte Produktpolitik bei elektrischen und elektronischen
Geräten zur Optimierung des Product-Life-Cycle**

155 Seiten, 91 Bilder, 17 Tabellen. 2005.
ISBN 3-87525-234-9

Band 170: Alexander Putz

**Grundlegende Untersuchungen zur Erfassung der realen Vorspannung von
armierten Kaltfließpresswerkzeugen mittels Ultraschall**

137 Seiten, 71 Bilder, 15 Tabellen. 2006.
ISBN 3-87525-237-3

Band 171: Martin Prechtl

Automatisiertes Schichtverfahren für metallische Folien – System- und Prozesstechnik

154 Seiten, 45 Bilder, 7 Tabellen. 2006.
ISBN 3-87525-238-1

Band 172: Markus Meidert

Beitrag zur deterministischen Lebensdauerabschätzung von Werkzeugen der Kaltmassivumformung

131 Seiten, 78 Bilder, 9 Tabellen. 2006.
ISBN 3-87525-239-X

Band 173: Bernd Müller

Robuste, automatisierte Montagesysteme durch adaptive Prozessführung und montageübergreifende Fehlerprävention am Beispiel flächiger Leichtbauteile

147 Seiten, 77 Bilder, 0 Tabellen. 2006.
ISBN 3-87525-240-3

Band 174: Alexander Hofmann

Hybrides Laserdurchstrahlsschweißen von Kunststoffen

136 Seiten, 72 Bilder, 4 Tabellen. 2006.
ISBN 978-3-87525-243-9
ISBN 3-87525-243-8

Band 175: Peter Wölflick

Innovative Substrate und Prozesse mit feinsten Strukturen für bleifreie Mechatronik-Anwendungen

177 Seiten, 148 Bilder, 24 Tabellen. 2006.
ISBN 978-3-87525-246-0
ISBN 3-87525-246-2

Band 176: Attila Komlódi

Detection and Prevention of Hot Cracks during Laser Welding of Aluminium Alloys Using Advanced Simulation Methods

155 Seiten, 89 Bilder, 14 Tabellen. 2006.
ISBN 978-3-87525-248-4
ISBN 3-87525-248-9

Band 177: Uwe Popp

Grundlegende Untersuchungen zum Laserstrahlstrukturieren von Kaltmassivumformwerkzeugen

140 Seiten, 67 Bilder, 16 Tabellen. 2006.
ISBN 978-3-87525-249-1
ISBN 3-87525-249-7

Band 178: Veit Rückel

Rechnergestützte Ablaufplanung und Bahngenerierung Für kooperierende Industrieroboter

148 Seiten, 75 Bilder, 7 Tabellen. 2006.
ISBN 978-3-87525-250-7
ISBN 3-87525-250-0

Band 179: Manfred Dirscherl

Nicht-thermische Mikrojustiertechnik mittels ultrakurzer Laserpulse

154 Seiten, 69 Bilder, 10 Tabellen. 2007.
ISBN 978-3-87525-251-4
ISBN 3-87525-251-9

Band 180: Yong Zhuo

Entwurf eines rechnergestützten integrierten Systems für Konstruktion und Fertigungsplanung räumlicher spritzgegossener Schaltungsträger (3D-MID)

181 Seiten, 95 Bilder, 5 Tabellen. 2007.
ISBN 978-3-87525-253-8

Band 181: Stefan Lang

Durchgängige Mitarbeiterinformation zur Steigerung von Effizienz und Prozesssicherheit in der Produktion

172 Seiten, 93 Bilder. 2007.
ISBN 978-3-87525-257-6

Band 182: Hans-Joachim Krauß

Laserstrahlinduzierte Pyrolyse präkeramischer Polymere

171 Seiten, 100 Bilder. 2007.
ISBN 978-3-87525-258-3

Band 183: Stefan Junker

**Technologien und Systemlösungen für die flexibel automatisierte Bestückung
permanent erregter Läufer mit oberflächenmontierten Dauermagneten**
173 Seiten, 75 Bilder. 2007.

ISBN 978-3-87525-259-0

Band 184: Rainer Kohlbauer

**Wissensbasierte Methoden für die simulationsgestützte Auslegung
wirkmedienbasierter Blechumformprozesse**
135 Seiten, 50 Bilder. 2007.

ISBN 978-3-87525-260-6

Band 185: Klaus Lamprecht

**Wirkmedienbasierte Umformung tiefgezogener Vorformen unter besonderer
Berücksichtigung maßgeschneiderter Halbzeuge**
137 Seiten, 81 Bilder. 2007.

ISBN 978-3-87525-265-1

Band 186: Bernd Zolleiß

**Optimierte Prozesse und Systeme für die Bestückung
mechatronischer Baugruppen**
180 Seiten, 117 Bilder. 2007.

ISBN 978-3-87525-266-8

Band 187: Michael Kerausch

**Simulationsgestützte Prozessauslegung für das Umformen lokal
wärmebehandelter Aluminiumplatten**

146 Seiten, 76 Bilder, 7 Tabellen. 2007.

ISBN 978-3-87525-267-5

Band 188: Matthias Weber

**Unterstützung der Wandlungsfähigkeit von Produktionsanlagen
durch innovative Softwaresysteme**

183 Seiten, 122 Bilder, 3 Tabellen. 2007.

ISBN 978-3-87525-269-9

Band 189: Thomas Frick

**Untersuchung der prozessbestimmenden Strahl-Stoff-Wechselwirkungen
beim Laserstrahlschweißen von Kunststoffen**

104 Seiten, 62 Bilder, 8 Tabellen. 2007.

ISBN 978-3-87525-268-2

Band 190: Joachim Hecht

**Werkstoffcharakterisierung und Prozessauslegung für die wirkmedienbasierte
Doppelblech-Umformung von Magnesiumlegierungen**

107 Seiten, 91 Bilder, 2 Tabellen. 2007.

ISBN 978-3-87525-270-5

Band 191: Ralf Völkl

**Stochastische Simulation zur Werkzeuglebensdaueroptimierung und
Präzisionsfertigung in der Kaltmassivumformung**

178 Seiten, 75 Bilder, 12 Tabellen. 2008.

ISBN 978-3-87525-272-9

Band 192: Massimo Tolazzi

Innenhochdruck-Umformen verstärkter Blech-Rahmenstrukturen

164 Seiten, 85 Bilder, 7 Tabellen. 2008.

ISBN 978-3-87525-273-6

Band 193: Cornelia Hoff

**Untersuchung der Prozesseinflussgrößen beim
Presshärten des höchstfesten Vergütungsstahls 22MnB5**

133 Seiten, 92 Bilder, 5 Tabellen. 2008.

ISBN 978-3-87525-275-0

Band 194: Christian Alvarez

**Simulationsgestützte Methoden zur effizienten Gestaltung von
Lötprozessen in der Elektronikproduktion**

149 Seiten, 86 Bilder, 8 Tabellen. 2008.

ISBN 978-3-87525-277-4

Band 195: Andreas Kunze

**Automatisierte Montage von makromechatronischen
Modulen zur flexiblen Integration in hybride Pkw-Bordnetzsysteme**

160 Seiten, 90 Bilder, 14 Tabellen. 2008.

ISBN 978-3-87525-278-1

Band 196: Wolfgang Hußnätter
Grundlegende Untersuchungen zur experimentellen Ermittlung und zur Modellierung von Fließortkurven bei erhöhten Temperaturen
152 Seiten, 73 Bilder, 21 Tabellen 2008.
ISBN 978-3-87525-279-8

Band 197: Thomas Bigl
Entwicklung, angepasste Herstellungsverfahren und erweiterte Qualitätssicherung von einsatzgerechten elektronischen Baugruppen
175 Seiten, 107 Bilder, 14 Tabellen 2008.
ISBN 978-3-87525-280-4

Band 198: Stephan Roth
Grundlegende Untersuchungen zum Excimerlaserstrahl-Abtragen unter Flüssigkeitsfilmen
113 Seiten, 47 Bilder, 14 Tabellen 2008.
ISBN 978-3-87525-281-1

Band 199: Artur Giera
Prozesstechnische Untersuchungen zum Rührreischweißen metallischer Werkstoffe
179 Seiten, 104 Bilder, 36 Tabellen 2008.
ISBN 978-3-87525-282-8

Band 200: Jürgen Lechler
Beschreibung und Modellierung des Werkstoffverhaltens von presshärtbaren Bor-Manganstählen
154 Seiten, 75 Bilder, 12 Tabellen 2009.
ISBN 978-3-87525-286-6

Band 201: Andreas Blankl
Untersuchungen zur Erhöhung der Prozessrobustheit bei der Innenhochdruck-Umformung von flächigen Halbzeugen mit vor- bzw. nachgeschalteten Laserstrahlfügeoperationen
120 Seiten, 68 Bilder, 9 Tabellen 2009.
ISBN 978-3-87525-287-3

Band 202: Andreas Schaller
Modellierung eines nachfrageorientierten Produktionskonzeptes für mobile Telekommunikationsgeräte
120 Seiten, 79 Bilder, 0 Tabellen 2009.
ISBN 978-3-87525-289-7

Band 203: Claudius Schimpf
Optimierung von Zuverlässigkeitsuntersuchungen, Prüfabläufen und Nacharbeitsprozessen in der Elektronikproduktion
162 Seiten, 90 Bilder, 14 Tabellen 2009.
ISBN 978-3-87525-290-3

Band 204: Simon Dietrich
Sensoriken zur Schwerpunktslagebestimmung der optischen Prozessemissionen beim Laserstrahliefschweißen
138 Seiten, 70 Bilder, 5 Tabellen 2009.
ISBN 978-3-87525-292-7

Band 205: Wolfgang Wolf
Entwicklung eines agentenbasierten Steuerungssystems zur Materialflussorganisation im wandelbaren Produktionsumfeld
167 Seiten, 98 Bilder, 2009.
ISBN 978-3-87525-293-4

Band 206: Steffen Polster
Laserdurchstrahlschweißen transparenter Polymerbauteile
160 Seiten, 92 Bilder, 13 Tabellen 2009.
ISBN 978-3-87525-294-1

Band 207: Stephan Manuel Dörfler
Rührreibschweißen von walzplattiertem Halbzeug und Aluminiumblech zur Herstellung flächiger Aluminiumschaum-Sandwich-Verbundstrukturen
190 Seiten, 98 Bilder, 5 Tabellen 2009.
ISBN 978-3-87525-295-8

Band 208: Uwe Vogt
Seriennahe Auslegung von Aluminium Tailored Heat Treated Blanks
151 Seiten, 68 Bilder, 26 Tabellen 2009.
ISBN 978-3-87525-296-5

Band 209: Till Laumann
Qualitative und quantitative Bewertung der Crashtauglichkeit von höchstfesten Stählen
117 Seiten, 69 Bilder, 7 Tabellen 2009.
ISBN 978-3-87525-299-6

Band 210: Alexander Diehl
Größeneffekte bei Biegeprozessen- Entwicklung einer Methodik zur Identifikation und Quantifizierung
180 Seiten, 92 Bilder, 12 Tabellen 2010.
ISBN 978-3-87525-302-3

Band 211: Detlev Staud
Effiziente Prozesskettenauslegung für das Umformen lokal wärmebehandelter und geschweißter Aluminiumbleche
164 Seiten, 72 Bilder, 12 Tabellen 2010.
ISBN 978-3-87525-303-0

Band 212: Jens Ackermann
Prozesssicherung beim Laserdurchstrahlenschweißen thermoplastischer Kunststoffe
129 Seiten, 74 Bilder, 13 Tabellen 2010.
ISBN 978-3-87525-305-4

Band 213: Stephan Weidel
Grundlegende Untersuchungen zum Kontaktzustand zwischen Werkstück und Werkzeug bei umformtechnischen Prozessen unter tribologischen Gesichtspunkten
144 Seiten, 67 Bilder, 11 Tabellen 2010.
ISBN 978-3-87525-307-8

Band 214: Stefan Geißdörfer
Entwicklung eines mesoskopischen Modells zur Abbildung von Größeneffekten in der Kaltmassivumformung mit Methoden der FE-Simulation
133 Seiten, 83 Bilder, 11 Tabellen 2010.
ISBN 978-3-87525-308-5

Band 215: Christian Matzner
Konzeption produktspezifischer Lösungen zur Robustheitssteigerung elektronischer Systeme gegen die Einwirkung von Betauung im Automobil
165 Seiten, 93 Bilder, 14 Tabellen 2010.
ISBN 978-3-87525-309-2

Band 216: Florian Schüßler
Verbindungs- und Systemtechnik für thermisch hochbeanspruchte und miniaturisierte elektronische Baugruppen
184 Seiten, 93 Bilder, 18 Tabellen 2010.
ISBN 978-3-87525-310-8

Band 217: Massimo Cojutti
Strategien zur Erweiterung der Prozessgrenzen bei der Innhochdruck-Umformung von Rohren und Blechpaaren
125 Seiten, 56 Bilder, 9 Tabellen 2010.
ISBN 978-3-87525-312-2

Band 218: Raoul Plettke
Mehrkriterielle Optimierung komplexer Aktorsysteme für das Laserstrahljustieren
152 Seiten, 25 Bilder, 3 Tabellen 2010.
ISBN 978-3-87525-315-3

Band 219: Andreas Dobroschke

Flexible Automatisierungslösungen für die Fertigung wickeltechnischer Produkte

184 Seiten, 109 Bilder, 18 Tabellen 2011.
ISBN 978-3-87525-317-7

Band 220: Azhar Zam

Optical Tissue Differentiation for Sensor-Controlled Tissue-Specific Laser Surgery

99 Seiten, 45 Bilder, 8 Tabellen 2011.
ISBN 978-3-87525-318-4

Band 221: Michael Rösch

Potenziale und Strategien zur Optimierung des Schablonendruckprozesses in der Elektronikproduktion

192 Seiten, 127 Bilder, 19 Tabellen 2011.
ISBN 978-3-87525-319-1

Band 222: Thomas Rechtenwald

Quasi-isothermes Laserstrahlsintern von Hochtemperatur-Thermoplasten - Eine Betrachtung werkstoff- prozessspezifischer Aspekte am Beispiel PEEK

150 Seiten, 62 Bilder, 8 Tabellen 2011.
ISBN 978-3-87525-320-7

Band 223: Daniel Craiovan

Prozesse und Systemlösungen für die SMT-Montage optischer Bauelemente auf Substrate mit integrierten Lichtwellenleitern

165 Seiten, 85 Bilder, 8 Tabellen 2011.
ISBN 978-3-87525-324-5

Band 224: Kay Wagner

Beanspruchungsangepasste Kaltmassivumformwerkzeuge durch lokal optimierte Werkzeugoberflächen

147 Seiten, 103 Bilder, 17 Tabellen 2011.
ISBN 978-3-87525-325-2

Band 225: Martin Brandhuber

Verbesserung der Prognosegüte des Versagens von Punktschweißverbindungen bei höchstfesten Stahlgüten

155 Seiten, 91 Bilder, 19 Tabellen 2011.
ISBN 978-3-87525-327-6

Band 226: Peter Sebastian Feuser

Ein Ansatz zur Herstellung von pressgehärteten Karosseriekomponenten mit maßgeschneiderten mechanischen Eigenschaften: Temperierte Umformwerkzeuge. Prozessfenster, Prozesssimulation und funktionale Untersuchung

195 Seiten, 97 Bilder, 60 Tabellen 2012.
ISBN 978-3-87525-328-3

Band 227: Murat Arbak

Material Adapted Design of Cold Forging Tools Exemplified by Powder Metallurgical Tool Steels and Ceramics

109 Seiten, 56 Bilder, 8 Tabellen 2012.
ISBN 978-3-87525-330-6

Band 228: Indra Pitz

Beschleunigte Simulation des Laserstrahlumformens von Aluminiumblechen

137 Seiten, 45 Bilder, 27 Tabellen 2012.
ISBN 978-3-87525-333-7

Band 229: Alexander Grimm

Prozessanalyse und -überwachung des Laserstrahlhärtings mittels optischer Sensorik

125 Seiten, 61 Bilder, 5 Tabellen 2012.
ISBN 978-3-87525-334-4

Band 230: Markus Kaupper

Biegen von höhenfesten Stahlblechwerkstoffen - Umformverhalten und Grenzen der Biegebarkeit

160 Seiten, 57 Bilder, 10 Tabellen 2012.
ISBN 978-3-87525-339-9

Band 231: Thomas Kroiß

Modellbasierte Prozessauslegung für die Kaltmassivumformung unter Berücksichtigung der Werkzeug- und Pressenauffederung

169 Seiten, 50 Bilder, 19 Tabellen 2012.
ISBN 978-3-87525-341-2

Band 232: Christian Goth

Analyse und Optimierung der Entwicklung und Zuverlässigkeit räumlicher Schaltungsträger (3D-MID)

176 Seiten, 102 Bilder, 22 Tabellen 2012.
ISBN 978-3-87525-340-5

Band 233: Christian Ziegler

Ganzheitliche Automatisierung mechatronischer Systeme in der Medizin am Beispiel Strahlentherapie

170 Seiten, 71 Bilder, 19 Tabellen 2012.
ISBN 978-3-87525-342-9

Band 234: Florian Albert

Automatisiertes Laserstrahllöten und -reparaturlöten elektronischer Baugruppen

127 Seiten, 78 Bilder, 11 Tabellen 2012.
ISBN 978-3-87525-344-3

Band 235: Thomas Stöhr

Analyse und Beschreibung des mechanischen Werkstoffverhaltens von presshärtbaren Bor-Manganstählen

118 Seiten, 74 Bilder, 18 Tabellen 2013
ISBN 978-3-87525-346-7

Band 236: Christian Kägeler

Prozessdynamik beim Laserstrahlschweißen verzinkter Stahlbleche im Überlappstoß

145 Seiten, 80 Bilder, 3 Tabellen 2013
ISBN 978-3-87525-347-4

Band 237: Andreas Sulzberger

Seriennahe Auslegung der Prozesskette zur wärmeunterstützten Umformung von Aluminiumblechwerkstoffen

153 Seiten, 87 Bilder, 17 Tabellen 2013
ISBN 978-3-87525-349-8

Band 238: Simon Opel

Herstellung prozessangepasster Halbzeuge mit variabler Blechdicke durch die Anwendung von Verfahren der Blechmassivumformung

163 Seiten, 108 Bilder, 207 Tabellen 2013
ISBN 978-3-87525-350-4

Band 239: Rajesh Kanawade

In-vivo Monitoring of Epithelium Vessel and Capillary Density for the Application of Detection of Clinical Shock and Early Signs of Cancer Development

124 Seiten, 58 Bilder, 15 Tabellen 2013
ISBN 978-3-87525-351-1

Band 240: Stephan Busse

Entwicklung und Qualifizierung eines Schneidclinchverfahrens

119 Seiten, 86 Bilder, 20 Tabellen 2013
ISBN 978-3-87525-352-8

Band 241: Karl-Heinz Leitz

Mikro- und Nanostrukturierung mit kurz und ultrakurz gepulster Laserstrahlung

154 Seiten, 71 Bilder, 9 Tabellen 2013
ISBN 978-3-87525-355-9

Band 242: Markus Michl

Webbasierte Ansätze zur ganzheitlichen technischen Diagnose

182 Seiten, 62 Bilder, 20 Tabellen 2013
ISBN 978-3-87525-356-6

Band 243: Vera Sturm

Einfluss von Chargenschwankungen auf die Verarbeitungsgrenzen von Stahlwerkstoffen

113 Seiten, 58 Bilder, 9 Tabellen
ISBN 978-3-87525-357-3

Band 244: Christian Neudel

Mikrostrukturelle und mechanisch-technologische Eigenschaften widerstandspunkgeschweißter Aluminium-Stahl-Verbindungen für den Fahrzeugbau

178 Seiten, 171 Bilder, 31 Tabellen
ISBN 978-3-87525-358-0

Band 245: Anja Neumann

Konzept zur Beherrschung der Prozessschwankungen im Presswerk

162 Seiten, 68 Bilder, 15 Tabellen

ISBN 978-3-87525-360-3

Band 246: Ulf-Hermann Quentin

Laserbasierte Nanostrukturierung mit optisch positionierten Mikrolinsen

137 Seiten, 89 Bilder, 6 Tabellen

ISBN 978-3-87525-361-0

Band 247: Erik Lamprecht

Der Einfluss der Fertigungsverfahren auf die Wirbelstromverluste von Stator-Einzelzahnblechpaketen für den Einsatz in Hybrid- und Elektrofahrzeugen

148 Seiten, 138 Bilder, 4 Tabellen

ISBN 978-3-87525-362-7

Band 248: Sebastian Rösel

Wirkmedienbasierte Umformung von Blechhalbzeugen unter Anwendung magnetorheologischer Flüssigkeiten als kombiniertes Wirk- und Dichtmedium

148 Seiten, 61 Bilder, 12 Tabellen

ISBN 978-3-87525-363-4

Band 249: Paul Hippchen

Simulative Prognose der Geometrie indirekt pressgehärteter Karosseriebauteile für die industrielle Anwendung

163 Seiten, 89 Bilder, 12 Tabellen

ISBN 978-3-87525-364-1

Band 250: Martin Zubeil

Versagensprognose bei der Prozesssimulation von Biegeumform- und Falzverfahren

171 Seiten, 90 Bilder, 5 Tabellen

ISBN 978-3-87525-365-8

Band 251: Alexander Kühl

Flexible Automatisierung der Statorenmontage mit Hilfe einer universellen ambidexteren Kinematik

142 Seiten, 60 Bilder, 26 Tabellen 2014

ISBN 978-3-87525-367-2

Band 252: Thomas Albrecht

Optimierte Fertigungstechnologien für Rotoren getriebeintegrierter PM-Synchronmotoren von Hybridfahrzeugen

198 Seiten, 130 Bilder, 38 Tabellen 2014

ISBN 978-3-87525-368-9

Band 253: Florian Risch

Planning and Production Concepts for Contactless Power Transfer Systems for Electric Vehicles

185 Seiten, 125 Bilder, 13 Tabellen 2014

ISBN 978-3-87525-369-6